Light Ignition of Carbon Nanotubes for the Initiation of Energetic Materials

Flinders
UNIVERSITY

Thesis submitted to the School of Chemical and Physical Sciences,

Faculty of Science and Engineering, Flinders University

in fulfilment of the requirements for the degree of

Doctor of Philosophy

December 2014

Steven Trewartha

Supervisors: Prof. Joe Shapter, Dr Rodney Appleby and Dr Jason Gascooke

Table of Contents

Summary

Carbon nanotubes have been shown to ignite when exposed to an intense flash of light such as from a camera flash or laser. This phenomenon has been proposed as a novel initiation method for fuels or explosives. Light initiation of materials provides many advantages over traditional initiation methods for fuels and explosives such as reduced degradation of the initiator over time, reduced interference from electrical fields, improved safety and faster ignition by initiating many points of a material at once. The purpose of this work was to investigate the use of light initiated carbon nanotubes in mining explosive initiators to replace the sensitive primary explosives currently used.

In order to investigate this, experimental methods and instruments needed to first be developed to control and reproducibly measure the ignition of carbon nanotubes by light. Subsequently, those experimental methods were used to comparably optimise the ignition output of carbon nanotubes by exploring the variables and investigating various additives and novel techniques.

Results were successfully recorded with the combination of a high speed camera and a high speed pyrometer. A comparison of the reactions when subjected to a camera flash and a laser was performed. It was found that a camera flash unit produced a slow, surface propagated deflagration while a laser produced a much faster explosion-like result which was determined to be preferable for controllable initiation of energetic materials.

The addition of ferrocene to carbon nanotube powder was found to increase the temperature and reaction of light initiated nanotubes and these mixtures were used to successfully ignite pentaerythritol tetranitrate (PETN). Incomplete combustion was found as a result of particle scattering and limited thermal transfer.

Growth of vertically aligned carbon nanotubes on a silicon substrate was performed and investigated as an alternative to randomly aligned nanotube powders. Light initiation of these samples demonstrated higher temperatures and greater reactivity due to the aligned nature of the nanotubes and the strong thermal conductivity of carbon nanotubes along their length. Vertically aligned carbon nanotubes coated in PETN produced explosive results when initiated by a laser and demonstrated great promise for the ignition of energetic materials.

Declaration

I certify that this thesis does not incorporate without acknowledgment any material previously submitted for a degree or diploma in any university; and that to the best of my knowledge and belief it does not contain any material previously published or written by another person except where due reference is made in the text.

_____

Steven Trewartha

Acknowledgements

Firstly, I would like to deeply express my thanks to everyone in my life, all of whom have contributed either directly or indirectly to my work and my ability to complete this thesis. I would like to make specific mention of some people without whom this project would not have been possible.

I specifically thank my primary supervisor, Joe Shapter, who is incredible to work with. Your patience and flexibility are matched by a willingness to support students by being available to discuss or answer questions at any time and provide excellent feedback to drafts in very short time. I also acknowledge and thank my secondary supervisor, Rodney Appleby from Orica, Australia who provided invaluable input particularly into the energetic materials portion of the experiments and the overall directions of the project along the way. Jason Gascooke, thank you for assisting with the laser operation in training me and expanding my knowledge.

I would like to acknowledge and thank the Flinders University Faculty of Science and Engineering for the scholarship which enabled me to continue study. I also acknowledge and thank Orica for proposing the project and providing financial assistance for the research. I also thank Marilyn Karaman from Orica for performing the TGA experiments presented.

I would like to acknowledge the excellent Technical Services Unit in the school, and in particular John Pesor who initially setup the photodiode system and LabView program, and Wayne Peacock who refined and helped troubleshoot the equipment right up to the last days where everything broke down.

I acknowledge DSTO who, through our Centre for Expertise in Energetic Materials (CEEM), provided me with safety training and access to PETN as well as the use of a high speed camera for a portion of the project.

Thanks go to Ashley Slattery for first providing me with samples of vertically aligned nanotubes and then training me to make them myself and always being available and helpful in answering questions about the process. Thanks also to Dan Tune who introduced me to the method of horizontally aligned nanotubes.

I thank the whole Smart Surface Structures labgroup who always listened intently and provided thought provoking questions and feedback whenever I presented portions of my results.

Lastly, but definitely not least, I thank my family for their unconditional support throughout my whole time studying, plus my girlfriend and all my friends for being there for me or just providing welcome distraction and relaxation when I needed it as well as the Flinders University Volleyball Club for much the same.

List of Figures

Chapter 1: Introduction and Literature Review

1.1: Overview

Carbon nanotubes have recently been found to ignite when exposed to a simple photoflash.[1] This phenomenon potentially has a wide range of applications in research and technology. The broad aim of this project is to use carbon nanotubes to ignite mining explosives using a light source as the initiation mechanism. The overall objective is to use this technology in commercial blasting systems if it is found to be reliable for the initiation of bulk explosives. Therefore the research will focus on discovering and investigating the variables that effect the ignition of nanotubes from light and thus control and accurately predict an explosive reaction. Reproducibility and energy outputs will be the primary factors investigated initially, and work will aim to optimise the efficiency, power and time of ignition. Finally and most importantly, experiments will be performed to use light initiated carbon nanotubes to ignite energetic materials.

1.2: History of Carbon Nanotubes

A carbon nanotube is a cylindrical nanostructure with the walls made up of sp^2 hybridized carbon bonded in a hexagonal one-atom thick structure like graphene. The structure is commonly described as individual sheets of graphene rolled up into a tube. Additionally, nanotubes can be formed with concentric layers of walls making up multi-walled carbon nanotubes. They have attracted great interest recently in the scientific community due to their unique nanoscale properties.

Sumio Iijima is widely credited with the discovery of carbon nanotubes in a paper in Nature in 1991.[2] However, early observations of carbon nanotubes and

similar carbon structures can be traced back to the 1950s and 1960s. Roger Bacon of Union Carbide in Ohio published a paper on what he termed 'Graphite Whiskers'; a carbon material with extremely high tensile strength (~20GPa) and Young's Modulus (~700GPa).[3] Graphite filaments had been observed previously[4] but Bacon was the first to grow them in a lab with measurable properties. At the time, it was the strongest material known to man, though Bacon was unaware exactly what he had made. Electron microscopy at the time did not have high enough resolution, but it showed a distinctive scroll-like structure[3] (Figure 1.1), which led to the high strength properties due to the hexagonal crystal structure, which would bend under pressure rather than break the strong bonds.

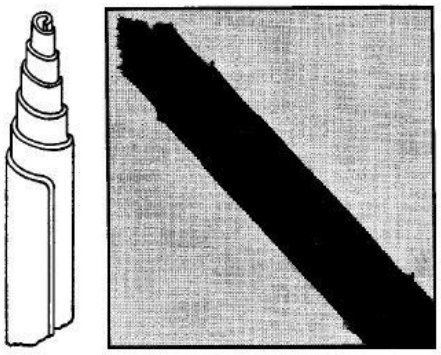

Figure 1.1: Left; Schematic model of a graphite whisker. Right; Electron microscope image of the scroll (2500X). (*Bacon, 1960*)

Perhaps the most interesting claim to an early discovery of carbon nanotubes can be traced to Russia in 1952, in the *Soviet Journal of Physical Chemistry*.[5] Radushkevich *et al.* reports tubular carbon nano-filaments and goes as far as to produce transmission electron microscopy images of them to verify the structure, as displayed in Figure 1.2.

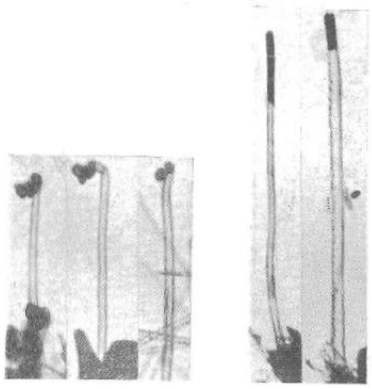

Figure 1.2: TEM images of carbon nanotubes approx. 50nm in diameter produced in 1952. (*Radushkevich et al., 1952*)

This paper was not widely recognized until 2006,[6] for several reasons. It was published in Russian, which cut it off from much of the Western World, and it was published at the height of the Cold War. Radushkevich also did not know what the structure of the material produced was and the TEM images were only precise enough to show the clear shape of the nanotubes, not the helical structure or multiple walls of nanotubes.

Several letters were produced in hindsight of Iijima's paper referencing earlier papers that showed images of nanotubes, but at the time their structure was not understood. For instance, Boehm (1997) suggested in *Carbon* that images produced in 1972 clearly showed carbon nanotubes by electron microphotographs.[7] In a short letter to *Nature*, Gibson (1992) suggested that similar carbon filaments have been reported in *Nature* as far back as 1953,[8] where firebricks at 450˚C and dissociating carbon monoxide formed helical carbon structures which were described to be observed coalesced together forming thicker 'ropes' as shown in Figure 1.3.[9]

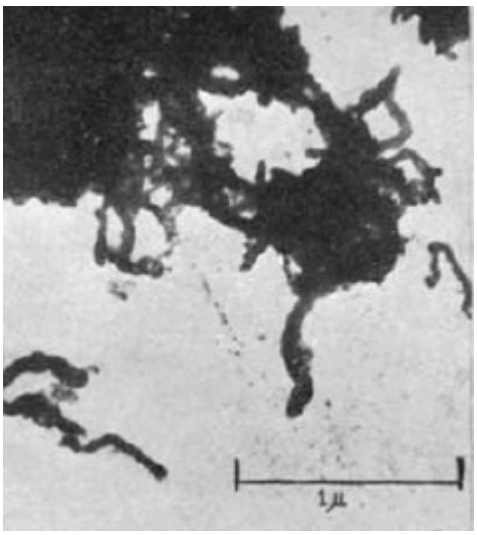

Figure 1.3: Stereoscopic examination of carbon growth in firebricks with an iron catalyst. (*Davis, 1953*)

In 1975, Morinobu Endo published a PhD thesis in Orleans, France[10] about carbon fibres based at Shinshu University, Japan, collaborating with Agnes Oberlin (France). In the thesis, Endo successfully made carbon fibres by decomposing hydrocarbons and growing them in the vapour phase. The aim of his work was to synthesis cheaper carbon fibres for use in the aerospace industry. Thus the fact that single-walled carbon nanotubes grew first as a basis for the carbon fibres was completely overlooked, since at the time they had no practical applications. Details of the experiment and images of the nanotubes (Figure 1.4) were published in 1976.[11]

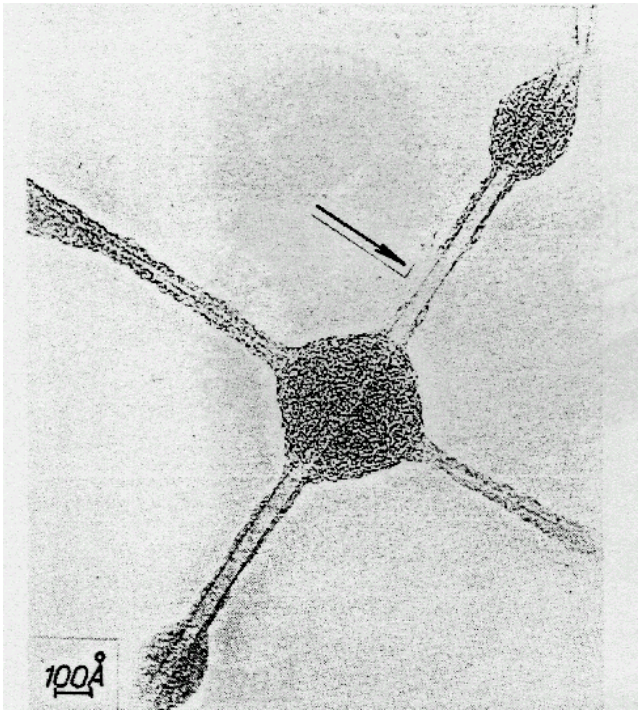

Figure 1.4: TEM image displaying a single-walled carbon nanotube in a cross-linked carbon fibre. (*Oberlin, 1976*)

Sumio Iijima's paper in Nature 1991[2] caught the attention of the scientific community, and is credited for the discovery of multi-walled carbon nanotubes (MWCNT). This is because he was able to outline a synthesis technique much like the method for producing fullerenes[12] called arc-discharge evaporation. It produced multi-walled carbon nanotubes, verified by electron microscopy which showed concentric tubes ranging in diameter from 4-30nm.[2] The structure was also proposed and shown to be different to the scroll structure shown by Bacon.[3]

The next significant step in carbon nanotube history followed a year after Iijima's paper. Experiments on characterizing CNTs fell short due to the tiny quantities of nanotubes synthesized thus only theoretical calculations could be performed. In 1992 in a letter to *Nature*, Ebbesen and Ajayan from NEC in Japan, where Iijima worked, published a method to optimize the conversion of graphitic carbon to carbon nanotubes and produce macroscopic amounts of nanotubes.[13] This allowed much more work to be performed characterizing the properties of

carbon nanotubes. Their method was the same as reported by Iijima[2] but they altered the current, voltage and relative graphitic rod size to reach optimal conditions for growth. Another key factor of their experiment was using an inert gas at high pressure in the chamber, helium at 500 Torr was applied which resulted in ~75% conversion of the graphite rod to nanoparticles, mostly made up of MWCNTs.[13]

Uniform single-walled carbon nanotubes (SWCNT) were grown and isolated simultaneously and independently by Iijima at NEC in Japan[14] and by Bethune at IBM in the USA.[15] Both papers were published in *Nature* on June 17, 1993. The arc-discharge technique was used but the SWCNTs were found to grow from carbon in the vapour phase rather than on the filament and deposit on the walls of the chamber under an atmosphere of inert gas. Both groups found these nanotubes to contain only a single atom thick wall and only 1-2nm wide, catalysed by iron (Iijima) or cobalt (Bethune). The original aim of the latter experiment was to produce nanotubes containing metal using iron, nickel or cobalt. The cobalt products displayed different properties to the other two catalysts, and upon investigation it was discovered that they had grown single-walled carbon nanotubes on beads of cobalt nanoparticles and soot clusters. A transmission electron microscopy image of Bethune's sample is shown in Figure 1.5.

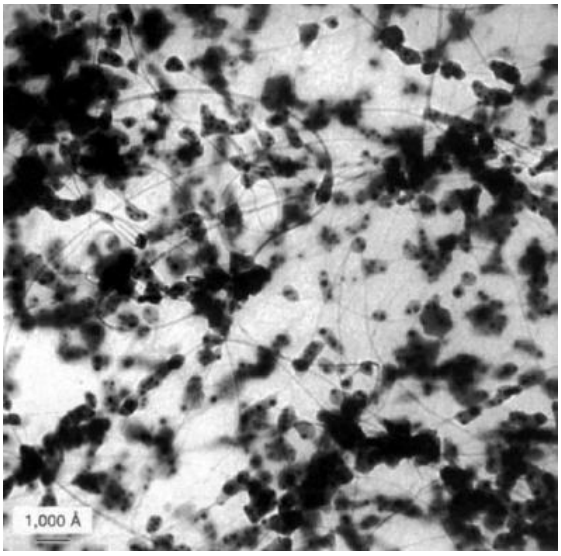

Figure 1.5: TEM image of SWCNTs attached to cobalt and soot clusters. (*Bethune, 1993*)

1.3: Synthesis of Carbon Nanotubes

There are several growth mechanisms established in the literature to produce carbon nanotubes, and recent experiments have led to much cheaper nanotube synthesis in larger quantities. However, purified samples of nanotubes are still expensive and difficult to grow. Methods to synthesise carbon nanotubes include; laser ablation, high-pressure CO conversion (HiPCO), chemical vapour deposition (CVD) and electric arc-discharge. Unlike fullerenes, which are commonly found in space dust, nanotubes cannot be found in nature, either on earth or in space.[16]

The first method used to produce carbon nanotubes was the arc-discharge method, and it is still commonly used today by many commercial producers. A schematic representation is shown in Figure 1.6. A system contains two carbon (graphitic) electrodes; a larger cathode is fixed, and a smaller anode is moveable. The two electrodes are moved together until a current passes through them (<1mm distance) and a plasma is formed in the gap. This plasma charged area, under the atmosphere of a pressurised inert gas, heats up to the range of 2000-

5000˚C, which is hot enough to sublimate the anode. As the anode evaporates and forms nanotubes on the cathode, it is moved closer to keep the distance small and the current flowing until the anode is completely used up.[16]

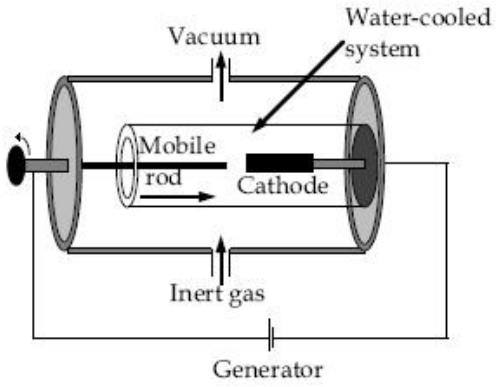

Figure 1.6: Schematic representation of an electric arc-discharge system to produce CNTs. (*Journet, 1998*)

This method of synthesis can produce both MWCNTs and SWCNTs. When just the graphite electrodes are used, the deposit growing on the cathode is a mixture of nanotubes of varying number of layers and lengths up to a micrometer as well as graphitic nanoparticles. The MWCNTs form the majority of the product, though some is unusable since the heat fuses it to the surroundings.[17]

To produce SWCNTs, metallic nanoparticles are used as growth sites for the nanotubes. This was the experiment performed by Iijima[14] and Bethune[15] in the discovery of SWCNTs. A hollow graphitic anode is used and filled with a metal catalyst and some fine graphite powder. This metal will then be evaporated with the anode and form part of the product. Under optimal conditions and with cobalt or nickel mixtures, SWCNTs are formed in high quantities.[18]

In 2002, Jeannette Benavides at the NASA Goddard Space Flight Center patented a method for synthesizing single-walled carbon nanotubes based on arc-discharge.[19] This method used helium arc welding to vaporise carbon. From there, the carbon could be deposited on a graphitic cathode and grown as nanotubes in arc-discharge. The process differs because it can produce nanotubes at a greater yield and a faster rate than normal arc-discharge, leading to cheaper nanotubes. It also does not require a metal catalyst at all, which is usually a significant cost both to manufacture and to remove from the nanotubes during purification. The complete absence of metal makes this method usable in medical applications that need highly pure products.

Chemical vapour deposition (CVD) is another technique often used by commercial companies to produce nanotubes. During CVD, a substrate is prepared with a catalyst, most commonly cobalt, nickel or iron, on the surface. The surface is then annealed at 600-1000˚C which causes the catalyst to form into nanoparticles to act as growth sites for nanotubes. Two gases are introduced to the system – a process or carrier gas (such as nitrogen or argon) and a hydrocarbon to act as a carbon source (such as methane or acetylene).[20] The catalyst sites break down the carbon source gas and carbon nanotubes grow from the catalyst particles. This technique means residual metal catalyst particles in the unrefined nanotubes are only present at the tips.

An example of a CVD system is shown in Figure 1.7 by Andrews *et al*., 2002.[21] Ferrocene ($Fe(C_5H_5)_2$) and xylene ($C_6H_4C_2H_6$) were used as the carbon based molecules to produce MWCNTs.[21] This mixture of powders was injected into the system with a heavy stream of inert gases to entrain them, and then high temperatures (~750˚C) in the reaction chamber cause decomposition of the molecules. No pressure seals are required since the reaction chamber is kept at atmospheric pressure. From the ferrocene, iron nanoparticles are nucleated and deposited on the substrate surface to act as a catalyst. Carbon can then self-

assemble on the substrate surface in the form of MWCNTs. The substrate is an extremely flat quartz surface.

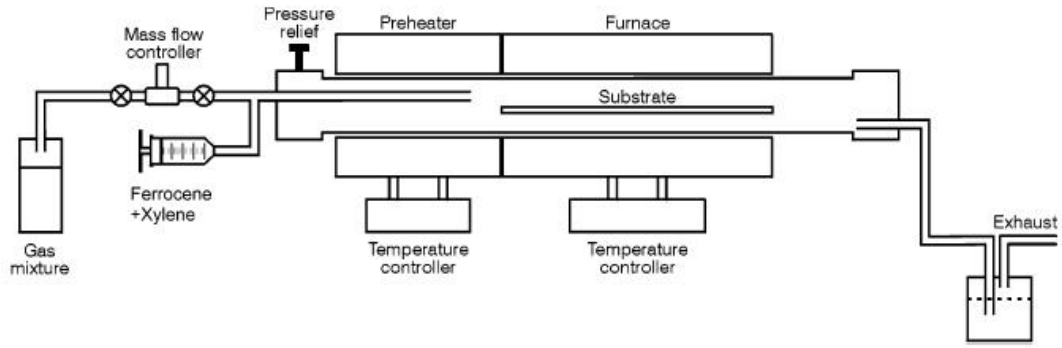

Figure 1.7: Example of a catalytic CVD system for MWCNT growth. (*Andrews, 2002*)

The nanotubes grow extremely quickly at the site once iron nanoparticles are deposited, and form in highly aligned 'forests' as shown in the SEM image in Figure 1.8. This is different to many other nanotube growth techniques which form tangled bundles, often likened to cooked spaghetti.

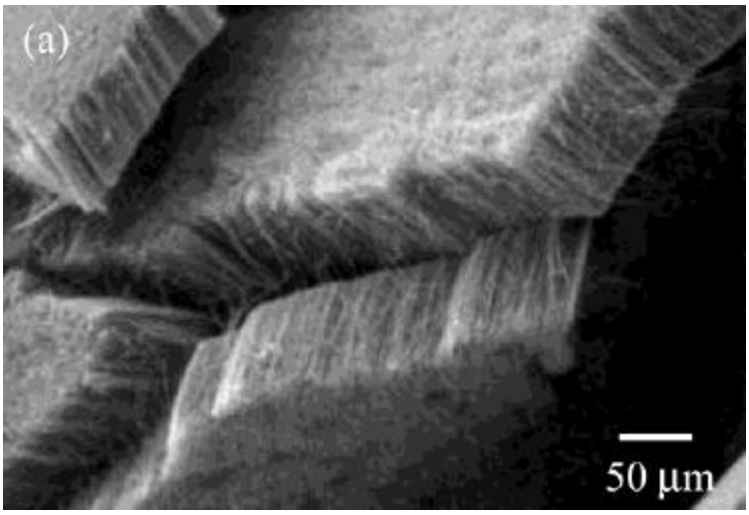

Figure 1.8: SEM image displaying highly aligned multi-walled carbon nanotubes produced via CVD on iron. (*Andrews, 2002*)

Laser ablation is a growth technique similar in principle to arc-discharge in that a furnace with a steady flow of inert gas and a graphite rod is used. It was first reported by Smalley *et al*. in 1995.[22] A laser is directed at a carbon sample in a furnace with a high flow of inert gas, carbon is vaporised by the laser and deposited further down the apparatus on a cooled collector, growing as carbon nanotubes and carbon soot.[16]

The laser is a pulsed laser, it is scanned across the surface to provide an even ablation and smooth surface. The collector is usually water-cooled copper to move the carbon out of the gas phase and produce fast deposition which allows nanotubes to grow instead of closing their structure to form fullerenes. The temperature of the oven can affect both the products formed and the purity; at 900˚C MWCNTs form with some defects and a lot of soot while at 1200˚C the MWCNTs have been found in higher yield and containing no defects.[23]

To produce SWCNTs from laser ablation, transition metals must be added to the graphite target, which reduces the yield. Alternatively to increase the yield, methods were developed to use two targets; one of pure carbon and the other of a mixture of carbon and a transitional metal alloy.[24] This was found to increase the yield and quality of SWCNTs.

High pressure carbon monoxide (HiPCO) growth is commonly used for bulk synthesis as it is capable of producing up to 10 grams per day of single-walled carbon nanotubes.[25] The technique was developed by Smalley *et al*. in 1999 and it works by thermally decomposing iron pentacarbonyl ($Fe(CO)_5$) to act as the catalyst for growth under a high pressure atmosphere of carbon monoxide, which is the carbon source.[26] The temperature in the reaction chamber is increased to 1000˚C and pressurised with carbon monoxide gas. Subsequently, the organometallic molecule $Fe(CO)_5$ is fed into the reaction chamber as a further source of CO and to provide the iron catalyst. The high temperature decomposes

the $Fe(CO)_5$ and clusters of iron form in the gas phase. The growth is catalysed and occurs on the surface of the iron. Growth can be performed continuously without waste of CO and the technique allows controlled growth of high quality SWCNTs with purity yields of up to 90%.[27]

1.4: Properties of Carbon Nanotubes

Carbon nanotubes have a very wide variety of potential uses due to their unique properties. Electronically, the π bonding and anti-bonding orbitals cross at the Fermi level of the molecule so carbon nanotubes can be either metallic or semi-conducting.[28]

The structure of a carbon nanotube falls into two categories named armchair and zigzag. These configurations are based on the way a theoretical sheet of graphene is rolled up into a nanotube, illustrated in Figure 1.9. Rolling symmetrically through the hexagonal rings from a corner to a corner produces the (n, n) configuration nanotube, or armchair. On the other hand, rolling symmetrically through a ring side will produce the (n, 0) configuration, or zigzag. Any other angle will produce chiral conformations which are combinations of the two main conformations.[29] Figure 1.10 displays the three conformations of nanotubes.

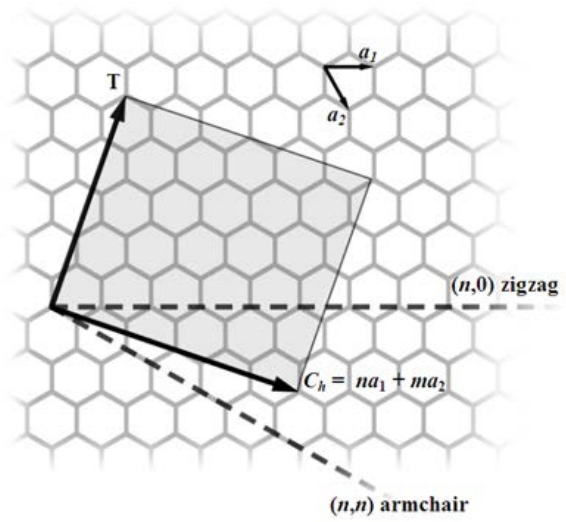

Figure 1.9: Schematic showing the vectors responsible for different nanotube conformations. (*Odom, 2000*)

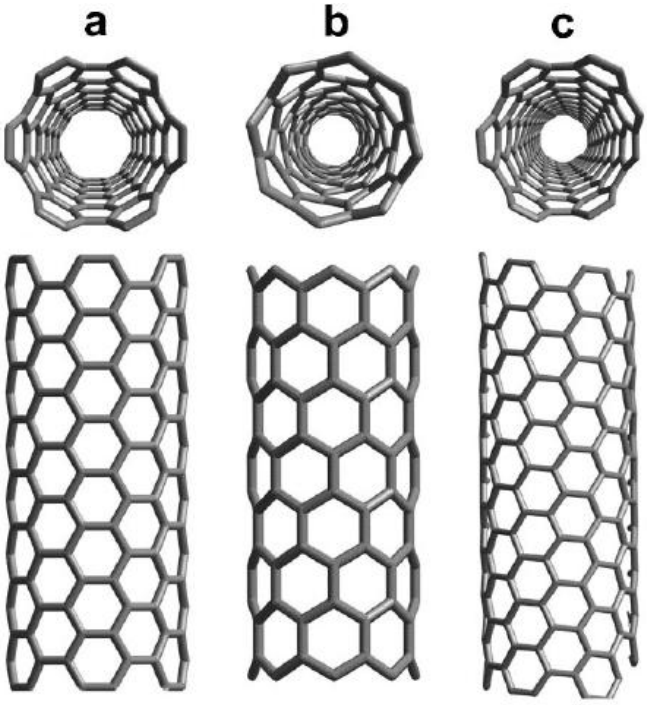

Figure 1.10: Molecular models of single-walled carbon nanotubes; a) armchair configuration, b) zigzag configuration, c) chiral conformation. (*Terrones, 2003*)

The armchair conformation SWCNTs are always metallic due to the symmetry of the density of states. The zigzag conformation is almost metallic, but curvature effects from the tube open up a small band-gap which is related to the diameter of the tube; as the diameter increases the band-gap decreases by the

inverse of the diameter squared. Thus the zigzag conformation is a small band-gap semi-conductor, and the chiral formation is a large band-gap semi-conductor with the band-gap determined by the angle of the bonds with respect to the length of the tube and the diameter.[30] The conductance of a pure and defect free metallic carbon nanotube is excellent due to the high mean-free path; as an electron is very unlikely to scatter along the length of a nanotube. Electrical current density has been measured at over 1000 times greater than that of copper.[31]

The carbon-carbon sp^2 hybridized chemical bond in a graphene sheet is one of the strongest covalent bonds known, thus carbon nanotubes are extremely strong materials. Their tensile strength is unmatched by any material; some 30 times stronger than steel. However, under compression their hollow structure and massive length to diameter ratio leads to buckling or bending.[30] The density of a carbon nanotube is much lower than metals, so as well as being much stronger carbon nanotubes are far lighter than metals, which makes their mechanical strength properties even more desirable.[32]

The thermal conductivity of carbon structures such as diamond and graphite is extremely high due to a stiff sp^3 bonding arrangement,[33] this leads to predictions that the thermal conductivity of nanotubes along the tube length may be the highest of all materials due to their even higher strength sp^2 bonds.[31] Phonon activity dominates the acoustic and thermal properties of carbon nanotubes; a large phonon mean free path is thought to be responsible for the high thermal conductivity. Early experiments determined that the thermal conductivity of CNTs is dependent on temperature.[33] At room temperature a theoretical thermal conductivity of 6600 W/m.K. has been predicted by Berber *et al.*, which far eclipses the thermal conductivity of copper; 385 W/m.K.[33] In a time dependent reaction such as ignition, the thermal diffusivity should be considered which is the thermal conductivity divided by the density and specific heat capacity.[34] This means sample density is an important parameter to consider.

1.5: Explosives Classifications and Terminology

Energetic materials are typically classified into two main categories; primary and secondary explosives. A primary explosive is highly sensitive to stimuli such as impact, friction, heat and spark.[35] The sensitivity of these explosives means great care and consideration is needed in handling and transportation. Primary explosives are commonly used in detonators, blasting caps and as triggers to explode charges of less sensitive explosives.[36] A commonly used rule of thumb is if an explosive is more sensitive than pentaerythritol tetranitrate (PETN) it is classed as a primary explosive.[37]

A secondary explosive tends to require a large amount of energy to be initiated. They are often used in high volume and are initiated by the explosion of a small quantity of primary explosive.[35]

A complimentary classification method for explosives splits them into high and low explosives, related to the velocity of explosion. Low explosives are those that are primarily propagated by deflagration and are commonly used as propellants. High explosives are propagated by a shockwave through detonation of the material. A high explosive can be classified as primary or secondary based on its sensitivity.[38]

1.6: Current Explosives Initiation Devices

There are many types of initiating devices currently available in the mining industry to detonate explosives. Most fall into one of three primary categories; non-electric initiators, hot-wire initiators and exploding bridgewire detonators. Non-electric initiators are the simplest type and usually work by loading a small amount of primary explosive next to the mechanism of initiation.

The initiator mechanism can either be heat, flame or spark.

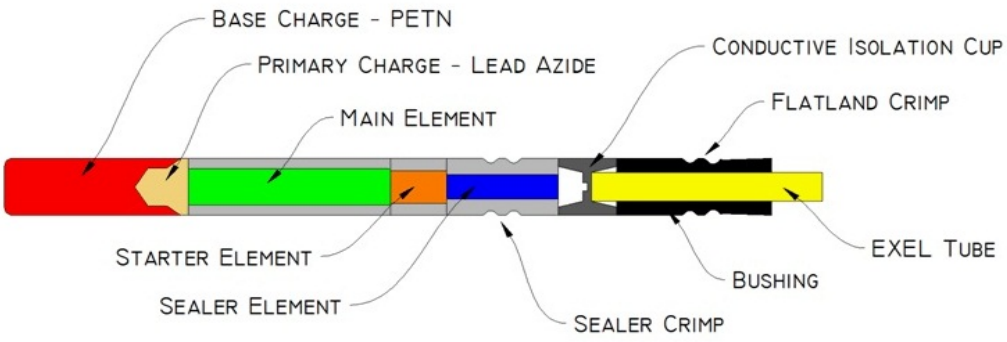

Figure 1.11: Schematic of a non-electric detonator. (*From Orica Australia general document in correspondence with Rodney Appleby*)

A schematic of a typical commercial non-electric detonator is displayed in Figure 1.11. The detonator will have the heat source supplied by the detonation reaction of the explosive powder in the attached signal tube (exel tube), usually octogen (HMX) and aluminium, which then ignites the pyrotechnic delay element that sits on top of the primary explosive. The heat from the burning pyrotechnic initiates the sensitive primary explosive (lead azide) which in turn detonates the high energy secondary explosive (PETN) base charge.[39]

Hot-wire initiators utilize electricity to initiate an explosion. The primary part of the initiator is a pair of wires embedded in a primary explosive, connected by a bridgewire. A current is passed through the wire which causes heating of the bridgewire and subsequent heating of the initiating material. When the ignition temperature of the material is reached, a burning reaction begins which propagates to the secondary explosive part of the device. A schematic of such a device is shown in Figure 1.12. The most common initiating material used is lead (III) azide. In most current initiators, a pyrotechnic material is used in contact with the bridgewire with the lead (III) azide loaded further down. This produces a controllable delay in the explosive initiator.[40]

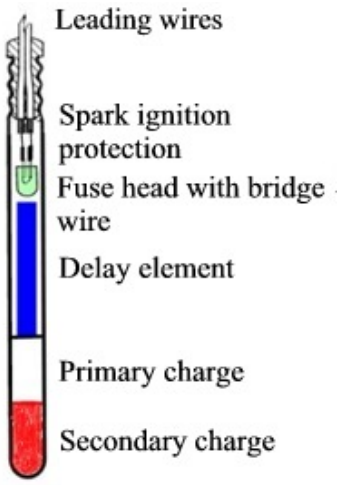

Figure 1.12: Schematic representation of a hot-wire initiator, also representative of an exploding bridgewire detonator.

(*From Science Partners http://www.sp.se/en/index/services/detonators/detonators/Sidor/default.aspx accessed September 2014*)

Hot-wire initiators can be unreliable since very small electrical differences in the leads or bridgewire will affect the time it takes to heat up, and thus the time to initiate the explosive. Imprecise contact between the bridgewire and the primary explosive will also affect how quickly initiation occurs. Of major concern with these systems is that stray electric fields can result in premature ignition of the system if not handled properly.

Exploding bridgewire detonators are very similar in design to the hot-wire initiators. The key difference is that the bridgewire is made of very thin, high density material such as gold or nichrome and the very high current is applied in a short time period. This means that instead of heating up, the bridgewire itself vaporises and produces an explosive shockwave to initiate detonation, providing a much faster and more reliable reaction than hot-wire initiation.[39] Pentaerythritol tetranitrate (PETN) is used in contact with the bridgewire so accidental detonation from heating the bridgewire (even to its melting point) does not occur.[40] An issue

with exploding bridgewire systems is that a large power supply is required to generate the current surge necessary to vaporise the bridgewire.

Carbon nanotubes are not classed as explosive materials and are considered non-hazardous for transportation according to their MSDS. Therefore this project will investigate the possibility of using carbon nanotubes in combination with other nanomaterials to replace the primary explosives of traditional initiators. Carbon nanotubes also offer the possibility of more reliable and safer methods of initiation via light initiation. Optical signals (solid state light emitting devices such as lasers) are largely immune to electromagnetic interference and less susceptible to degradation over time.[41] The combination of these two properties offers a novel method of initiation which can overcome the shortfalls of previous devices discussed in this section.

1.7: Literature Review of the Light Ignition of Nanomaterials

Carbon nanotubes have been found to ignite when subjected to a burst of light, such as from a camera flash. This phenomenon was first discovered accidentally by Ajayan *et al.* in 2002 and believed to be a photoacoustic effect.[1] It was found that a photoflash at close range (~2cm) ignited 'fluffy' (term used to describe the low density nanotube powder) single-walled carbon nanotubes (SWCNT). The proposed mechanism was that due to the high absorption of light energy from the photoflash and subsequent conversion into vibration and thermal energy, excess energy that is unable to be efficiently dissipated causes sufficient localised heating in the nanotubes thus exothermic oxidation and propagation occurs leading to ignition. In support of this theory, SWCNTs were found by High Resolution Transition Election Microscopy (HRTEM) to undergo significant reconstruction as a result of the photoflash even when ignition did not occur as shown in Figure 1.13. This suggests it is a property of the nanotubes responding to the light which causes the effect. This phenomenon was found to not occur in multi walled carbon nanotubes (MWCNT), carbon soot, C_{60}, or graphite powder. Interestingly, purified SWCNT were also found to not ignite. The initial explanation for this was that the increased density of purified SWCNTs allowed more nanotubes to be in contact with each other thus efficient heat dispersal is possible.[1]

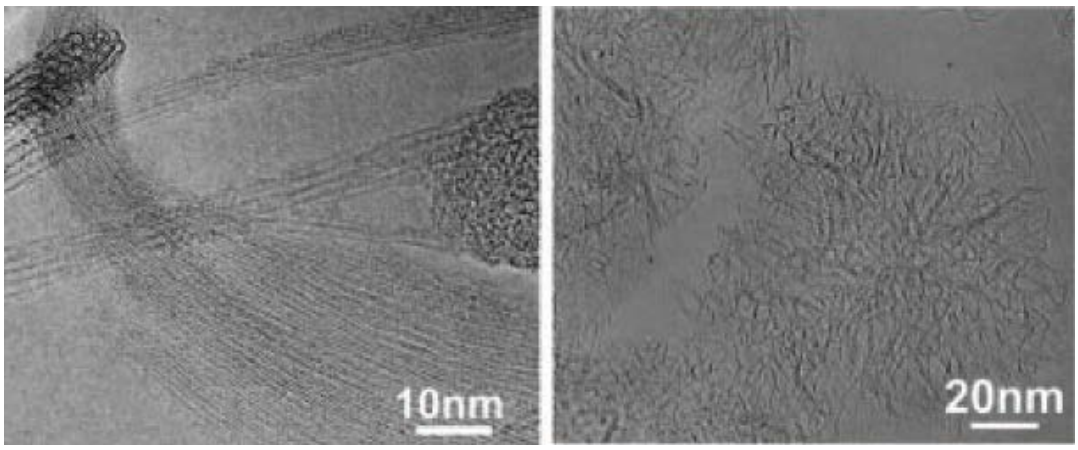

Figure 1.13: High Resolution Transmission Electron Microscopy images of SWCNTs pristine (left) and reconstructed carbonaceous material after photoflash (right). (*Ajayan, 2002*)

Bockrath *et al.* hypothesised, in response, that the catalyst particles play a crucial role in the ignition process and are more likely to be the cause of the phenomenon.[42] Purifying nanotubes removes these catalyst particles thus would also remove the ignition properties, regardless of nanotube density. Experiments were performed coating thin layers of metal nanoparticles onto carbon sheets and it was found ignition readily occurred when exposed to a photoflash. This led to the theory that carbon nanotubes merely act as a stabilizing medium for the metal nanoparticles and once the carbon begins to oxidize and expose the metal to air, much more energetic oxidation of the metal nanoparticles can occur. This alternate theory does not explain why physically compressed SWCNTs and MWCNTs with large percentages of metal catalyst do not ignite.

The initial photoflash ignition experiment was repeated by Braidy *et al.* in 2002 to begin investigating the phenomenon further on raw HiPCO SWCNTs containing Fe (23% wt/wt) particles of 1-5nm diameter.[43] The researchers observed a bright orange residual material in the sample at the precise spots where burning was most intense. X-ray powder diffraction analysis of this material showed it to be iron oxide (Fe_2O_3 with trace amounts of Fe_3O_4), and TEM showed that the particles also agglomerated into larger clumps. A similar experiment performed before ignition confirmed that they were iron nanoparticles with no

oxidized material until exposure to flash. The iron does not oxidize naturally since it is protected by shells of amorphous carbon or contained within the walls of nanotubes. This oxidation and agglomeration of particles suggests localized temperatures of 1500-2000˚C – temperatures required for the aforementioned SWCNT reconstructions.[1]

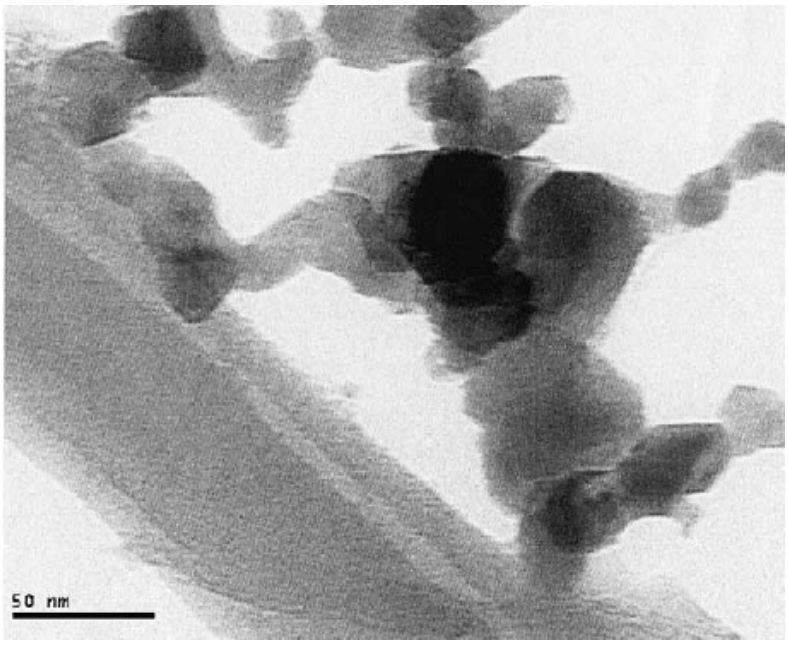

Figure 1.14: TEM image of single-walled carbon nanotubes post flash ignition showing large formations of iron oxide. ***(Smits, 2003)***

Smits *et al.* in 2003 expanded this work by exposing iron microparticles (6-10μm diameter) to the same photoflash as SWCNTs and found they ignited and oxidized as well with no nanotubes present.[44] This supports the theory of Bockrath that the metal nanoparticles are the crucial part for ignition. HRTEM was performed on SWCNTs before and after photoflash ignition to investigate the size and location of iron catalyst particles. Before ignition, particles were found mostly inside the nanotubes and attached to the outside, ranging 1-5nm in diameter. Figure 1.14 shows that after ignition the nanotubes were damaged and chemically changed. In addition the iron nanoparticles oxidized to Fe_2O_3 and agglomerated into particles 50-150nm in diameter. Electron energy loss

spectroscopy (EELS) showed an amorphous carbon coating around the Fe_2O_3 particles. This reaction again suggests localized temperatures above 1500˚C. Purified SWCNTs with little to no residual catalyst were again found to not ignite in the study, and HRTEM showed that the few remaining iron nanoparticles did not undergo oxidation.

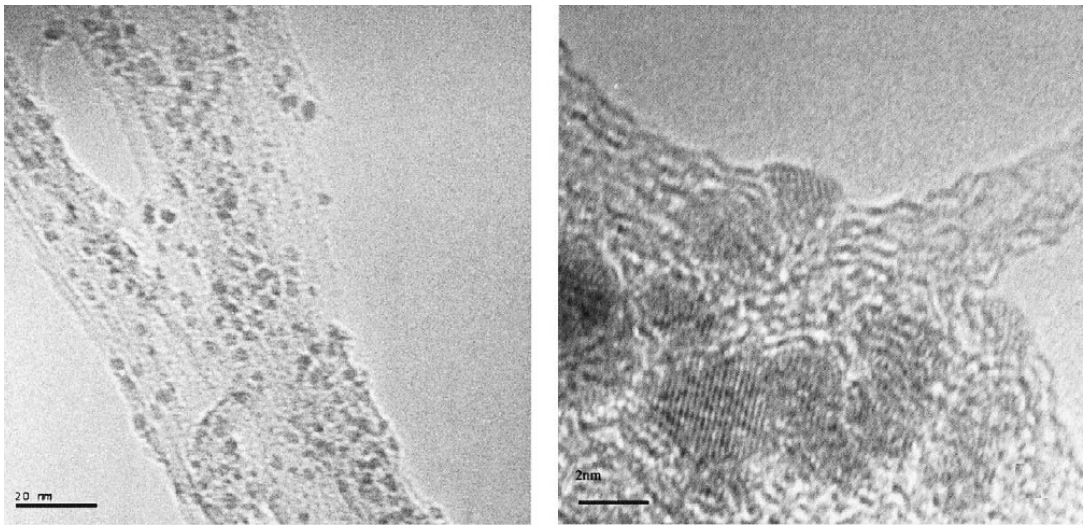

Figure 1.15: TEM image of as-prepared single walled carbon nanotubes showing the distribution of iron nanoparticles (20nm scale) (left) and high-resolution TEM of a bundle showing that most of the iron appears to be encased in carbon (2nm scale) (right). (*Smits, 2003*)

It was suggested from the TEM images shown in Figure 1.15 that the iron nanoparticles within the nanotubes are well insulated by carbon and thus unable to easily disperse heat, while the nanotube bundles are conductive and interconnected thus easily able to disperse heat. The study concluded that ignition was purely due to the pyrophoric nature of fine iron powder rather than any unique properties of the carbon nanotubes and subsequently, heat released from the exothermic oxidation of the iron nanoparticles was sufficient to cause melting of the particles as well as promote deformations and restructuring of the carbon nanotubes.[44] However, the paper made no experimental investigation into MWCNTs or why a sample of MWCNTs with an equal weight percentage of iron catalyst would not also oxidize and ignite.

A Raman study with a He-Ne laser (633nm) was performed on carbon nanotube/polyurethane composite matrices by Singamaneni *et al*. in 2006.[45] The experiment showed spontaneous ignition of the composite when the laser was focused at a power of just 25mW. The nanotubes chosen were 70% pure and contained nickel/yttrium as the catalyst rather than iron. The combustion only occurred when the nanotubes were highly dispersed in the matrix, and no ignition was found from either material individually or with other polymer matrices. It was hypothesized that poor thermal conduction between the nanotubes and the polymer resulted in rapid localized heating of the nanotubes, oxidation, a release of gases, and thermal degradation of the surrounding polymer matrix. Figure 1.16 shows SEM images of the sample displaying burned craters that are 3-4 times larger than the spot size of the laser which suggests there is some propagation of the reaction, but not through the entire material.

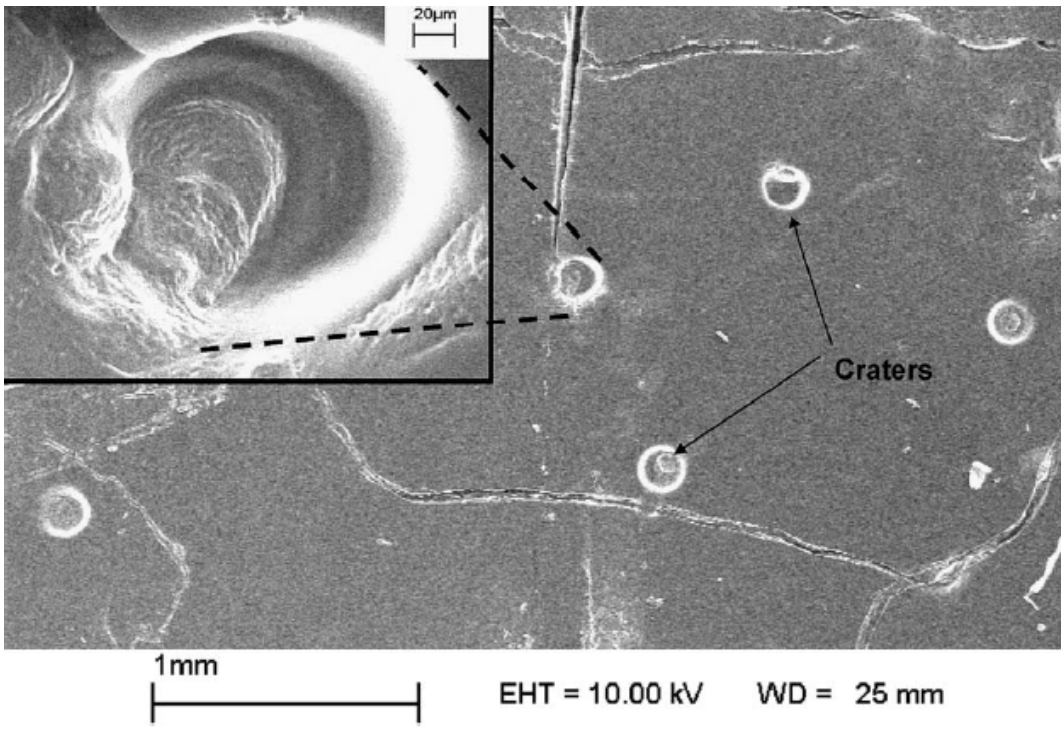

Figure 1.16: SEM image of nanotube/polymer film after ignition of laser showing the large craters. (*Singamaneni, 2006*)

The G-band peak of carbon nanotubes is known to shift downwards with an increase in temperature due to bond softening and thermal expansion.[46] Using this relationship, Singamaneni was able to perform real-time Raman spectroscopy on the sample and estimate the ignition point to be 385˚C (with an estimated peak temperature of 750˚C), which correlates with the oxidation temperature and the initial thermal decay of carbon nanotubes.[47] Additionally, the polyurethane is optically inactive in the 633nm range, while carbon nanotubes have an absorption maximum at 650nm[48] which strongly suggests a property of the nanotubes in this experiment is responsible for the ignition behaviour. The polymer matrix insulated the nanotubes enough that they could not easily disperse the absorbed heat thus they were able to rapidly oxidize.[45]

Carbon nanotubes are known to have photoconductive properties which have been extensively investigated for their potential use in optoelectronic devices.[49-53] An experiment performed by Liu *et al*. in 2007 investigated and measured the photocurrent generated in SWCNTs as a result of exposure to a camera flash.[54] The experiment utilized an aligned bundle of SWCNTs on a silicon wafer. Each end of the bundle was connected to a drop of silver paint with platinum wires attached to create a circuit (optical image is displayed in Figure 1.17). The camera flash was applied under different pressures, gas environments and flash intensities for optimization. The significant point from this research is that a measurable photocurrent was produced in the nanotubes as a result of a camera flash. This strongly supports the ignition mechanism theory that the SWCNTs perform a crucial part of the reaction and it is not simply due to the pyrophoric nature of metal nanoparticles. Ignition should not be possible in this system due to the closely packed and aligned nature of the bundle being able to disperse heat quickly and efficiently.

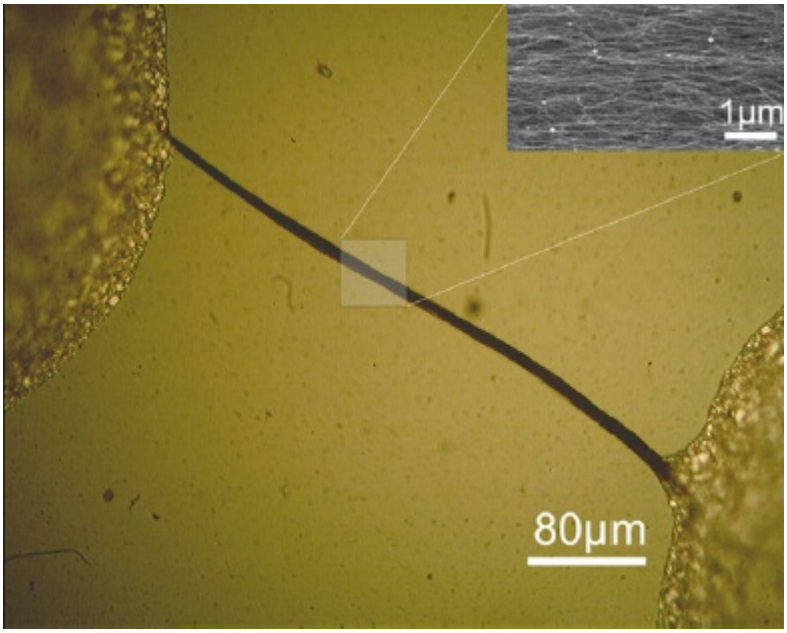

Figure 1.17: Optical image of the two-terminal device used to measure photocurrent. A drop of silver paint is at either end with an aligned bundle of SWCNTs connecting the drops. Inset: SEM image of the aligned nanotubes. (*Liu, 2007*)

Previously reported studies have supported the theory that an acoustic wave is generated upon ignition causing a popping sound.[1,42] A detailed study into the photoacoustic and ignition characteristics of carbon nanotubes was performed by Tseng *et al.* in 2007.[55] Experiments involved a sensitive microphone to record the intensity of the photoacoustic effect in an anechoic (non-echoing) room. Materials investigated included as-prepared 'fluffy' SWCNTs (CVD grown, 13.8% wt/wt iron catalyst) and purified SWCNTs, multi-walled carbon nanotubes, carbon fibres (8-10µm diameter), C_{60} fullerenes, graphite powder, carbon paste and diamond nanopowder. Density was considered an important factor for ignition possibility due to heat dispersal pathways and was reported with SWCNTs and MWCNTs having the lowest density. The authors proposed that a photoacoustic mechanism was occurring – the rapid increase in temperature from camera flash absorption causes an instant thermal expansion of air which triggers the acoustic wave. Theoretically and proven experimentally, materials which accumulate heat faster than they dissipate it produce a much stronger acoustic wave than materials which can readily dissipate heat.[55-57] Results showed 'fluffy' SWCNTs as the most reactive followed by 'fluffy' MWCNTs, compacted

SWCNTs, carbon fibre, carbon powder and purified SWCNTs. There was no detectable acoustic wave or reaction from C_{60}, carbon paste or diamond nanopowder.

As a crude method to quantify the temperature reached in nanotubes as a result of a photoflash, ferrocene was sprayed onto samples. It was found to have an ignition temperature of 480˚C,[55] therefore any samples showing an instant ignition and flame had to have reached at least 480˚C. Ferrocene on its own was not reactive to the flash. An increased flame from ferrocene acting as a fuel is useful for some explosive applications.

Tseng *et al.* also measured CO_2 concentrations in an enclosed system before and after exposure to a photoflash to prove oxidation of nanotubes occurred. It was found that even in samples that did not ignite, sound was recorded and CO_2 levels increased which suggests that there needs to be sufficient enough amounts of heat and metal nanoparticles to cause enough exothermic oxidation for ignition to occur otherwise the reaction begins but dissipates before ignition. Experiments were performed in a vacuum and an argon atmosphere which showed no iron oxide formation, highlighting the importance of atmospheric oxygen. The study concluded that the mechanism for ignition could be due to heating and oxidation of the nanotubes exposing trapped catalyst particles to air which subsequently allows the exothermic oxidation formation of Fe-O which causes a chain reaction due to the heat released to the surroundings. This suggests that the carbon acts as a shell around the catalytic nanoparticles and stops them spontaneously combusting until enough energy is input to oxidize and deform the nanotubes.

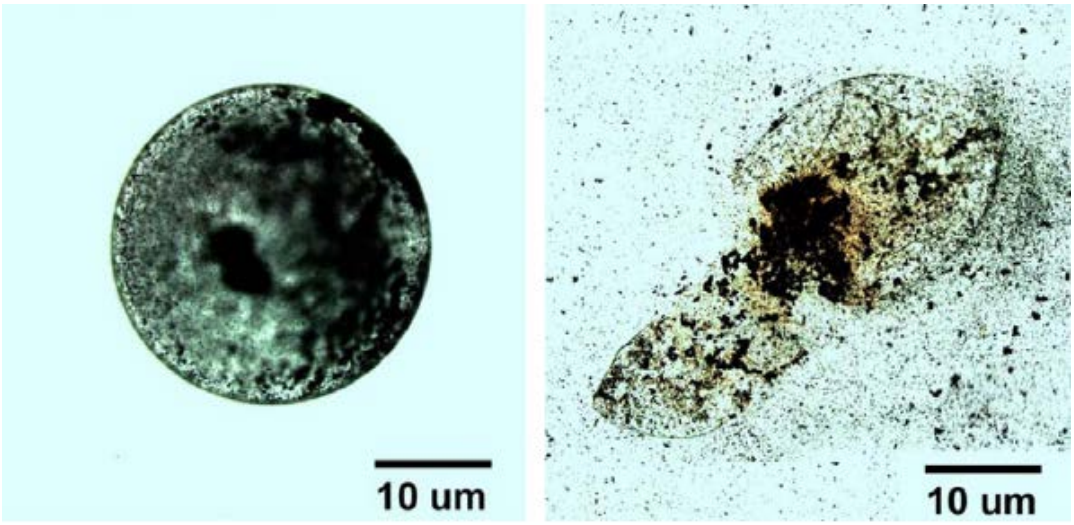

Figure 1.18: SWCNT enwrapped in a polymer microcapsule before laser irradiation (left) and after laser irradiation (right). *(Kang, 2008)*

In 2008, Kang *et al.* used an infrared laser as the light source to ignite single walled carbon nanotubes.[58] SWCNTs were suspended in water by sonication and irradiated by the laser, which produced small bubbles and shock waves. This suggested that the nanotubes could be undergoing detonation rather than just deflagration. The SWCNTs were then wrapped in 20µm polymer capsules and ignited, which caused the capsules to break apart, Figure 1.18, demonstrating the destructive power of light initiated SWCNTs and showing evidence that it could be detonation rather than deflagration. Kang investigated as-prepared SWCNTs (~20 wt.% metal) and purified (~8 wt.% metal) samples and found no difference in their ignition properties or photoacoustic spectra, which suggested that catalyst oxidation is not the mechanism for ignition in this case. Rather Kang proposed the photoacoustic response of SWCNTs coupled with their inability to efficiently disperse heat when suspended in solution as the mechanism for ignition.

In 2012, Chehroudi published a study thoroughly investigating the minimum ignition energy (MIE) from a camera flash required for as-prepared SWCNTs and performed experiments investigating the effect of wavelength and

pulse duration.[59] The results showed that over a range of long pass and short pass wavelength filters, MIE did not change implying that wavelength is a fairly insignificant variable. On the other hand, changing the pulse duration between 0.2ms and 7ms produced a large change in the MIE from ~30-35mJ/pulse for the 0.2ms pulse up to 80-95mJ/pulse for the 7ms pulse setting. This result agrees with the mechanism that for ignition to occur, heat dissipation must be slower than incident energy – a shorter time for the light pulse means the sample is heated over a shorter time period and is thus given less time to dissipate heat.

Chehroudi *et al*. has also devised a more complete experimental setup for measuring the light ignition of carbon nanotubes.[60] A high speed camera and sensitive microphone were used to view the ignition in slow-motion and record the acoustic spectra. As an extended experimental setup, a pyrometer measured temperature versus time and an IR spectrometer measured spectral emission. However, results from these instruments have not yet been detailed in the literature.[60,61] Results conclude that samples with a higher degree of compaction require more energy to ignite.

1.8: Energetic Materials with the Light Ignition of Nanotubes

Manaa *et al.* first combined nanotubes with explosives in an initiator in 2005.[62] SWCNTs (as-prepared, containing iron 29wt.%) were combined with PETN (10mg of each material) and exposed to a camera flash, which produced bright illumination and burning. Subsequently, SWCNTs (0.020g) were loaded into a copper cylinder that was filled with K-6 explosive (30g) and initiated with a flash bulb. Deflagration occurred followed by detonation 1.5 minutes after deflagration started, characterised by a witness plate and pins along the cylinder to measure the speed of the shockwave.

Carbon nanotubes have been wrapped in energetic materials and ignited. The thermoelectric effect is a phenomenon where an electric voltage is caused by a thermal gradient by charged carriers diffusing from the hot side to the cold side of a circuit.[63] Nanotubes have been used as the thermoelectric conductor between two temperature controlled metal plates.[64-67] There is a concept called thermopower waves which has recently gained momentum in the literature as a nanoscale extension of the thermoelectric effect and far exceeds classical theoretic limits for thermoelectric energy creation.[68]

A thermopower wave is a phenomenon by which a nanomaterial with large axial thermal conductivity can self-propagate a reactive wave along its length which drives electrical carriers with the thermopower wave when an exothermic reaction is triggered at one end.[69] The process is aided by a material coated on the nanowire that undergoes exothermic degradation. A schematic of the process is shown in Figure 1.19B. Experiments to create a device were published by Choi *et al*. in 2010.[70] Vertically aligned arrays of MWCNTs on silicon were synthesized by CVD then the explosive material cyclotrimethylene trinitramine (RDX) was added by dissolving it in acetonitrile and evaporating it into the nanotubes. TEM showed this process created a 6-9nm layer of RDX around individual nanotubes, Figure 1.19A. Sodium azide was added by evaporation with water after the RDX reportedly to allow initiation at ambient temperature and pressure.

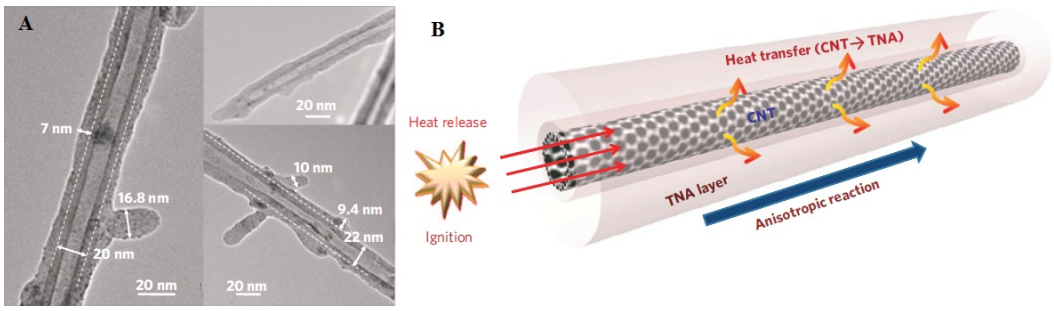

Figure 1.19: A) TEM image of RDX coated MWCNTs with dashed line showing the boundary between the materials. B) Schematic of the mechanism of reaction to create the thermopower wave. (*Choi, 2010*)

The reaction and subsequent thermopower wave was successfully initiated both by laser irradiation and by electrical discharge. A reaction wave was measured with a velocity along the length of the nanotubes more than four orders of magnitude faster than the typical combustion rate of RDX. A large electrical impulse was also measured from the reaction. Control experiments suggest that alignment of the nanotubes is required for a reaction to occur – randomly oriented samples did not work. The authors discuss the potential of this system for single-use power sources, however, there is also potential for explosive devices using similar systems as the light initiated portion to produce an explosion.

Malec *et al*. published results of a study in 2010 to investigate the light ignition of nanotubes mixed with various ratios of ferrocene and sodium perchlorate ($NaClO_4$).[71] A camera flash unit was used as the light source for experiments and a photodiode measured intensity of explosions to optimize mixtures. MWCNTs were found to not react to the camera flash unless mixed with ferrocene (MWCNTs/ferrocene 1:4 wt/wt) whereby samples would burn by a surface propagated deflagration for several minutes. The addition of $NaClO_4$ as an oxidant was found to change the reaction from a steady burn to a violent combustion of total time 50-100ms. Malec *et al*. found that the optimal ratio of MWCNT/ferrocene/$NaClO_4$ was 1:4:20 wt/wt. A lower amount resulted in incomplete combustion, while a higher amount absorbed the released energy.

Porous silicon has previously been found to be explosive when combined with an oxidizer and triggered by a spark electrode due to its high surface area to volume ratio.[72] It may also be initiated by laser pulse, but not by a camera flash. Malec *et al*. added the optimised mixture of MWCNTs/ferrocene/$NaClO_4$ to porous silicon and successfully used it as an initiator via camera flash triggering to explode the porous silicon film.[71]

Xiang *et al*. investigated the photo-responsive sensitivity of energetic materials when supported by carbon nanotubes in 2012.[73] The energetic materials used were a mixture of metal powder and an oxidant – namely zirconium (~100μm diameter) and potassium perchlorate ($KClO_4$) in the paper. The authors had previously found various metal/oxidant mixtures were sensitive to exothermic oxidation when initiated by a laser,[74,75] but proved insensitive to the lower intensity of a photoflash.

SWCNTs were added in a reported optimal ratio of Zr/$KClO_4$/SWCNT (9:1:3) and the resultant mixture underwent combustion from a photoflash, showing that nanotube addition was responsible for initiating the reaction. Excess of carbon nanotubes in the mixture decreased the reaction due to the extra heat dissipation pathways present. X-ray diffraction displayed oxidation of the zirconium into ZrO_2 and Raman spectroscopy showed removal of the radial breathing mode (RBM) of SWCNTs and increase in the D-band which is attributed to amorphous carbon. This result suggests that the photoflash ignition has destroyed the microstructure of the nanotubes and created defects. High-resolution transmission electron microscopy of samples after the flash ignition is shown in Figure 1.20 with onion-like structures formed as a result of reconstruction of the nanotubes which supports the Raman results.

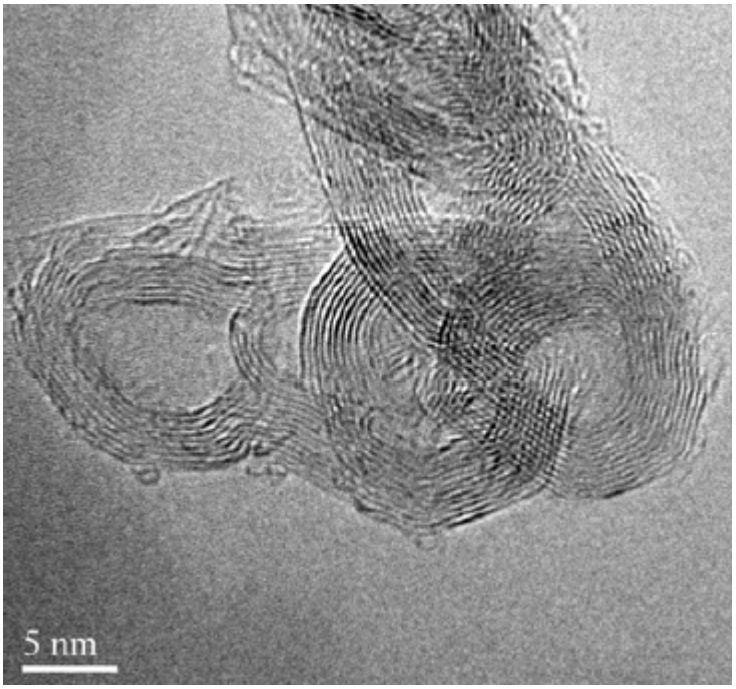

Figure 1.20: High-resolution TEM image of Zr/$KClO_4$/SWCNT after ignition from a photoflash displaying onion-like structures from significant reconstruction of nanotube structure. (*Xiang, 2012*)

A similar study was published by Kim *et al*. in 2013 with energetic nanomaterials initiated by SWCNTs.[76] Aluminium nanoparticles (80nm diameter) and copper oxide nanoparticles (50nm diameter) were combined at a ratio of 3:7 and subsequently sonicated in ethanol with various ratios of SWCNTs. The authors found some ignition from repeated camera flashes in the absence of nanotubes, however, the reaction was significantly enhanced by SWCNTs. A high speed camera was used in their study to measure the speed of explosions, and the fastest reaction was found with 1wt.% SWCNTs in the reaction. The ignition was suppressed by heat dissipation from the nanotubes at concentrations higher than 5wt.%. The method of mixing in this study produces a close contact between the nanotubes and the energetic nanomaterials to allow heat transfer from the light induced oxidation of nanotubes and their metallic nanoparticles to the energetic nanomaterials.

1.9: Addition of Fuels to the Light Ignition of Nanotubes

Light initiation of carbon nanotubes has also sparked great interest in engines, in particular combustion engines. The ignition technique for such engines is critical and failure can lead to catastrophe in systems such as rocket engines.[77] The most common ignition system is electric spark igniters, however, its drawbacks include heavy components that are susceptible to degradation and require high voltage and high energy. Most significantly as well, a spark is a single-point stimulus – it only initiates one point in the system.[77] Carbon nanotubes mixed with fuels and fuel sprays then initiated by a camera flash could potentially form cheap, lightweight and multiple point initiation systems where a controlled area of fuel could be ignited simultaneously by exposure to a widespread light source.

Carbon nanotubes were combined with a variety of fuels including liquid jet fuels, liquid hydrocarbons, nitro-methane, ionic liquids and solid oxidizing agents by Danczyk *et al.* in 2005.[77] Experiments performed found that the fuels could be ignited using a camera flash to initiate the ignition of nanotubes and subsequently the fuels. To ignite, nanotubes need oxygen from the air so experiments where the SWCNTs were completely submerged in fuel proved unsuccessful. The nanotubes were placed next to a drop of fuel, or alternatively, the fuel was left to evaporate until parts of the nanotubes were exposed before ignition. Additionally, purified SWCNTs (~97% containing 3% wt/wt iron) were investigated and found to ignite only in an oxygen rich environment. Higher purifications than 97% SWCNTs would not even ignite in pure oxygen. The study also proposed the idea of a liquid fuel spray with SWCNTs that could be ignited by a light source, and found that ignition was more intense in oxygen rich environments.

Berkowitz *et al*. used a combustion chamber with a mix of ethylene and air with suspended nanotubes to investigate the potential light initiation of the fuel mixture in 2011.[78] A camera flash was used to initiate the nanotubes, and subsequent combustion in the reaction chamber was observed. This result was compared to the same experiment initiated by a spark plug. High speed camera results (Figure 1.21) showed that the camera flash initiation produced a distributed ignition across the whole chamber at once while the spark ignition produced a single ignition point which expanded in a combustion wave across the chamber. The camera flash initiation created a much higher pressure rise and higher peak pressure than the spark initiated system.

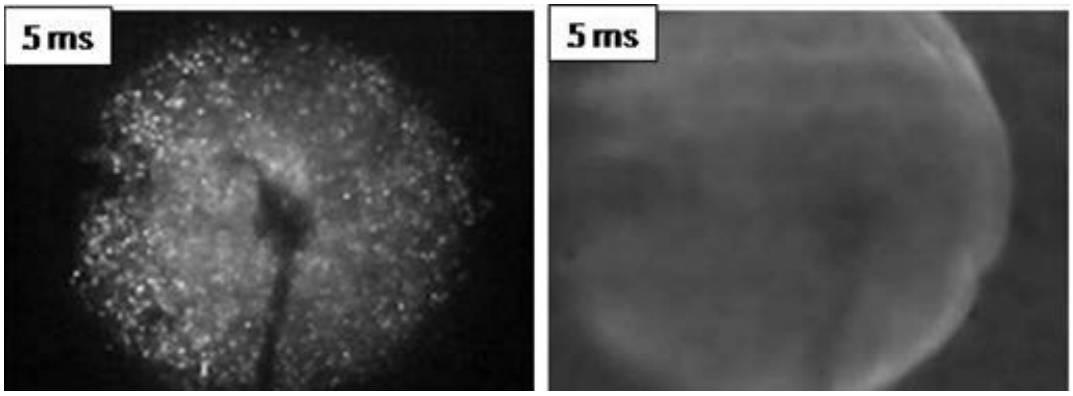

Figure 1.21: High frame rate photo (5ms after initiation) comparison of camera flash initiated ignition of SWCNTs in ethylene/air creating a distributed ignition across many points (left) and spark initiated comparison that created a combustion wave which expanded from the centre (right). (*Berkowitz, 2011*)

A separate study into flash ignition of nanotubes suspended in fuel mixtures was performed by Finigan *et al*. in 2011.[79] The fuel mixture used was ethylene/oxygen/nitrogen and the deflagration-to-detonation transition (DDT) of the mixture was examined and compared to single point spark ignition. Results found the flash ignition of nanotubes in the chamber produced a DDT ~2x faster than the spark ignition. It was hypothesized that distributed flash initiation increases the energy release rate, accelerates the flame area expansion and amplifies the DDT. The most sensitive mixture detonated fast enough that the authors proposed it was possible for the reaction to directly detonate without initial deflagration.

1.10: Overview of Previous Work

The majority of studies into the light initiation of carbon nanotubes have so far concentrated on the residue of an ignition and physical changes made to nanotube structure as a result of a photoflash and ignition. Research has also sought to understand the fundamental phenomenon better and what conditions will optimise ignition, however, the mechanism for what causes ignition is not yet properly understood. Very little work has been performed in regards to the changes in the nanotubes during ignition and what is happening within the first 10 ms after initiation from a light source. The change in temperature, speed of explosion, and whether deflagration or detonation is occurring are important factors for an initiation device. In order for carbon nanotubes to successfully and safely work in the mining industry, their reaction must be predictable and repeatable within millisecond time frames, which will be a large focus of this project.

Infrared laser radiation has been found to ignite SWCNTs[58] but different wavelengths have not been properly investigated, nor has a comparison between the energy generated from a photoflash compared to the energy from a laser been investigated or the differences in the produced reactions. The use of a laser instead of a photoflash offers several experimental advantages including a much more controlled input of energy which can be directed to very specific small areas of samples and with the input light controlled in a beam rather than flooded across a large area. Any light sensitive detectors will record less interference from a laser than from a photoflash.

Additionally, there has been little work performed in examining different additives besides ferrocene and oxidants to boost or sensitise the ignition properties. This work will aim to accurately and reproducibly measure light

initiated ignitions then to maximize the measured output of reactions. This will also be investigated as a primary goal in this PhD project, and subsequently, experiments into whether the produced nanotube mixtures can be used to detonate insensitive explosives will be performed.

Previously at Flinders University, Chris Malec investigated the camera flash ignition of carbon nanotubes in 2008.[80] The measuring apparatus for these experiments was made in-house and involved a photodiode to measure the intensity of ignitions and a UV-Vis spectrometer to measure the temperature of the ignitions through black body radiation emission. Experiments found that SWCNTs were more sensitive to the photoflash than MWCNTs, which did not react at all in many cases. Purified nanotubes were also found to be insensitive. The reaction of all samples was enhanced by the inclusion of ferrocene. Additionally, sodium perchlorate was added as an oxidizer to speed up the ignition and mixtures were used to initiate the explosion of porous silicon.[71]

1.11: Structure of the Thesis

This thesis will build towards measuring the light initiated ignitions of carbon nanotubes with reproducible methods and then, using novel additives and techniques, to attempt to improve the output energy and reaction rate with the overall goal of initiating the explosion of insensitive secondary energetic materials.

Chapter 2 is a materials and methods chapter where details of the nanotubes and other chemicals used in this thesis are shown, along with details of analytical techniques used throughout the experimental sections and the methods for measuring the light initiated ignitions. Chapter 3 attempts to replicate and improve upon the work of Malec[80] and investigates the limitations of the

experimental setup and potential solutions. New ignition measuring equipment is introduced and the chapter investigates the use of a laser to initiate carbon nanotubes instead of a camera flash. In Chapter 4, the parameters and variables of laser ignition are investigated thoroughly and reproducible experimental techniques are outlined. Subsequently several types of nanotubes are investigated and the effect of ferrocene addition with laser initiation is examined. Chapter 5 explores novel modifications and additives to nanotubes to attempt to enhance the output ignition of samples as a result of laser initiation. In Chapter 6 an energetic material is added to a variety of samples to investigate the transfer of energy from light initiated carbon nanotube mixtures to the insensitive energetic material. Finally, in Chapter 7, overall conclusions are provided along with a discussion of potential future work and areas of investigation.

1.12: References

1 Ajayan, P. M. *et al.*, Nanotubes in a Flash--Ignition and Reconstruction. *Science* **296** (5568), 705- (2002).

2 Iijima, Sumio, Helical Microtubules of Graphitic Carbon. *Nature* **354**, 56-58 (1991).

3 Bacon, Roger, Growth, Structure, and Properties of Graphite Whiskers. *Journal of Applied Physics* **31** (2), 283-290 (1960).

4 R. Iley, H. L. Riley, The Deposition of Carbon on Vitreous Silica. *Journal of the Chemical Society* (1948).

5 Radushkevich and Lukyanovich, (Translated) About the Structure of Carbon Formed by Thermal Decomposition of Carbon Monoxide on Iron Substrate. *Soviet Journal of Physical Chemistry*, p88-95 (1952).

6 Monthioux, Marc and Kuznetsov, Vladimir L., Who Should Be Given the Credit for the Discovery of Carbon Nanotubes? *Carbon* **44**, 1621 (2006).

7 Boehm, H. P., The First Observation of Carbon Nanotubes. *Carbon* **35** (4), 581-584 (1997).

8 Davis, W. R., Slawson, R. J., and Rigby, G. R., An Unusual Form of Carbon. *Nature* **171** (4356), 756-756 (1953).

9 Gibson, J. A. E., Early Nanotubes? *Nature* **359** (6394), 369-369 (1992).

10 Endo, M, Mecanisme De Croissance En Phase Vapeur De Fibres De Carbone, PhD Thesis, University of Orleans, 1975.

11 Oberlin, A., Endo, M., and Koyama, T., Filamentous Growth of Carbon through Benzene Decomposition. *J. Cryst. Growth* **32**, 335-349 (1976).

12 Kroto, H. W. *et al.*, C60: Buckminsterfullerene. *Nature* **318** (6042), 162-163 (1985).

13 Ebbesen, T. W. and Ajayan, P. M., Large-Scale Synthesis of Carbon Nanotubes. *Nature* **358** (6383), 220-222 (1992).
14 Iijima, Sumio and Ichihashi, Toshinari, Single-Shell Carbon Nanotubes of 1-nm Diameter. *Nature* **363** (6430), 603-605 (1993).
15 Bethune, D. S. *et al.*, Cobalt-Catalysed Growth of Carbon Nanotubes with Single-Atomic-Layer Walls. *Nature* **363** (6430), 605-607 (1993).
16 Journet, C. and Bernier, P., Production of Carbon Nanotubes. *Applied Physics A: Materials Science & Processing* **67** (1), 1-9 (1998).
17 Ebbesen, T. W., Carbon Nanotubes. *Annual Review of Materials Science* **24** (1), 235-264 (1994).
18 Maser, W. K. *et al.*, Elaboration and Characterization of Various Carbon Nanostructures. *Synthetic Metals* **81** (2-3), 243-250 (1996).
19 Benavides, J. M., Patent No. 10/292,952 (2002).
20 Dupuis, Anne-Claire, The Catalyst in the CCVD of Carbon Nanotubes—a Review. *Progress in Materials Science* **50** (8), 929-961 (2005).
21 Andrews, Rodney, Jacques, David, Qian, Dali, and Rantell, Terry, Multiwall Carbon Nanotubes: Synthesis and Application. *Accounts of chemical research* **35** (12), 1008-1017 (2002).
22 Guo, Ting *et al.*, Self-Assembly of Tubular Fullerenes. *The Journal of Physical Chemistry* **99** (27), 10694-10697 (1995).
23 Rinzler, A. G. *et al.*, Unraveling Nanotubes: Field Emission from an Atomic Wire. *Science* **269** (5230), 1550-1553 (1995).
24 Yudasaka, Masako, Ichihashi, Toshinari, Komatsu, Toshiki, and Iijima, Sumio, Single-Wall Carbon Nanotubes Formed by a Single Laser-Beam Pulse. *Chemical Physics Letters* **299** (1), 91-96 (1999).
25 Bronikowski, M. J. *et al.*, Gas-Phase Production of Carbon Single-Walled Nanotubes from Carbon Monoxide Via the HiPCO Process: A Parametric Study. *Journal of Vacuum Science & Technology A: Vacuum, Surfaces, and Films* **19**, 1800 (2001).
26 Nikolaev, P. *et al.*, Gas-Phase Catalytic Growth of Single-Walled Carbon Nanotubes from Carbon Monoxide. *Chemical Physics Letters* **313** (1), 91-97 (1999).
27 Isaacs, J. A., Tanwani, A., Healy, M. L., and Dahlben, L. J., Economic Assessment of Single-Walled Carbon Nanotube Processes. *J Nanopart Res* **12** (2), 551-562 (2010).
28 Reich, S., Thomsen, C., and J.Maultzsch, *Carbon Nanotubes: Basic Concepts and Physical Properties*. (Wiley-VCH, Weinheim, Germany, 2004).
29 Odom, T. W., Hafner, J. H., and Lieber, C. M., Scanning Probe Microscopy Studies of Carbon Nanotubes. *Topics in Applied Physics* **80**, 173-212 (2000).
30 Dresselhaus, M. S., Dresselhaus, G., and Jorio, A., Unusual Properties and Structure of Carbon Nanotubes. *Annual Review of Materials Research* **34**, 247 (2004).
31 Terrones, Mauricio, Science and Technology of the Twenty-First Century: Synthesis, Properties, and Applications of Carbon Nanotubes. *Annual Review of Materials Research* **33** (1), 419-501 (2003).
32 Yakobson, B. I. and Avouris, P., Mechanical Properties of Carbon Nanotubes. *Topics in Applied Physics* **80**, 287-328 (2000).
33 Berber, Savas, Kwon, Young-Kyun, and Tománek, David, Unusually High Thermal Conductivity of Carbon Nanotubes. *Physical Review Letters* **84** (20), 4613 (2000).

34 Xie, Huaqing, Cai, An, and Wang, Xinwei, Thermal Diffusivity and Conductivity of Multiwalled Carbon Nanotube Arrays. *Physics Letters A* **369** (1–2), 120-123 (2007).

35 Meyer, Rudolf, Köhler, Josef, and Homburg, Axel, *Explosives*, 6th edition. pp 265-277 (Wiley-VCH Verlag GmbH & Co. KGaA, 2007).

36 Sickler, Robert A, *Explosive Principles: An Essential Guide to Understanding Explosives and Detonations*. (Paladin Press, 1992).

37 Matyáš, Robert, Šelešovský, Jakub, and Musil, Tomáš, Sensitivity to Friction for Primary Explosives. *Journal of hazardous materials* **213**, 236-241 (2012).

38 Meyer, Rudolf, Köhler, Josef, and Homburg, Axel, *Explosives*, 6th edition. pp 250-269 (Wiley-VCH Verlag GmbH & Co. KGaA, 2007).

39 Hopler, RB, *Blasters' Handbook*, 17th edition. p. 117-134 (International Society of Explosives Engineers, Cleveland, Ohio, 1998).

40 Cooper, PW, *Explosives Engineering*. p. 321-354 (Wiley-Vch New York, 1996).

41 Bourne, N.K., On the Laser Ignition and Initiation of Explosives. *Proceedings of the Royal Society of London. Series A: Mathematical, Physical and Engineering Sciences* **457** (2010), 1401-1426 (2001).

42 Bockrath, Bradley *et al.*, Igniting Nanotubes with a Flash. *Science* **297** (5579), 192-193 (2002).

43 Braidy, Nadi, Botton, Gianluigi A., and Adronov, Alex, Oxidation of Fe Nanoparticles Embedded in Single-Walled Carbon Nanotubes by Exposure to a Bright Flash of White Light. *Nano Letters* **2** (11), 1277-1280 (2002).

44 Smits, Jan *et al.*, Response of Fe Powder, Purified and as-Produced HiPCO Single-Walled Carbon Nanotubes to Flash Exposure. *Materials Science and Engineering A* **358** (1-2), 384-389 (2003).

45 Singamaneni, Srikanth, Shevchenko, Valeriy, and Bliznyuk, Valery, Unusual Ignition Behavior of Polyurethane/Carbon Nanotube Composites with a He-Ne Laser Excitation (632.8 nm) During Micro-Raman Spectroscopy. *Carbon* **44** (11), 2191-2195 (2006).

46 Raravikar, Nachiket R. *et al.*, Temperature Dependence of Radial Breathing Mode Raman Frequency of Single-Walled Carbon Nanotubes. *Physical Review B* **66** (23), 235424 (2002).

47 Landi, Brian J., Cress, Cory D., Evans, Chris M., and Raffaelle, Ryne P., Thermal Oxidation Profiling of Single-Walled Carbon Nanotubes. *Chemistry of Materials* **17** (26), 6819-6834 (2005).

48 Hartschuh, Achim *et al.*, Single Carbon Nanotube Optical Spectroscopy. *ChemPhysChem* **6** (4), 577-582 (2005).

49 Barone, Paul W., Baik, Seunghyun, Heller, Daniel A., and Strano, Michael S., Near-Infrared Optical Sensors Based on Single-Walled Carbon Nanotubes. *Nat Mater* **4** (1), 86-92 (2005).

50 Levitsky, I. A. and Euler, W. B., Photoconductivity of Single-Wall Carbon Nanotubes under Continuous-Wave near-Infrared Illumination. *Applied Physics Letters* **83** (9), 1857-1859 (2003).

51 Misewich, J. A. *et al.*, Electrically Induced Optical Emission from a Carbon Nanotube FET. *Science* **300** (5620), 783-786 (2003).

52 Wu, Zhuangchun *et al.*, Transparent, Conductive Carbon Nanotube Films. *Science* **305** (5688), 1273-1276 (2004).

53 Zhang, Y. and Iijima, S., Elastic Response of Carbon Nanotube Bundles to Visible Light. *Physical Review Letters* **82** (17), 3472-3475 (1999).

54 Liu, Guangtong *et al.*, Large Photocurrent Generated by a Camera Flash in Single-Walled Carbon Nanotubes. *Journal of Physics D: Applied Physics* **40** (22), 6898 (2007).
55 Tseng, Shih H. *et al.*, Ignition of Carbon Nanotubes Using a Photoflash. *Carbon* **45** (5), 958-964 (2007).
56 Chen, H. and Diebold, G., Chemical Generation of Acoustic Waves: A Giant Photoacoustic Effect. *Science* **270** (5238), 963-966 (1995).
57 McDonald, F. Alan and Wetsel, Grover C., Generalized Theory of the Photoacoustic Effect. *Journal of Applied Physics* **49** (4), 2313-2322 (1978).
58 Kang, Bin, Dai, Yaodong, Chang, Shuquan, and Chen, Da, Explosion of Single-Walled Carbon Nanotubes in Suspension Induced by a Large Photoacoustic Effect. *Carbon* **46** (6), 978-981 (2008).
59 Chehroudi, Bruce, Minimum Ignition Energy of the Light-Activated Ignition of Single-Walled Carbon Nanotubes (SWCNTs). *Combustion and Flame* **159** (2), 753-756 (2012).
60 Chehroudi, B., Danczyk, S.A., Morgan, C., and Badakhshan, A., in *55th JANNAF Propulsion/4th LPS/3rd SPS/6th MSS Joint Meeting* (Orlando, Florida, 2008).
61 Chehroudi, B, Distributed Ignition Using Single-Walled Carbon Nanotubes (SWCNTs) with Applications in Aerospace and Future Automotive Engines. *Recent Patents on Space Technology* **2**, 67-75 (2010).
62 Manaa, M. Riad *et al.*, Flash Ignition and Initiation of Explosives−Nanotubes Mixture. *Journal of the American Chemical Society* **127** (40), 13786-13787 (2005).
63 DiSalvo, Francis J., Thermoelectric Cooling and Power Generation. *Science* **285** (5428), 703-706 (1999).
64 Hone, J. *et al.*, Thermal Properties of Carbon Nanotubes and Nanotube-Based Materials. *Applied Physics A: Materials Science & Processing* **74** (3), 339-343 (2002).
65 Hone, J., Whitney, M., Piskoti, C., and Zettl, A., Thermal Conductivity of Single-Walled Carbon Nanotubes. *Physical Review B* **59** (4), R2514 (1999).
66 Kim, P, Shi, Li, Majumdar, A, and McEuen, PL, Thermal Transport Measurements of Individual Multiwalled Nanotubes. *Physical Review Letters* **87** (21), 215502 (2001).
67 Yu, Choongho *et al.*, Thermal Conductance and Thermopower of an Individual Single-Wall Carbon Nanotube. *Nano Letters* **5** (9), 1842-1846 (2005).
68 Abrahamson, Joel T. *et al.*, Excess Thermopower and the Theory of Thermopower Waves. *ACS Nano* **7** (8), 6533-6544 (2013).
69 Choi, Wonjoon, Abrahamson, Joel T., Strano, Jennifer M., and Strano, Michael S., Carbon Nanotube-Guided Thermopower Waves. *Materials Today* **13** (10), 22-33 (2010).
70 Choi, Wonjoon *et al.*, Chemically Driven Carbon-Nanotube-Guided Thermopower Waves. *Nat Mater* **9** (5), 423-429 (2010).
71 Malec, Christopher D., Voelcker, Nicolas H., Shapter, Joseph G., and Ellis, Amanda V., Carbon Nanotubes Initiate the Explosion of Porous Silicon. *Materials Letters* **64** (22), 2517-2519 (2010).
72 Plummer, Andrew *et al.*, The Burning Rate of Energetic Films of Nanostructured Porous Silicon. *Small* **7** (23), 3392-3398 (2011).
73 Xiang, Xu *et al.*, Photo-Responsive Behaviors and Structural Evolution of Carbon-Nanotube-Supported Energetic Materials under a Photoflash. *Materials Letters* **88**, 27-29 (2012).

74 Xiang, Shi-Biao, Xiang, Xu, and Feng, Chang-Gen, Effects of Temperature on Laser Diode Ignition. *Optik - International Journal for Light and Electron Optics* **120** (2), 85-88 (2009).

75 Xiang, Shi-biao *et al.*, Investigation on Oxygen-Equilibrium Effects of Laser Ignition of Energetic Materials. *Modern Physics Letters B* **20** (07), 353-358 (2006).

76 Kim, Ji Hoon, Ahn, Ji Young, Park, Hyun Seol, and Kim, Soo Hyung, Optical Ignition of Nanoenergetic Materials: The Role of Single-Walled Carbon Nanotubes as Potential Optical Igniters. *Combustion and Flame* **160** (4), 830-834 (2013).

77 Danczyk, SA *et al.*, in *53rd JANNAF Joint Propulsion Meeting, 2nd Liquid Propulsion Subcommittee and Spacecraft Propulsion Subcommittee* (Monterey, CA, 2005).

78 Berkowitz, Andrew M. and Oehlschlaeger, Matthew A., The Photo-Induced Ignition of Quiescent Ethylene/Air Mixtures Containing Suspended Carbon Nanotubes. *Proceedings of the Combustion Institute* **33** (2), 3359-3366 (2011).

79 Finigan, Daniel J, Dohm, Brian D, Mockelman, Jeffrey A, and Oehlschlaeger, Matthew A, Deflagration-to-Detonation Transition Via the Distributed Photo Ignition of Carbon Nanotubes Suspended in Fuel/Oxidizer Mixtures. *Combustion and Flame* **159** (3), 1314-1320 (2012).

80 Malec, Christopher, The Use of Carbon Nanotubes as an Energetic Material Initiator, Honours Thesis, Flinders University, 2008.

Chapter 2: Materials and Experimental Methods

2.1: Materials

The single-walled carbon nanotubes (SWCNT) used as a standard for experiments were as-prepared SWCNTs (APSWCNT) purchased from Carbon Solutions, Inc. These nanotubes are prepared via the electric arc-discharge method, and have a reported carbonaceous purity of 60-70% wt/wt. They are produced using a Ni/Y catalyst which is reported to be at 35% wt/wt residual in samples as determined by TGA. The individual nanotubes of length 0.5-3.0μm and diameter 1.4nm tend to occur as bundles in lengths 1-5μm and width 2-10nm.

Carbon nanotubes were also sourced from several other manufacturers to compare the ignition of nanotubes with different properties. Shenzhen Nanotech Port Co., Ltd. (NTP) are prepared by chemical vapour deposition with an iron catalyst and boast purities of >97% with almost no residual metal catalyst. These multi-walled carbon nanotubes (MWCNT) have a length of 5-15μm and an outer diameter of 7-15nm. SWCNTs of the same purity were also purchased from NTP that had a length of 2-5μm and a diameter of <3nm. Bundle sizes were not reported.

SWCNTs from Unidym are synthesized by the HiPCO method and the raw unpurified nanotubes were used. These are produced with an iron catalyst of reported 35wt.% residual in samples. The individual nanotubes of length 0.1-1.0μm and diameter 1.0nm tend to occur as bundles in lengths 0.5-3μm and width 2-8nm.

Iron nanoparticles (26nm and 100nm diameter) were received from CANano Technologies. Size variation of particles was reported as ±6nm with up to 1% impurities.

Nickel nanoparticles (20nm diameter) were purchased from Skyspring Nanomaterials Inc. with size variation ±4nm and 99.9% reported purity.

Dicyclopentadienyl iron (ferrocene) and sodium perchlorate were purchased from Sigma-Aldrich. Purity is reported as >98%.

Pentaerythritol tetranitrate (PETN) is a white crystalline secondary explosive known for its high explosive nature. It is commonly used as a component of the materials in boosters and detonators as well as in detonator cord. A sample was obtained from DSTO (Defence, Science and Technology Organisation), Edinburgh. The sample was primarily made up of conventional (106µm diameter) particles with some ultrafine (1µm diameter) particles present due to sample aging.[1,2] The density is reported as 1.39g/cm^3.

2.2: Powder Mixing of Nanotubes

Most experiments required two or more powders to be mixed as homogeneously and consistently as possible. Commonly, nanotubes were mixed with ferrocene and/or PETN in varying ratios. A Stuart SF1 Flask Shaker was used at a speed of 800 oscillations/minute for 10 minutes to mix all dry samples.

2.3: Carbon Nanotube Purification

For some experiments, carbon nanotubes samples were cut and purified by an acid treatment method.[3-5] Firstly, an acid mixture of sulphuric acid (98%) and nitric acid (70%) was prepared in a 3:1 (v/v) ratio and lowered to 0˚C in an ice bath. APSWCNTs were then added to the solution in a concentration of 1mg/mL and it was placed in an ultrasonic bath (Elma S30 H, 280W) then sonicated at 0˚C for 6 hours. Upon completion, the reaction was quenched in milliQ water (500mL) to dilute the acid and refrigerated overnight.

To isolate the purified and cut carbon nanotubes from the dilute acid solution, they were vacuum filtered through a 0.4µm polytetrafluoroethylene (PTFE) membrane with extra milliQ water constantly added to raise the solution to pH 6. The membrane and nanotubes were then oven dried at 80˚C for 24 hours prior to use.

2.4: Chemical Vapour Deposition (CVD) CNT Synthesis

Vertically aligned carbon nanotube arrays were grown via CVD on silicon wafers (Siltronix, France) with a water assisted technique first published by Hata *et al*.[6,7] The silicon wafers were first prepared by washing with acetone, ethanol and water, dried under a stream of nitrogen after each step. A schematic of the following synthesis process is shown in Figure 2.1. A Quorum Technologies K575X sputter coater with film thickness monitor was used to sputter a 10nm layer of aluminium onto the surface. This is to add roughness to the surface and help prevent the iron catalyst from agglomerating. In addition, it acts as a buffer between the iron and the silicon to stop diffusion and unwanted FeSi products forming which could retard CNT growth. Following this treatment, a 5nm layer of iron was sputtered onto the surface to act as catalytic growth sites for nanotubes.

The sputtered silicon wafer was then placed in a quartz tube inside a Labec HTF40/12 tube furnace. The gas delivery system was a MKS 647C controller with a MF1 type mass flow controller. The sample was heated to 800˚C under an atmosphere of argon (1000 standard cubic centimetres per minute (sccm)). Once at the required temperature, hydrogen (40sccm) was added to the tube furnace and the argon flow rate was lowered to 960sccm for 10 minutes in order to reduce the iron oxide film into iron nanoparticles suitable for growth of carbon nanotubes. The carbon source used for CNT growth was acetylene (C_2H_2). It was introduced as a mixture of acetylene/hydrogen/argon (5/40/955sccm) for 10 minutes during which the growth occurred. The system was capable of bubbling the argon gas through water which introduces water vapour to the system to wash away the amorphous carbon, however, CNT growth was found to occur without water. The current system is unable to accurately measure the flow rate of water into the reaction chamber. The sample was then left to cool under argon (1000sccm).

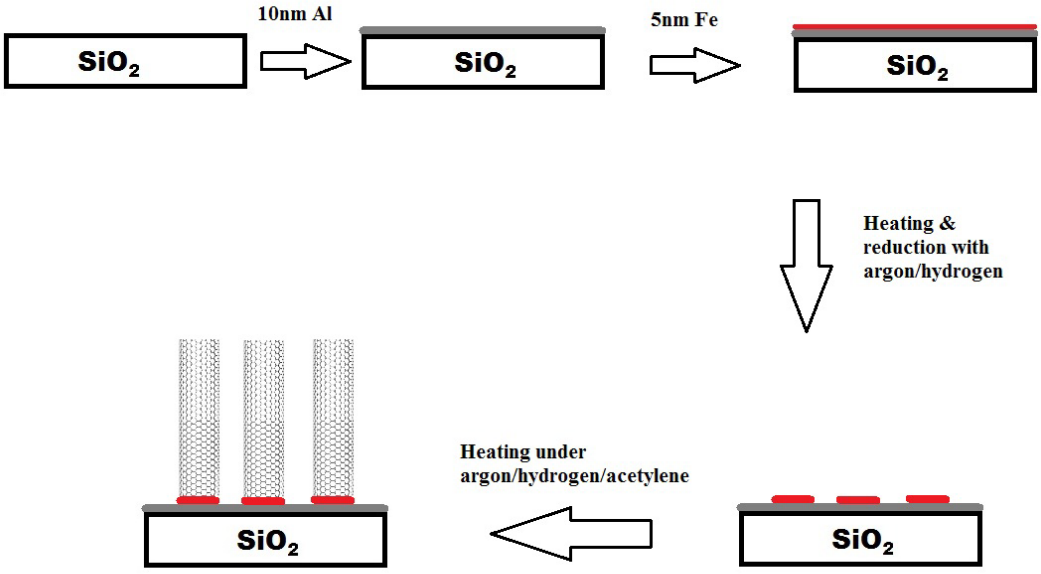

Figure 2.1: Schematic of CNT growth by chemical vapour deposition.

The mechanism of carbon nanotube growth in CVD has been the subject of considerable investigation. There are two potential growth pathways based on the mechanism of carbon filament growth.[8] In both modes, gaseous molecular decomposition and carbon deposition occur at one side of the catalytic nanoparticles which supersaturates them and begins diffusion through the catalyst.[9] Precipitation at the other side begins the growth of carbon fibres. The two growth pathways are differentiated by tip-growth, where the catalyst particle lifts off of the surface, and base-growth, where the nanotubes grow off of the surface bound catalyst, Figure 2.2.[10] In carbon nanotube growth, it is expected that base-growth strongly dominates due to the interactions of the catalyst particle with the surface.[10-12] Other mechanisms may dominate at the nanoscale making tip-growth impossible.[10,13] Therefore in experiments with CVD grown carbon nanotubes, the catalyst particles are expected to be entirely at the base of nanotubes on the silicon surface, differing from unpurified powder nanotube samples where catalyst particles are found throughout the sample.

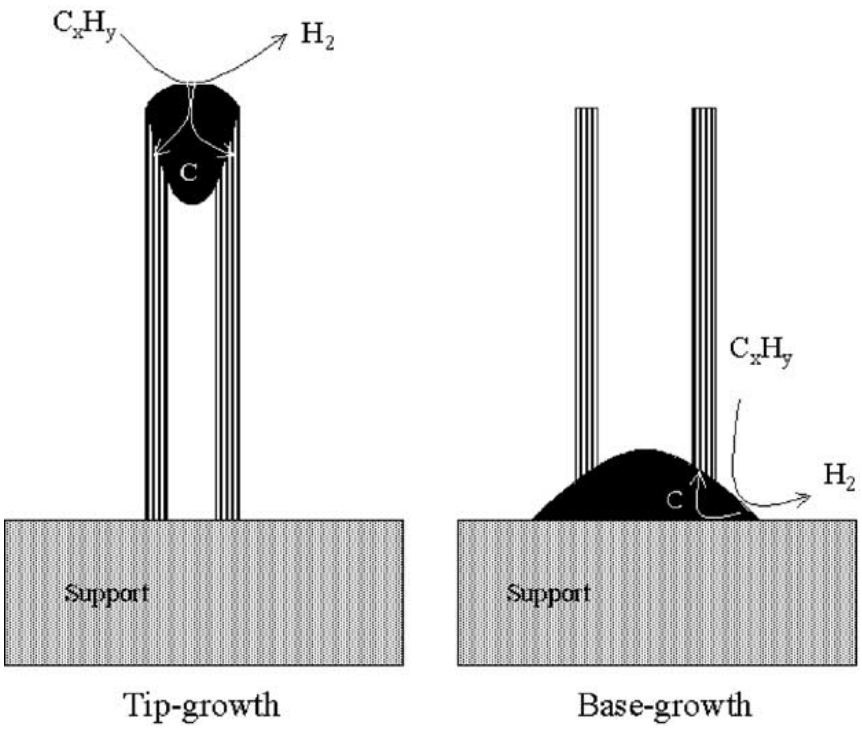

Figure 2.2: The two growth models of carbon filaments from a supported catalyst. (*Dupuis, 2005*)

2.5: PETN Loading on Surface Bound MWCNTs

As a further treatment to the CVD grown vertically aligned carbon nanotubes, some samples were charged with PETN in Chapter 6 by the following technique. PETN (10mg) was added directly to the surface, and then acetone was added in 15µL aliquots through a micropipette until the PETN crystals had dissolved and dispersed on the sample. Samples were left to air dry for 20 minutes in a fume hood.

2.6: Camera Flash Unit

A Luxtronics TUMAX DA880Z camera flash unit was used for all camera flash initiated experiments. It was modified in-house to run on mains power

instead of battery for consistent energy. The camera flash unit was remotely controlled by LabView 8.2 software to allow the flash to be triggered at the same time as data acquisition begins. Front panel of the LabView program is displayed in Appendix A.1 where 'Enable Acquisition' triggered the flash and data recording.

According to the manufacturer, the capacitance of the flash unit is 600µF and the voltage is 330V. From this, the energy of the flash of light is calculated to be 32.67J, which equates to a power of 3267W and power density of 148.5W.cm^{-2} based on the area of the flash unit being 6.5x3.4cm. The pulse of light lasts for ~10ms. The wavelength range of the emitted light from the camera flash unit was measure using an Ocean Optics USB4000 UV-Vis Spectrometer and is displayed in Figure 2.3. Photons are observed from 380-770nm from the camera flash, with the highest intensity recorded at 515nm.

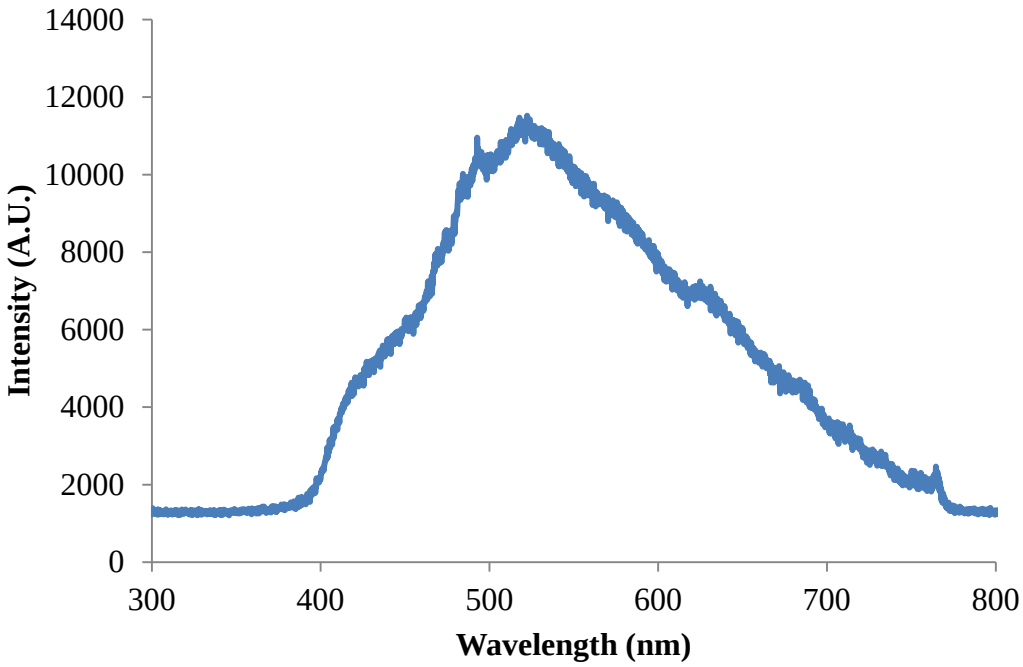

Figure 2.3: Measured wavelength range and intensity of the light from the camera flash unit.

2.7: Photodiode/UV-Vis Spectrometer

A Centronic OSD5-5T Photodiode (548-728) with an operating range of 430-900nm was coupled with a National Instruments USB6009 data acquisition box operated by LabView 8.2 to record the light intensity of the sample ignition. The LabView VI block diagram is shown in Appendix A.2. The photodiode signal was captured via a fibreoptic cable (50µm) mounted 10cm above the sample stage. The software was programmed to trigger the camera flash unit and the photodiode recording at the same time and produce a plot of light intensity against time with a resolution of 0.1ms.

An Ocean Optics USB4000 UV-Vis Spectrometer with a spectral range of 300-1100nm was used in conjunction with the photodiode. Signal was received via the same fibreoptic cable as was used for the photodiode for consistency.

2.8: Initial Experimental Setup

A photo of the initial custom-made experiment setup is shown in Figure 2.4. This is an adaptation of previous work by Malec *et al.*[14,15] The camera flash unit was mounted directly beneath a glass sample stage in order to provide the intense light source at direct close range while also protecting it from the risk of damage due to ignition or smoke residue. The fibreoptic collector was a split cable connected to both the photodiode and UV-Vis Spectrometer. It was mounted directly above the sample stage to maximize the amount of light absorbed and with a glass slide to protect it from smoke residue and ignition.

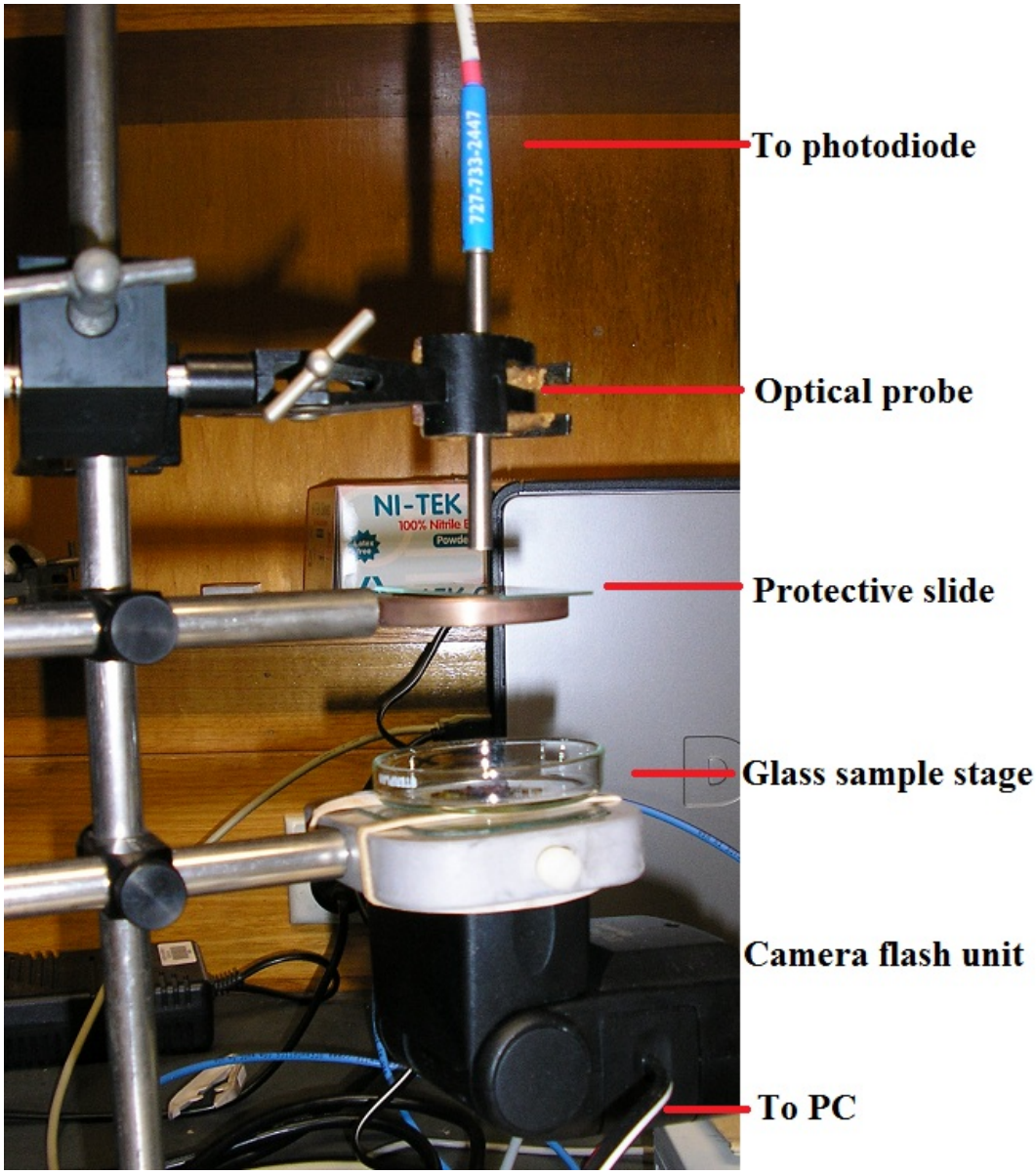

Figure 2.4: Photograph of initial camera flash initiation experimental setup.

2.9: Nd-YAG Laser and Experimental Setup

A Surelite SLIII Nd-YAG 1064nm laser was used for initiation of samples as an alternate light source to the flash unit. The laser beam was directed horizontally across a bench then vertically down onto the sample stage, as shown by the red line in Figure 2.5. The fibreoptic sensor was also placed above the sample offset from the laser beam to maximize the light collected collection of ignition results and prevent laser light from directly entering the sensors and

damaging them. Single pulse settings were used to produce a 5ns pulsewidth beam on the sample. The energy was tuneable by altering the Q-switching time of the laser from 15mJ-1000mJ. Experiments were performed at 150mJ unless otherwise noted which produced a 2mm radius laser spot on the sample. This energy level results in a power of $3.04*10^{7}$W and a power density of $2.42*10^{9}$W.cm^{-2}.

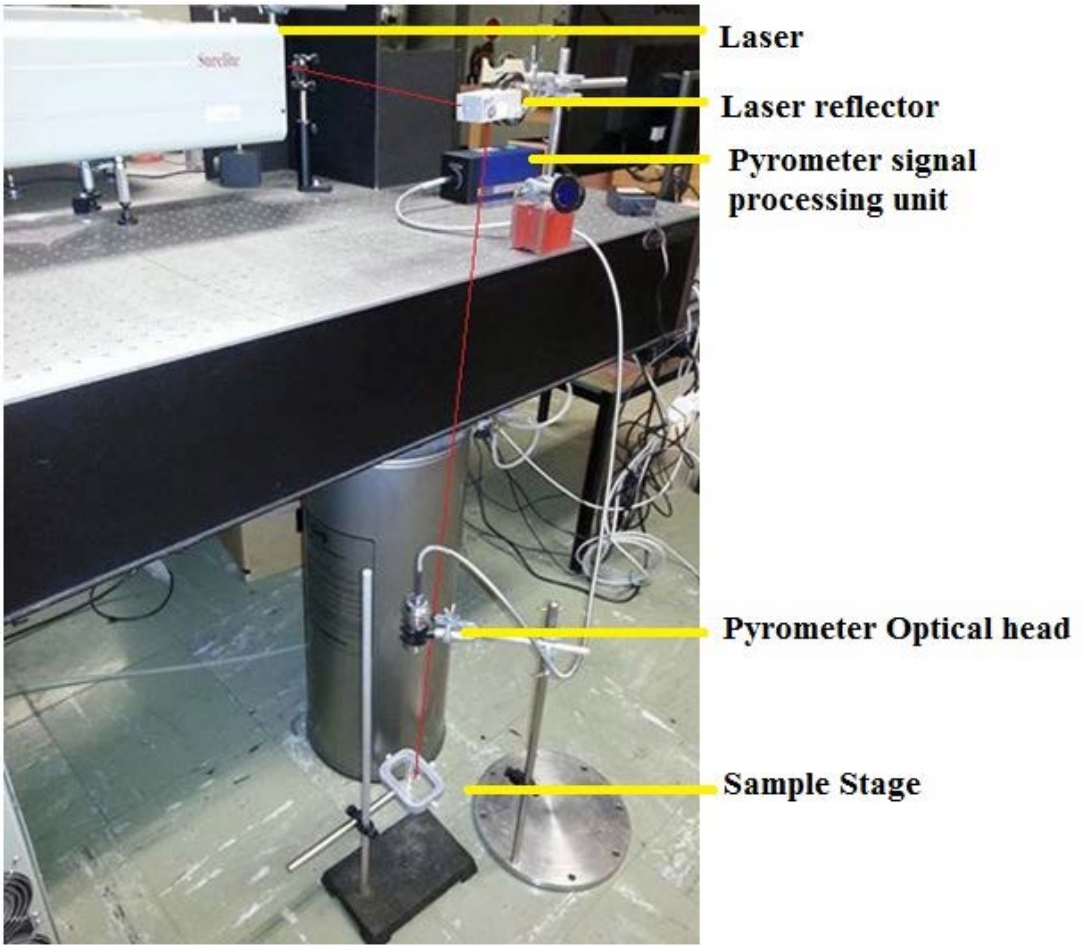

Figure 2.5: Nd-YAG laser setup showing the path of the laser to the sample stage (red line).

An Ophir Optronics Nova II laser power and energy meter was used to calibrate the energy of the laser. New flash lamps were installed and used for the entirety of the project to maintain continuity of laser energy. The Q-switch time was recorded against the measured energy of the laser. Each data point was collected by pulsed lasing at 10Hz on the energy meter for 5 minutes to reduce the

error margins to less than 2%, or ±3mJ. The calibration graph is shown in Figure 2.6. Above a Q-switch time of 465µs (<20mJ) lasing is inconsistent and unreliable due to the high Q-switch time.

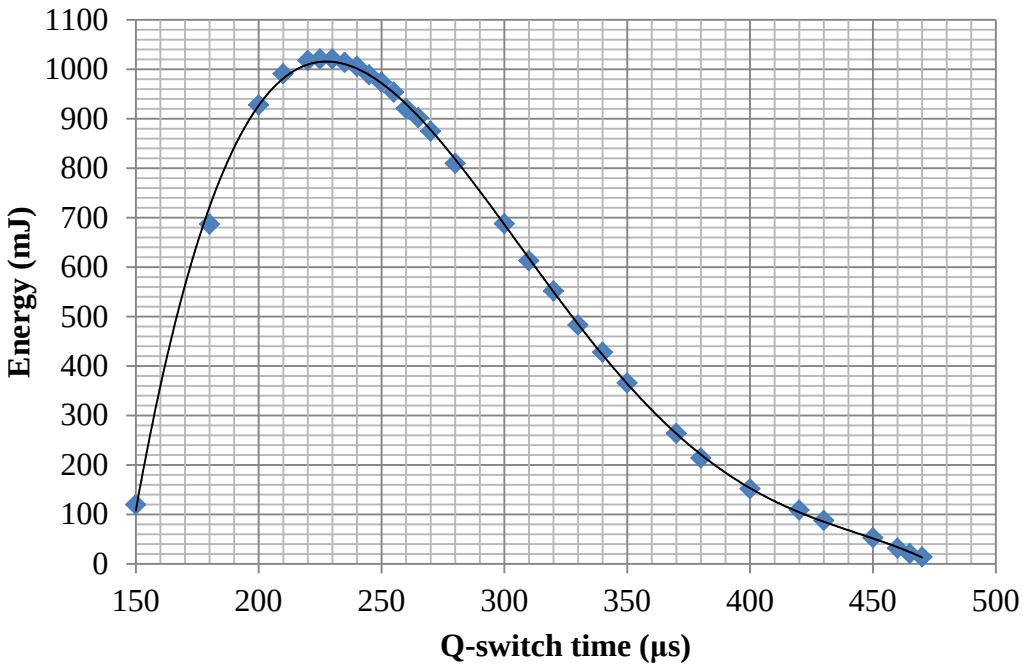

Figure 2.6: Laser calibration of the measured output energy as a function of the Q-switch time in the laser.

2.10: Pyrometer

A Lumasense IMGA 740-LO high speed pyrometer was used to measure the temperature of the sample and its resultant ignition over time. Included was an LVO35 optical sensor head on a fibreoptic cable to focus the collection spot directly onto the sample stage at the point where the laser beam hit. The optical sensor head (seen in Figure 2.5) was held 30cm above the sample stage as close to the beam of the laser as possible to provide the best collection angle. The pyrometer had a range of 400-3000˚C and a temporal resolution of 10µs. Manufacturer software recorded spectra directly onto a PC and the instrument was triggered by the temperature rising above 400˚C so data recording began at the

exact data point where the sample was initiated via laser/camera flash unit in order to capture consistent time-resolved results.

2.11: High Speed Camera

A Photron Fastcam SA3 high speed camera with a Nikon brand zoom lens was used to video the ignition of some samples. Supplementary lighting was provided by a 150 watt halogen flood light. Results were recorded at 6000fps or a shutterspeed of one frame every 0.16ms and with a resolution of 512x512 pixels. Computer software dissected the videos into individual images of each frame. These results were recorded to visually observe the process of ignition to better understand the reaction.

The high speed camera was on loan from Defence, Science and Technology Organisation (DSTO) Edinburgh, South Australia. As it was not available for the duration of the project, a Casio EX-F1 high speed camera owned by Orica Australia was also used. The EX-F1 was capable of 1200fps (one frame every 0.83ms) with a resolution of 336x96 pixels. Supplementary lighting was provided by a 150 watt halogen flood light.

2.12: Confocal Raman Spectroscopy

Raman scattering is a phenomena that was first described by Sir Chandrasekhara Ventaka Raman in 1928. It is a spectroscopy technique that measures the low frequency modes in a sample such as vibration and rotation. Incident monochromatic light from a laser can interact with the molecules exciting them to highly unstable virtual energy levels, the relaxation then occurs in one of three ways illustrated in Figure 2.7. Elastic reflection is where the molecule returns to the same energy level it started in due to no vibrational

interaction with the photon, it is most common and referred to as Rayleigh scattering. The molecule may also relax to a higher energy state than it started causing inelastic scattering called Stokes Raman scattering. Finally and most rarely at room temperature, relaxation may return it to a lower energy level than it started which is called anti-Stokes Raman scattering.[16]

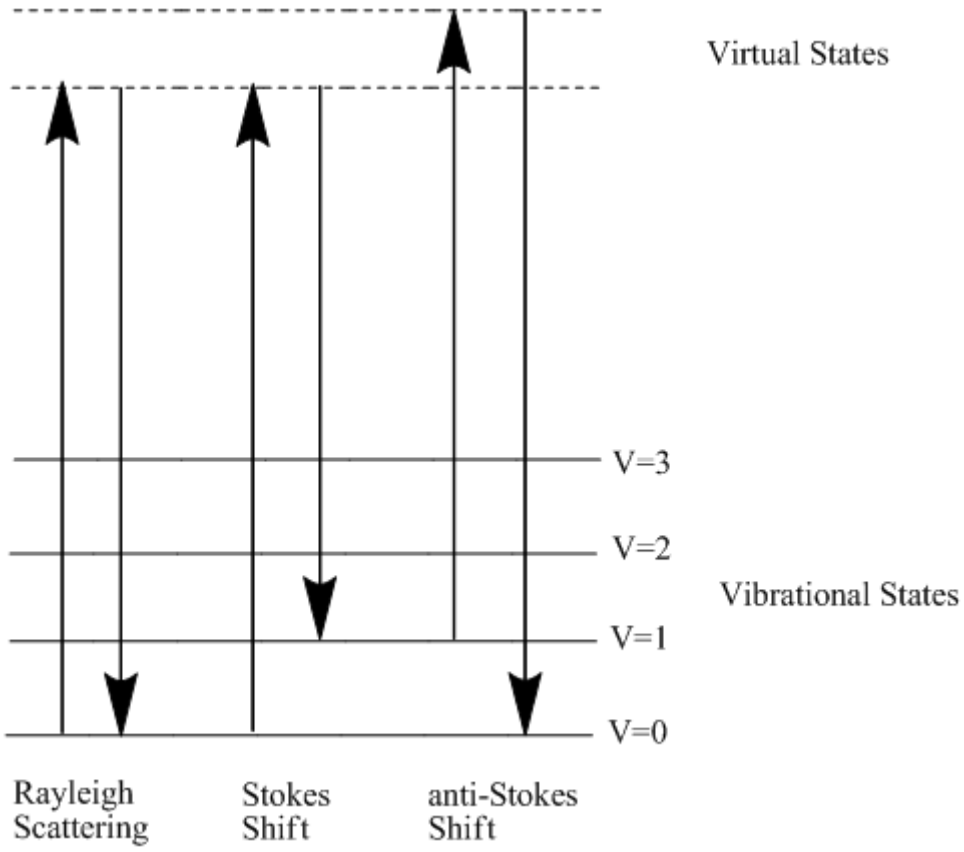

Figure 2.7: Energy level diagram showing the Raman Effect. Rayleigh scattering is inelastic while Stokes and anti-Stokes are elastic and the energy change can be measured by emitted photons.

The resultant change in energy level is measured in Raman spectroscopy to provide information about the vibrational modes in the system. Raman spectroscopy is a good technique to identify specific chemical bonds. In carbon nanotubes an indication of carbonaceous purity can be found by differentiating the amorphous and graphitic carbon bonds.[17] There are three peaks of significance in carbon nanotubes – the radial breathing mode (RBM), the disorder band (D-band) and the graphitic band (G-band).[18] These are illustrated in Figure 2.8.

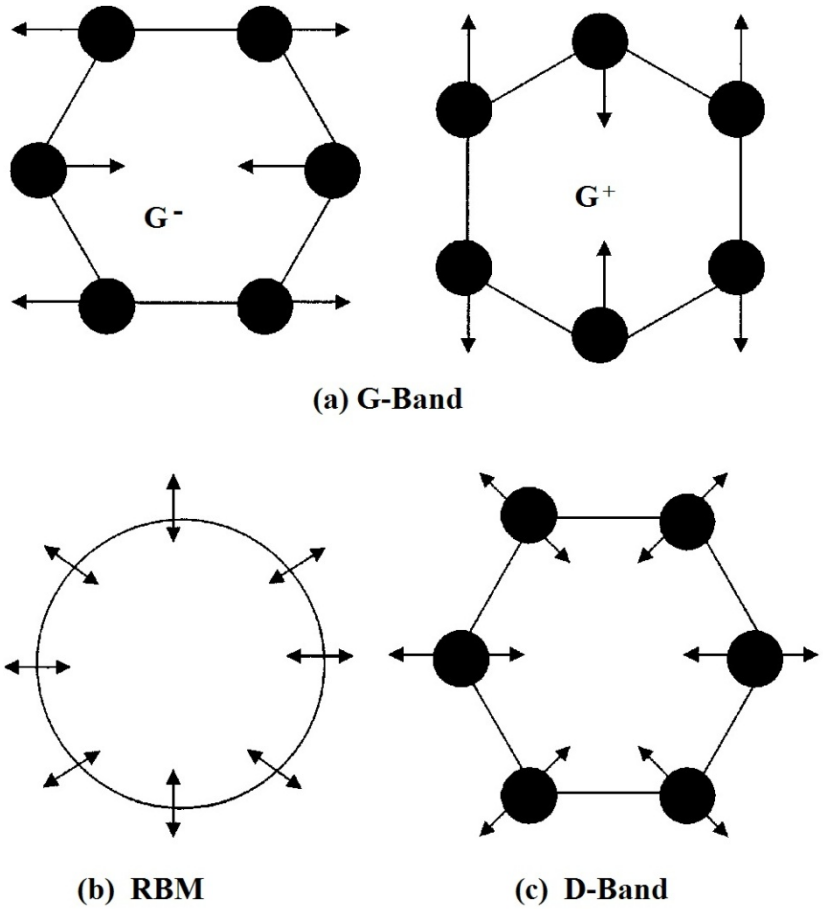

Figure 2.8: Vibrational modes of carbon in carbon nanotubes. (a) Vibrations of G-band showing G^+ vibrations along the tube axis and G^- vibrations around the tube circumference, (b) cross-section of a nanotube showing the RBM of the tube and (c) vibrations of the D-band. (*modified from Raravikar, 2002*)

The G-band is the tangential stretching of carbon-carbon bonds, and is possible in two directions (Figure 2.8 (a), one hexagonal ring of carbon atoms on the surface of a nanotube). G^- occurs as a result of vibrations around the circumference of nanotubes with the Raman peak at ~1570cm^{-1}, G^+ occurs as a result of vibrations along the length of a nanotube with the Raman peak at ~1590cm^{-1}. In MWCNTs the G-band peaks combine into one peak.[18] The size of the G-band peak is approximately dependent on the concentration of nanotubes.[19]

The D-band corresponds to in-plane vibrations of carbon atoms towards and away from the centre of the covalently bonded hexagons on the surface of carbon nanotubes (Figure 2.8 (c), one hexagonal ring of carbon atoms on the surface of a nanotube).[20] The Raman peak occurs at 1300-1350cm^{-1}. In pristine samples of nanotubes, the curvature of the structure restricts these vibrations and minimizes the peak. Therefore the size of the D-band is related to the degree of impurities and surface defects in a sample.[18]

The RBM is the symmetric radial 'breathing' of a nanotube as the carbon atoms move towards and away from the centre of the carbon nanotube axis (Figure 2.8 (b), cross-sectional view of a nanotube). The Raman peak occurs at 100-300cm^{-1} and is unique to SWCNTs thus it can be used to determine whether a sample is single-walled or multi-walled.[20]

A WITec Alpha300RS Confocal Raman Microscope was used. A schematic of the system is shown in Figure 2.9. A 40x zoom objective (numerical Aperture 0.60) was used producing a laser spot size of approx. 500nm coupled with a UHTS 300 CCD spectrometer. A 532nm laser was used for all experiments. A 600 g.mm^{-1} grating was used resulting in a spectral resolution of 4cm^{-1}. The reflected light from the sample is beamed through the same objective and through a pinhole detector to ensure only light from the image focal plane is recorded; penetration depth for the laser is significantly less than the thickness of samples prepared. A 532nm edge filter is employed to reduce Rayleigh scattered light.

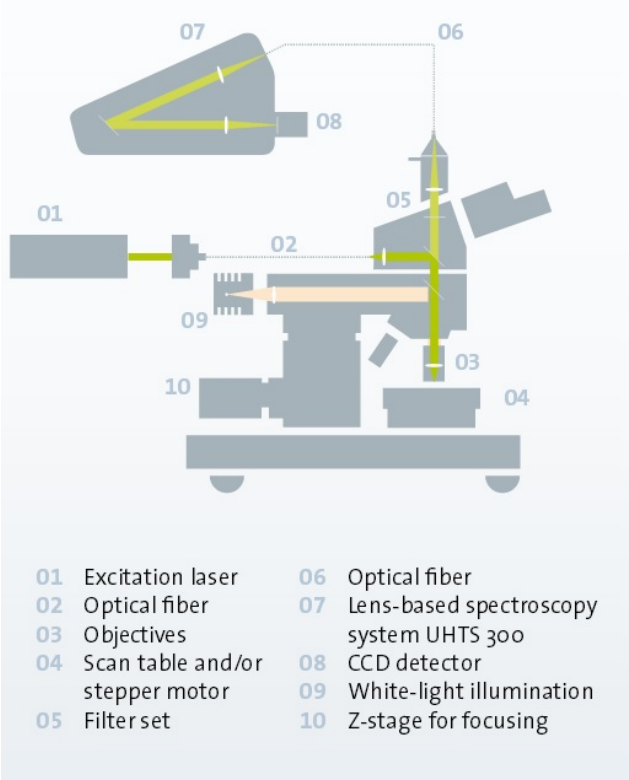

Figure 2.9: Schematic of the Confocal Raman microscope used. (*WITec product catalogue*)

In addition to recording single-point spectra of samples, the Raman microscope is capable of scanning an area up to 70x70µm by performing scans at multiple points along a line and multiple lines on an area. This technique allows mapping of the chemical composition of an area and production of an image of the relative concentration of a chosen vibration in the area. In the example of a bundle of horizontal nanotubes on glass in Figure 2.10, a 35x35µm area was scanned with 25 lines recording the spectra at 30 points along each line. The intensity image of the G-band (1580cm^{-1}) across the sample was produced; the brighter areas correspond to higher concentration. The spectra where the nanotubes are present also shows a strong RBM at 170cm^{-1} indicating that the sample is single-walled and a small D-band at 1350cm^{-1} indicating that the sample is very pure. Also observed is the elastic Rayleigh scattering at 0cm^{-1} and a G'-band at 2670cm^{-1} from second-order scattering.[18]

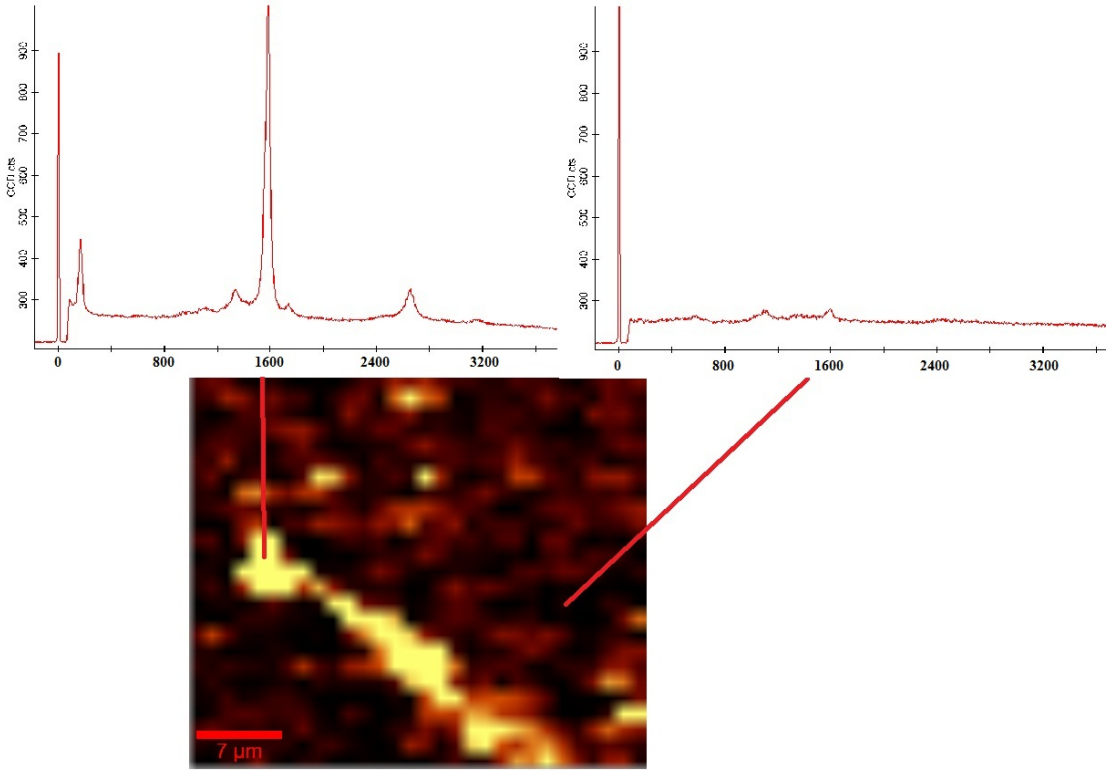

Figure 2.10: Raman intensity image of the G-band (1580cm^{-1}) peak of carbon nanotubes horizontally on a surface with reference to the point spectra highlighted. X-axis is relative wavenumber (cm^{-1}), y-axis is CCD counts.

2.13: Thermogravimetric Analysis (TGA)

TGA is a mass-loss measuring technique used to determine the stability and decomposition of a chemical sample over a large temperature range (25-1000˚C). A small amount of the sample is placed on a suspended pan in an inert atmosphere and the mass is precisely recorded as the sample is heated at a constant rate. The mass loss recorded can show when a sample begins to break down. In carbon nanotubes, this is a good test for purity since the carbon ash burns off at a lower temperature than the nanotubes. The residual metal catalyst remains in the sample at 1000˚C so the weight percentage of metal can be determined. TGA of SWCNTs by Chiang *et al.* is displayed in Figure 2.11.[21] For as-prepared (unpurified) nanotubes (a) the weight % remaining is ~30%, which is the amount of catalyst by weight in the sample. A small peak due to carbon oxidation is observed immediately before the carbon loss at ~350-400˚C. By

contrast, in the purified sample (b), the weight remaining at the end is near zero suggesting there is no residual metal and the range over the carbon mass loss is smaller since there is less carbon impurities. Temperature stability of purified nanotubes was reported to be higher than as-prepared nanotubes.[21]

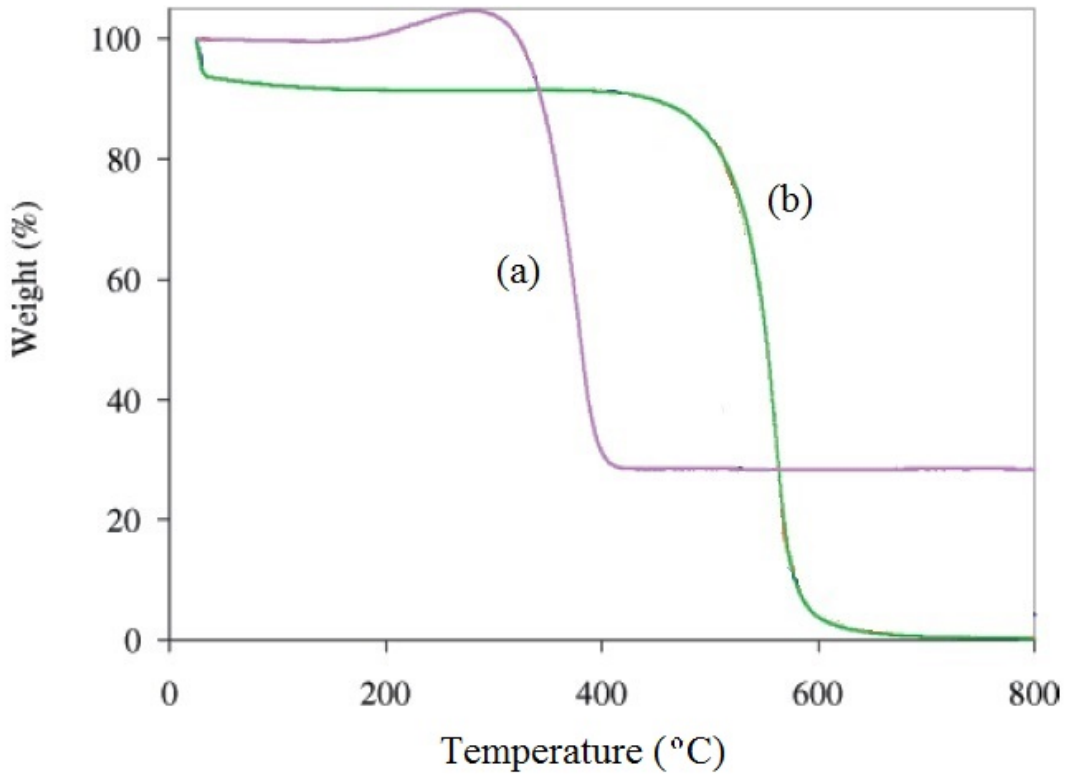

Figure 2.11: TGA profile of as-prepared unpurified SWCNTs (a) and purified SWCNTs (b). (*Modified from Chiang, 2001*)

A Mettler Toledo TGA/DSC 1 was used at Orica Australia, Kurri Kurri. TGA curves were acquired from 25˚C-1000˚C at a rate of 10˚C/min. Approximately 1mg of sample was used, and all results were normalised to a percentage mass loss. The same method was used for all TGA data presented in this thesis.

2.14: References

1 Foltz, MF, Aging of Pentaerythritol Tetranitrate (PETN), Report No. LLNL-TR-415057, (2009).

2 Young, Sharissa, Method Development and Validation for Measuring the Particle Size Distribution of Pentaerythritol Tetranitrate (PETN) Powders, New Mexico Institute of Mining and Technology, 2005.

3 Chen, Jian *et al.*, Dissolution of Full-Length Single-Walled Carbon Nanotubes. *The Journal of Physical Chemistry B* **105** (13), 2525-2528 (2001).

4 Liu, Jie *et al.*, Fullerene Pipes. *Science* **280** (5367), 1253-1256 (1998).

5 Marshall, Matthew W., Popa-Nita, Simina, and Shapter, Joseph G., Measurement of Functionalised Carbon Nanotube Carboxylic Acid Groups Using a Simple Chemical Process. *Carbon* **44** (7), 1137-1141 (2006).

6 Hata, Kenji *et al.*, Water-Assisted Highly Efficient Synthesis of Impurity-Free Single-Walled Carbon Nanotubes. *Science* **306** (5700), 1362-1364 (2004).

7 Yamada, Takeo *et al.*, Revealing the Secret of Water-Assisted Carbon Nanotube Synthesis by Microscopic Observation of the Interaction of Water on the Catalysts. *Nano Letters* **8** (12), 4288-4292 (2008).

8 Wagner, RS and Ellis, WC, The VLS Mechanism of Whisker Growth. *Trans Met Soc AIME* **233**, 1054-1064 (1965).

9 Tibbetts, Gary G., Why Are Carbon Filaments Tubular? *Journal of Crystal Growth* **66** (3), 632-638 (1984).

10 Dupuis, Anne-Claire, The Catalyst in the CCVD of Carbon Nanotubes—a Review. *Progress in Materials Science* **50** (8), 929-961 (2005).

11 Charlier, Jean-Christophe and Iijima, Sumio, in *Carbon Nanotubes* (2001), pp. 55-81.

12 Nikolaev, Pavel *et al.*, Gas-Phase Catalytic Growth of Single-Walled Carbon Nanotubes from Carbon Monoxide. *Chemical Physics Letters* **313** (1), 91-97 (1999).

13 Dai, Hongjie *et al.*, Single-Wall Nanotubes Produced by Metal-Catalyzed Disproportionation of Carbon Monoxide. *Chemical Physics Letters* **260** (3), 471-475 (1996).

14 Malec, Christopher, The Use of Carbon Nanotubes as an Energetic Material Initiator, Honours Thesis, Flinders University, 2008.

15 Malec, Christopher D., Voelcker, Nicolas H., Shapter, Joseph G., and Ellis, Amanda V., Carbon Nanotubes Initiate the Explosion of Porous Silicon. *Materials Letters* **64** (22), 2517-2519 (2010).

16 Colthup, Norman B, Daly, Lawrence H, and Wiberley, Stephen E, *Introduction to Infrared and Raman Spectroscopy*. (Elsevier, 1990).

17 Dresselhaus, MS *et al.*, Raman Spectroscopy on Isolated Single Wall Carbon Nanotubes. *Carbon* **40** (12), 2043-2061 (2002).

18 Dresselhaus, M. S., Dresselhaus, G., Saito, R., and Jorio, A., Raman Spectroscopy of Carbon Nanotubes. *Physics Reports* **409** (2), 47-99 (2005).

19 Picher, Matthieu, Anglaret, Eric, Arenal, Raul, and Jourdain, Vincent, Self-Deactivation of Single-Walled Carbon Nanotube Growth Studied by in Situ Raman Measurements. *Nano Letters* **9** (2), 542-547 (2009).

20 Raravikar, Nachiket R. *et al.*, Temperature Dependence of Radial Breathing Mode Raman Frequency of Single-Walled Carbon Nanotubes. *Physical Review B* **66** (23), 235424 (2002).

21 Chiang, I. W. *et al.*, Purification and Characterization of Single-Wall Carbon Nanotubes (SWNTs) Obtained from the Gas-Phase Decomposition of CO (HiPCO Process). *The Journal of Physical Chemistry B* **105** (35), 8297-8301 (2001).

Chapter 3: Photodiode, Camera Flash and Laser Initiation

In this Chapter, the light initiation of carbon nanotubes with a camera flash unit is discussed including the effect of ferrocene addition. Several limitations and difficulties are presented in light of the analysis of results. Methods of measuring light initiated reactions are explored and a laser is proposed as an alternate light initiation source. The differences between the energy of the two light initiation sources are investigated and the subsequent differences in the light initiated reactions of the nanotubes are examined.

3.1: Camera Flash Unit Results

Experiments to ignite carbon nanotubes were setup with the photodiode detector and the camera flash unit as described in Chapter 2.8, a photo of the setup is seen in Figure 3.1. Carbon Solutions as-prepared single walled carbon nanotubes (APSWCNT) were used as the sample to be initiated. Upon ignition from the camera flash unit, a small amount of glowing was observed which does not propagate across the sample. The glow is not intense enough for any recording on the photodiode and no results could be recorded.

Ferrocene was added to the sample to oxidize and act as a fuel to promote ignition. With ferrocene added, an audible pop is heard upon initiation from the camera flash unit and a surface propagated flame burns across the sample for ~2-5 seconds. The ignition temperature of ferrocene is 475-480˚C,[1] so burning of the sample suggests that the nanotubes exceed that temperature from the camera flash unit initiation and successfully transfer heat to the ferrocene. Various ratios of APSWCNT/ferrocene (wt/wt) were tested from 1:1 to 1:8, less ferrocene tended to cause the sample to burn for a shorter time overall. Ratios above 1:8 did not ignite. As a control, ferrocene was exposed to the camera flash in the absence of

nanotubes, and no reaction was observed. This proves that the ignition is a property of the nanotubes and not the ferrocene, and that the nanotubes cause the subsequent combustion of ferrocene.

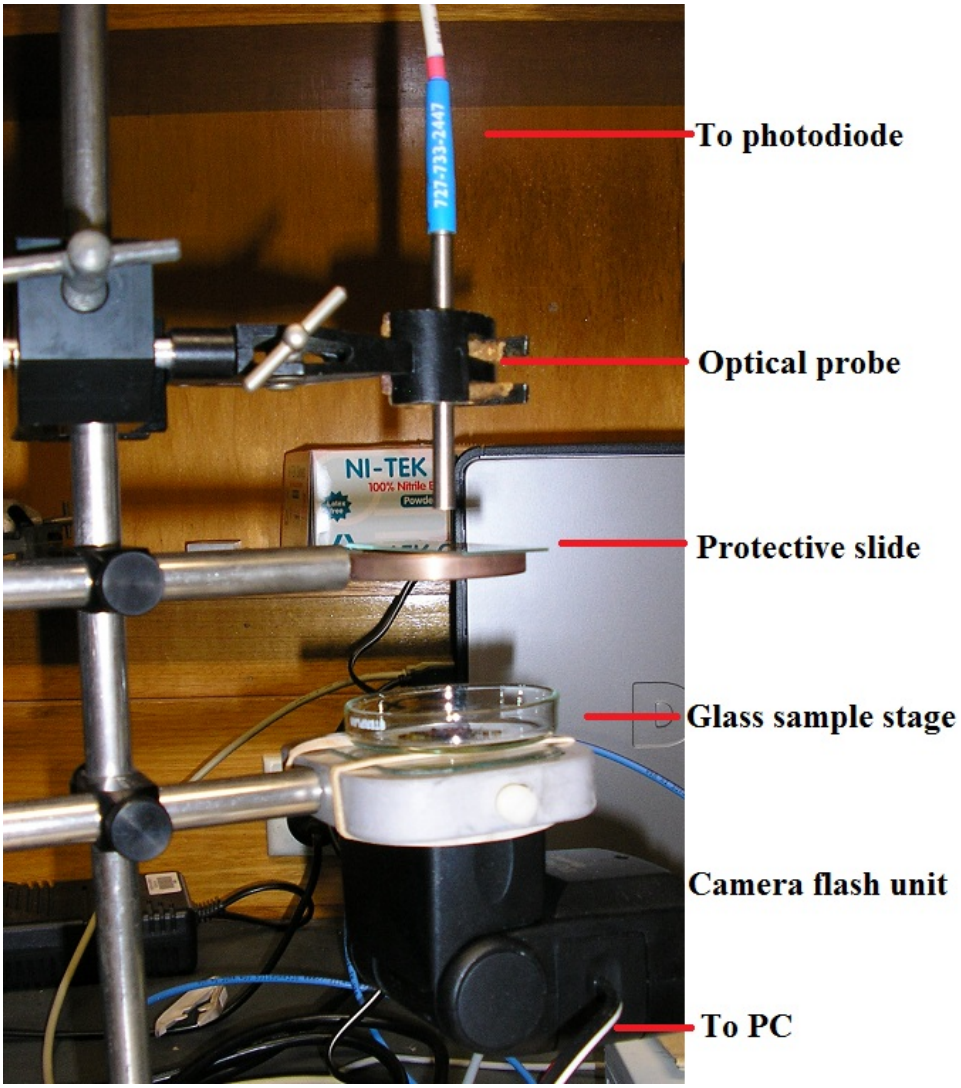

Figure 3.1: Photograph of the initial experimental setup to record the flash initiated ignition of nanotubes.

A mixed sample of APSWCNT/ferrocene (1:4, 5mg total) was prepared and initiated by the camera flash unit with the intensity recorded on the photodiode system, Figure 3.2. For the first 8ms, the photodiode is saturated by the light from the camera flash unit since the intensity is above the upper sensitivity limit of the photodiode. After this time, the intensity rises over the first

20ms as the sample glows brightly then deflagrates and begins a surface propagated burn. This continues for several seconds, however, only the first 100ms was recorded and displayed since this is the important timeframe for the initiation of an explosive device. The slow nature of the reaction strongly suggests that an explosion is not occurring. Instead the sample is transforming enough heat from the light absorption of the flash unit to set it on fire, then a combination of the ferrocene and carbon nanotubes provides fuel for it to continue to exothermically oxidize and burn the entire sample.

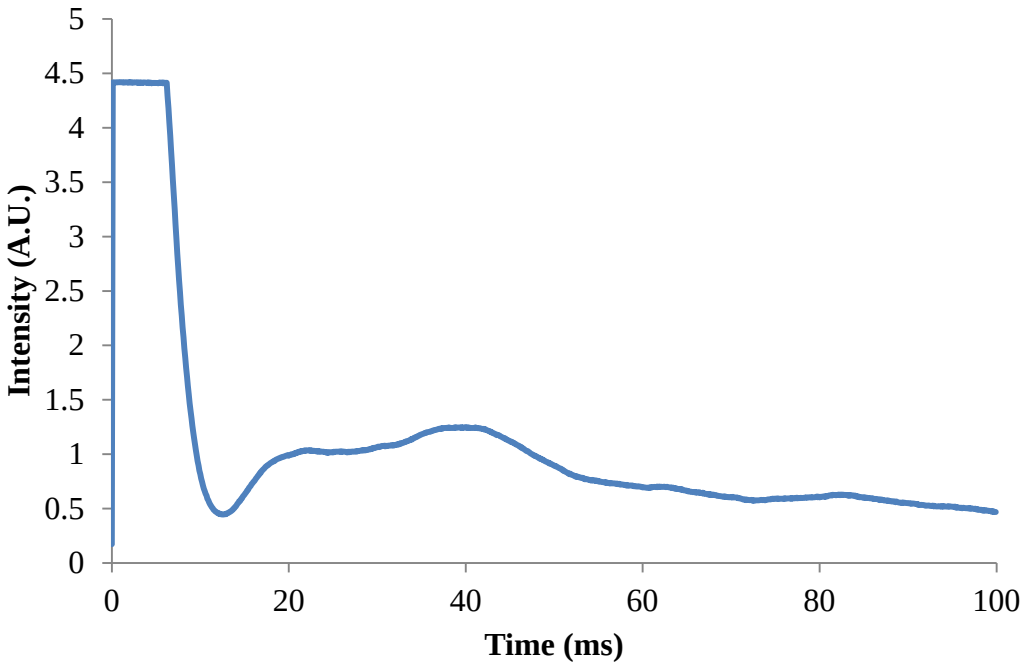

Figure 3.2: Camera flash unit initiation results of APSWCNT and ferrocene (1:4, 5mg total) recorded with a photodiode.

Figure 3.3 displays a photo of the residue from the ignition. Large areas of the sample have turned from black to orange, indicative of the oxidation of the iron from the ferrocene to Fe_2O_3 and traces of Fe_3O_4.[2] Bright yellow areas are also residual from the burnt ferrocene and stuck to the glass sample stage, and some areas of ash remain. APSWCNTs do not contain iron (they were produced with

nickel and yttrium) so when ignited without ferrocene present, no bright areas were observed after ignition.

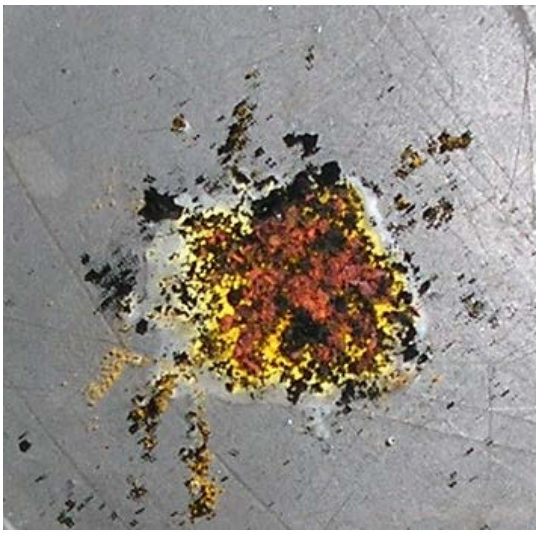

Figure 3.3: Photograph of a post-camera flash ignition sample of APSWCNT/ferrocene (1:4, 10mg total) displaying evidence of oxidation of metal particles.

A series of 6 identically prepared samples of APSWCNT/ferrocene (1:4, 5mg total) were ignited by the camera flash and recorded in order to examine the reproducibility of the experiment. Preparation of samples included shaking them in a flask shaker for 10 minutes to ensure homogenous mixing. These results are displayed in Figure 3.4. Three of the ignitions are very similar in character, but overall reproducibility of results was not good. All samples appeared to burn at different rates producing varying results from the photodiode. Initial ignition characteristics within the first 10ms are more likely to be consistent while the following surface-propagated burn (>10ms) is more likely to be unpredictable, however, saturation of the sensor from the camera flash prevented this section of the data being visible. Due to the peaks occurring at different times, it is not practical or representative to calculate a mean of the results.

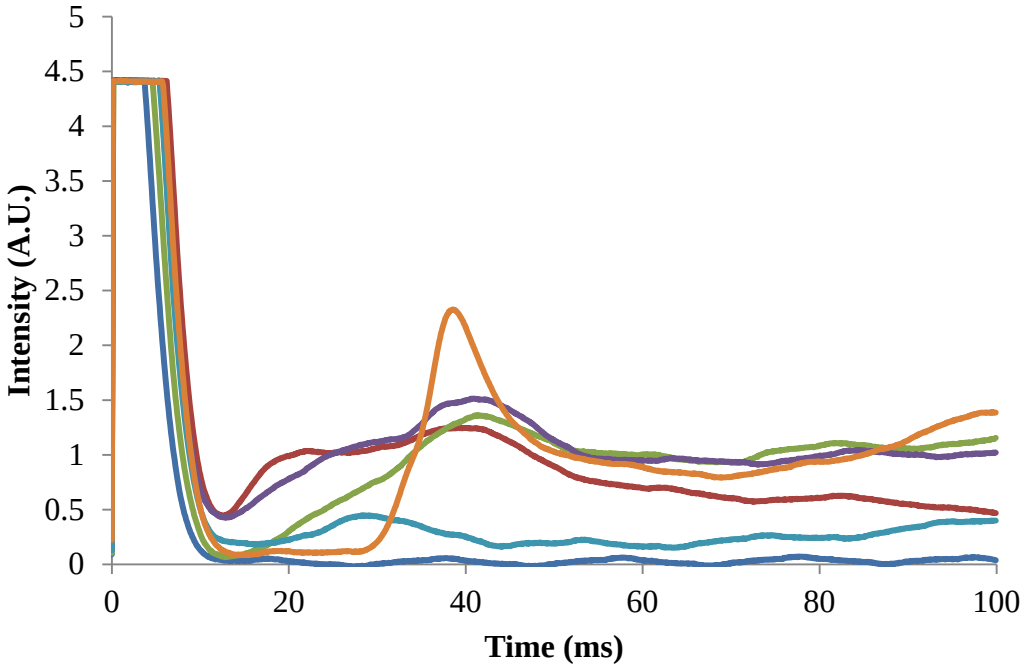

Figure 3.4: Camera flash initiation results of multiple identically prepared samples of APSWCNT/ferrocene (1:4, 5mg total) to examine reproducibility.

The mass of the sample was varied in order to see if the intensity or speed of the reaction changed significantly. Reducing the total mass of the sample below 5mg did not produce an ignition bright enough for the photodiode to detect. Ignition results of APSWCNT/ferrocene (1:4) were compared with two 5mg total samples and three 12mg total samples in Figure 3.5. This result highlights the lack of reproducibility since there is little correlation between sample size and the ignition intensity. There is also very little similarity between samples of the same mass.

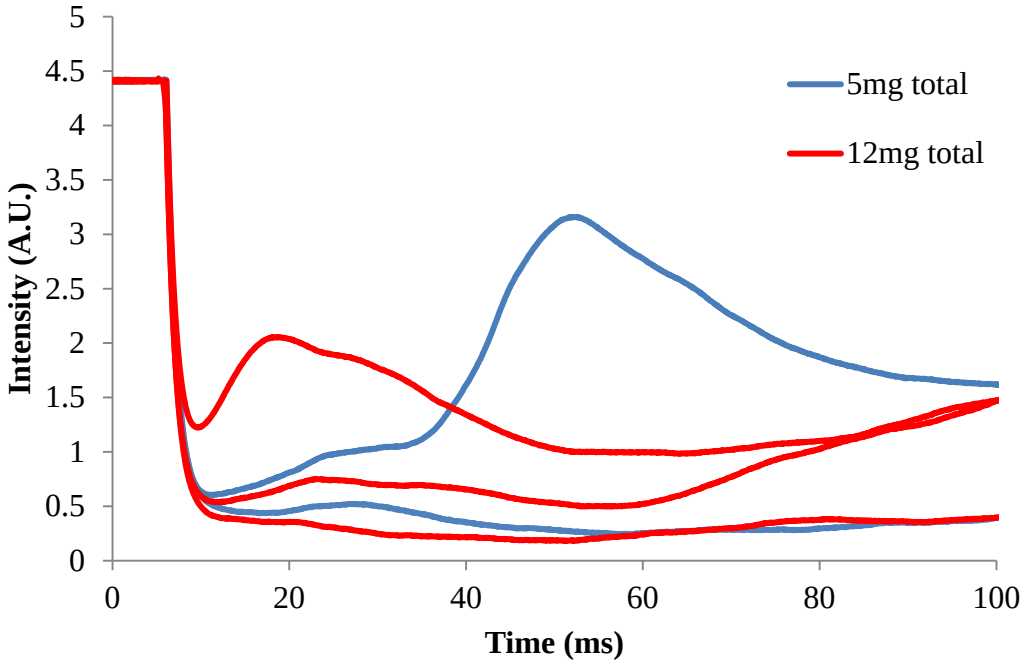

Figure 3.5: Comparison of camera flash initiation of APSWCNT/ferrocene (1:4) with two different total sample masses; 5mg and 12mg.

A UV-Vis spectrometer was also connected to the fibre sensor with the idea of collecting the black-body radiation peak and calculating the approximate temperature of the sample. Malec *et al.*[3,4] proposed that the broad peak visible in the UV-Vis spectrum was due to black body radiation and the temperature can be calculated from Wien's Displacement Law.[5] The instrument collected and averaged data over the first 100ms of the ignition. The spectra displayed in Figure 3.6 shows a carbon peak at 758nm over the top of a broader peak which is due to thermal radiation from the flames. Two sharp peaks at 547nm and 612nm are due to the fluorescent lights in the room. Altering the ratio of nanotubes and ferrocene did not change the peak intensity or peak location. In this spectral range, the calculated temperature using the broad peak at 670-870nm is ~3000˚C, which is double the predicted temperature for the flash initiation of nanotubes.[6] It was proposed that the broad peak is more likely due to a combination of many different carbon emissions from covalent bond reconstructions and deformations in the nanotubes as a result of the camera flash rather than black body radiation. As such, the UV-Vis spectrometer was not used further in this project.

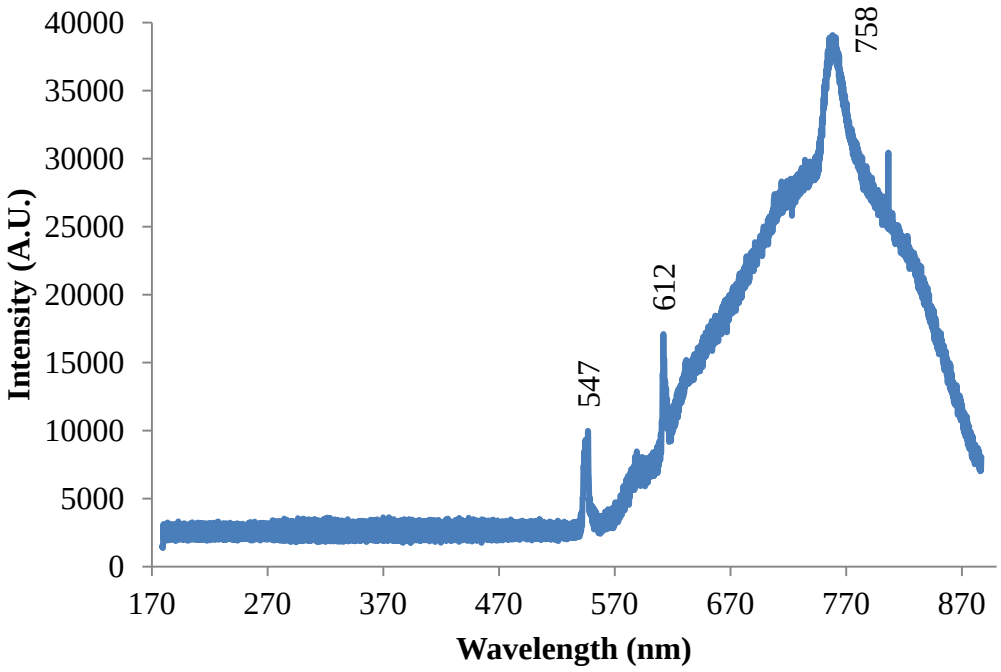

Figure 3.6: UV-Vis spectrum of the ignition of APSWCNT/ferrocene (1:4, 5mg total) in the first 100ms.

To support the photodiode results, a high speed camera was used to capture frames at a rate of 6000fps. This produced a frame-by-frame examination of the material during its ignition. Figure 3.7 shows 6 images captured of the ignition of a sample of APSWCNT/ferrocene (1:4, 5mg total) via the flash unit, times shown are the time since flash initiation. The sample cannot be seen clearly during the first 10ms of recording as the flash floods the image. The frame at 7.014ms (a) is the first frame where the sample is visible and the image isn't blanketed by the flash. Then (b) extracted at 10.02ms is the first frame where the background camera flash light is no longer visible at all. From 10-20ms (b-c), glowing and sparks can be seen spreading across the surface. After 20ms (d), visible flame is burning on the surface, which also spreads across the sample until 70ms (e) where the sample is completely burning. The flames continue for 4 seconds until the sample is completely oxidized. This is a relatively slow process for ignition and these images support the photodiode results which prove that the reaction is a deflagration and surface propagated burning rather than an explosion

or detonation.

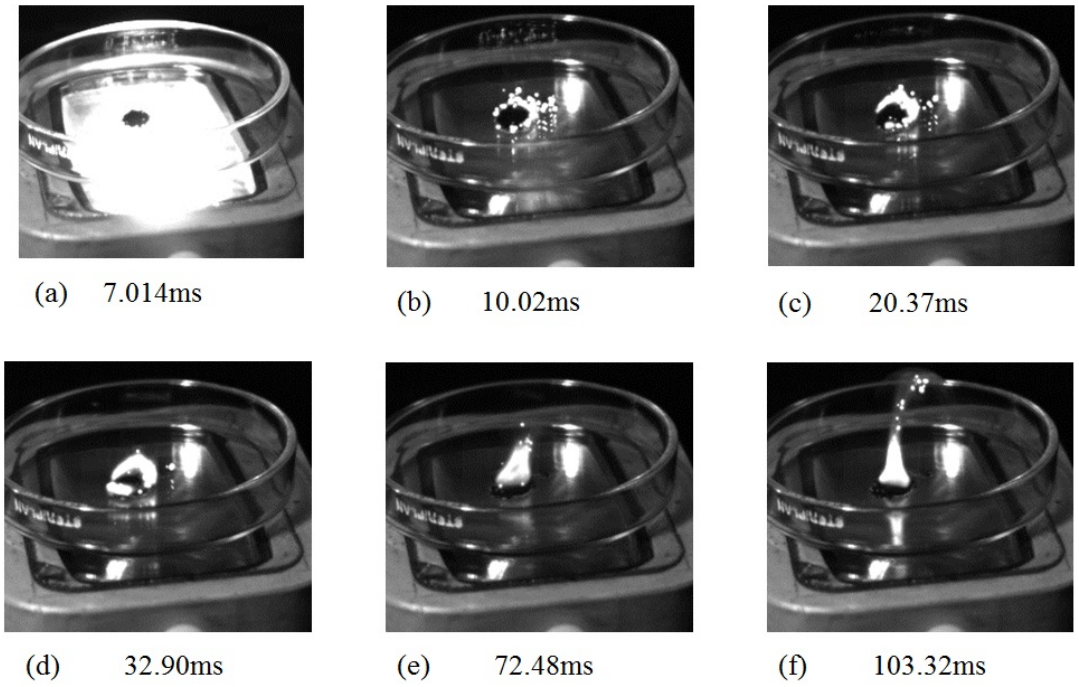

Figure 3.7: High speed camera showing the ignition of Carbon Solutions APSWCNT/ferrocene (1:4, 5mg) with the camera flash unit. Time shown refers to the amount of time passed since the flash unit was triggered.

3.2: Flash Ignition of Metal Nanoparticles

It has been shown in the literature review (Chapter 1.7) that other nanoparticles may ignite in the presence of an intense pulse of light due to their pyrophoric nature.[7] In addition, investigating metal nanoparticle ignition will aid in discovering the importance of metal catalyst particles in nanotubes during ignition. Metal nanoparticles have been exposed to the camera flash both in the presence and absence of carbon nanotubes to investigate their reaction.

Iron nanoparticles (100nm diameter) were found not to react to the camera flash unit, however, 26nm diameter iron nanoparticles glowed, displayed some sparks and oxidized. Smaller particles are more reactive due to the higher surface

area. An audible pop was also heard after the camera flash was initiated. Oxidation was determined by a colour change after exposure from black to rust brown/orange, shown in Figure 3.8. The reaction did not cause any flames, most likely due to a lack of fuel. The light intensity of the sparks on the iron nanoparticles was too low to be detected by the photodiode.

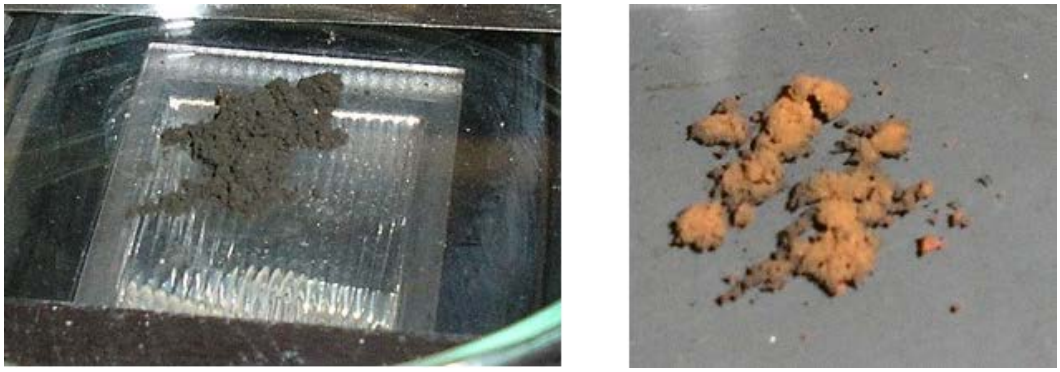

Figure 3.8: Iron nanoparticle (26nm diameter) shown before exposure to camera flash (left) and after initiation from the camera flash unit (right) having undergone oxidation.

When the iron nanoparticles were mixed with APSWCNT (1:1), no reaction was observed and nothing was visible on the photodiode. This was a curious result since both materials react under the camera flash independently. This is most likely because heat does not transfer as easily between the loosely packed metal nanoparticles and the nanotubes - the interaction with catalyst particles is easier because they are present either inside the nanotubes or encapsulated on the outside of the walls. As a result, additional metal nanoparticles added act as spacers and reduce the ratio of fuel in the sample. Nanotubes may also draw heat and oxygen away from the metal nanoparticles.

In addition, nickel nanoparticles were investigated since nickel and yttrium are the catalysts used for the production of Carbon Solutions nanotubes. Nickel nanoparticles (20nm) were exposed to the camera flash, the reaction was similar to the iron nanoparticles; a glow was observed which slowly propagated across the sample as oxidation occurred. Nickel nanoparticles appeared to be less

reactive than iron nanoparticles and only a slight colour change from black to grey was observed.

3.3: Limitations and Solutions

The first 10ms recorded on the photodiode of each flash ignition was masked by the light intensity from the camera flash unit saturating the photodiode sensor. Several techniques were employed to try to reduce the effect. The flash unit was masked by a plate so only ~5cm^2 in the middle under the sample was exposed to reduce the amount of excess flash light. However, this did not stop the saturation of the photodiode sensor. The fibreoptic cable was placed at different angles so it was not pointed directly into the flash, and various wavelength filters were utilized to reduce the broad spectrum of the flash but none of these approaches were successful in significantly reducing the interference from the camera flash on results.

The possibility of moving the camera flash to above the sample stage in line with the photodiode rather than below it was investigated to allow the fibreoptic sensor to only receive reflections of the flash not the direct light. An oscilloscope was used to measure the diminishing light intensity as a function of distance from the surface of the camera flash. This loss shown in Figure 3.9 appears to be a linear loss of light over the short range examined. Ignition of samples was not possible when the sample was further than 3cm away from the flash unit. This makes it impractical to mount the flash unit above the samples since it would have to be within 3cm and ignition may damage it.

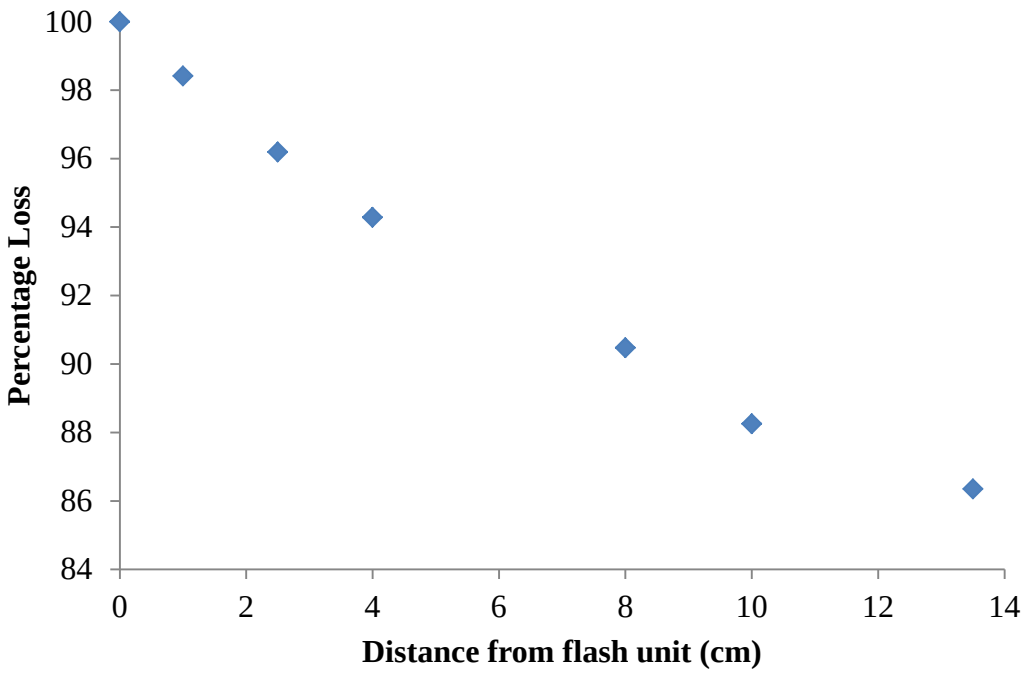

Figure 3.9: Light intensity loss from the camera flash as a function of distance from the flash unit.

To overcome the problems of flash light interference and inconsistent results, it was decided to change the light initiation source from the flash unit to a laser. This is a monochromatic coherent light source that will provide a more consistent initiation each time in a small focused part of the sample. The small spot size of 2mm means no direct light will enter the fibreoptic as was the case with the camera flash which spread light over a large area, and the laser energy is relatively lossless over short distances allowing the laser beam to hit the sample from above the sample stage while still having the fibreoptic sensor above the sample. This means only minor reflections from the laser on the sample will reach the sensor to interfere with it. In addition, the pulse length of the laser is 5ns compared to the 10ms of the camera flash so its interference with any sensor equipment will be minimized to the first data point at most (due to the temporal resolution of 100µs and 10µs in the photodiode and pyrometer respectively).

A series of 3 identically prepared samples of APSWCNT/ferrocene (1:4, 5mg total) were ignited by the laser at 100mJ and recorded with the pyrometer in

order to examine the reproducibility of the experiment. Preparation of samples included shaking them in a flask shaker for 10 minutes to ensure homogenous mixing. These results are displayed in Figure 3.10.

A sharp peak at 0ms is observed above the maximum sensitivity of the pyrometer, this is a result of the laser striking the sample. After ~5ms the signal rises sharply from the sample igniting. In some cases (seen in the green trace) the ignition saturates the photodiode. The ignition lasts for 80-200ms in total and displays a variance in the signal between samples. The small sharp peak observed in all samples at 101ms is due to the fluorescent lights in the room pulsing every 100ms. Reproducibility between samples is still not strong.

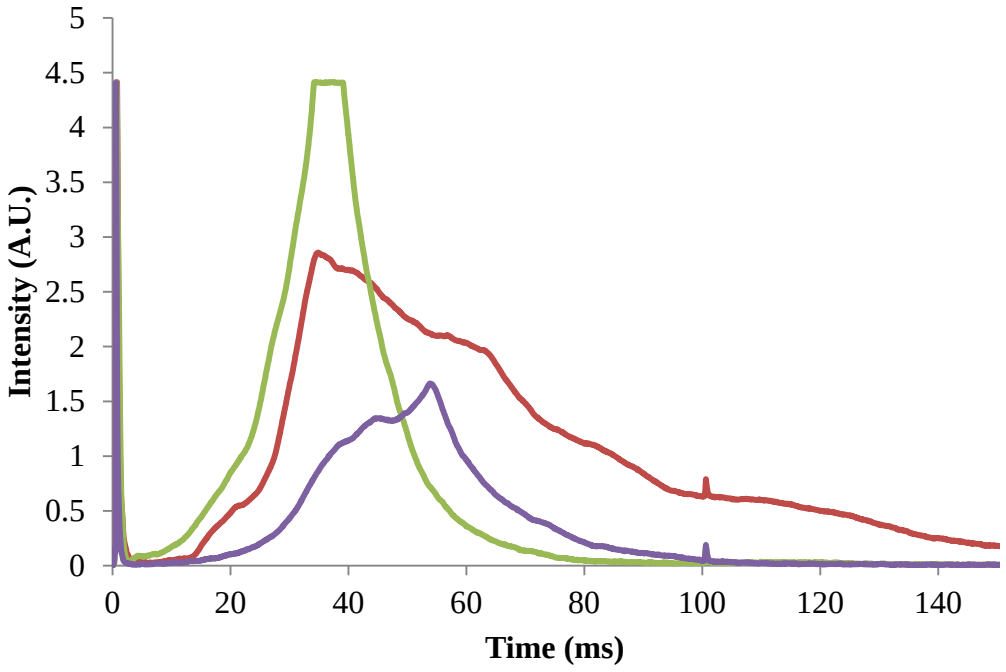

Figure 3.10: Laser initiation results of multiple identically prepared samples of APSWCNT/ferrocene (1:4, 5mg total) to examine reproducibility.

Another problem with data was that results acquired between multiple different samples prepared by the same method with the same mass were not as

consistent as was required for a thorough investigation and comparison. This exaggerated the already qualitative nature of the photodiode and made it difficult to draw comparisons between different types of samples and to extract meaningful data from the results.

A Lumasense IMGA 740-LO high speed pyrometer was purchased to replace the photodiode system and produce quantitative and comparable results. The pyrometer was trialled with a sample of APSWCNT/ferrocene (1:2, 10mg) initiated by flash unit. The lower ratio was chosen to reduce the amount of ferrocene residue on the sample stage so cleaning between experiments could be performed faster while the experimental technique was still being refined. The experimental setup was identical to that previously described and shown in Figure 3.1 except the fibreoptic above the sample stage for the photodiode was replaced with the pyrometer optical head. The camera flash unit was also initiated with no sample present as a blank to observe any interference from the flash unit on the pyrometer results. The initiation result is shown in Figure 3.11.

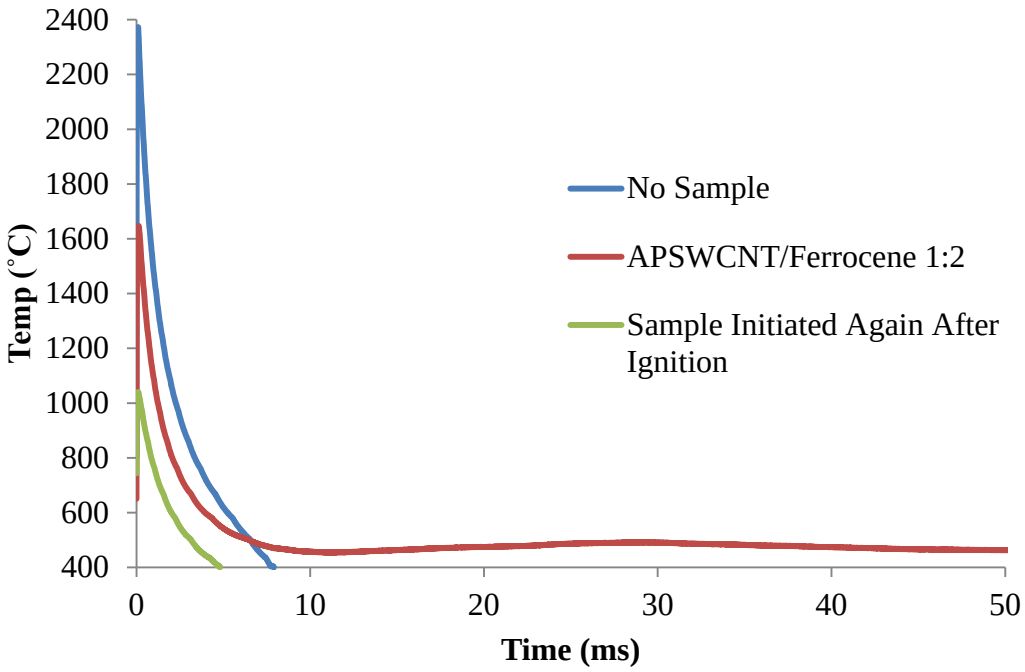

Figure 3.11: Camera flash initiation of APSWCNT/ferrocene (1:2, 10mg) recorded with the high speed pyrometer. A blank recording is also performed, and a second camera flash after the sample had completed flash ignition but was still physically blocking light on the sample stage.

With no sample present, a very large peak starting at 2400˚C was observed. This is the light from the camera flash travelling directly into the pyrometer sensor head, the interference lasts for 8ms. When there is a sample on the sample stage, it physically blocks a portion of the photoflash light from reaching the pyrometer sensor, so a sample that had already been ignited and burned was initiated again from the camera flash to show the reduced flash interference with a sample in place to block it (green line in Figure 3.11). This shows less interference from the camera flash, however, there is still a large peak starting at 1030˚C interfering with the collection of data for the first 5ms. No continued reaction shows that complete combustion of the sample is achieved from a single exposure to the flash unit.

The sample ignition is displayed as the red line. As the initiated sample burns, a steady temperature of deflagration occurs at ~480˚C. Only 50ms is displayed, the total reaction lasted for several seconds as the surface propagated

reaction burned across the whole sample. However, the area of interest for the potential initiation of energetic materials from a sample is within the first 10ms, where the camera flash significantly interferes with the data.

A sample of APSWCNT/ferrocene (1:2, 10mg) was prepared in a small glass sample vial and initiated with the laser (100mJ, single pulse) and recorded on the pyrometer. The pyrometer records temperature by measuring the ratio of two wavelengths of infrared light, so the monochromatic laser should not produce any direct interference. The overall reaction with the laser is much faster and more violent as evidenced by the pyrometer result in Figure 3.12. The entire reaction is complete in less than 200ms compared to the slow (>3 second) deflagration from the flash unit. A very sharp and high initial peak was seen when the laser first hit the sample, thereafter the results displayed are entirely due to the ignition of the sample without interference. The laser initiation caused the sample to rapidly scatter over the petri dish on the sample stage and a flash of light was observed on the sample. This scattering causes particles to cool faster and results in incomplete combustion of samples compared to the flash unit. Rapid ignition was not observed with camera flash unit initiation. The temperature of the sample burning is higher than that observed from the camera flash unit suggesting much more energy is in the reaction as a result of the increased power intensity of the laser. A secondary peak is observed rising from 5-20ms. This is most likely due to the ferrocene being ignited and oxidizing from the initial nanotube absorption.

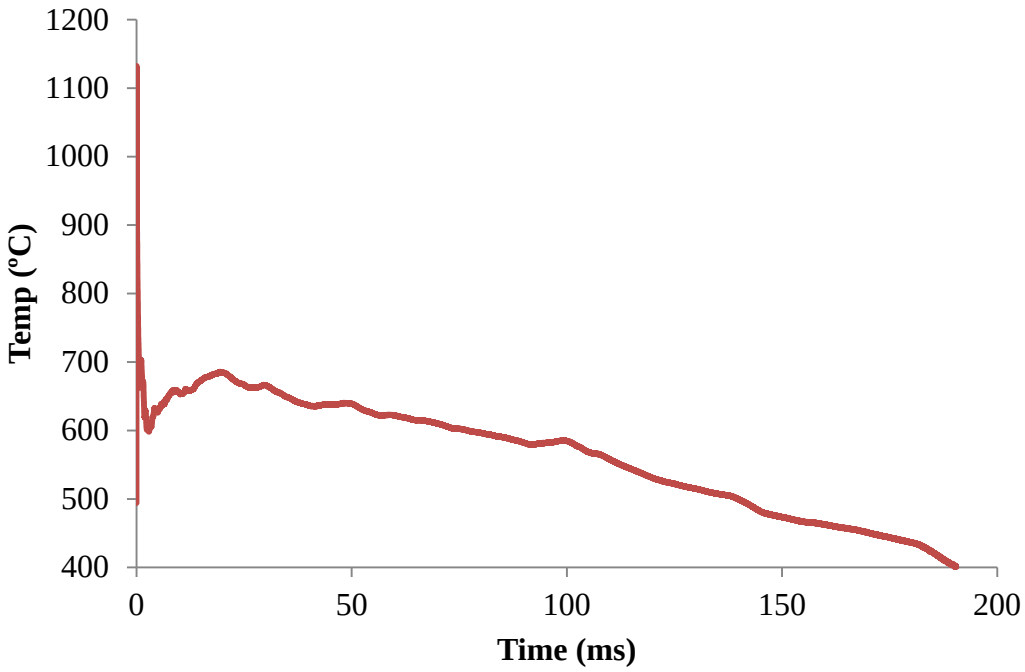

Figure 3.12: Laser ignition of a sample of APSWCNT/ferrocene (1:2, 10mg) using the pyrometer to record the data.

A high speed camera was used to record the laser ignition of a sample of APSWCNT/ferrocene (1:2, 10mg) to compare to the flash unit ignition previously described in Figure 3.7. Note that this experiment was recorded with a laser initiation at 50mJ so the overall reaction time is not directly comparable with the pyrometer result in Figure 3.12. Selected frames of the ignition are displayed in Figure 3.13. A different timescale was used in this series of photos since laser initiation was a much faster reaction than flash unit initiation (Figure 3.7). The entire ignition reaction was complete within 20ms, while the camera flash ignition was only beginning after 10ms and burned slowly for several seconds. The energy of the laser is enough to cause the material to scatter as opposed to remaining stationary, and the reaction looks much closer to an explosion than surface propagated deflagration. The first frame in Figure 3.13 (a) shows the first frame captured once the laser was triggered, the light and flame has already spread across a large amount of the sample before a much brighter flash is observed (b) from the explosion of the sample and the burning material becomes airborne (d-f). This high speed camera result also shows the laser ignition to be much faster than

the photodiode or pyrometer results suggest. This can be attributed to the sample being uncontained on the glass petri dish giving the particles more allowance to scatter and cool down while the flash unit did not scatter particles. Additionally, a laser pulsewidth of 5ns means energy is absorbed much faster than the sample can dissipate heat compared to the ~10ms of the flash unit.

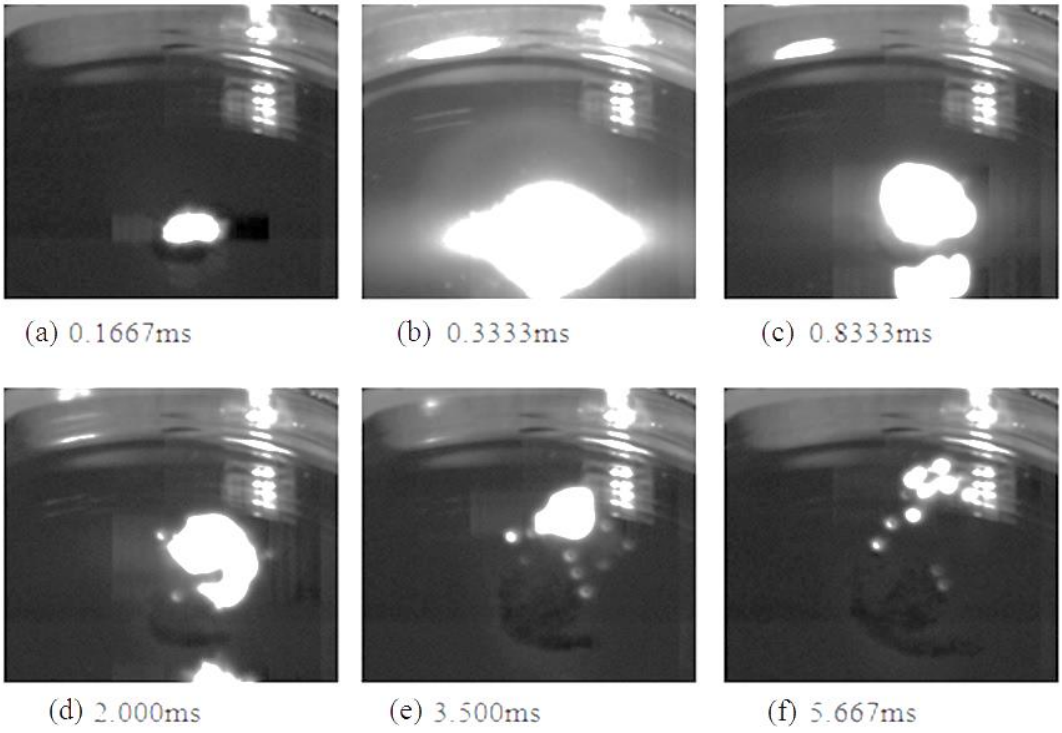

Figure 3.13: High speed camera frames showing the ignition of APSWCNT/ferrocene (1:2, 10mg) with the laser (50mJ). Time shown refers to the amount of time passed since the laser was triggered.

3.4: Energy Comparison of the Flash Unit and the Laser

There is a significant difference in the reaction of a sample when exposed to a laser as compared to when exposed to the camera flash unit. This could be due to the differences in power and surface power density (specific power) between the two light sources which is related to the different pulse times. Both were calculated and compared.

The theoretic maximum energy of the camera flash unit can be calculated based on the capacitance and voltage of the capacitor in the flash unit. The experimental energy will be lower due to losses to heat as the capacitor discharges. Energy stored in a capacitor is given as,

$$E = -\int[v.dq]$$

where v is the potential and dq is a charge. This resolves to $Q^2 / 2C$. We then substitute for C since

$$Q = C.V$$

to get

$$E = \frac{C.V^2}{2}$$

The capacitance and voltage were obtained from the manufacturer as 600µF and 330V respectively. This results in 32.7J of energy from the flash unit.

The laser used was a 100mJ single pulse, so the energy of the camera flash unit is several orders of magnitude higher. However, the power and power density are more important factors. The results recorded by the pyrometer (Figure 3.11) and high speed camera (Figure 3.7) show that the camera flash time is ~10ms. The pulse width of the laser is 5ns. Power is joules per second, which resolves to 3267W for the camera flash unit and $2.0*10^7$W for the laser. Therefore the power input on samples is significantly higher for the laser due to the much smaller pulse width. It should also be noted that the spot size of the laser is 2mm, while the camera flash spreads over a ~22cm^2 area (calculated by the size of the flash unit being 6.5x3.4cm) which creates a much smaller specific power; 148.5W.cm^{-2} for the camera flash unit and $2.42*10^9$W.cm^{-2} for the laser. It also means that 100% of the laser energy hits the sample due to the 2mm spot size, while only a small percentage of the camera flash unit energy directly hits the sample.

Since lasing is not possible below ~15mJ, an experiment was prepared to defocus the laser beam to further reduce the energy input to a sample and compare that to the camera flash unit. A concave lens was placed before the mirror in the laser setup (diagram in Chapter 2.9, Figure 2.5) in order to diverge the laser beam as shown in Figure 3.14. It was placed before the mirror rather than after since the beam did not diverge enough when placed after the mirror. Distance from the lens to the mirror was fixed at 4.5cm. The height of the sample stage was adjustable in order to vary the spot size of the beam.

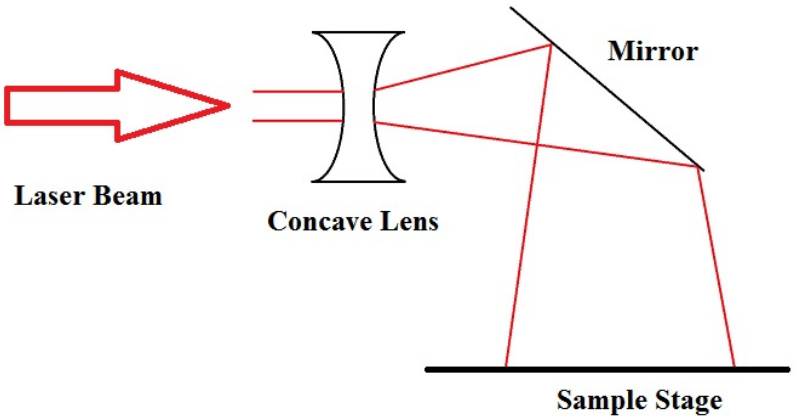

Figure 3.14: Side view diagram of the diverged laser beam path to the sample. Image not to scale.

The size of the laser spot could be measured with flash paper placed on the sample stage. Figure 3.15 shows a defocused laser spot burn on the flash paper. The red spot on the right side (highlighted by the arrow) is a comparison to the laser spot without divergence. A large portion of the radius is cut off due to the reflecting mirror being smaller than the beam width. The radius and thus specific power can be calculated from these burns.

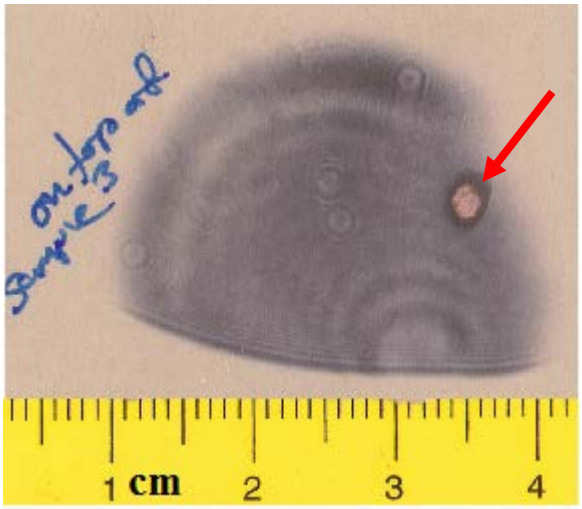

Figure 3.15: Flash paper measuring the spot size of the diverged laser beam. The laser spot without lens defocusing is indicated by the arrow for comparison.

A sample of APSWCNT/ferrocene (1:2, 10mg) was used in this experiment. No reaction was found with the laser beam at 100mJ at any distance below the mirror. The specific power of a 23mm radius laser spot (produced on the sample 55cm below the mirror) from a 100mJ pulse of the laser calculates to $1.20*10^{6}W.cm^{-2}$ which is four orders of magnitude higher than the camera flash unit ($148.5W.cm^{-2}$). It should be noted that the calculated specific power does not take into account energy lost due to the laser beam reflecting from the concave lens (see Figure 3.16). However, it can still be assumed that the specific power of the laser would be much higher than the camera flash unit. Therefore since the camera flash unit does ignite samples, and this laser setting does not while the beam is diverged despite a higher specific power, it suggests that other factors such as the wavelength of light may play a role in sample ignition.

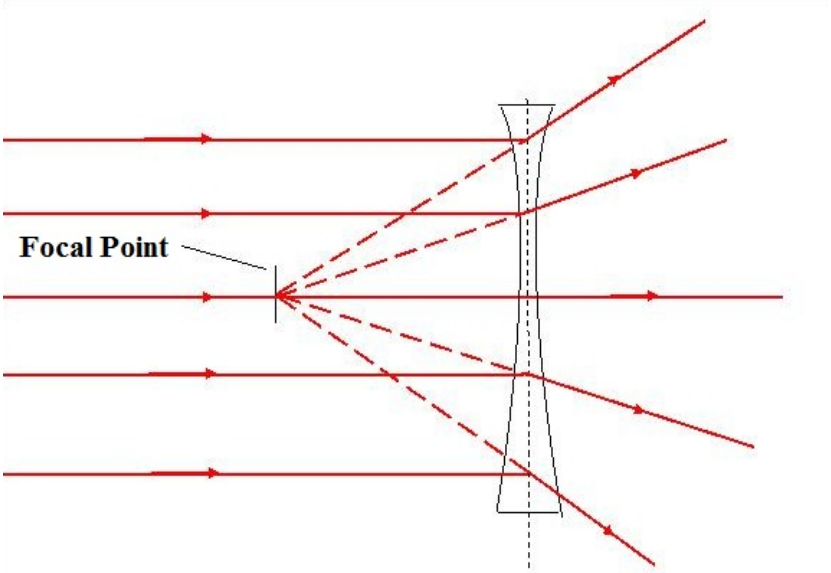

Figure 3.16: Schematic of light reflections and refractions through a concave lens showing the reflected focal point of light.

The sample stage was moved to a distance of 26cm from the mirror, and the laser energy was increased to 500mJ. This resulted in a laser spot radius of 15mm and a theoretical specific power of $1.31*10^{7}W.cm^{-2}$. At this power level, a sample was successfully ignited by the laser. The resultant laser initiation resembled ignitions from the camera flash unit rather than the focused laser. The sample underwent surface propagated deflagration and burnt with a steady flame for several seconds, and no scattering of the sample across the sample stage was observed.

It appears that the divergence of the light source may affect the ignition of samples, and the ignition characteristic of the sample can be controlled between a slow burning ignition (flash unit) and a faster more explosive reaction (focused laser) which may have different mechanisms. Another consideration is that with a divergent light source (camera flash or defocused laser) the entire sample is heated up at once which will limit the ability of particles to transfer heat to neighbouring particles, while the small laser spot only hits a 2mm radius of sample.

3.5: Chapter Conclusions

The light initiation of APSWCNTs from a flash unit was examined using a photodiode to measure the output light intensity over time. Samples successfully ignited and the reaction was greatly enhanced by the presence of ferrocene which produced a surface propagated deflagration over the whole sample. Additionally, iron and nickel nanoparticles were found to rapidly oxidise when exposed to the flash unit indicating a potential role in the reaction. Light interference from the flash unit was found to obscure data over the first ~10ms which prohibited complete analysis of reactions. Similar interference was found when a high speed pyrometer was employed to measure temperature over time for the reactions.

Using a laser as the light initiation source prevented interference on measured results since the pulse width was in the range of 5ns compared to the 10ms of the flash unit. Calculations showed that the input power from the laser was much higher than the power from the flash unit due to the shorter pulse width. As a result, samples were unable to dissipate heat that was rapidly gained from the light and the laser initiated ignition reaction of samples proceeded at a much faster rate; in the order of 100ms as opposed to several seconds for the flash unit.

A high speed camera analysis of sample reactions from both light sources indicated that from the laser, a reaction closer to an explosion occurs where a fireball rapidly (<10ms) engulfs the sample. However, the energy from the laser scatters the sample particles resulting in incomplete combustion. By contrast, no particle scattering was observed with the camera flash unit and instead the reaction appeared to propagate by a slow surface deflagration which allowed the complete combustion of the sample to occur over several seconds.

3.6: References

1 Tseng, Shih H. *et al.*, Ignition of Carbon Nanotubes Using a Photoflash. *Carbon* **45** (5), 958-964 (2007).

2 Braidy, Nadi, Botton, Gianluigi A., and Adronov, Alex, Oxidation of Fe Nanoparticles Embedded in Single-Walled Carbon Nanotubes by Exposure to a Bright Flash of White Light. *Nano Letters* **2** (11), 1277-1280 (2002).

3 Malec, Christopher, The Use of Carbon Nanotubes as an Energetic Material Initiator, Honours Thesis, Flinders University, 2008.

4 Malec, Christopher D., Voelcker, Nicolas H., Shapter, Joseph G., and Ellis, Amanda V., Carbon Nanotubes Initiate the Explosion of Porous Silicon. *Materials Letters* **64** (22), 2517-2519 (2010).

5 Hu, Lu, Narayanaswamy, Arvind, Chen, Xiaoyuan, and Chen, Gang, Near-Field Thermal Radiation between Two Closely Spaced Glass Plates Exceeding Planck's Blackbody Radiation Law. *Applied Physics Letters* **92** (13), 133106 (2008).

6 Ajayan, P. M. *et al.*, Nanotubes in a Flash--Ignition and Reconstruction. *Science* **296** (5568), 705- (2002).

7 Smits, Jan *et al.*, Response of Fe Powder, Purified and as-Produced HiPCO Single-Walled Carbon Nanotubes to Flash Exposure. *Materials Science and Engineering A* **358** (1-2), 384-389 (2003).

Chapter 4: Pyrometer Method with Laser Initiation

This chapter aims to achieve consistent and repeatable results by exploring the variables which influence nanotube ignition characteristics from laser initiation and subsequently to setup reproducible experimental conditions and methods. The laser properties such as wavelength and input energy will be examined. The confinement of samples is investigated to improve consistency. The chapter also explores the effect of ferrocene in samples with respect to the ignition and how different ratios of ferrocene react. Finally, the difference in laser initiation between several different types of nanotubes is investigated.

4.1: Laser Settings and Experiment Setup

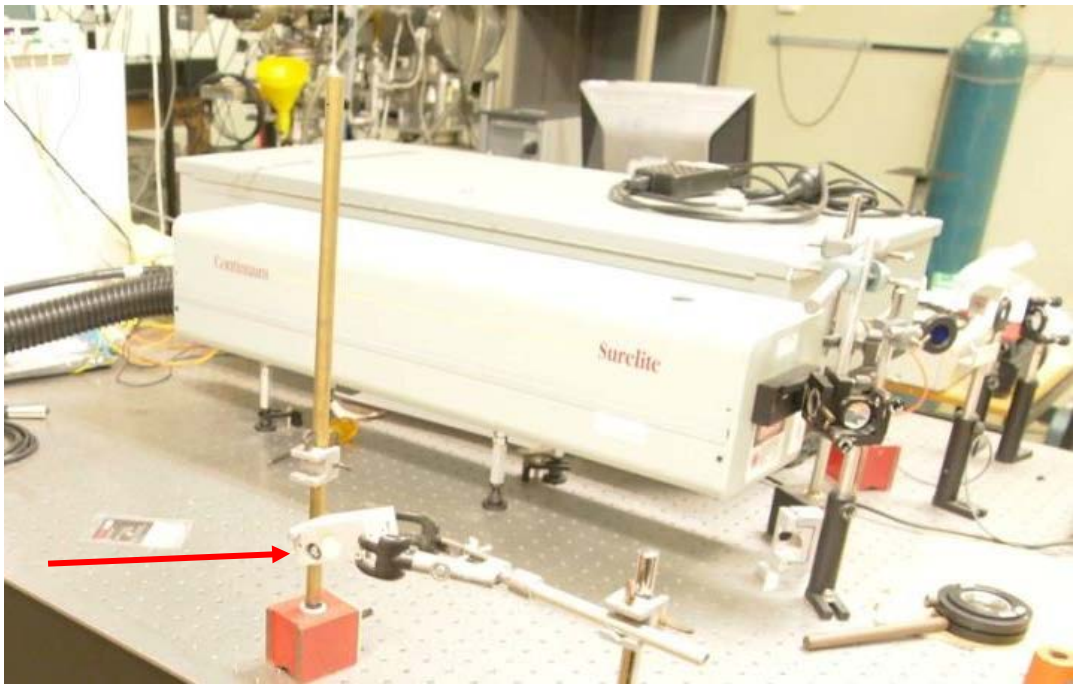

Figure 4.1: Photograph of the Surelite SLIII Nd-YAG laser. The arrow shows the mirror which reflects the beam down to the sample stage.

The infrared (1064nm) Nd-YAG laser (Figure 4.1) was set to a button-triggered single pulse mode to produce a 5ns pulsewidth beam and calibrated to 152mJ with a Q-switch time of 400µs. Five separate samples of Carbon Solutions as-prepared single walled carbon nanotubes (APSWCNTs) (10mg) were initiated and the ignitions recorded on the pyrometer. These results are displayed in Figure 4.2. Overall the reactions look very similar though there is some variance in the initial temperature and the total reaction time. Minor variations are expected in the ignition of samples of randomly oriented loose powder. For several samples a second peak was observed in the reaction. Carbon nanotubes are known to undergo significant reconstruction as a result of light initiation[1,2] and these reconstructions may be exothermic which would account for delayed secondary peaks. Throughout this thesis, various results and reactions are compared back to the ignition of APSWCNT as a standard which always refers to the Carbon Solutions brand. During many experiments, a new reference sample of APSWCNT was ignited to make the comparison but where that did not happen, one of the obtained results from Figure 4.2 was selected to compare.

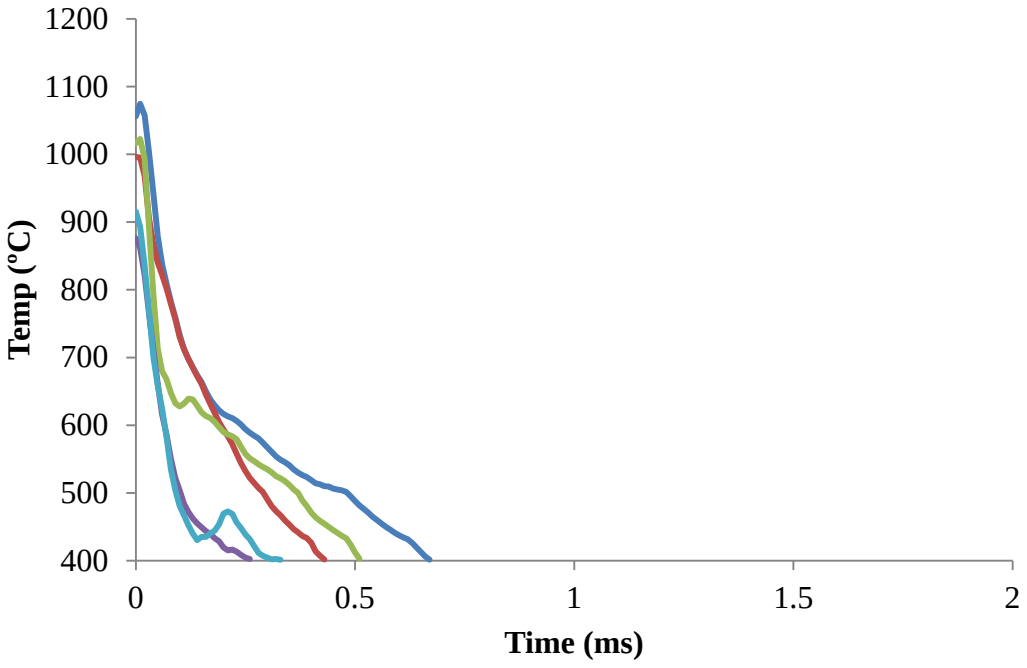

Figure 4.2: Laser initiation results of 5 separate samples of APSWCNT (10mg) ignited at 152mJ to examine consistency between samples.

Laser initiation has been shown to scatter samples all over the sample stage, as displayed in Figure 4.3 (reused from Figure 3.13). Fast moving airborne particles will cool down quicker and more easily than a stationary packed sample which leads to incomplete combustion of samples that may contribute to the variability in the measured results.

Explosives are commonly pressurised or confined in order to increase their explosive output. An initiation system will almost certainly be confined with the material packed densely. Therefore there is a need to understand the influence of confining the samples on the output reaction.

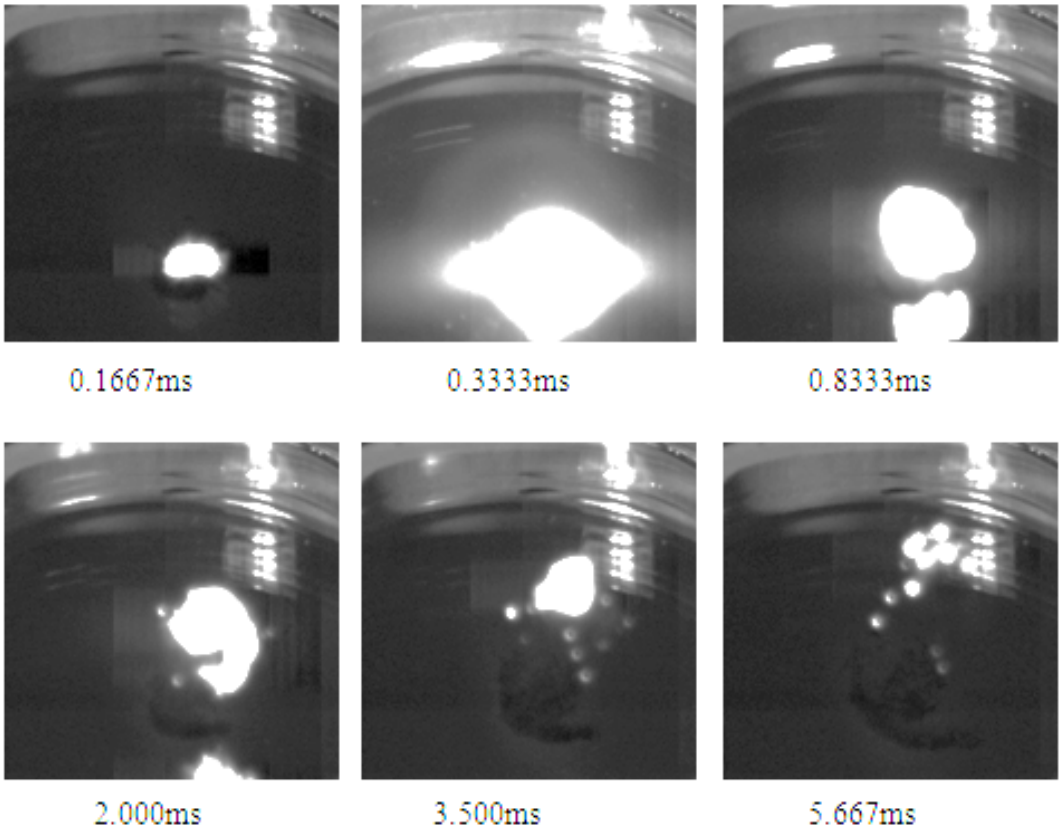

Figure 4.3: High speed camera frames showing the ignition of unconfined APSWCNT/ferrocene (1:2, 10mg total) with the laser. Time shown refers to the amount of time passed since the laser was triggered.

To test the effects of confinement, the first experiment attempted was to tape a powder sample of APSWCNT/ferrocene (1:2, 10mg total) onto a piece of double sided carbon tape. This was less about physically confining the sample and more about reducing the particle scattering from the laser impact. The results were similar to loose unconfined samples. A series of photos from the high speed camera is shown in Figure 4.4. The time shown on the figure is elapsed time after laser initiation. The first photo is the first frame of ignition visible. This result is very similar to the sample that wasn't stuck down (Figure 4.3) showing the same characteristic flame above the sample which extinguishes within 5ms. After this time, the sample does still appear to scatter despite being taped down, though most scattering is in an upward direction rather than sideways. The brighter initial flash is most likely because the carbon tape is optically active unlike glass. The laser does not travel through the carbon tape, so the entire laser beam reacts at the sample stage rather than a portion of it traveling through. Taping a sample to the stage appears to make little difference aside from the brighter initial flash.

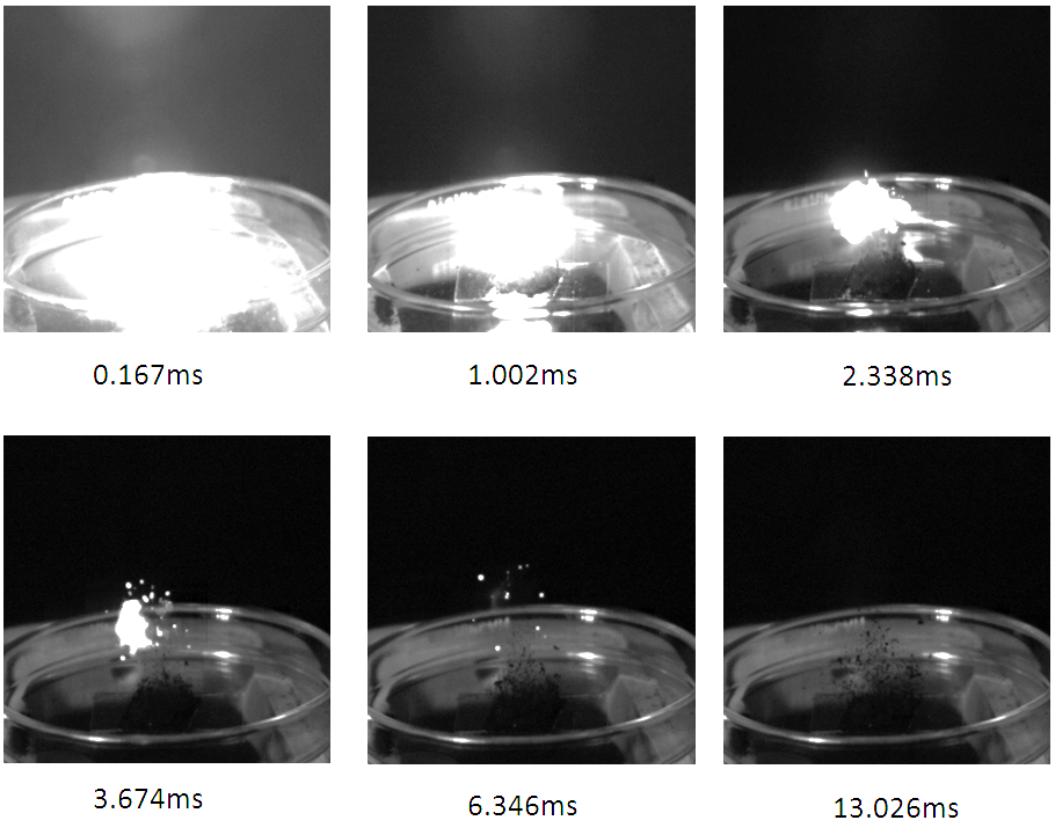

Figure 4.4: High speed camera frame series of APSWCNT/ferrocene (1:2, 10mg) taped to double sided carbon tape and initiated by the laser. Time shown is time after laser initiation.

To increase the density and compaction of the material, a sample of APSWCNT/ferrocene (1:2, 10mg total) was sandwiched between two glass slides. Initiating the sample with the laser showed no sign of ignition and no result on the pyrometer, though the particles did appear to still move slightly from the impact of the laser. Exposing the sample by removing the covering slide and initiating it again allowed it to ignite as normal, which supports the suggestion that air does play an important role in the light ignition of nanotubes.[3] Pressing the material together also increases the density and may lead to more energy dispersion pathways.

It was reported in the literature that density of nanotubes may be an important variable as a higher density allows easier transfer and dispersion of heat throughout the entire sample, while a low density creates localised hotspots where

the light energy is converted into thermal energy and causes rapid heating which cannot easily be released.[1,3]

A sample of APSWCNT/ferrocene (1:2, 10mg total) was prepared in a small glass sample vial (~1cm diameter and 3.5cm height). The sample in the glass tube was placed on the sample stage and initiated with the laser. This method confines the sample to a small area but does not compress or pressurise the sample at all. In addition, ignition from samples is forced upwards only due to radial confinement of the sample tube rather than spreading outwards over the whole petri dish sample stage. A series of frames from the high speed camera is shown in Figure 4.5. As with the unconfined samples, an initial bright flash is seen lasting over the first few milliseconds of the reaction (Figure 4.5a-c). After this, a secondary reaction begins at ~11ms (d) and a larger fireball rapidly fills the glass sample tube (e-f). This is due to the limited confinement of the sample restricting the ability of the particles to scatter and cool plus the glass tube contains the flames which allows the reaction to proceed.

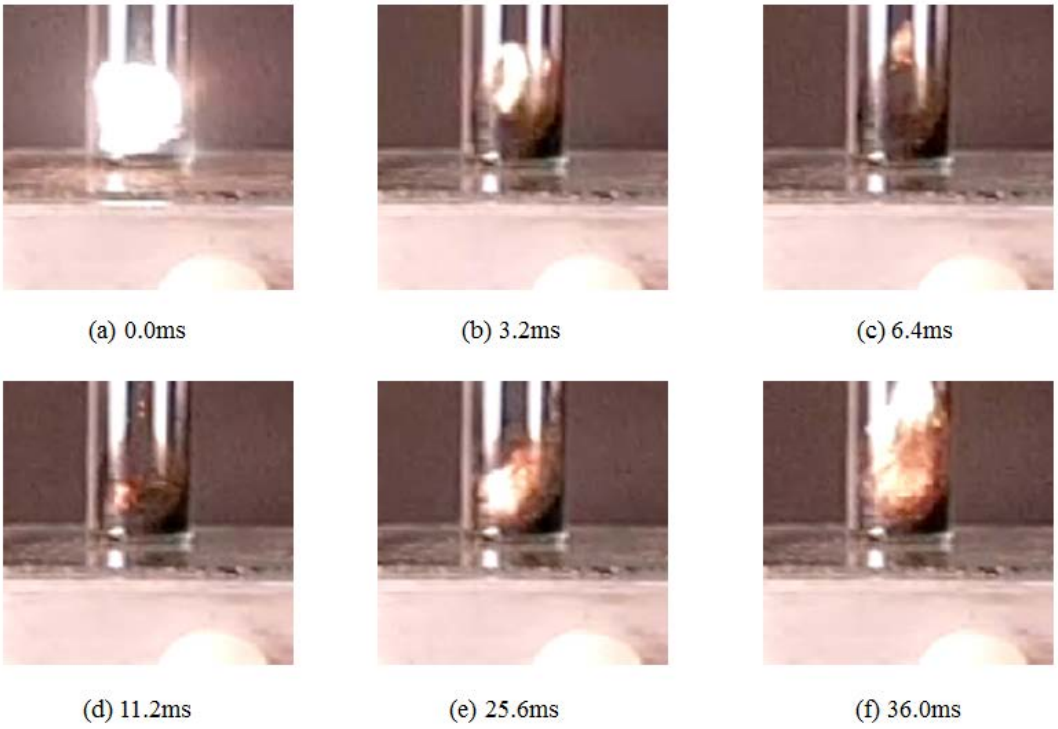

Figure 4.5: High speed camera photos of the laser initiation of APSWCNT/ferrocene (1:2, 10mg total) displaying the initial ignition (a-d) followed by a secondary ignition (e-f) when the ferrocene is initiated and oxidizes.

Confining samples provides two advantages over igniting samples on the flat glass petri dish sample stage. Firstly, the pyrometer focal spot on the sample collects more data from the ignition since the explosion is confined to a ~1cm wide area forcing it to travel upwards directly toward the pyrometer optical head. Secondly, particles from the sample cannot scatter across the sample stage and instead will remain in a small area potentially allowing them to remain hotter for longer.

Figure 4.6 displays a comparison of two different samples of APSWCNT/ferrocene (1:2, 10mg total) initiated in the glass sample tube at 152mJ. Most significantly from the figure, results between identically prepared samples are very consistent and reproducible when the glass tube is used. This is because the impact of the random nature of explosions on the results is reduced. The total ignition time for the sample was found to be much more reproducible

and consistent over multiple samples, whereas the samples completely unconfined on the flat petri dish varied in total ignition time significantly and often scattered before a complete reaction could occur.

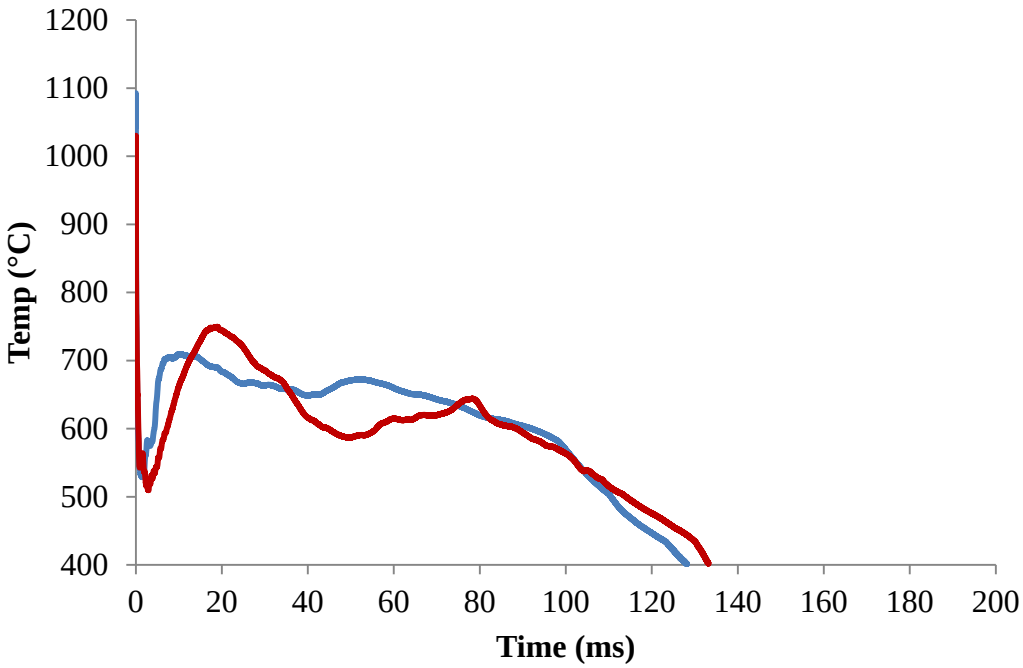

Figure 4.6: Laser initiation of two samples of APSWCNT/ferrocene (1:2, 10mg total) when initiated from within a glass sample tube demonstrating the consistency of results.

Several samples of APSWCNT/ferrocene (1:2, 10mg total) were prepared and ignited at various energy levels of the laser, shown in Figure 4.7. At 80mJ and below, there is not enough energy input into the sample from the laser to cause an ignition of the ferrocene shown by the secondary peak. Above that threshold energy input, samples ignite for a total ignition time of 100-200ms and display an initial drop in temperature immediately after the laser impact (0-2ms) followed by a rise as the sample ignites to a second peak. Increasing the energy of the laser appears to shorten the time to reach the secondary peak temperature. The energy of 152mJ caused the sample to peak in temperature at 5-9ms as opposed to the 15-20ms seen in the samples ignited with 110mJ and 120mJ.

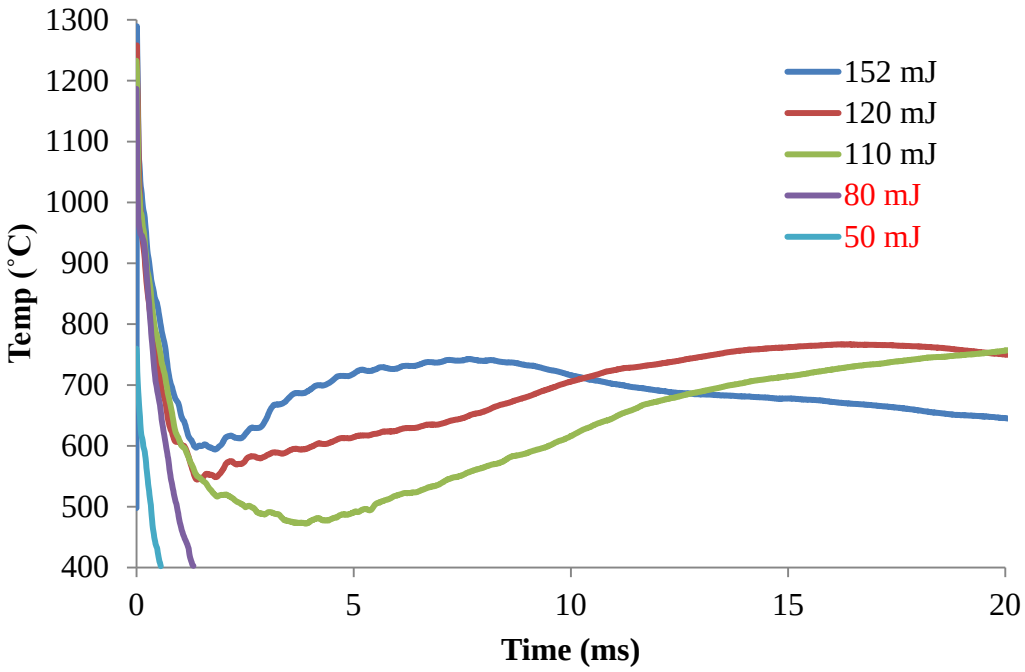

Figure 4.7: Pyrometer recorded ignition results of varying laser energy levels on samples of APSWCNT/ferrocene (1:2, 10mg total) using IR laser wavelength 1064nm. Complete initiation to 110ms not displayed.

Operating at high energy levels (>200mJ) is dangerous and may cause damage to equipment in addition to scattering the sample more violently. Operating at low energy levels (<100mJ) causes a higher variance in the Q-switch timing thus variance in the energy produced and input to samples. Therefore experiments were performed at 152mJ (Q-switch time of 400µs) in order to ensure reproducible results without using too much energy. This energy level produced a 2mm radius laser spot on the sample. Unless otherwise noted, all experiments were performed at this energy level to ensure comparability.

4.2: Ferrocene and Ratios of Ferrocene

Ferrocene was added into APSWCNTs as it was for the flash unit experiments. Adding ferrocene resulted in a higher initial temperature in the sample and a much longer burn time, as shown in Figure 4.8 comparing the

reaction of APSWCNT to APSWCNT/ferrocene (1:2, 10mg total). The data is presented in two graphs with different x-axis scales in order to display the full reaction as well as a zoomed version of the first 2ms. The peak temperature with ferrocene is 1130˚C while with no ferrocene present, it is 915˚C. APSWCNT completed the reaction within 0.5ms, but when there is ferrocene present the sample burned for ~150ms. Ferrocene was initiated without nanotubes and the result displayed two data points and no observable reaction. It does not ignite on its own from the laser. This means that the nanotubes are required to absorb the light energy and transfer it to the ferrocene.

The increased reaction with ferrocene was reported to be because ferrocene acts as a fuel and burns once the nanotubes have reacted to the laser and heated up.[3-5] A second peak is observed at ~20ms due to the ferrocene igniting. This agrees with the observations in the high speed camera frames that showed a secondary reaction occurring within the sample, Figure 4.5(d-f).

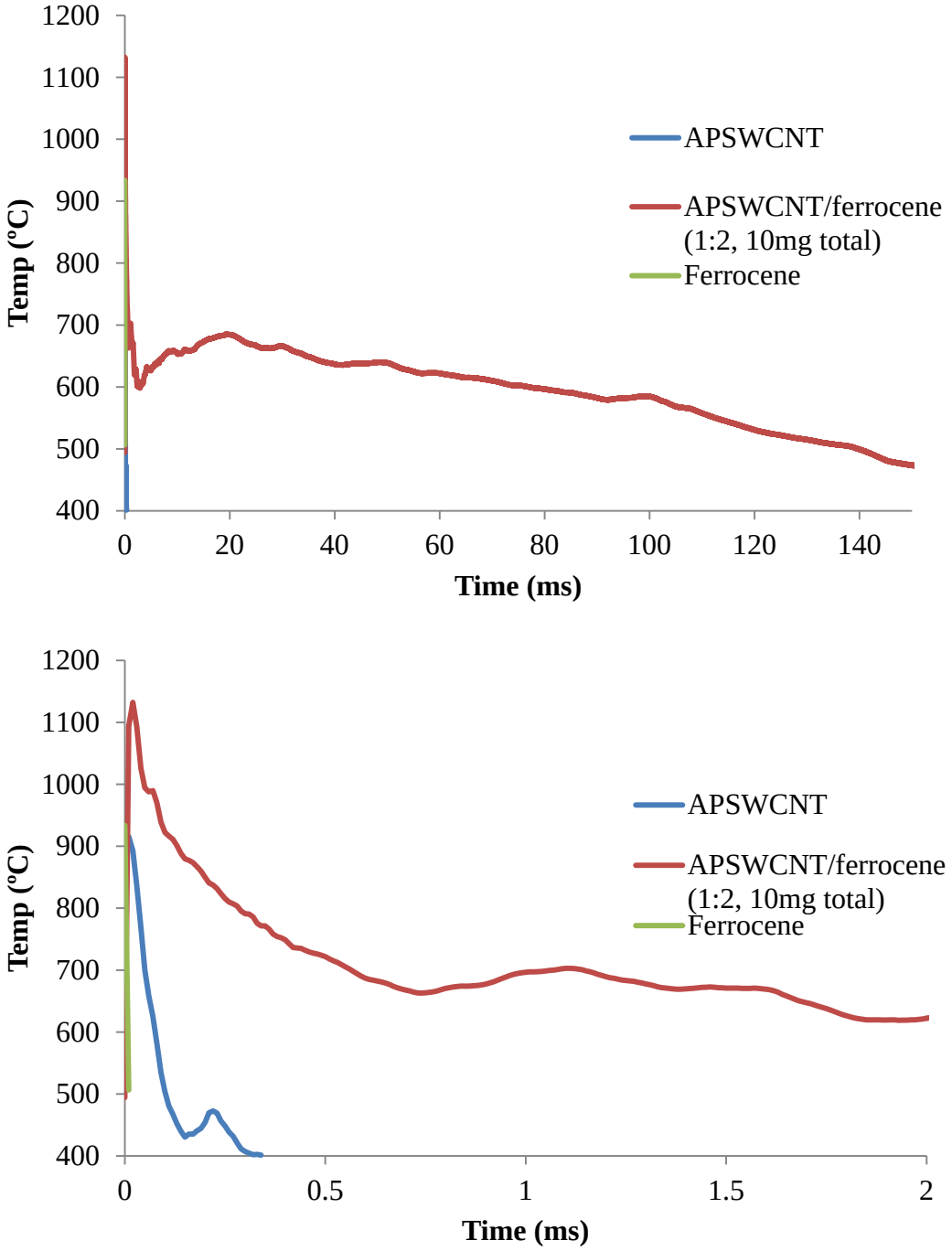

Figure 4.8: Comparison of the ignition of APSWCNT to APSWCNT/ferrocene (1:2, 10mg) displaying a higher temperature and longer burn time in the presence of ferrocene. The results are displayed at two different scales to show the full reaction of the APSWCNT/ferrocene (1:2, 10mg) (top) and then zoomed in on the first 2ms (bottom).

The secondary reaction observed with ferrocene was investigated further. This was believed to be the ignition of ferrocene as a result of the temperature reached in the nanotube bundles,[3-5] the auto-ignition temperature of ferrocene is

~480˚C.[3] In order to support the pyrometer result showing that the reaction was due to ferrocene, a sample of APSWCNT (10mg) was ignited in the glass tube with no ferrocene present. The recorded photo frames are displayed in Figure 4.9. No secondary reaction is observed without ferrocene. The initial bright flash lasts for <1ms in Figure 4.9a-b as compared to ~6ms with ferrocene present (Figure 4.5a-c) which suggests that the initial parts of the reaction are enhanced by ferrocene as well as the secondary reaction at ~10-20ms due to ferrocene.

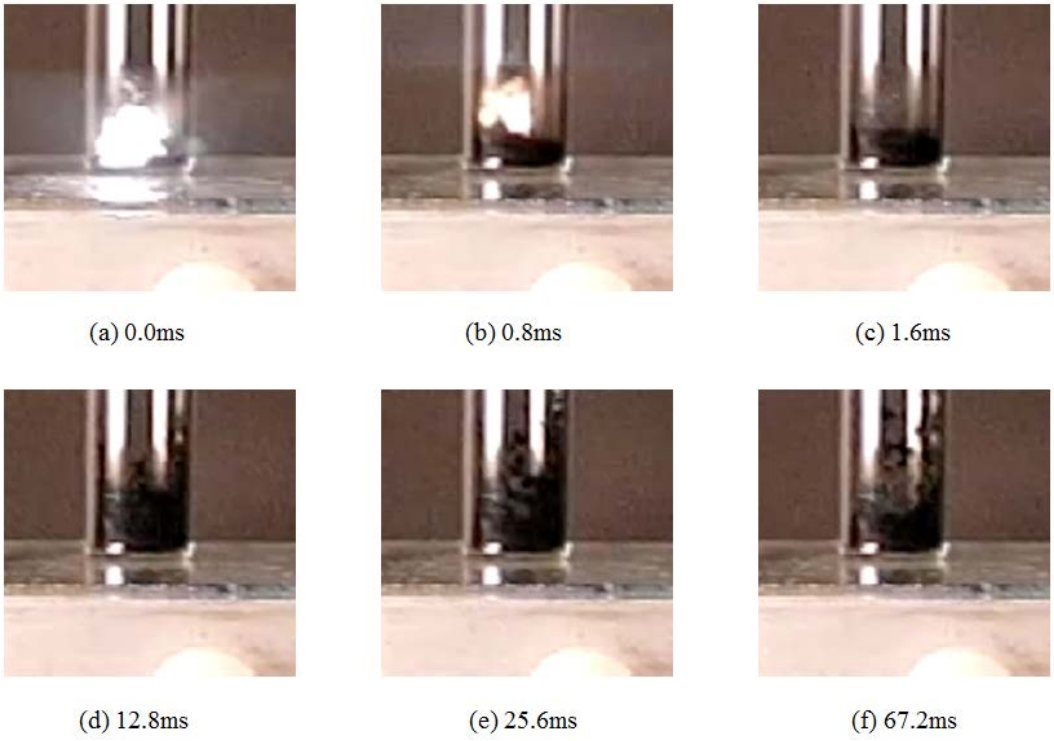

Figure 4.9: High speed camera photos of the laser initiation of APSWCNT (10mg) displaying the initial ignition (a-b) followed by some scattering of the nanotubes but no secondary ignition.

The mechanism by which ferrocene reacts has not been fully investigated as part of the scope of this thesis, however, a hypothesis is suggested. Ferrocene has previously been investigated as a soot reduction agent in fuel combustion by catalysing the combustion of carbonaceous waste.[6-11] The proposed mechanism during combustion was described in detail by Kasper *et al.* in 1999[6] as follows. Ferrocene first cracks open as a result of the fuel burning and the iron particles oxidise into iron oxide and agglomerate. The iron oxide particles then act as

condensation nuclei for carbonaceous soot to preferentially condense onto the surface in an endothermic process. Combustion of the carbon is catalysed by the iron oxide and the reaction proceeds by the same carbothermal reduction reactions as iron smelting from iron oxide and coal:

$2Fe_2O_3 + 3C \rightarrow 4Fe + 3CO_2$

and

$FeO + C \rightarrow Fe + CO$

The carbon oxidises to CO and CO_2 while the iron oxide reduces to iron nanoparticles. These metal nanoparticles are pyrophoric[2] so they ignite and oxidise again once the catalytic combustion of carbon is complete.

A similar mechanism can be applied to the reaction of carbon nanotubes and ferrocene as a result of laser initiation and is described here with reference to Figure 4.8. In the presence of ferrocene, a higher initial temperature (<1ms) is recorded and a brighter flash is observed than with nanotube initiation alone. The extra energy can be attributed to ferrocene cracking open and the iron particles exothermically oxidising due to the heat of the carbon nanotubes.[2] Ferrocene undergoes sublimation from ~100-200˚C[7,12,13] but it is chemically stable up to 500˚C.[7] This temperature is surpassed as the carbon nanotubes absorb light and convert it into thermal energy as the initial peak in Figure 4.8 is >800˚C. In the region 1-10ms, the temperature drops as a result of carbonaceous ash from the APSWCNT condensing onto the iron oxide nanoparticles. These nanoparticles catalyse the combustion of the carbon which reduces the iron oxide back to iron nanoparticles and produces heat. The reaction peaks at ~20ms because the hot, reduced iron nanoparticles are exposed to air again after combustion of the carbon coating, and they readily oxidise again producing more heat which resolves as the secondary ignition and extra peak. As the iron oxide acts as a catalyst, it is

possible this reaction repeats several times until the energy is exhausted which could account for the extra small peaks observed on the pyrometer at 28ms, 47ms and 100ms. In support of this theory, the publication of Smits *et al*. (detailed in Chapter 1.7) examined the residue of nanotubes after light initiation and found iron oxide particles coated with amorphous carbon.[2] When there is not enough heat left in the reaction for combustion of carbon to occur (after 100ms), it will remain attached to the iron oxide particles.

Experiments were performed to investigate various ratios of APSWCNT and ferrocene and determine what the optimal amount is when considering temperature of ignition and the ignition properties. The total mass of the samples to be ignited was kept constant at 3.5mg and samples of APSWCNT/ferrocene (1:1, 1:2, 1:4 and 1:8) were prepared. Ignition with different ratios was performed five times for each ratio and a representative initiation from each is presented in Figure 4.10 as a summary of results.

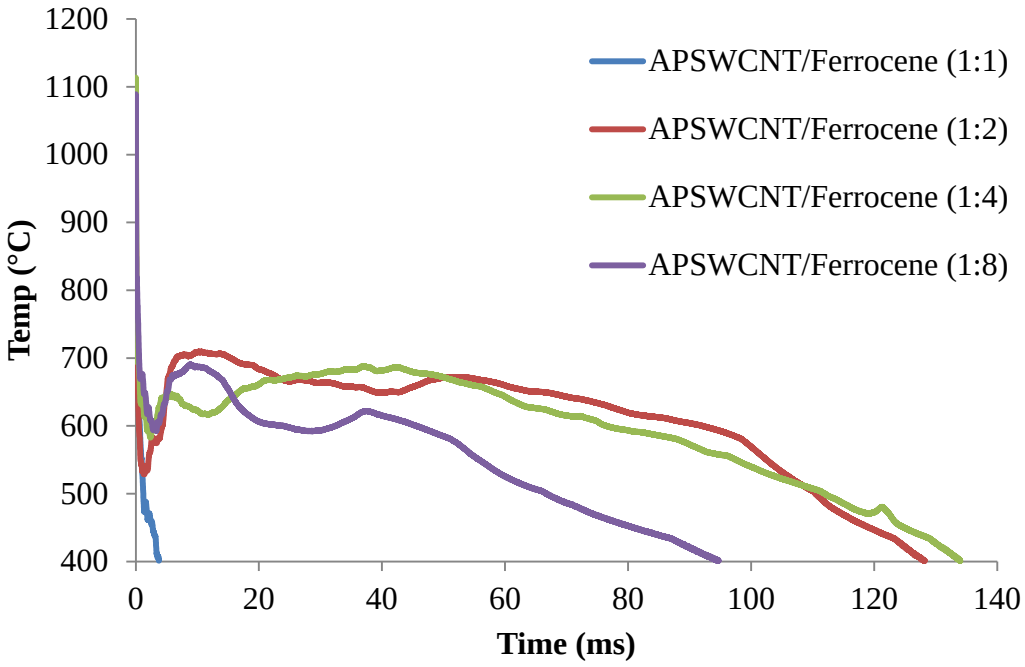

Figure 4.10: Laser initiation results for various ratios of APSWCNT/ferrocene (3.5mg total) at 152mJ.

The mean initial peak temperature of all samples for each ratio only varied by 70˚C with the hottest sample being (1:2) at 1010˚C compared to the (1:8) sample at 940˚C and the (1:1) sample at 977˚C. The (1:4) sample ignited at 1000˚C. Within the first 2ms the results for all samples was very similar. The (1:1) sample displayed an ignition characteristic of APSWCNT/ferrocene (secondary peak and extended ignition) only once out of the 5 samples ignited. This suggests that at a (1:1) ratio, there is not enough ferrocene present to cause a complete reaction reliably. On the other hand, after initiation of (1:8) samples, there was a visible amount of unreacted ferrocene remaining in the sample container. The reaction also created a less bright ignition, and the pyrometer results show a smaller explosion and less heat due to too much ferrocene.

Both the (1:2) and (1:4) samples ignited similarly to each other in terms of total reaction time and initial heat. Previous work by Malec *et al*. found that a (1:4) ratio was optimal and ignition results below that ratio were significantly decreased.[4] However, their experiments were performed with a camera flash unit as the light initiation source. In that case the reaction was significantly slower as detailed in Chapter 3.1 and the observed result was most likely due to the ferrocene simply undergoing slow, surface propagated deflagration rather than the rapid ignitions observed with a laser initiation. In Figure 4.10, the secondary peak for the (1:2) sample is at a higher temperature (705˚C) than the (1:4) sample (670˚C), and the initial temperature is higher. Thus it was concluded that APSWCNT/ferrocene (1:2) was the best ratio for laser ignition.

4.3: Altering the Wavelength and Energy of the Incident Laser Beam

The incident wavelength from the initiation light source may affect the absorption and thus energy of ignition of nanotubes. The camera flash unit

produced a broad spectrum of light from 380-770nm. A laser produces a monochromatic light thus far utilized at 1064nm.

The light absorption of carbon nanotubes has been previously investigated. Since carbon nanotubes naturally aggregate into bundles with strong electronic coupling, the absorption spectra is somewhat complicated to ascertain since the energy states from different nanotubes in the bundles becomes mixed.[14,15] The absorption spectra of a bundle of single-walled carbon nanotubes as reported by Hartschuh *et al*. is displayed in Figure 4.11.[16] Broad unresolved peaks for semiconducting nanotubes are seen at 1700nm and 950nm, while a peak for metallic nanotubes is seen at 650nm. Carbon nanotubes absorb strongly across the whole visible region and less strongly in the infrared up to ~2000nm. The laser at 1064nm falls on the edge of the 950nm peak.

Utilizing harmonic generation crystals, the laser beam can be shifted to the second (532nm) and third (355nm) harmonics. According to the optical absorption of single-walled carbon nanotubes, the absorption is greater at 532nm than at 1064nm thus sensitivity to light ignition should be higher.

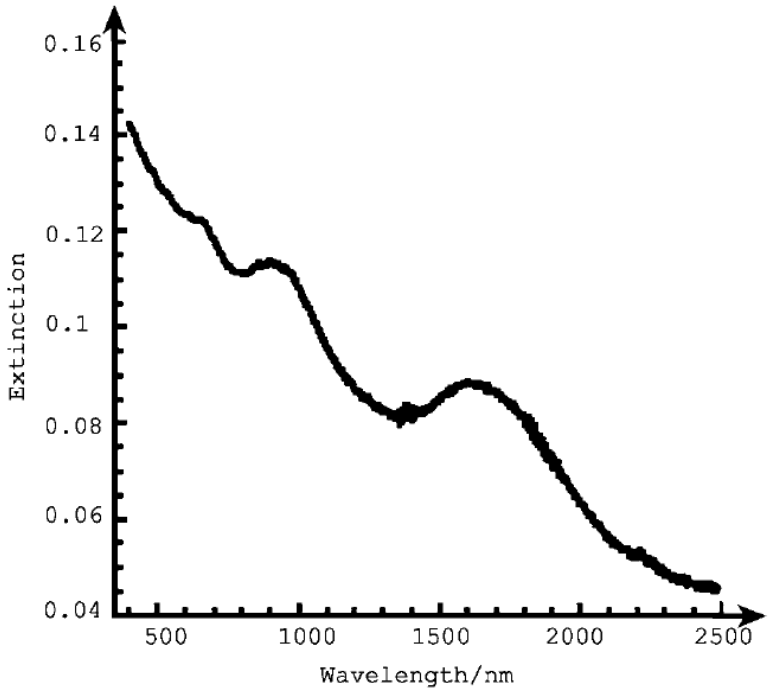

Figure 4.11: Optical absorption spectrum of SWCNTs spun-coated onto quartz. (*Hartschuh, 2005*)

The reported UV-Vis spectroscopy of ferrocene displays absorption at 225nm, 325nm and 440nm.[17-19] None of these absorption maxima align with the laser wavelengths used here so ferrocene is expected to ignite as a result of thermal energy transfer from the carbon nanotubes rather than its own absorption. Ferrocene has already been shown to be unresponsive to 1064nm laser and flash unit without nanotubes present. One published article reports ferrocene absorption at 528nm.[20] This was not found in other sources. If this absorption exists it may have a positive impact on results using the 532nm laser.

The reactivity of samples of APSWCNT/ferrocene (1:2, 10mg total) at various energies of the infrared (1064nm) laser has already been investigated and displayed in Figure 4.7. In summary, above 80mJ of laser energy there was enough heat and energy to ignite the ferrocene in the sample and produce a secondary peak due to exothermic oxidation of ferrocene while below 80mJ only a small reaction existed with no extended ignition from the ferrocene. At 152mJ, the secondary peak was onset faster (5-9ms as opposed to 15-20ms for lower

energies tested) which is favourable for the initiation of an explosion in energetic materials. The same axis of 20ms has been used for other wavelengths since this region displays the most significant differences and the rest of the data does not add to the conclusions presented.

A series of experiments were performed with the laser set at 532nm using various energy levels on APSWCNT/ferrocene (1:2, 10mg total) samples. The results are displayed in Figure 4.12. The initial peak temperature is consistently lower at 532nm (<1000˚C) than at 1064nm (1000-1300˚C) despite stronger nanotube absorption. This may be because the absorption peak at 650nm is for metallic nanotubes, and the APSWCNTs contain a ratio of semiconducting to metallic nanotubes of 2:1 so there are less nanotubes absorbing at 650nm.[21,22] The initial ignitions display shoulder peaks arising within 1ms which did not occur with the IR laser. This may be due to the absorption of ferrocene in this region allowing the cracking and oxidation of ferrocene to occur faster. The total reaction time (not shown) was less than 100ms for reactions with the 532nm laser. This is shorter than the ~120ms found with the IR laser. A shorter total reaction time also supports the idea of the reaction occurring faster.

A higher sensitivity to the 532nm laser was noted since a complete reaction including the ferrocene occurs as low as 65mJ of laser energy compared to 80mJ for the IR laser. Shoulder peaks to the initial reaction all appear within the first 5ms for the green laser indicating a stronger early reaction potentially due to enhanced absorption from ferrocene at 532nm providing greater energy as the ferrocene molecule cracks open. Secondary peaks appeared after 20ms which is in general slower than the IR results. There was still no reaction of ferrocene without any nanotubes present.

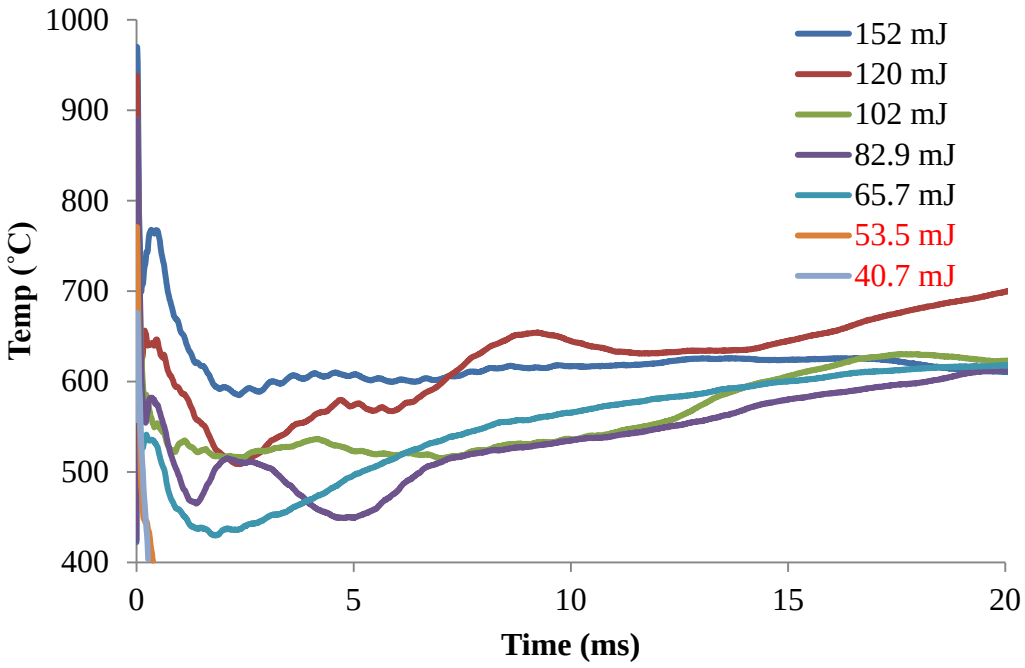

Figure 4.12: Pyrometer recorded ignition results of varying laser energy levels on samples of APSWCNT/ferrocene (1:2, 10mg total) using visible laser wavelength of 532nm.

The results appear contradictory since there are less metallic nanotubes in the sample absorbing at 532nm than there are semiconducting nanotubes absorbing at 1064nm, but the overall absorption is stronger in the visible region. As a result the reaction proceeds faster but a lower initial temperature is observed. To date, there are no studies in the literature investigating the light initiation of carbon nanotubes with respect to semiconducting versus metallic carbon nanotubes.

Reducing the laser to its third harmonic produces ultraviolet light at 355nm. A similar experiment was performed testing various energy levels with samples of APSWCNT/ferrocene (1:2, 10mg total) to test the sensitivity. Results are displayed in Figure 4.13. The energy output at the third harmonic is greatly reduced and the stability of the output energy is much less so the energy levels displayed contain an error margin of ±6mJ. In addition, due to the instability of

the system, the maximum laser energy that could be generated was ~140mJ at 355nm.

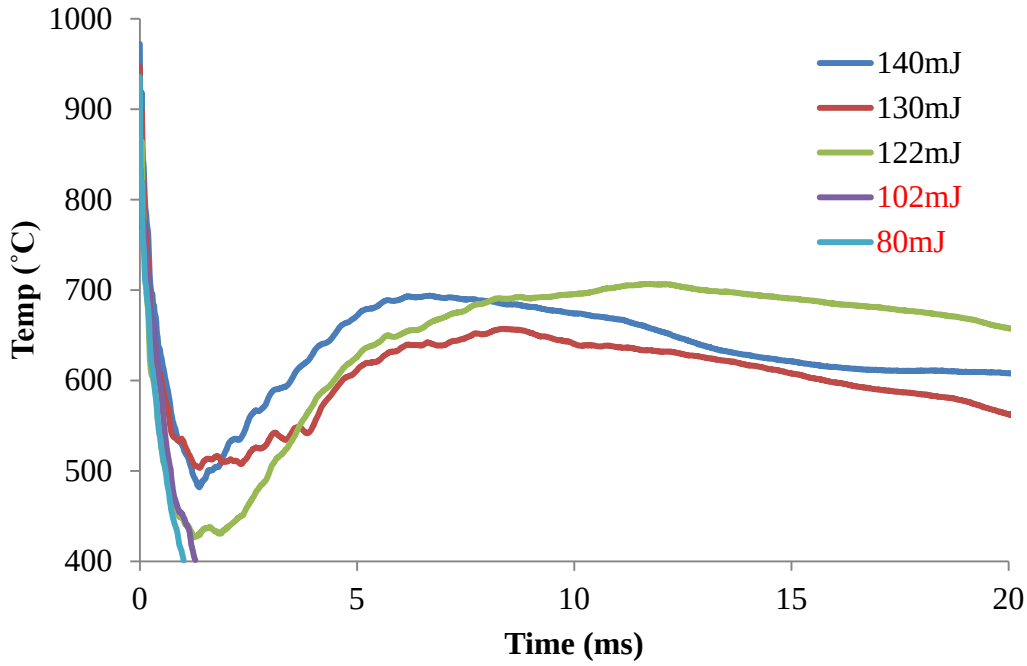

Figure 4.13: Pyrometer recorded ignition results of varying laser energy levels on samples of APSWCNT/ferrocene (1:2, 10mg total) using UV laser wavelength of 355nm.

Initial peak temperatures were found to be below 1000˚C as with the 532nm laser and overall sensitivity to the laser was greatly reduced since 122mJ was required to complete an ignition of the ferrocene in the samples. Secondary peaks do appear to occur earlier as the energy is increased. The peak with 140mJ is observed first at ~6ms, 130mJ produces the peak at ~8ms, and 122mJ does not peak until 11ms.

To conclude, any wavelength tested is capable of igniting APSWCNT/ferrocene samples. The nanotubes used appeared to be most sensitive and produced a faster reaction at 532nm compared to 1064nm and 355nm. However, the initial peak temperature was lower than that found at 1064nm most

likely due to the prevalence of semiconducting nanotubes compared to metallic nanotubes. Consideration of this should be made in selecting a wavelength to initiate nanotubes though further investigation is required. Experiments presented in the rest of this thesis were performed with the infrared (1064nm) laser.

4.4: Brands of Carbon Nanotubes

The residual metal catalyst in carbon nanotubes is thought to play a key role in the light initiation properties of carbon nanotubes.[2,23,24] The catalyst can vary by the type of metal and the weight percentage remaining in the sample after production. It is not yet fully understood what effect these properties have on the light ignition of carbon nanotubes.

APSWCNTs from Carbon Solutions have been used in the majority of experiments in this thesis to this point. They contain a Ni/Y catalyst at ~35wt%. Unidym SWCNTs were used containing Fe catalyst at ~35wt%. Additionally, Shenzhen Nanotech Port (NTP) SWCNTs containing Fe at <3wt% were used. Therefore a comparison study can be made between two samples of nanotubes with a similar wt% of residual catalyst but a different catalyst (Fe and Ni/Y) and a sample with almost no residual catalyst. A comparison of their light initiation at 152mJ is presented in Figure 4.14.

The Unidym SWCNTs initiated at the highest temperature (1130˚C) and burnt for a longer time than the other two samples. NTP nanotubes burnt at the lowest temperature (<900˚C) initially and for the shortest timeframe, though they showed a very similar profile to Carbon Solutions APSWCNTs overall.

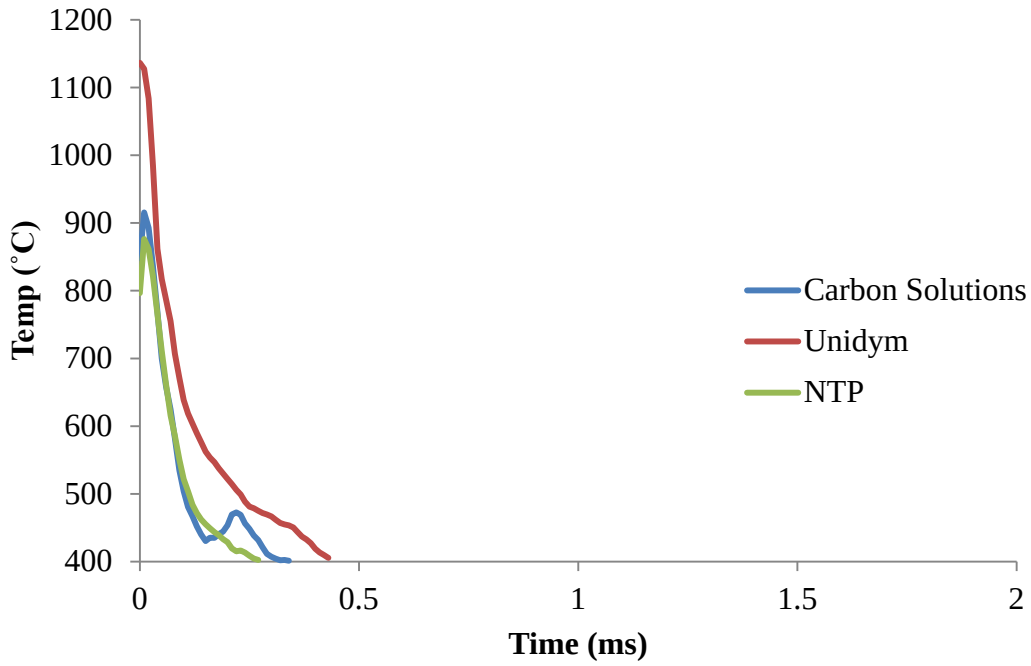

Figure 4.14: Comparison of the initiation of three different brands of SWCNTs. Carbon Solutions (~35wt% Ni/Y), Unidym (~35wt% Fe) and NTP (<3wt% Fe).

This result suggests that iron catalyst is favourable for light initiation over nickel/yttrium, and that a higher residual weight percentage is more favourable. However, other properties may affect results which have not been investigated. For example, the length of individual nanotubes for the Unidym sample was 0.1-1.0µm compared to 0.5-3.0µm for Carbon Solutions and 2-5µm for NTP. Reactivity may be increased for smaller nanotubes. Additionally, the ratio of semiconducting to metallic nanotubes in each sample was not examined.

Samples of Carbon Solutions, Unidym and NTP brand SWCNTs were prepared with ferrocene (1:2, 10mg total) and initiated with the laser at 152mJ. The results are presented in Figure 4.15 at two different x-axis scales to examine both the initial reaction (2ms) and the total reaction (100ms).

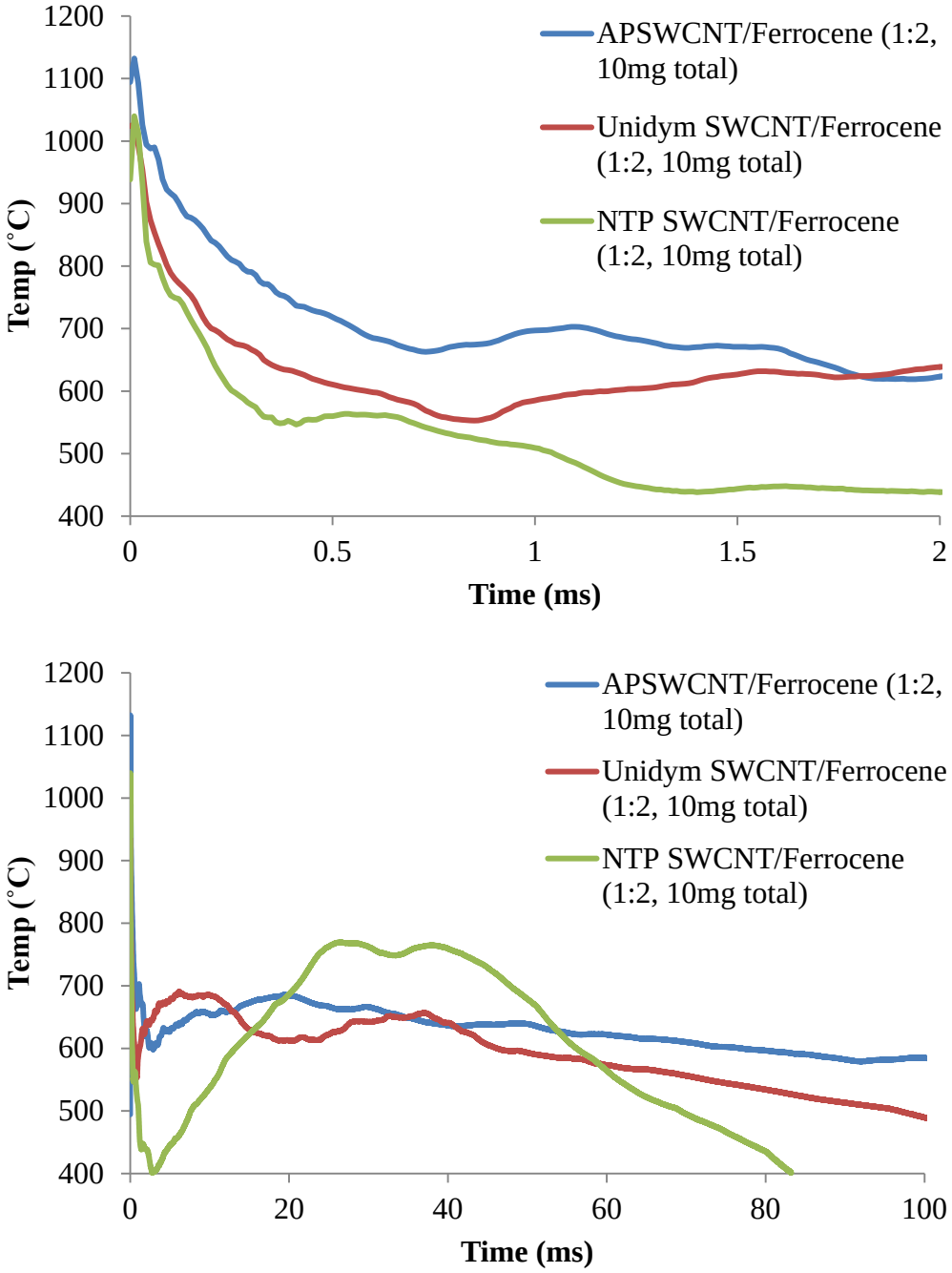

Figure 4.15: Laser initiation of APSWCNT/ferrocene (1:2, 10mg total) compared to Unidym and NTP SWCNT/ferrocene (1:2, 10mg total) displaying a 2ms scale (top) to see the initial reaction and a 100ms scale (bottom) to show the complete reaction.

The Carbon Solutions sample displayed the highest initial temperatures at 1130˚C compared to 1030˚C for Unidym and NTP samples. The Carbon Solutions nanotubes also maintained the most heat, remaining above 600˚C while Unidym and NTP dropped to 550˚C and 400˚C respectively. The NTP sample

contains the least amount of metal nanoparticles so there are far less hot metal parts in the sample compared to the other two samples. Total reaction time for the Unidym nanotubes was 125ms, which is comparable to the Carbon Solutions reaction. Two clear peaks are visible in the Unidym reaction which may be due to the oxidation of iron from leftover catalyst and from ferrocene respectively.

4.5: Single-Walled and Multi-Walled Carbon Nanotubes

Multi-walled carbon nanotubes (MWCNTs) have been reported to not ignite from a light source.[1,4] Conversely, there are also reports of MWCNTs successfully igniting by a light source.[3,25] It appears that the ability of MWCNTs to absorb heat is lower than for SWCNTs due to their multiple walls.[2,3] SWCNTs have a reported thermal conductivity of 3500W/K.m[26] compared to 3000W/K.m for MWCNTs[27] which may increase their sensitivity to light ignition.

A sample of NTP brand MWCNTs (containing Fe<3%) (10mg) was initiated by the laser at 152mJ and compared to APSWCNTs in Figure 4.16. The initial temperature reached is higher for the MWCNT sample and the overall ignition lasted longer than the APSWCNT. It was previously found that NTP MWCNTs do not ignite from a flash unit.[4] It can be postulated that the sensitivity of MWCNTs to light initiation is lower than for SWCNTs, but above a threshold energy (not investigated here) they ignite as effectively as SWCNTs. The NTP MWCNTs ignited at a higher temperature than the NTP SWCNTs (Figure 4.14). The reason for this has not been determined.

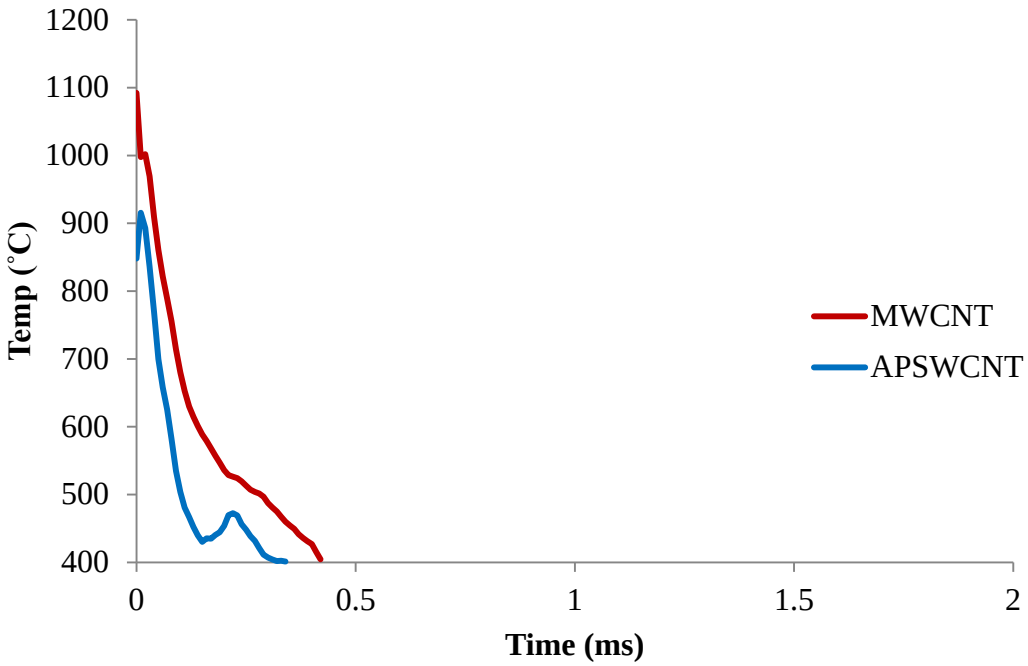

Figure 4.16: Laser initiation of a sample of NTP MWCNTs (10mg) compared to APSWCNTs (10mg).

A sample of MWCNT/ferrocene (1:2, 10mg total) was prepared and initiated by the laser. The results are shown in comparison to APSWCNT/ferrocene (1:2, 10mg total) in Figure 4.17 at two different x-axis scales to examine the initial and total reactions.

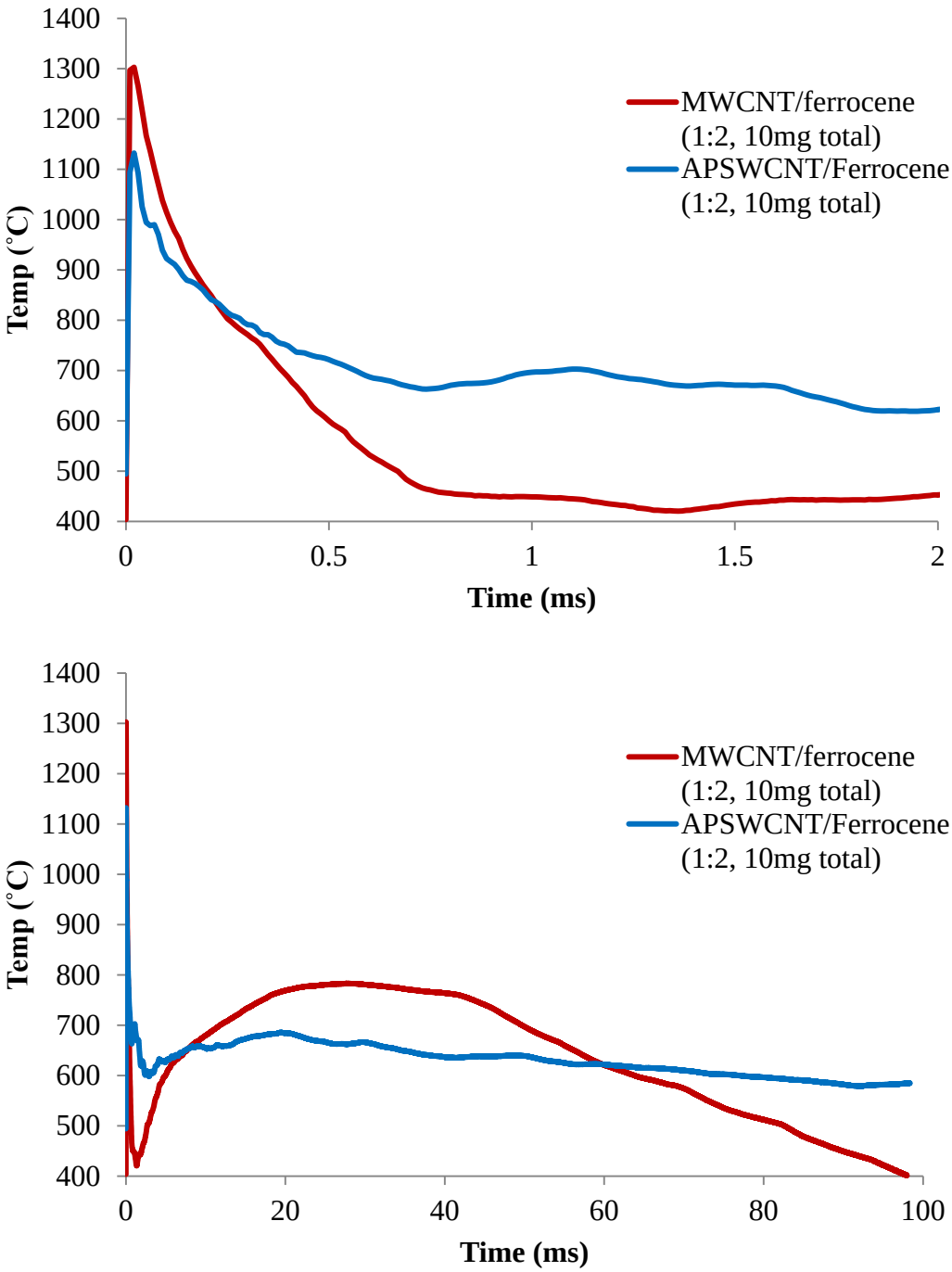

Figure 4.17: Laser initiation of NTP MWCNT/ferrocene (1:2, 10mg total) compared to APSWCNT/ferrocene (1:2, 10mg total) displaying a 2ms scale (top) to see the initial reaction and a 100ms scale (bottom) to show the complete reaction.

The initial temperature for the MWCNT sample is much higher than the APSWCNT sample. However, in the MWCNT sample the temperature rapidly drops to ~400˚C at 1.4ms. This is more drastic than the drop in temperature with

APSWCNT/ferrocene samples which may be due to the residual metal catalyst in the samples. The MWCNTs contain <3wt% iron as a catalyst which means there are a lot less potential hotspots in the sample than for APSWCNTs which contain ~35wt% Ni/Y catalyst, so the ability to retain more heat is greater for the APSWCNT sample. A similar trend in the NTP SWCNTs (Figure 4.15) suggests that the result is not from a difference in reaction between single and multi-walled carbon nanotubes. The existence of the strong secondary reaction in the MWCNT sample still suggests that there is enough energy to ignite the sample and oxidize the ferrocene.

The secondary peak produced from the ferrocene oxidation is higher in the MWCNT sample (800˚C) but it takes longer to reach, peaking at ~27ms. Due to the MWCNT/ferrocene reaction being hotter and consuming more of the sample at the peak, the total reaction time is shorter for the MWCNT sample than for the APSWCNT sample (<100ms compared to 130ms).

4.6: Thermogravimetric Analysis of Samples

Thermogravimetric Analysis (TGA) is a technique that measures mass loss as a sample is heated. This gives an indication of the purity of a sample since impurities will burn off at different temperatures, and it also shows the various components of a sample burning off at different temperatures.

Carbon Solutions APSWCNTs with ferrocene at various ratios is displayed in Figure 4.18 along with a comparison to raw APSWCNT and ferrocene alone. A sharp drop at ~180˚C is due to the sublimation of ferrocene.[12,13] In the (1:2) ratio sample, ferrocene sublimes at a lower temperature than any of the other samples or the raw material. This may suggest that at this ratio there is a greater extent of molecular interaction between nanotubes and

ferrocene than at other ratios causing it to react at a lower temperature. The raw nanotube sample shows 33.5% mass left at 1000˚C, which is the metal catalyst residue present as an oxide. This percentage is comparable to the manufacturer's specification of 35% residual catalyst within experimental error. Since ferrocene leaves very little residue at 1000˚C, as the portion of ferrocene in mixed samples is increased the mass percentage remaining decreases.

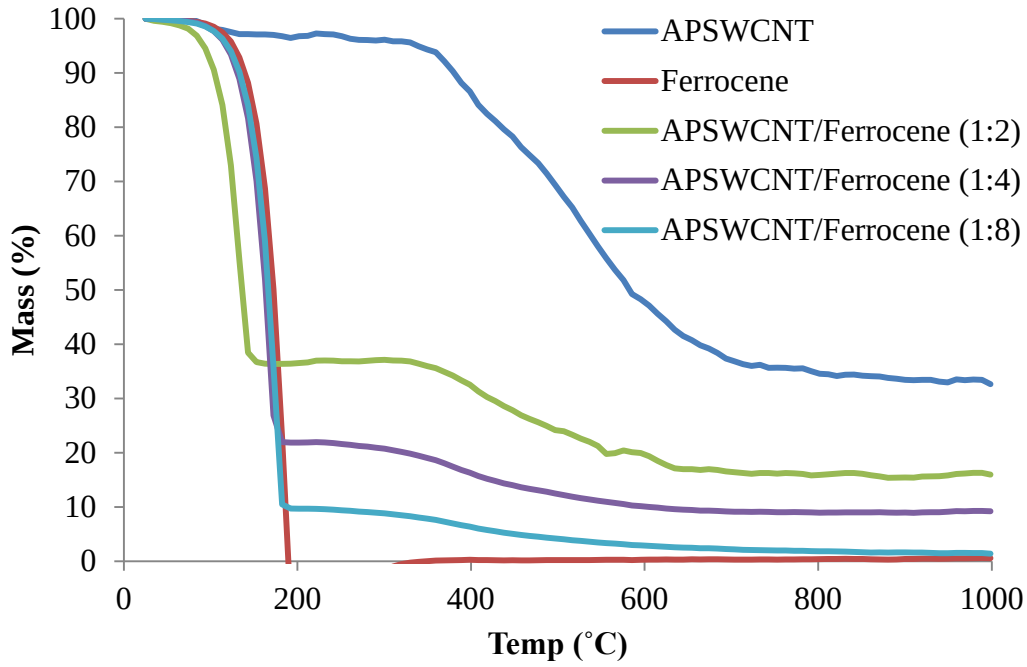

Figure 4.18: TGA results of Carbon Solutions APSWCNTs and ferrocene in various ratios and neat. Ferrocene sublimes at ~170˚C while other mass loss is carbon combustion.

A similar investigation was performed on NTP brand SWCNTs, the results are displayed in Figure 4.19. The NTP nanotubes appear to be the most pure sample with only 4.9% residual mass at 1000˚C due to the metal catalyst. In addition, the sharp drop in mass at ~465˚C means that all the organic matter is burning off at the same time which suggests that the NTP nanotube sample is very pure compared to the Carbon Solutions sample. Decomposition is significantly broadened when ferrocene is present at a (1:2) ratio, which may indicate an interaction between nanotubes and ferrocene which alters the decomposition of

the material.

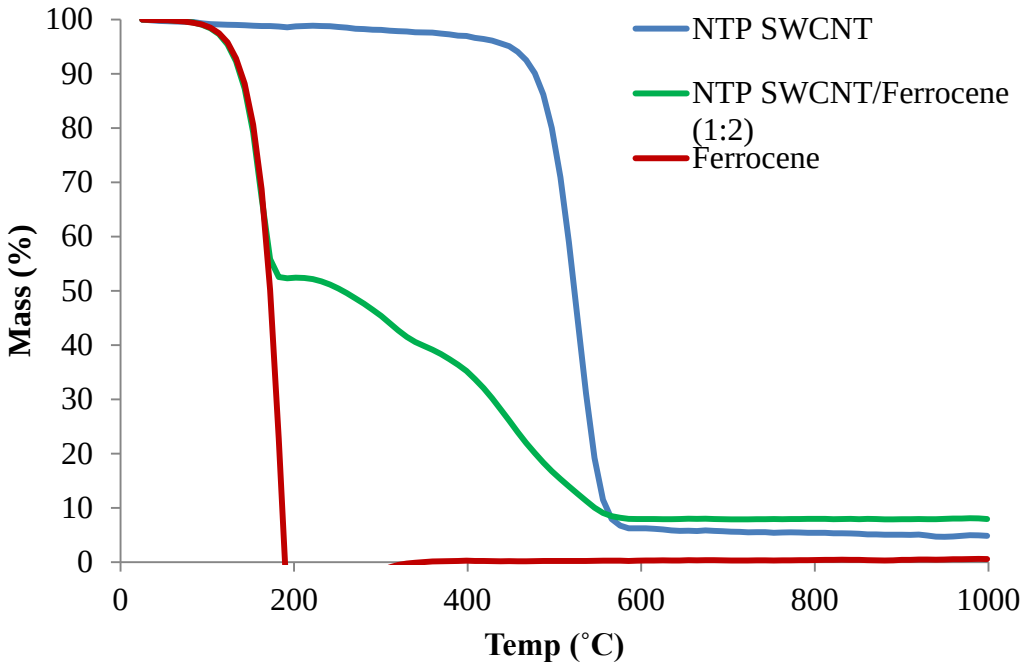

Figure 4.19: TGA results of NTP SWCNTs and ferrocene at (1:2) and neat. Ferrocene sublimes at ~170˚C while other mass loss is carbon combustion.

In this case, the remaining mass after ferrocene sublimation (at ~200˚C) is 52% compared to only 36.4% in the Carbon Solutions APSWCNT sample. Of a total sample of SWCNT/ferrocene (1:2), there is 33% SWCNTs and 66% ferrocene, so ferrocene has not completely sublimed in this sample. Rather, it shows that some of the ferrocene has attached to the SWCNTs and aided in the thermal degradation. This result may be enhanced here due to the residual catalyst in NTP nanotubes being iron rather than nickel/yttrium as in Carbon Solutions. Unidym SWCNTs were not available at the time when TGA was performed.

4.7: Chapter Conclusions

Reproducible results between samples were achieved. It was found that confining samples in glass sample vials restricted their ability to scatter thus maintained heat in the reaction better and allowed more complete combustion. Laser initiation was performed with input radiation at various wavelengths including 355nm, 532nm and 1064nm. The reaction rate and temperature at different input energy levels was examined. A lower energy of 65mJ was capable of initiating samples at 532nm indicating higher sensitivity to that wavelength, however, reaction with 1064nm was found to be more favourable for ignition due to higher temperatures realised. Increasing the energy up to 152mJ increased the reaction rate.

Various ratios of nanotube/ferrocene were investigated and it was determined that a 1:2 ratio was optimal for laser initiation of samples. A mechanism for the effect of ferrocene on nanotubes igniting was proposed. This mechanism was based on the catalytic soot reduction that ferrocene is capable of via a carbothermic reduction around iron oxide nuclei.

Several different brands of SWCNTs were investigated and comparisons were made between their reactions with respect to the type of residual metal catalyst and weight percentage. Nickel/yttrium (35%) containing nanotubes were compared to iron (<3% and 35%) and the higher percentage of catalyst produced a better ignition. Nanotubes with iron were found to react at higher temperatures than the Carbon Solutions nanotubes with Ni/Y. However, the Carbon Solutions nanotubes produced a better reaction when combined with ferrocene.

Comparisons were made between single-walled and multi-walled nanotubes with no reduction in reaction from the MWCNT sample suggesting that

with enough input light energy, MWCNTs ignite as well as SWCNTs. The directly comparable NTP MWCNTs showed a better ignition than the NTP SWCNTs. Evidently, more variables influence the ignition of nanotubes than have been investigated here.

Concluding the standard experiment for reproducibility, a method was determined. Laser initiation experiments performed best when samples were loosely confined in glass sample vials to reduce particle scattering, this method was maintained throughout the rest of this thesis. Infrared (1064nm) laser was determined to be the appropriate wavelength going forward with the input energy at ~150mJ. Carbon Solutions APSWCNTs were chosen as the standard brand of nanotube and it was determined that, when combined with ferrocene, a ratio of 1:2 was optimal.

4.8: References

1 Ajayan, P. M. *et al.*, Nanotubes in a Flash--Ignition and Reconstruction. *Science* **296** (5568), 705- (2002).

2 Smits, Jan *et al.*, Response of Fe Powder, Purified and as-Produced HiPCO Single-Walled Carbon Nanotubes to Flash Exposure. *Materials Science and Engineering A* **358** (1-2), 384-389 (2003).

3 Tseng, Shih H. *et al.*, Ignition of Carbon Nanotubes Using a Photoflash. *Carbon* **45** (5), 958-964 (2007).

4 Malec, Christopher, The Use of Carbon Nanotubes as an Energetic Material Initiator, Honours Thesis, Flinders University, 2008.

5 Malec, Christopher D., Voelcker, Nicolas H., Shapter, Joseph G., and Ellis, Amanda V., Carbon Nanotubes Initiate the Explosion of Porous Silicon. *Materials Letters* **64** (22), 2517-2519 (2010).

6 Kasper, M. *et al.*, The Influence of Fuel Additives on the Formation of Carbon During Combustion. *Journal of Aerosol Science* **30** (2), 217-225 (1999).

7 Mitchell, J. B. A., Smoke Reduction from Burning Crude Oil Using Ferrocene and Its Derivatives. *Combustion and Flame* **86** (1–2), 179-184 (1991).

8 Ritrievi, K. E., Longwell, J. P., and Sarofim, A. F., The Effects of Ferrocene Addition on Soot Particle Inception and Growth in Premixed Ethylene Flames. *Combustion and Flame* **70** (1), 17-31 (1987).

9 Howard, Jack B. and Kausch Jr, William J., Soot Control by Fuel Additives. *Progress in Energy and Combustion Science* **6** (3), 263-276 (1980).

10 Bonczyk, P. A., Effect of Ferrocene on Soot in a Prevaporized Iso-Octane/Air Diffusion Flame. *Combustion and Flame* **87** (3–4), 233-244 (1991).
11 Matter, U and Siegmann, K, The Influence of Particle Filter and Fuel Additives on Turbo Diesel Engine Exhaust. *Journal of Aerosol Science* **28** (1001), 51-52 (1997).
12 de Souza, A. C., Pires, A. T. N., and Soldi, V., Thermal Stability of Ferrocene Derivatives and Ferrocene-Containing Polyamides. *Journal of Thermal Analysis and Calorimetry* **70** (2), 405-414 (2002).
13 Harada, Akira, Hu, Ying, Yamamoto, Shyoko, and Takahashi, Shigetoshi, Preparation and Properties of Inclusion Compounds of Ferrocene and Its Derivatives with Cyclodextrins. *Journal of the Chemical Society, Dalton Transactions* (3), 729-732 (1988).
14 O'Connell, Michael J. *et al.*, Band Gap Fluorescence from Individual Single-Walled Carbon Nanotubes. *Science* **297** (5581), 593-596 (2002).
15 Reich, S., Thomsen, C., and Ordejón, P., Electronic Band Structure of Isolated and Bundled Carbon Nanotubes. *Physical Review B* **65** (15), 155411 (2002).
16 Hartschuh, Achim *et al.*, Single Carbon Nanotube Optical Spectroscopy. *ChemPhysChem* **6** (4), 577-582 (2005).
17 Jolly, William L., *The Synthesis and Characterization of Inorganic Compounds*. pp. 487 (Englewood Cliffs, N.J., Prentice-Hall, Englewood Cliffs, N.J., 1970).
18 Kaplan, Louis, Kester, William L., and Katz, Joseph J., Some Properties of Iron Biscyclopentadienyl. *Journal of the American Chemical Society* **74** (21), 5531-5532 (1952).
19 Wilkinson, Geoffrey, Rosenblum, M., Whiting, M. C., and Woodward, R. B., The Structure of Iron Bis-Cyclopentadienyl. *Journal of the American Chemical Society* **74** (8), 2125-2126 (1952).
20 Scott, Donald R. and Becker, Ralph S., Comprehensive Investigation of the Electronic Spectroscopy and Theoretical Treatments of Ferrocene and Nickelocene. *The Journal of Chemical Physics* **35** (2), 516-531 (1961).
21 Itkis, M. E. *et al.*, Purity Evaluation of as-Prepared Single-Walled Carbon Nanotube Soot by Use of Solution-Phase near-Ir Spectroscopy. *Nano Letters* **3** (3), 309-314 (2003).
22 Maser, W. K. *et al.*, Elaboration and Characterization of Various Carbon Nanostructures. *Synthetic Metals* **81** (2-3), 243-250 (1996).
23 Bockrath, Bradley *et al.*, Igniting Nanotubes with a Flash. *Science* **297** (5579), 192-193 (2002).
24 Braidy, Nadi, Botton, Gianluigi A., and Adronov, Alex, Oxidation of Fe Nanoparticles Embedded in Single-Walled Carbon Nanotubes by Exposure to a Bright Flash of White Light. *Nano Letters* **2** (11), 1277-1280 (2002).
25 Choi, Wonjoon *et al.*, Chemically Driven Carbon-Nanotube-Guided Thermopower Waves. *Nat Mater* **9** (5), 423-429 (2010).
26 Pop, Eric *et al.*, Thermal Conductance of an Individual Single-Wall Carbon Nanotube above Room Temperature. *Nano Letters* **6** (1), 96-100 (2005).
27 Kim, P, Shi, Li, Majumdar, A, and McEuen, PL, Thermal Transport Measurements of Individual Multiwalled Nanotubes. *Physical Review Letters* **87** (21), 215502 (2001).

Chapter 5: Novel Techniques and Additives

Chapter 4 investigated many variables with respect to carbon nanotube laser ignition and determined standard experimental parameters. In Chapter 5, more novel additives to nanotubes are investigated such as oxidizers and fuel sources to attempt to enhance the light initiated reaction. Modification of carbon nanotubes is performed by purification of a sample. Ordered samples of nanotubes are investigated by horizontally aligning nanotubes on a glass surface and by growing vertically aligned arrays of nanotubes.

5.1: Metal Nanoparticles

It has been proposed in the literature that the residual metal catalyst left in carbon nanotubes after growth plays a crucial role in the light initiation mechanism and process.[1-4] This has been investigated by initiating metal nanoparticles with the camera flash unit (Chapter 3.2) and with the laser. Iron nanoparticles (26nm) were chosen since they readily oxidize and are commonly used as catalysts for CNT growth. Nickel nanoparticles (20nm) were also investigated as they are the primary catalyst in Carbon Solutions nanotubes. Figure 5.1 displays the laser ignition of pure iron and nickel nanoparticles (10mg each sample) at 150mJ as well as Carbon Solutions as-prepared single-walled carbon nanotubes (APSWCNT) as a comparison.

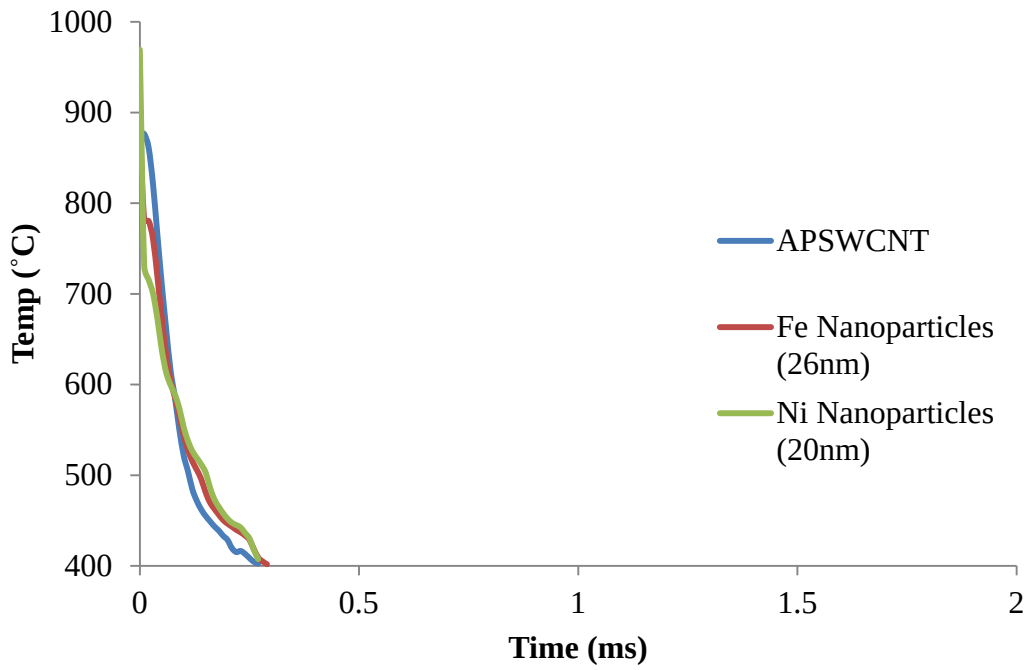

Figure 5.1: Laser ignition characteristic of iron (26nm) and nickel (20nm) nanoparticles compared to APSWCNTs.

The temperature profile of all three samples is very similar. However, visually, the nanotubes exhibit a bright flash of light as they ignite and burn. The nanoparticles alone do not display such behaviour, most likely due to a lack of fuel to combust. Residual iron nanoparticles were observed to change colour from black to orange upon light initiation, pictured in Figure 5.2. This is due to the oxidation of iron into iron oxide. Nickel nanoparticles changed colour from black to grey. The most common nickel oxide is green or black, indicating that rather than significant oxidation much of the reaction could be the fusing of nickel nanoparticles into larger nickel particles, though oxidation is still expected.

Figure 5.2: Photograph of iron nanoparticles (26nm) after camera flash unit initiation displaying an orange colour due to oxidation. (Reproduced from Chapter 3.2)

From these results, it is possible that metal nanoparticles could initiate the ignition of other materials since their temperature profile is similar to APSWCNTs. However, a close contact between materials would be required to facilitate a transfer of thermal energy since combustion does not appear to occur.

5.2: Cut and Purified Nanotubes

It has been reported that purified nanotubes either do not ignite at all from light initiation or at least show a much lower sensitivity compared to unpurified samples.[3-6] This was thought to be a combination of two factors; less residual catalyst to ignite and greater density in the nanotube bundles allowing easier heat transfer and dissipation rather than localised hotspots.

A sample of Carbon Solutions APSWCNT was purified as detailed in Chapter 2.3. This process purifies the nanotubes by removing the amorphous carbon and the metal catalyst particles. In the process it also cuts the nanotubes to a shorter length and adds defect sites and functionality to nanotubes.[7-9] A final result of the vacuum filtration process is that the previously ‘fluffy’ sample is

extracted as a thin, brittle wafer. This meant it could not be powder-mixed with other materials. The purified sample was ignited by the laser at 150mJ and compared to a 'fluffy' sample of APSWCNT in Figure 5.3. Contrary to the literature,[3-5] the purified sample ignited at least as well as the APSWCNT sample. The total ignition time is very similar and the initial temperature is ~80ºC higher for the purified sample. This particular APSWCNT sample exhibited a secondary peak at 0.22ms. This does not occur all the time in the absence of ferrocene but may indicate a delay in the reaction of the nanotubes and the subsequent heating and oxidation of catalytic metal nanoparticles in the sample. This secondary reaction did not occur with any filtered samples since they no longer contain metal catalyst particles.

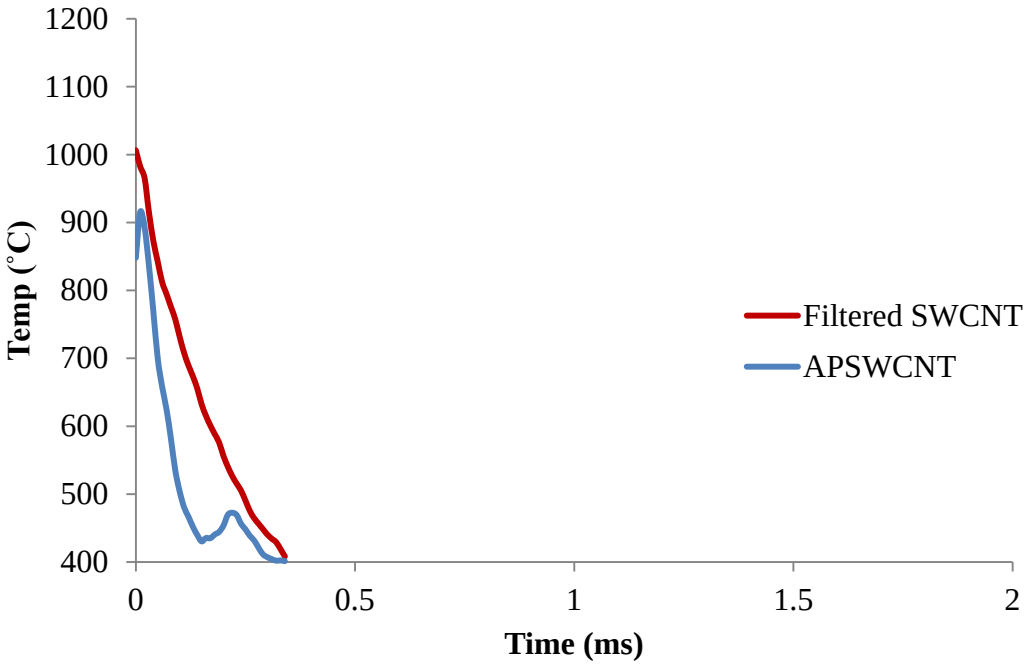

Figure 5.3: Laser initiation of filtered and purified SWCNT compared to APSWCNTs.

This result contradicts the literature that purified samples do not initiate. It also contradicts the finding in Chapter 4.4 that NTP SWCNTs were less reactive due to the lower catalyst content. The increased functionality of the purification

process here may lead to greater reactivity. Future investigations are required to properly understand this.

5.3: Addition of Oxidizer to Carbon Nanotubes

Addition of oxidizers and fuels to nanotubes to enhance their light ignition presents a range of possibilities. Ferrocene as a fuel has been reported in Chapter 4.2 of this thesis and in the literature.[4] Malec *et al*. have added sodium perchlorate to MWCNT/ferrocene mixtures and loaded them on explosive porous silicon for ignition via a photoflash.[6]

Experiments were performed to test the addition of sodium perchlorate ($NaClO_4$) and potassium nitrite (KNO_2) to nanotube samples. Both materials are strong oxidizers and KNO_2 in particular is often used to accelerate the combustion of materials.

Both oxidizers were separately mixed with samples of APSWCNTs in a ratio of nanotube/oxidizer (1:2, 10mg total). Samples were initiated via laser pulse at 150mJ, the results are displayed in Figure 5.4. The initial temperature for the KNO_2 mixture was significantly lower (700˚C) than the other samples suggesting it may have reflected some of the laser beam or aided in heat dissipation. The $NaClO_4$ mixture initiated with the same temperature as APSWCNTs but no enhancement of the reaction was evident.

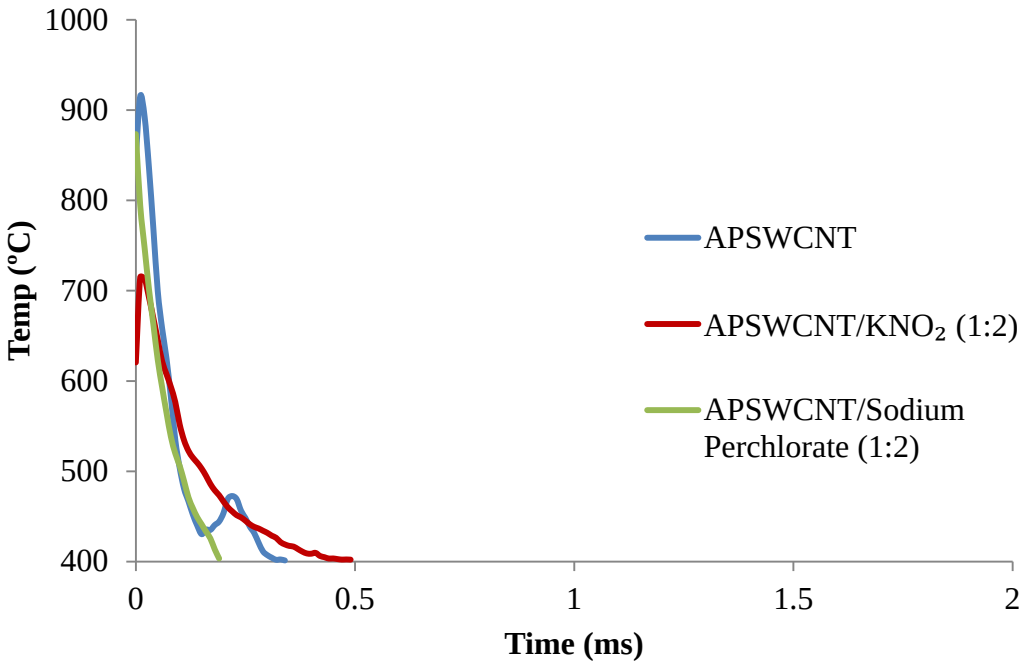

Figure 5.4: Ignition of APSWCNT mixed with potassium nitrite and sodium perchlorate respectively at a ratio of (1:2).

It was found by Malec *et al*. that the optimal ratio of APSWCNT/$NaClO_4$ was 1:6.[6] This ratio was used in addition to ferrocene in a sample for a mixture of APSWCNT/ferrocene/$NaClO_4$ (1:2:6, 18mg total) to utilise the optimal ratio of both additives. The results are displayed in Figure 5.5 with comparison to APSWCNT/ferrocene (1:2, 10mg total). The overall reaction time was shorter at 90ms with oxidizer compared to 128ms without, suggesting that the material gets consumed faster. A lower initial temperature was observed with $NaClO_4$, and before the secondary peak the temperature drops to 400˚C. With sodium perchlorate present, a clear peak is seen at 65ms. Since the first peak was attributed to ferrocene based on the delay time it is reasonable to assume that the second peak is a reaction from the $NaClO_4$. A 65ms response is too slow for practical use in an explosive initiating device.

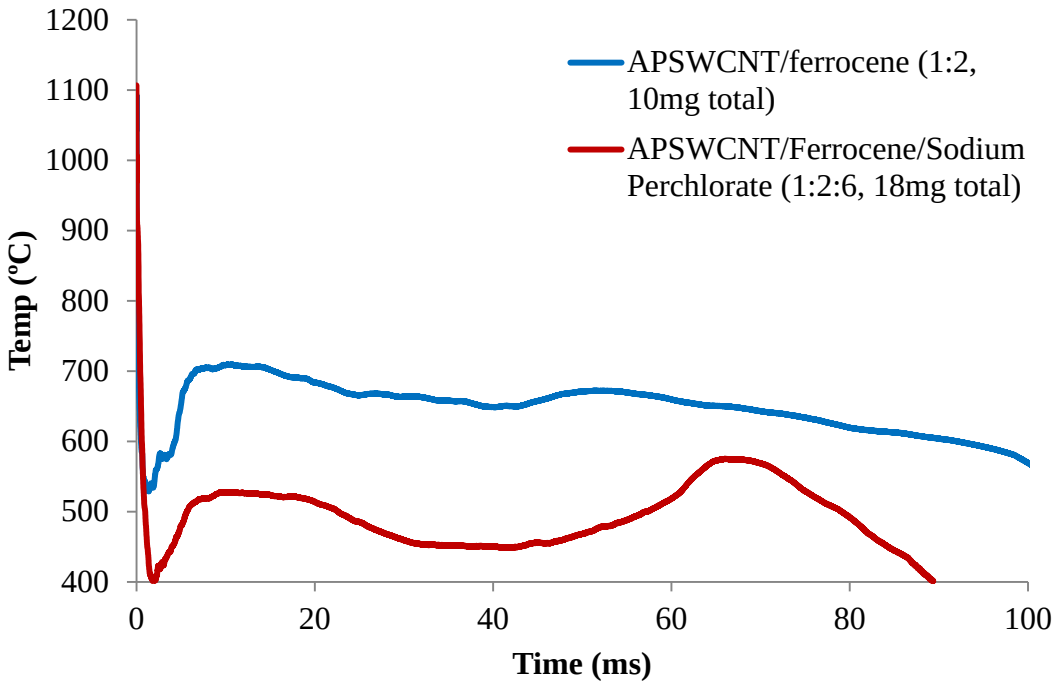

Figure 5.5: Laser initiation of a sample of APSWCNT/ferrocene/sodium perchlorate (1:2:6, 18mg total) displaying two ignition peaks. Firstly for ferrocene igniting, and secondly for the sodium perchlorate igniting. APSWCNT/ferrocene (1:2, 10mg total) is displayed as a comparison.

Overall, some enhancement in the overall reaction is achieved with oxidizer present. A larger flame was observed and a stronger combustion occurred. However, the delay in the extra reaction makes it impractical for the goals of this thesis.

5.4: Polymer Wrapping Around Carbon Nanotubes

One alternative to add more fuel and oxygen into the system is by wrapping APSWCNT in polystyrene sulfonate (PSS). PSS is a polymer with the structure shown in Figure 5.6. It is easy to wrap around carbon nanotubes and potentially provides more fuel to the reaction. The SO_3^- group also adds extra oxygen into the system.

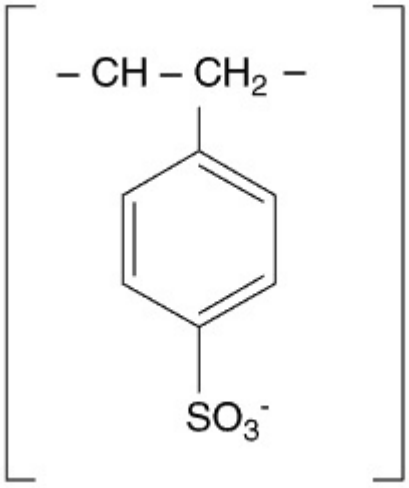

Figure 5.6: Chemical structure of polystyrene sulfonate.

APSWCNT (10mg) and PSS (20mg) were added to distilled water (50mL) and sonicated at room temperature for 10 minutes. This process separates the bundles of nanotubes into individual tubes, cuts them and wraps them in PSS. Proof of successful chemical attachment is demonstrated by the nanotubes remaining suspended in water indefinitely when carbon nanotubes are normally insoluble in water.[10] The solution was vacuum filtered through a 0.4µm polytetrafluoroethylene (PTFE) membrane. The membrane and nanotubes were then oven dried at 80˚C for 24 hours prior to use. In addition to adding fuel and oxygen to the reaction, it was thought that spacing the nanotubes with a polymer would create localized hotspots in the sample upon exposure to the laser and not allow the nanotubes to disperse heat as easily.[5]

As a control to investigate the effect of the nanotubes being wrapped in PSS, the dry monomer was mixed with a dry sample of APSWCNT without chemical wrapping and ignited to compare. The results are displayed in Figure 5.7. PSS was also laser initiated on its own to see if any reaction occurred. Figure 5.7 shows that it heats up to 650˚C from the laser but rapidly cools and no ignition of the material was observed.

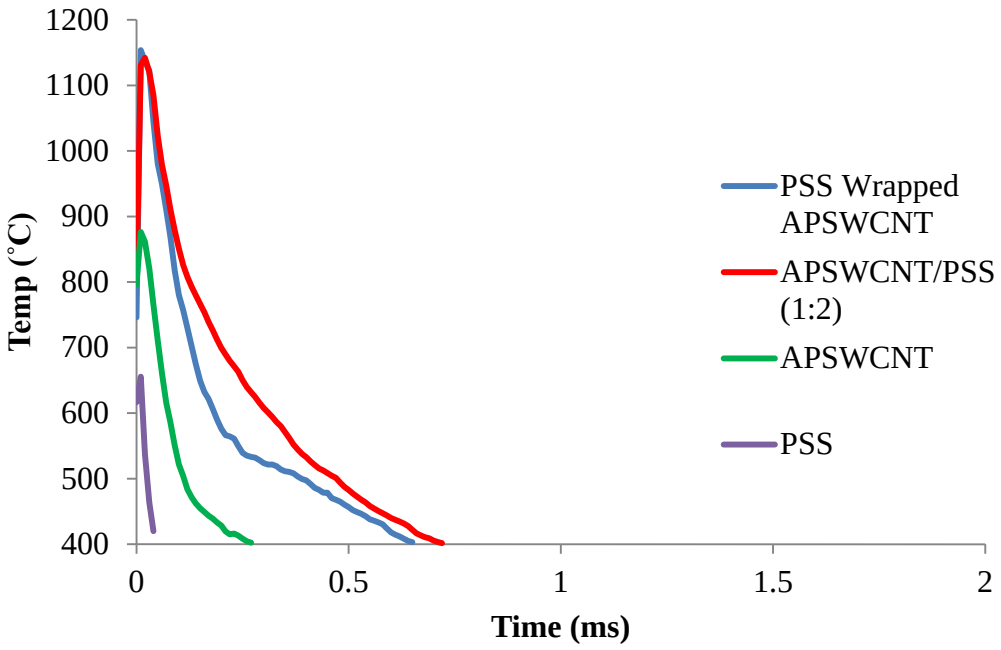

Figure 5.7: Laser ignition results of APSWCNT wrapped in polystyrene sulfonate and the monomer dry mixed with APSWCNT compared to the raw chemicals.

A much higher initial temperature is observed when PSS is present in the nanotubes suggesting that light is transformed into heat more effectively. There appears to be little difference between PSS wrapped nanotubes and monomer mixed, with the simple mixing process showing a slightly higher temperature over the duration of the ignition. This is most likely because wrapping the nanotubes involves sonicating, which cuts them and may destroy some nanotubes.

As a fuel additive to carbon nanotubes, PSS does not burn as long or effectively as ferrocene, compared in Figure 5.8. CNT/ferrocene mixtures were shown to burn for >100ms and produce more flame and smoke from the reaction. Although both additives reached the same initial temperature, ferrocene released significantly more heat than PSS. This is because the iron content in ferrocene absorbs heat more effectively than the polymer material and oxidises which releases heat for a longer timeframe so it was concluded that ferrocene is a more effective additive.

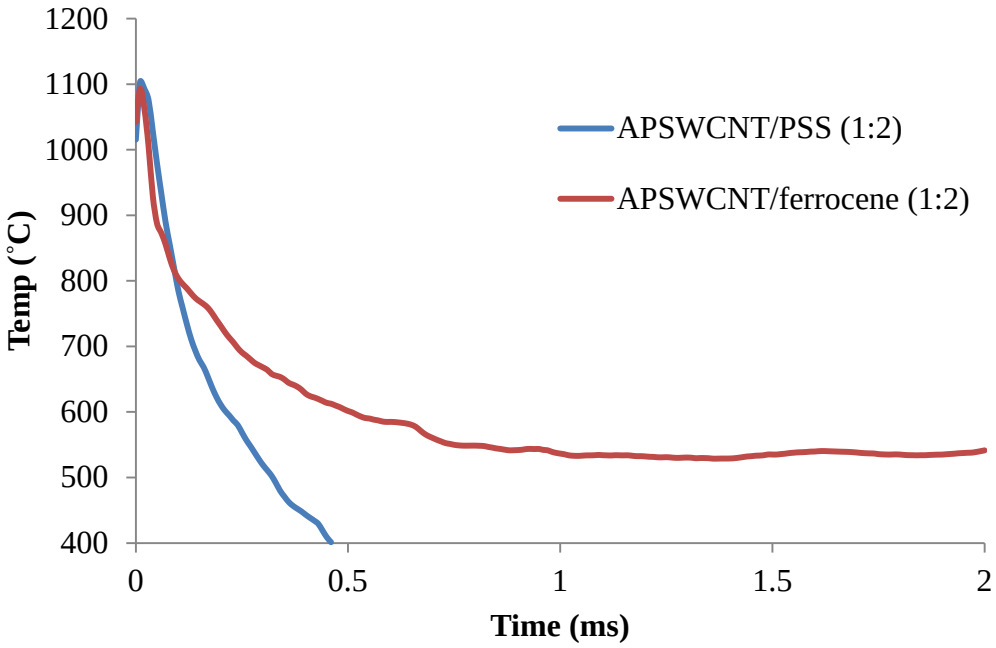

Figure 5.8: Comparison of the ignition of APSWCNT/ferrocene (1:2, 10mg total) and APSWCNT/PSS (1:2, 10mg total).

5.5: Horizontally Aligned Carbon Nanotubes

The potential propagation of energy into surrounding nanotubes has been investigated by making horizontally aligned carbon nanotube arrays on glass. Nanotubes are very good thermal conductors along their length[11-13] and they could potentially be used in fuse wire if they can propagate a light initiated reaction onto neighbouring nanotubes. Additionally, aligning nanotubes allows energy to transfer between them easier than when they are in their tangled 'fluffy' form due to their excellent thermal and electrical conductivity along their length.[14-19]

The arrays were produced by suspending APSWCNT (5mg) in dimethyl sulfoxide (DMSO) (20mL) - a polar aprotic solvent that is very effective in dispersing nanotubes. The horizontal nanotubes were then formed by evaporating the solution overnight at 80˚C. This created the 'coffee ring effect' which is a

capillary flow action induced by the edge evaporating faster than the middle of the solution.[20] As a result, nanotubes flow to the edge of the solution and align themselves on the glass. This produces rows of horizontally aligned nanotubes on the surface as photographed in Figure 5.9. The thickness and spacing of the rows can be somewhat controlled by the concentration of nanotubes in solution, thus it was observed that over the ~5cm tube photographed in Figure 5.9 the lines are spaced further and are lighter in colour towards the top of the tube before DMSO evaporated and increased the concentration of remaining SWCNTs resulting in closer and darker rows towards the bottom.

Figure 5.9: Horizontally aligned rows of carbon nanotubes on glass produced by the 'coffee cup effect' during evaporation.

Confocal Raman microscopy was performed on the horizontally aligned nanotubes to confirm their alignment. A Raman spectrum of the sample at a point on one of the rows of nanotubes is displayed in Figure 5.10. The RBM peak at 174cm^{-1} confirms that the nanotubes are single walled. The very low D-band peak at 1345cm^{-1} indicates a high purity of SWCNT since mainly the nanotubes align

with the evaporation edge while the amorphous carbon impurities deposit mostly between the nanotube rings and on the bottom of the container.

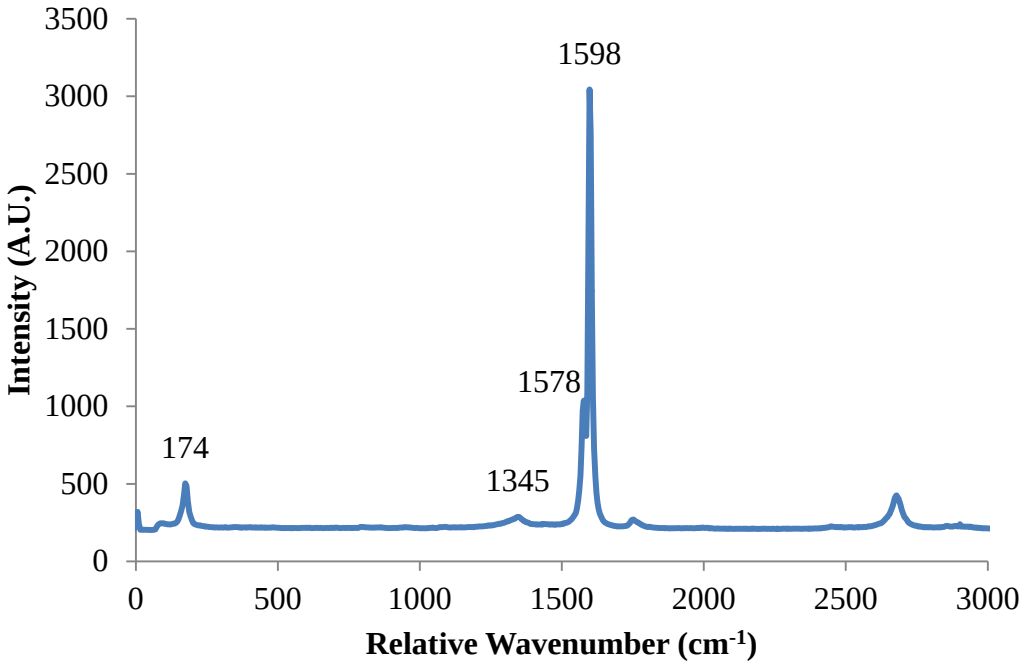

Figure 5.10: Raman spectrum of horizontally aligned SWCNTs on glass displaying a high purity as a result of the very low D-band (1345cm^{-1}).

An optical microscopy image is shown in Figure 5.11. A row of the nanotube array is seen horizontally across the middle of the image. Bundles of nanotubes are aligned where the evaporation ring occurred with some amorphous carbon randomly oriented in other areas.

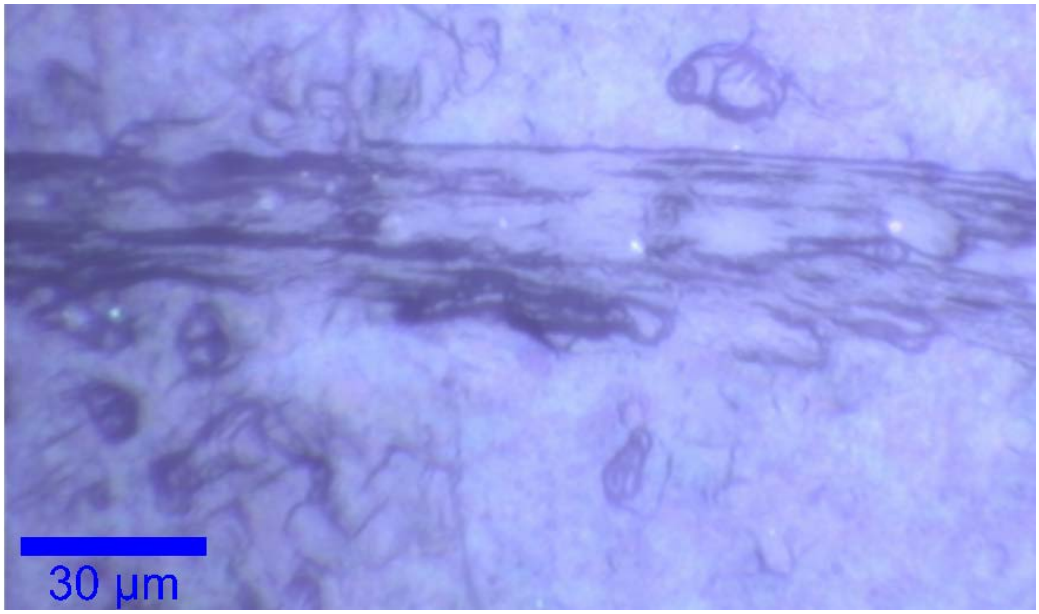

Figure 5.11: Optical microscopy image of horizontally aligned SWCNTs on glass.

From the optical image, a Raman intensity image of the G-band peak at 1598cm^{-1} was mapped. The image in Figure 5.12 shows intense horizontal lines where the carbon nanotube bundles are aligned and confirms the formation of horizontally aligned carbon nanotubes.

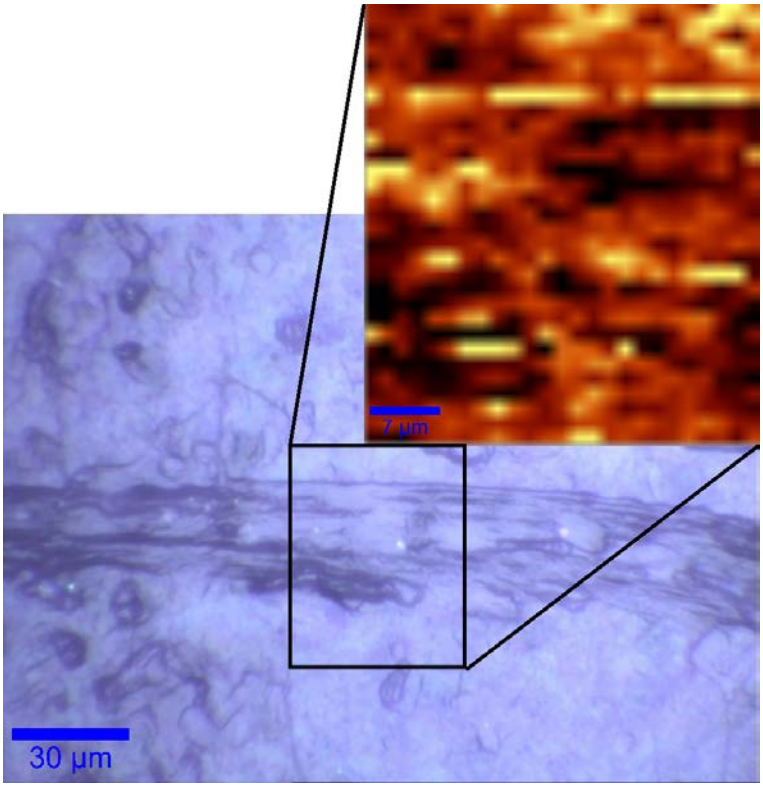

Figure 5.12: Optical microscopy image of horizontally aligned SWCNTs on glass. Inset: Raman intensity image of the 1598cm^{-1} carbon peak showing alignment of the array. Scale bar in the Raman image is 7µm.

A key difference between the aligned arrays and raw APSWCNT is that the amorphous carbon portion of the material does not tend to dissolve in DMSO as nanotubes do. Amorphous carbon floats on the surface and after evaporation, most is found at the bottom of the glass vessel. However, some parts stick to the walls and disrupt the line as observed near the top of the vessel in Figure 5.9. As a result, the horizontal arrays are purer than the tangled 'fluffy' powder.

Horizontally aligned nanotubes on glass will have a higher density than ‘fluffy’ APSWCNT since the bundles are pressed together as the solution dissolves. The surface layer is very thin so fewer nanotubes will be exposed to the laser spot. Figure 5.13 shows the laser ignition of the horizontally aligned sample compared to an as-prepared ‘fluffy’ nanotube sample. The temperature was below 600˚C for the aligned surface and only a small flash of light was observed during the ignition at the point where the laser spot hit. The sample was ablated off the

glass surface from the laser. Figure 5.14 shows an elliptic circle after the laser has hit the sample. There appears to be no propagation of the reaction past the spot of the laser so energy and reaction transfer has not successfully travelled along the lengths of the nanotubes.

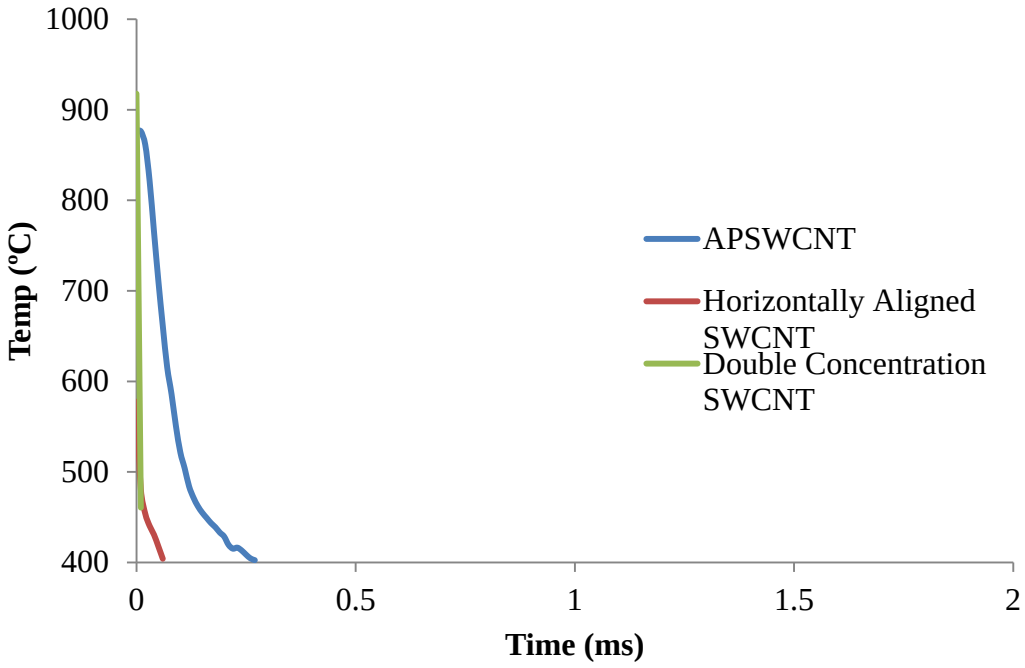

Figure 5.13: Laser ignition of horizontally aligned SWCNTs on glass at two concentrations and compared to 'fluffy' APSWCNT.

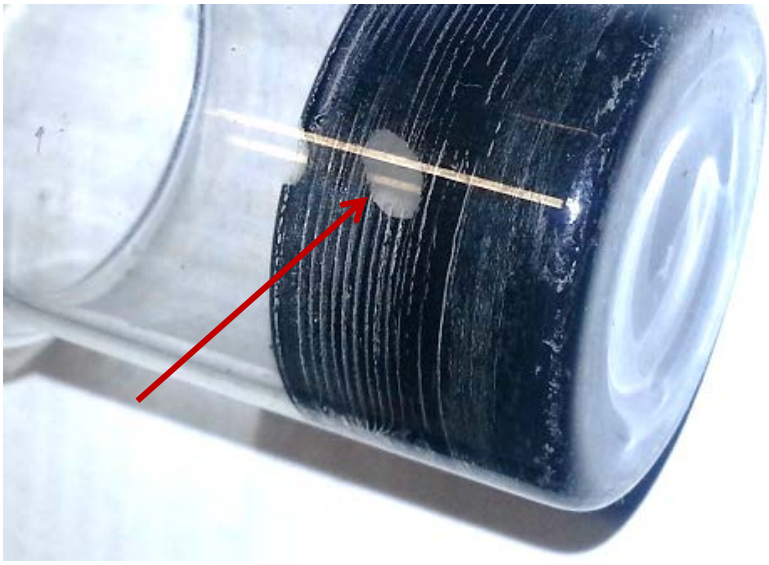

Figure 5.14: Photo of a horizontally aligned sample of SWCNTs after ignition by the laser showing an ablation spot where the laser hit the sample.

The concentration of the SWCNTs was doubled to examine the reaction of a thicker line of nanotubes. APSWCNTs (10mg) were suspended in DMSO (20mL) and evaporated at 80˚C. This produced a much thicker sample of aligned nanotubes, shown in Figure 5.15. The ignition result is displayed in Figure 5.13 and shows a higher initial temperature but very little reaction. This sample could disperse the heat more easily and not create the local hotspots required to ignite properly. The result suggests that a horizontally aligned sample facilitates better heat dispersal rather than heat transfer and propagated reaction.

In the timeframe of this reaction (<0.01ms) it is most likely occurring too fast for the maximum sensitivity of the pyrometer to collect complete data. Even the initial peak temperature was not observed on several samples and only a single data point was collected. An audible pop and visual flash were observed but it is difficult to tell if any ignition occurred or if the sample simply ablated off the surface. Finally, complete ablation did not occur with a single shot from the laser when the thickness of the nanotube layer was high. Figure 5.15 shows the sample after several laser shots on the same spot with incomplete ablation of the sample in that location.

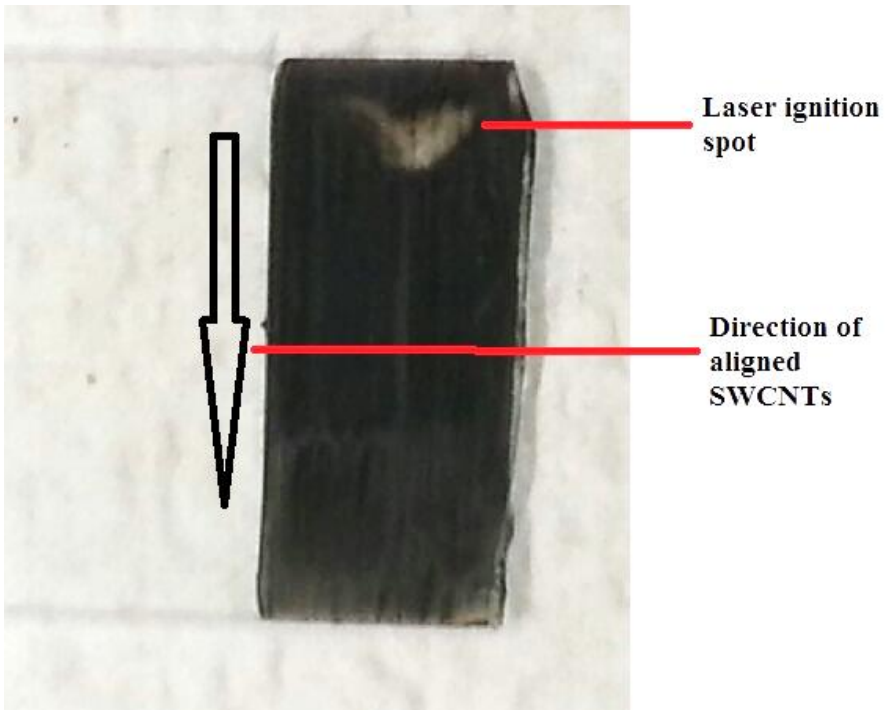

Figure 5.15: Horizontally aligned SWCNTs with double concentration of the original sample showing the spot where ignition and partial ablation occurred from the laser.

Another sample was prepared with ferrocene added. APSWCNTs (5mg), ferrocene (20mg) and DMSO (20mL) were subjected to the same sample preparation of horizontally aligned nanotubes described in this section. Ferrocene was added at a higher ratio (1:4) to ensure enough ferrocene was deposited with the carbon nanotubes during evaporation since the solubility of ferrocene is much higher.

The results of the sample ignition are shown in Figure 5.16 with comparison to the horizontally aligned sample and 'fluffy' APSWCNTs. Characteristic of the powder samples, the presence of ferrocene has caused a higher initial temperature, though it dropped rapidly to a secondary shoulder peak where ferrocene may have exothermally oxidized. Further reaction was most likely inhibited by the comparatively very small amount of sample in the aligned experiment and the rapid ablation. The sample has ignited and ablated at a higher

temperature than without ferrocene present, though it is still significantly weaker than the APSWCNT sample. A bright flash was observed upon initiation of the sample and the laser ablated the sample in the spot where it hit. No reaction outside the laser spot was observed.

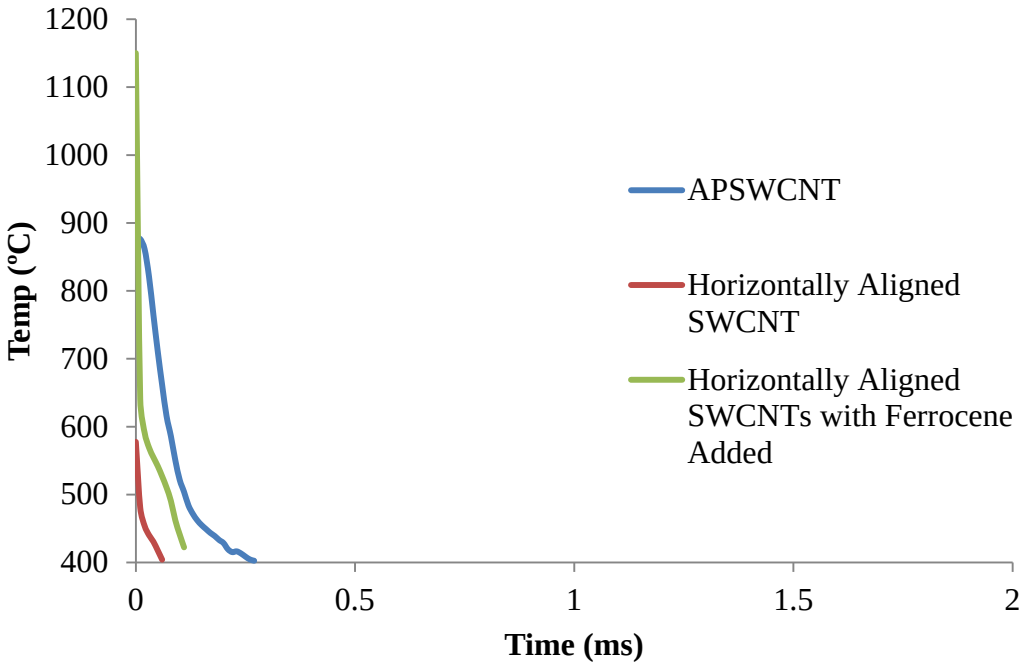

Figure 5.16: Laser initiation of horizontally aligned SWCNTs with ferrocene added compared to no ferrocene and APSWCNTs.

Results suggest that the horizontally aligned nanotubes do not ignite significantly and powder samples are more effective. It is expected that this is because there was only a small amount of sample exposed to the laser spot and removal of the sample from the glass (via ablation or vaporisation) occurs much faster than exothermic oxidation. Individual nanotubes are excellent thermal conductors along their length. The thermal diffusivity from one nanotube to another is much harder to realise and in these arrays there was no significant thermal diffusivity to neighbouring nanotubes that were not directly initiated by the laser beam despite the horizontal alignment.

5.6: Vertically Aligned Surface Bound CVD Grown Nanotubes

Multi-walled carbon nanotubes (MWCNTs) were grown via the Chemical Vapour Deposition (CVD) technique outlined in Chapter 2.4 on a silicon wafer with a sputtered layer of aluminium and iron. This growth method presents a range of differences when compared to the powder samples. Firstly, they are surface bound rather than free, which should reduce ablation from the laser and heat losses to kinetic energy. Secondly, growth of the nanotubes initiates from iron nanoparticles on the surface and as a result, residual catalyst is typically found at the base of the nanotubes only.[21,22] Thirdly and most significantly for this project, the process creates vertically aligned arrays of nanotubes on the surface, Figure 5.17. Since individual nanotubes are photoconductors and transfer light strongly along their length,[23-26] the laser beam directed from above the sample surface will travel down the length of the nanotubes rather than hitting a random array as with the powder samples. Further, the bulk thermal conductivity of aligned arrays of carbon nanotubes has been found to be higher than the thermal conductivity of randomly oriented carbon nanotubes.[27,28] Finally, these samples will be laser initiated on an optically active wafer of silicon/Al/Fe rather than glass which may enhance the reaction.

The alignment of nanotubes in regard to their sensitivity to light initiated ignition has never been previously investigated. There are smaller bundles and limited cross-linking of nanotubes in a vertical array so effective heat dissipation to the surrounds will be inhibited. The length of nanotubes produced by this method was in the range of 150-300µm, which is much longer than the Carbon Solutions APSWCNTs, quoted at 0.5-3.0µm by the manufacturer.

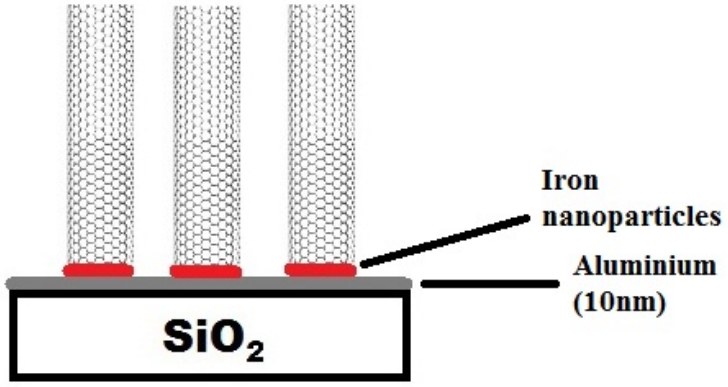

Figure 5.17: Schematic of CVD grown MWCNTs showing the vertically arrayed nature and the location of the catalyst nanoparticles.

Control of sample preparation in the CVD growth chamber is not fully realised yet so it is currently not possible to grow two samples exactly the same with our equipment. Nanotube densities on the surface and nanotube length were two properties that differed between samples. This somewhat limits exact reproducibility of results. However, general trends between samples were still observable. For this reason, samples of at least $2cm^2$ were prepared so one part of the sample could be ignited first as prepared before any modification to the sample was performed and analysis of the effect of surface modification could be made with the same nanotubes.

Figure 5.18 presents a comparison of three samples prepared in the same way but at different times. The samples were all initiated by the 1064nm laser at 150mJ. The average initial temperature was 1400˚C and total ignition time varied between 1.2ms and 1.8ms. Ignition of powder APSWCNTs is also shown as a comparison and much better results were observed with the surface bound nanotubes.

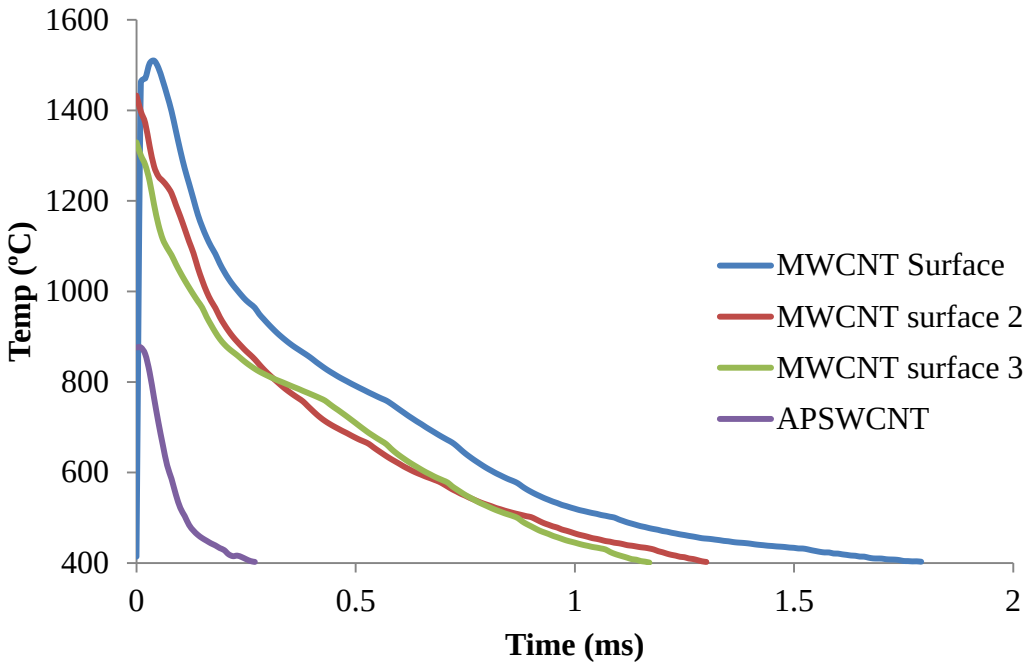

Figure 5.18: Comparison of the ignition of three samples of CVD grown vertically aligned MWCNTs with APSWCNT as a reference.

The vertical arrays of nanotubes appear to absorb light more efficiently since optically they are much darker than APSWCNTs. The much higher initial temperature achieved in Figure 5.18 compared to APSWCNTs also suggests that they convert the light into thermal energy more effectively. High speed video was recorded and frames are shown in Figure 5.19. The first photo is the first frame where ignition is apparent on the sample; a fireball has risen above the sample which disappeared within ~1.5ms. There was very little ablation and airborne particles for these samples. A small piece circled in red moving upwards from the surface was all that was observed. Compared to the powder samples where material scattered across the sample stage this is very minimal which would contribute to converting the light energy into thermal energy rather than dissipating it via kinetic energy. An audible pop was heard from the samples upon ignition from the laser.

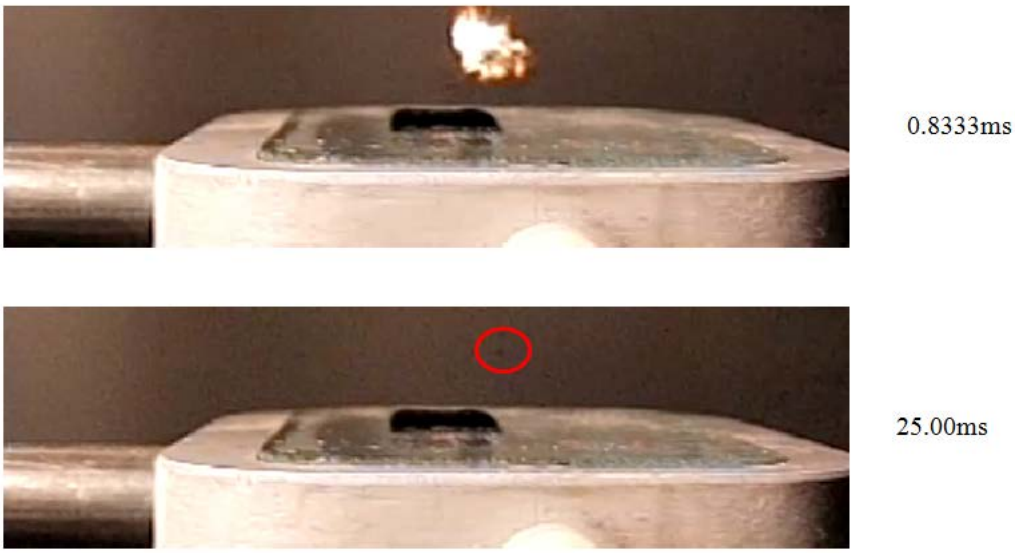

Figure 5.19: High speed video frames of laser initiation of MWCNT surface. Top: 1 frame after the laser initiation showing a small fireball above the sample. Bottom: 25ms after laser initiation with airborne material circled in red.

Complete ablation does not always occur in samples when hit by the laser beam which indicates complete combustion does not occur. Ignition appears to be very localised to the laser spot area, with a small region of damage around the central area, Figure 5.20. The same sample was initiated in the same place multiple times to test the sample degradation as shown in Figure 5.21. The second ignition was diminished somewhat, third and fourth were significantly reduced, and the sample showed no ignition after the fourth laser beam.

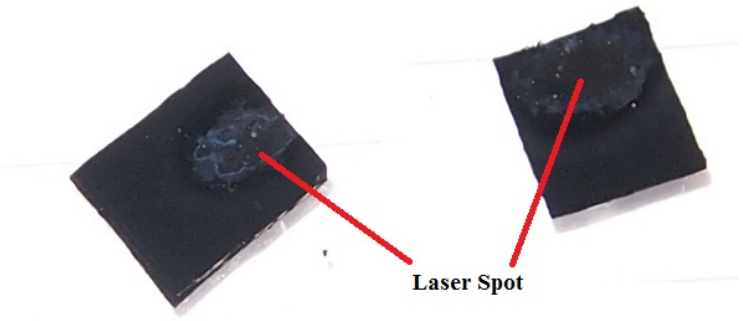

Figure 5.20: Photo of vertical MWCNT arrays after initiation by the laser showing the burnt spot where the laser beam hit the sample.

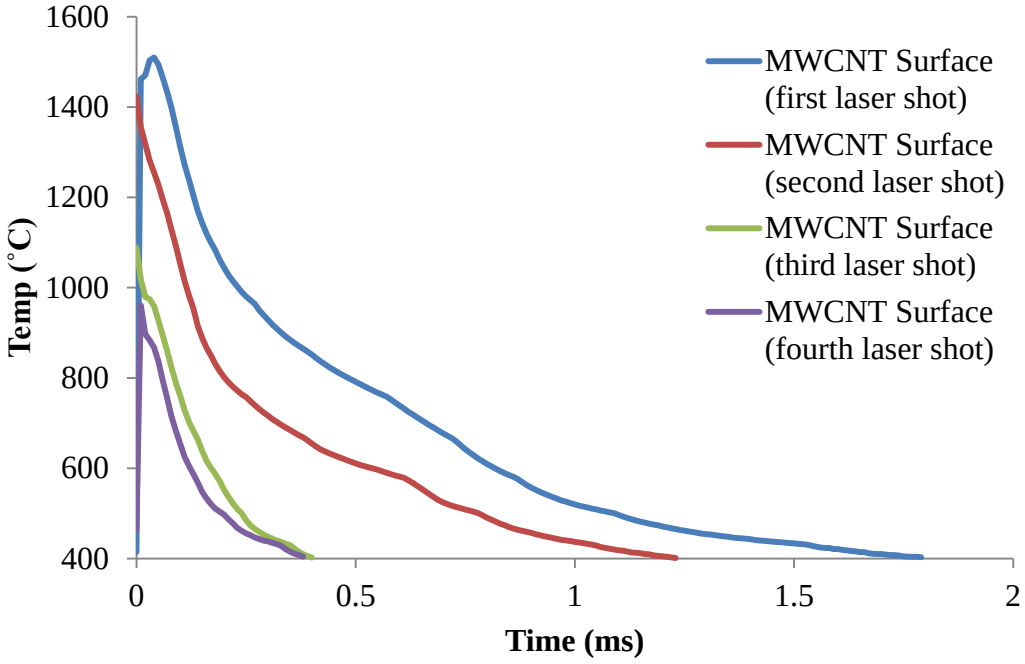

Figure 5.21: Laser initiation at 150mJ of the same MWCNT surface four times in succession displaying the lowering reaction as more of the sample is oxidized and ablated.

An optional step in the CVD growth is to sputter a 10nm layer of aluminium onto the silicon before adding the catalyst. This adds surface roughness to promote the formation of catalytic nanoparticles to grow nanotubes instead of agglomeration of the iron into larger non-catalytic pieces. It also puts a protective layer between the silicon and the catalyst to prevent silicon by-products

from forming with the catalyst. It was hypothesized that this nanoscale aluminium layer would also assist the ignition properties of the carbon nanotubes since aluminium has a high enthalpy of combustion and is often added to explosives to increase the energy yield.[29] Additionally aluminium nanopowders and oxide mixtures are increasingly being used as potential components in energetic material research.[30-33]

When exposed to air, the sputtered pure aluminium layer rapidly oxidizes to Al_2O_3. It was proposed that the temperature in the CVD furnace with a flow of argon would reduce the aluminium oxide back to aluminium then the carbon nanotube growth on top would prevent atmospheric oxygen from reaching the aluminium and oxidizing it. Carbothermal reduction of aluminium oxide at high temperatures in an inert gas is possible via a two-step process.[34] However, it is an energetically favourable reaction only above the melting point of aluminium (~700˚C) and requires temperatures up to 2500˚C for complete reduction to occur.[35] Reduction times of 10 hours have been reported.[35] The CVD synthesis method used in this research was operated for 10 minutes at 800˚C before introduction of carbon via acetylene, then 10 minutes with acetylene for nanotube growth and potential aluminium oxide reduction. Thus some reduction of aluminium oxide is to be expected but not a significant amount due to the limited time, competing reaction of nanotube growth and subsequent steric hindrance.

It has been shown that the protective oxide layer on aluminium is ~4nm thick,[36,37] so under this aluminium oxide layer there still remains nanoscale aluminium. Additionally, despite being classed as a ceramic, aluminium oxide is reported as having a relatively high thermal conductivity (~35W/m.K.) which will facilitate the propagation of heat across the surface.[38] Aluminium oxide nanoparticles have been used to increase the thermal conductivity of nanofluids.[39,40]

Nagayama *et al*. used a laser to ignite pentaerythritol tetranitrate (PETN) on a poly(methyl methacrylate) (PMMA) surface and found that a roughened layer of aluminium (100nm thick) on the PMMA increased the speed and strength of the shockwave.[41]

This process was tested by growing nanotubes without the aluminium layer and igniting them, Figure 5.22. Results suggest that the hypothesis is correct since the sample without aluminium ignited at a lower peak temperature and burned for a much shorter time. Visually a much smaller flash was observed as well.

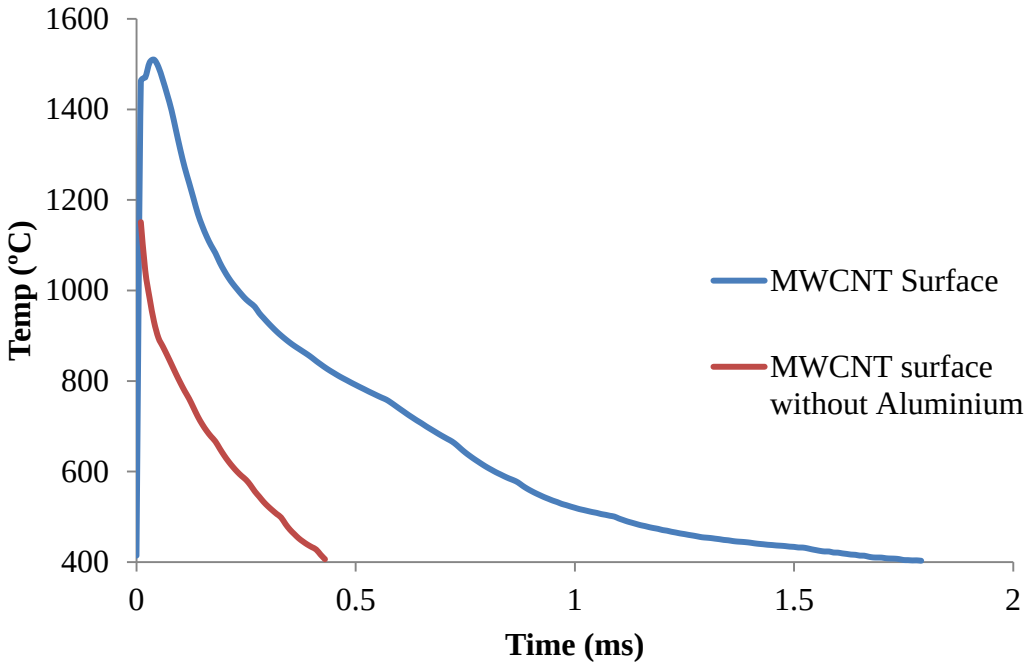

Figure 5.22: Comparison of the ignition of MWCNT arrays with and without the supporting sputter coated layer of aluminium.

Powder mixing of surface bound samples is not possible as it was with the powder APSWCNTs so preparing additives for samples presents a unique challenge. Ferrocene presented as the most effective additive for APSWCNT so it

was primarily used with the surface bound MWCNTs too. Firstly, ferrocene was added to the surface of the sample with a spatula and lightly pressed. This was a very loose contact that allowed easy ablation of the ferrocene from the surface when initiated via a laser. Results of the laser ignition are shown in Figure 5.23. The sample does burn at a higher temperature than with no ferrocene present and it burned for a longer time. However, it was observed that a lot of the ferrocene scattered off of the sample unreacted when exposed to the laser.

The ferrocene was physisorbed to a sample by dissolving it in acetone, adding it drop-wise to the MWCNT surface and then evaporating the acetone away in a fume hood. This intercalated the ferrocene to the sample by creating a bright yellow layer on the surface. This result is displayed in Figure 5.23. The initial temperature is much lower than the other samples at 1050˚C, which is closer to the APSWCNTs. This could be due to the ferrocene reflecting some of the laser energy away from the sample surface or the acetone interacting with the nanotube structure. A crystalline shape of ferrocene rather than a powder may also aid in heat dissipation.

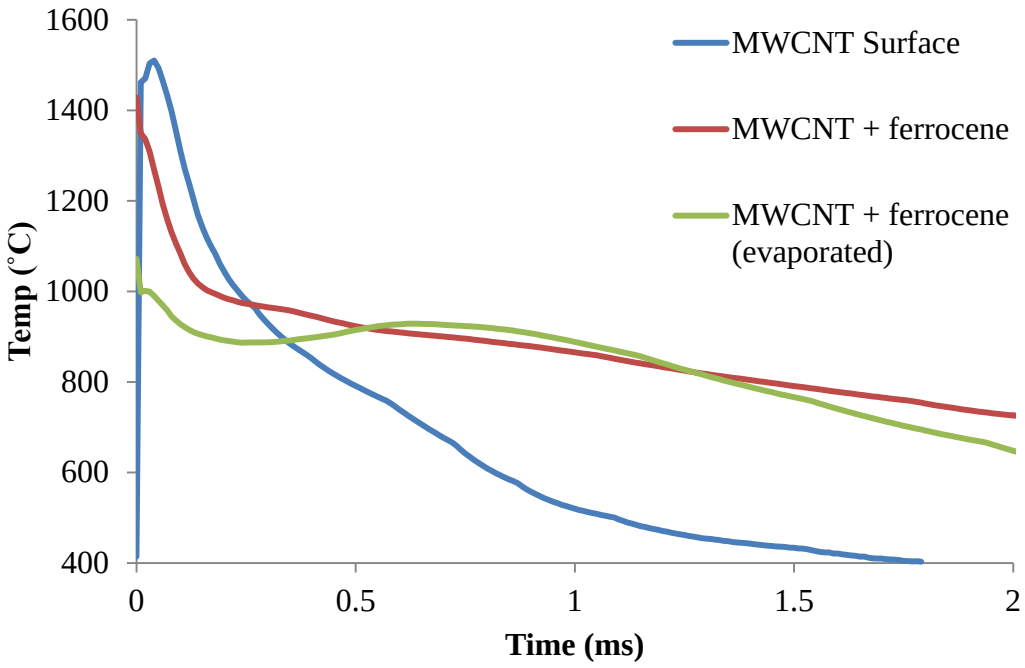

Figure 5.23: Laser ignition of vertically aligned MWCNT surface with ferrocene sprinkled on top compared to ferrocene evaporated into the nanotubes via acetone.

As the ferrocene loaded samples burn for longer than the standard display of 2ms, the full scale data of Figure 5.23 is presented in Figure 5.24 to show the complete ignition of the samples. A secondary peak in the ferrocene evaporated sample is seen at 0.7ms which agrees with powder blends of APSWCNTs and ferrocene. This peak is due to the ferrocene oxidising from the reaction of the nanotubes, and is not present when the ferrocene is sprinkled loosely on the surface. This is because the ferrocene is bound and cannot easily scatter from the laser beam. The total ignition time for both samples is very similar at 5.1ms.

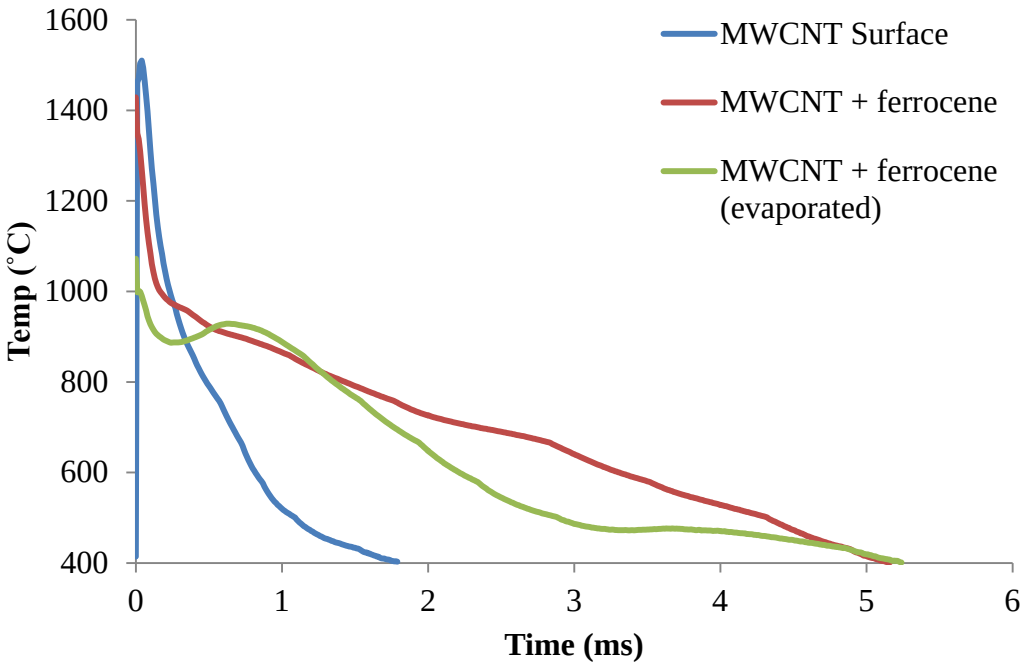

Figure 5.24: Data as presented in Figure 5.23 with a broader x-axis scale to display the full reaction.

5.7: Chapter Conclusions

The purification of APSWCNTs was performed by acid treatment and laser initiation was performed which showed that purification did not significantly alter the output energy of the reaction. This outcome provides a platform for future studies involving light initiation of functionalised nanotubes. Purification can lead to the attachment of novel functional groups on carbon nanotubes and there is potential for them to enhance the light initiation properties.

Addition of the oxidizers potassium nitrite and sodium perchlorate was investigated. Reaction enhancement was very limited in the absence of ferrocene. In the presence of ferrocene, sodium perchlorate at a ratio of APSWCNT/ferrocene/$NaClO_4$ (1:2:6) produced a large but delayed ignition triggered by the light initiated nanotubes. These reactions may have potential in other applications, but the reaction delay inhibits the use in this thesis.

APSWCNTs were wrapped in polystyrene sulfonate in an attempt to add fuel and oxygen into the sample. Results displayed some enhancement of the reaction through higher initial temperatures. However, the enhancement was not as significant as that found by ferrocene addition. The wrapping technique also appeared to have little effect on the reaction compared to simply powder mixing with the monomer.

Horizontally aligned arrays of APSWCNTs on glass were prepared to investigate the axial thermal conductance along the length of nanotubes and the energy transfer to neighbouring nanotubes aligned in the same direction. No evidence of energy transfer was found, which was attributed to the laser ablation of the sample where the beam contacted. The light initiated reaction was limited due to the reduced volume of sample radiated by the laser. Results suggest that if anything, the horizontal alignment allowed the sample to dissipate heat easier and reduce the reaction rather than enhance it by propagating energy.

CVD grown vertically aligned arrays of nanotubes were synthesized and produced a significantly enhanced reaction compared to the randomly oriented APSWCNT samples. This was attributed to the vertical alignment whereby the laser radiation impacts at the tip of nanotubes which allows the energy to transfer along their length. The surface bound nature also restricted particle scatter from laser radiation. The further use of vertically aligned arrays of nanotubes in light initiation presents new possibilities without many of the drawbacks of using powder samples. The optically active layer of aluminium on the silicon wafer was shown to enhance the reaction which suggests other surfaces could be used to aid in the light initiation of carbon nanotubes.

A drawback of surface bound samples was that powder mixing is no longer possible. Ferrocene was evaporated onto the surface with a far more

limited reaction enhancement compared to the powder mixed APSWCNT and ferrocene samples. Other techniques to combine materials may need to be explored.

5.8: References

1 Bockrath, Bradley *et al.*, Igniting Nanotubes with a Flash. *Science* **297** (5579), 192-193 (2002).

2 Braidy, Nadi, Botton, Gianluigi A., and Adronov, Alex, Oxidation of Fe Nanoparticles Embedded in Single-Walled Carbon Nanotubes by Exposure to a Bright Flash of White Light. *Nano Letters* **2** (11), 1277-1280 (2002).

3 Smits, Jan *et al.*, Response of Fe Powder, Purified and as-Produced HiPCO Single-Walled Carbon Nanotubes to Flash Exposure. *Materials Science and Engineering A* **358** (1-2), 384-389 (2003).

4 Tseng, Shih H. *et al.*, Ignition of Carbon Nanotubes Using a Photoflash. *Carbon* **45** (5), 958-964 (2007).

5 Ajayan, P. M. *et al.*, Nanotubes in a Flash--Ignition and Reconstruction. *Science* **296** (5568), 705- (2002).

6 Malec, Christopher D., Voelcker, Nicolas H., Shapter, Joseph G., and Ellis, Amanda V., Carbon Nanotubes Initiate the Explosion of Porous Silicon. *Materials Letters* **64** (22), 2517-2519 (2010).

7 Chen, Jian *et al.*, Dissolution of Full-Length Single-Walled Carbon Nanotubes. *The Journal of Physical Chemistry B* **105** (13), 2525-2528 (2001).

8 Liu, Jie *et al.*, Fullerene Pipes. *Science* **280** (5367), 1253-1256 (1998).

9 Marshall, Matthew W., Popa-Nita, Simina, and Shapter, Joseph G., Measurement of Functionalised Carbon Nanotube Carboxylic Acid Groups Using a Simple Chemical Process. *Carbon* **44** (7), 1137-1141 (2006).

10 Hassam, Christopher and Lewis, David A., Dispersion of Single and Multiwalled Nanotubes with Poly(Sodium Styrene Sulfonate) – Effect of pH and Ionic Strength on Dispersion Stability. *Australian Journal of Chemistry* **67** (1), 66-70 (2014).

11 Fujii, Motoo *et al.*, Measuring the Thermal Conductivity of a Single Carbon Nanotube. *Physical Review Letters* **95** (6), 065502 (2005).

12 Kim, P, Shi, Li, Majumdar, A, and McEuen, PL, Thermal Transport Measurements of Individual Multiwalled Nanotubes. *Physical Review Letters* **87** (21), 215502 (2001).

13 Yu, Choongho *et al.*, Thermal Conductance and Thermopower of an Individual Single-Wall Carbon Nanotube. *Nano Letters* **5** (9), 1842-1846 (2005).

14 Berber, Savas, Kwon, Young-Kyun, and Tománek, David, Unusually High Thermal Conductivity of Carbon Nanotubes. *Physical Review Letters* **84** (20), 4613 (2000).

15 Che, Jianwei, Cagin, Tahir, and Iii, William A. Goddard, Thermal Conductivity of Carbon Nanotubes. *Nanotechnology* **11** (2), 65-69 (2000).

16 Dai, H., Carbon Nanotubes: Synthesis, Integration, and Properties. *Accounts of chemical research* **35** (12), 1035-1044 (2002).

17 Hone, J. *et al.*, Electrical and Thermal Transport Properties of Magnetically Aligned Single Wall Carbon Nanotube Films. *Applied Physics Letters* **77** (5), 666-668 (2000).
18 O'Connell, Michael J., *Carbon Nanotubes: Properties and Applications*, 3rd edition. (CRC Press, Boca Raton, FL, 2006).
19 Terrones, Mauricio, Science and Technology of the Twenty-First Century: Synthesis, Properties, and Applications of Carbon Nanotubes. *Annual Review of Materials Research* **33** (1), 419-501 (2003).
20 Deegan, Robert D. *et al.*, Capillary Flow as the Cause of Ring Stains from Dried Liquid Drops. *Nature* **389** (6653), 827-829 (1997).
21 Hata, Kenji *et al.*, Water-Assisted Highly Efficient Synthesis of Impurity-Free Single-Walled Carbon Nanotubes. *Science* **306** (5700), 1362-1364 (2004).
22 Yamada, Takeo *et al.*, Revealing the Secret of Water-Assisted Carbon Nanotube Synthesis by Microscopic Observation of the Interaction of Water on the Catalysts. *Nano Letters* **8** (12), 4288-4292 (2008).
23 Dresselhaus, M. S., Dresselhaus, G., and Avouris, Phaedon, *Carbon Nanotubes : Synthesis, Structure, Properties, and Applications*. (Berlin London : Springer, 2001).
24 Dresselhaus, M. S., Dresselhaus, G., and Jorio, A., Unusual Properties and Structure of Carbon Nanotubes. *Annual Review of Materials Research* **34**, 247 (2004).
25 Freitag, M. *et al.*, Photoconductivity of Single Carbon Nanotubes. *Nano Letters* **3** (8), 1067-1071 (2003).
26 Fujiwara, Akihiko *et al.*, Photoconductivity in Semiconducting Single-Walled Carbon Nanotubes. *Japanese Journal of Applied Physics* **40** (11B), L1229 (2001).
27 Shaikh, S., Li, L., Lafdi, K., and Huie, J., Thermal Conductivity of an Aligned Carbon Nanotube Array. *Carbon* **45** (13), 2608-2613 (2007).
28 Xie, Huaqing, Cai, An, and Wang, Xinwei, Thermal Diffusivity and Conductivity of Multiwalled Carbon Nanotube Arrays. *Physics Letters A* **369** (1–2), 120-123 (2007).
29 Stamatis, Demitrios, Jiang, Xianjin, Beloni, Ervin, and Dreizin, Edward L, Aluminum Burn Rate Modifiers Based on Reactive Nanocomposite Powders. *Propellants, Explosives, Pyrotechnics* **35** (3), 260-267 (2010).
30 Jouet, R. J. *et al.*, Preparation and Reactivity Analysis of Novel Perfluoroalkyl Coated Aluminium Nanocomposites. *Materials Science and Technology* **22** (4), 422-429 (2006).
31 Lee Perry, W. *et al.*, Energy Release Characteristics of the Nanoscale Aluminum-Tungsten Oxide Hydrate Metastable Intermolecular Composite. *Journal of Applied Physics* **101** (6), - (2007).
32 Umbrajkar, Swati M. *et al.*, Aluminum-Rich Al-MoO3 Nanocomposite Powders Prepared by Arrested Reactive Milling. *Journal of Propulsion and Power* **24** (2), 192-189 (2008).
33 Walter, Kevin C., Pesiri, David R., and Wilson, Dennis E., Manufacturing and Performance of Nanometric Al/MoO3 Energetic Materials. *Journal of Propulsion and Power* **23** (4), 645-650 (2007).
34 Cox, J. H. and Pidgeon, L. M., An Investigation of the Aluminium-Oxygen-Carbon System. *Canadian Journal of Chemistry* **41** (3), 671-683 (1963).
35 Halmann, M., Frei, A., and Steinfeld, A., Carbothermal Reduction of Alumina: Thermochemical Equilibrium Calculations and Experimental Investigation. *Energy* **32** (12), 2420-2427 (2007).

36 Campbell, Timothy *et al.*, Dynamics of Oxidation of Aluminum Nanoclusters Using Variable Charge Molecular-Dynamics Simulations on Parallel Computers. *Physical Review Letters* **82** (24), 4866 (1999).

37 Campbell, Timothy J *et al.*, Oxidation of Aluminum Nanoclusters. *Physical Review B* **71** (20), 205413 (2005).

38 Hoch, Michael and Silberstein, A, Thermal Conductivity of Aluminium Oxide, Technical Report, Air Force Materials Laboratory, Research and Technology Division, Air Force Systems Command, United States Air Force, (1966).

39 Lee, S., Choi, S. U. S., Li, S., and Eastman, J. A., Measuring Thermal Conductivity of Fluids Containing Oxide Nanoparticles. *Journal of Heat Transfer* **121** (2), 280-289 (1999).

40 Maddah, Heydar, Rezazadeh, Mahdokht, Maghsoudi, Mojtaba, and NasiriKokhdan, Syamak, The Effect of Silver and Aluminum Oxide Nanoparticles on Thermophysical Properties of Nanofluids. *J Nanostruct Chem* **3** (1), 1-6 (2013).

41 Nagayama, Kunihito, Inou, Kazunari, and Nakahara, Motonao, Initiation of PETN Powder by Pulse Laser Ablation. *Shock Compression of Condensed Matter: 12th APS Topical Conference* **620** (1), 995-998 (2002).

Chapter 6: Energetic Materials and Carbon Nanotubes

This chapter will firstly introduce the methods by which lasers have previously initiated energetic materials and provide a brief description of some of the important variables which affect the sensitivity of energetic materials. A review of the relevant research into the chosen energetic material, pentaerythritol tetranitrate (PETN), is presented. Drawing upon these findings and the findings of previous chapters, a series of experiments to investigate the addition of PETN to carbon nanotubes and the subsequent laser initiated reactions is explored.

6.1: Introduction

The primary motivation for this thesis was to attempt to use light initiated carbon nanotubes to ignite explosive materials. Typically in explosive devices, the material is initiated by incident heat or shock from electrical heating or a spark. It has been proposed that a laser could provide a better initiation source since it can be delivered with immunity to electrical interference or chemical failure.[1] There are two main potential pathways a laser can be used to assist the initiation of energetic materials. The first is an indirect method where a metallic flyer plate is launched at the energetic material and vaporised by laser energy to create a high pressure zone which initiates the material's deflagration and subsequent detonation.[1-3] In the second method, the laser is shone directly onto the explosive material which absorbs the light energy subsequently converting it into thermal energy which triggers the explosion.[1,4-6] The focus of this work is primarily on the direct initiation of nanotube and energetic material mixtures from light energy.

Explosive materials tend not to be very good absorbers of light.[2,7] A technical study at Defence, Science and Technology Organisation (DSTO) of

several explosive materials including trinitrotoluene (TNT), Research Department Explosive (RDX), 2,2',4,4',6,6'-hexanitrostilbene (HNS), octogen (HMX) and pentaerythritol tetranitrate (PETN) found that all of the materials reflected light across the visible spectrum and absorbed strongly in the ultraviolet region(<300nm).[7] This has driven research into the indirect laser initiation of materials by a laser driven metal plate as described earlier since direct initiation is considered inefficient.[8] This thesis attempted to enhance the direct ignition of a secondary energetic material by blending it with carbon nanotubes so that the heat and ignition of nanotubes from laser absorption can act as hotspots within the PETN and thermally initiate it hence increasing the light sensitivity of the explosive material.

PETN was used in these experiments since it is commonly used as an ingredient in many boosters and detonators and it was easy to obtain from DSTO. It is classed as a secondary explosive, yet it is among the more sensitive of secondary explosives.[9] PETN is an odourless, white crystalline material which is soluble in acetone,[10] making it easy to combine with other materials.

Quantitative sensitivity measurements for explosive materials is complicated by the vast number of variables such as particle size, density, surface area (governed by particle shape) and confinement of bulk materials that greatly affect their sensitivity and the properties of their explosions.[3,11,12] Porosity of materials or location of voids in materials is also an important variable.[13] In comparison to other explosive materials, PETN is relatively insensitive to friction[14] but sensitive to shock.[15] The deflagration point of PETN is 202˚C.[9] Smaller grain size (~1μm diameter) particles of PETN have been found to be more sensitive to stimuli than conventional grain size (106μm diameter) particles.[3]

Tarzhanov *et al*. investigated the laser absorption in PETN at 1060nm and found it was heavily dependent on the density and particle size of the sample.[16] Energy transfer between loosely bound particles was difficult thus a higher density was required for initiation and smaller particle sizes were more sensitive.

One of the most important and extensively studied parameters of explosive materials is the critical diameter or critical thickness. This is defined as the smallest length scale of a charge that can support a self-sustained detonation.[12] If an explosive material is below the critical diameter, a shockwave cannot propagate through the material since too much energy is lost at the edges so deflagration occurs but not detonation. Detonation velocity is said to be dependent on diameter of a cylinder of explosives, thus below the critical diameter no explosion will occur regardless of the velocity of the initiating shockwave.[17] Critical diameter is most commonly measured by a steel column of explosive material being initiated at one end. For PETN the mechanism of deflagration to detonation has been investigated and shown that a shockwave is required to transition to detonation.[11]

The critical thickness is studied less often and is described as the minimum thickness required to detonate a material. It is more commonly used for high-density samples such as pellets and films.[18] Critical thickness of a material is theoretically at least two times smaller than critical diameter and experimentally up to four times smaller[19] since the shockwave expansion is geometrically confined to one dimension while the shockwave in a cylinder expands radially, as illustrated in Figure 6.1.

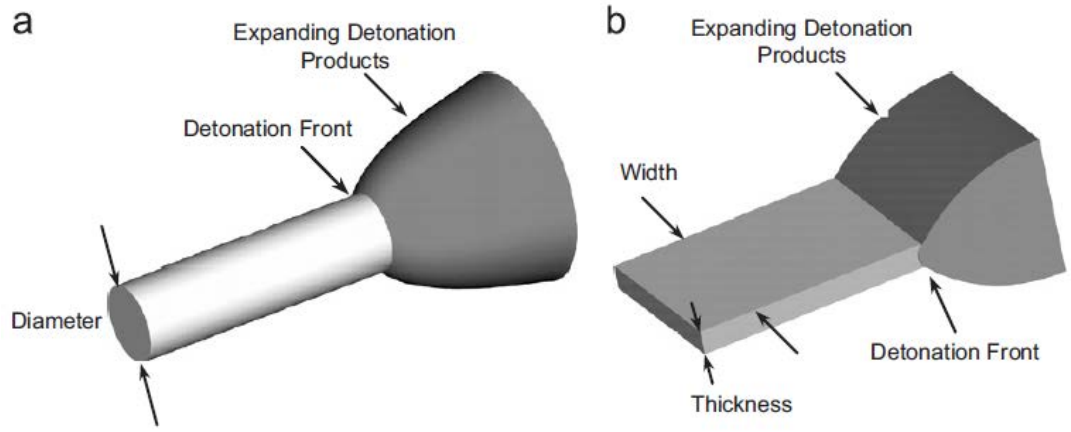

Figure 6.1: Schematic of the expanding detonation shockwave when propagating through a charge (a) in a cylindrical charge with a radial shockwave and (b) in a film charge with a 1-dimensional shockwave. (*Petel, 2007*)

The critical thickness of PETN was investigated by Tappan *et al*. in 2011 by physical vapour deposition of PETN films on fused silica substrates.[18] Critical thickness for their samples was found to be ~90-150µm. Deposition parameters were found to have a large influence on critical thickness and very minor changes in the film properties resulted in large changes in the critical thickness curves. It was concluded that differences in the microstructure of the films was responsible and there was a high dependence on grain size, porosity and density.

In 2001, Nagayama *et al*. used a 1064nm laser to produce a shockwave on a roughened surface of poly(methyl methacrylate) (PMMA).[2] The researchers then found that a layer of aluminium (100-420nm thickness) on the PMMA surface greatly increased the laser induced shockwave. Subsequently, PETN was initiated by the shockwave in 10-20mg quantities and detonation occurred below the critical diameter of the material.[2]

The absorption spectrum from 300-1100nm of PETN was measured by Aluker *et al*. in 2008.[6] As previously reported,[7] absorption was found in the UV region with very low absorption across the visible and IR regions, Figure 6.2. Difference spectra at the maximum sensitivity of the instrument were recorded in

the experiment which made it possible to detect a weak absorption peak with maxima at ~1020nm, inset Figure 6.2. In their experiment to laser initiate molten PETN at temperatures of up to 176˚C, this peak was given as the reason ignition was successful with a laser at 1060nm but not at 530nm.[4]

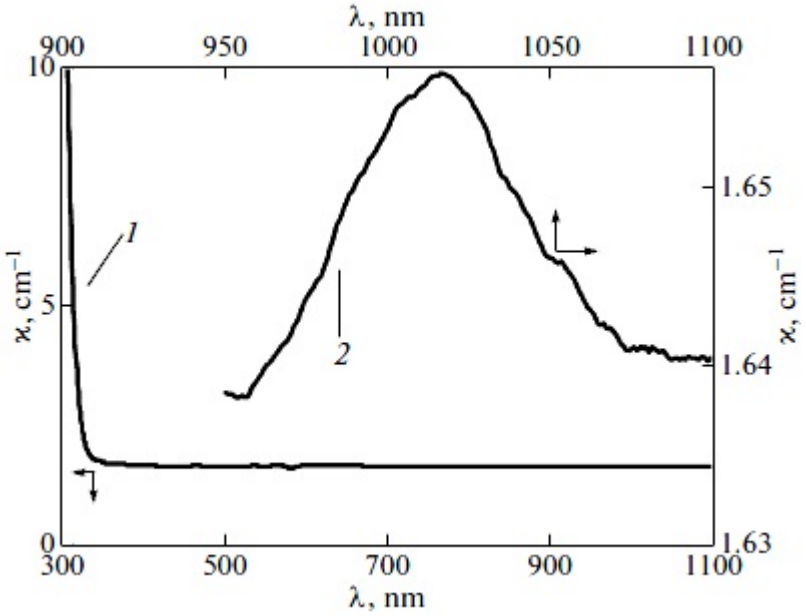

Figure 6.2: Absorption spectra of PETN. (1) Overview spectrum left and bottom axis, (2) maximum sensitivity spectrum right and top axis. (*Aluker, 2008*)

The small peak in the infrared region may assist ignition of PETN with the laser used in this thesis at 1064nm. No significant difference in absorption is to be expected across the visible and IR region since the peak observed in Figure 6.2 is very small. The sensitivity to laser initiation of PETN was found to be three to four times greater at 250nm than at 1060nm.[20] Using the third harmonic of the Surelite laser used in previous chapters can produce 355nm laser radiation at the cost of reduced energy and causes larger margins of error in the output energy, plus it is still outside the absorbing region for PETN. For this reason the 1064nm laser was used for all experiments involving PETN in this chapter with the expectation that carbon nanotubes will trigger the ignition.

6.2: Laser Ignition of PETN with APSWCNTs

The first experiment performed was to attempt to initiate the PETN with the laser without any nanotubes present as a control. In Figure 6.3, upon initiation from the laser at 150mJ, PETN showed a temperature of 1250˚C which rapidly declined within 2 data points (0.02ms). This suggests that the original high peak is mostly from sample scattering of the laser beam onto the optical pyrometer head rather than a thermal heating and cooling event. Visually, no reaction occurred and the PETN sample did not ignite. PETN's weak absorption in the IR region accounts for the lack of reaction.[6] These experiments were performed at room temperature with the sample in its crystalline state, whereas the ignition of PETN performed by Aluker *et al*. was performed above room temperature with PETN in a molten state.[4-6] Those conditions were not replicated in these experiments. A sample was also initiated at 800mJ laser power, and no ignition or change in appearance was observed.

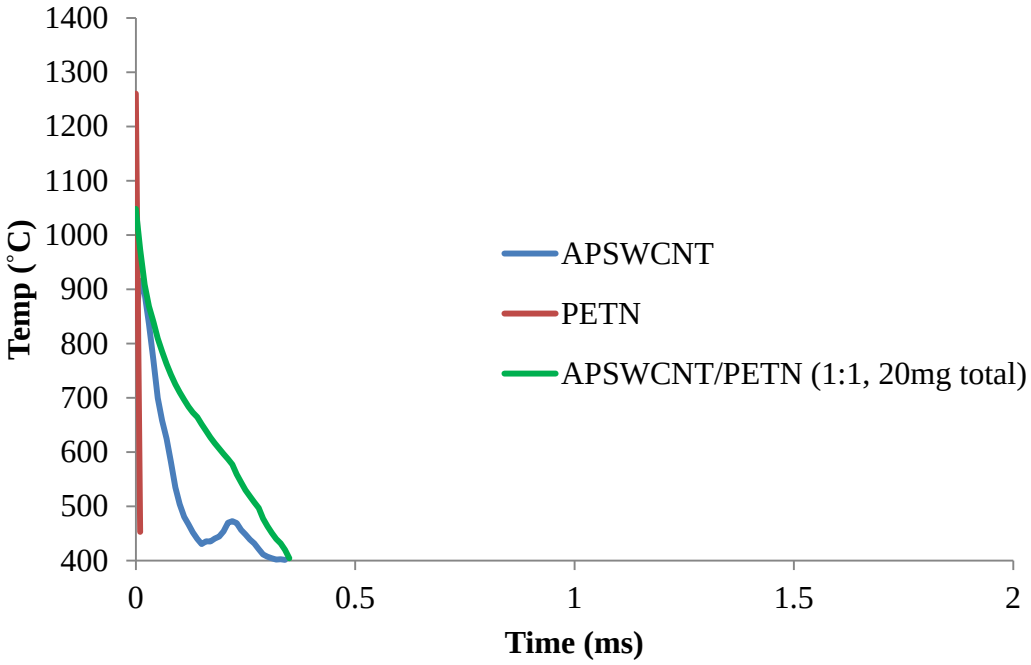

Figure 6.3: Laser ignition response of PETN, APSWCNTs and a mixture of both displaying that there is no reaction for PETN in the absence of nanotubes.

APSWCNT and PETN (10mg each) were combined and mixed using the flask shaker. The ignition is displayed in Figure 6.3 alongside an ignition of raw APSWCNT for comparison. The initial temperature of the mixed sample is 1050˚C compared to 900˚C of just nanotubes, and the area of the reaction under the curve is larger indicating that the sample stayed hotter for longer. However, the total ignition time is the same for both. After ignition, the sample still contained white crystals indicating at least some of the PETN was unreacted as a result of the APSWCNT igniting and an incomplete ignition occurred. This means that the heat transfer from the APSWCNT to the PETN was relatively poor and there was insufficient energy to initiate the complete reaction of the PETN in the sample.

High speed video of the ignition of APSWCNTs and PETN was recorded. Captured frames are shown in Figure 6.4. An initial bright flash was seen when the laser first impacted the sample (a) and the next frame captured (b) shows a bright fireball in the sample. In the following frame (c) the flames have already mostly extinguished, 1.6ms after the laser pulse. The frame rate of the camera (1200fps) limits the precision of the photo frames compared to the pyrometer when the reaction completes in <1ms. The powder sample is seen to scatter in the sample tube (d-f). This rapid particle scattering aids in cooling the sample particles and reduces heat transfer between nanotubes and PETN. It also prevents any shockwave from propagating. To support that, the small remaining hotspot in (d) is completely extinguished rapidly as a result of the particles scattering.

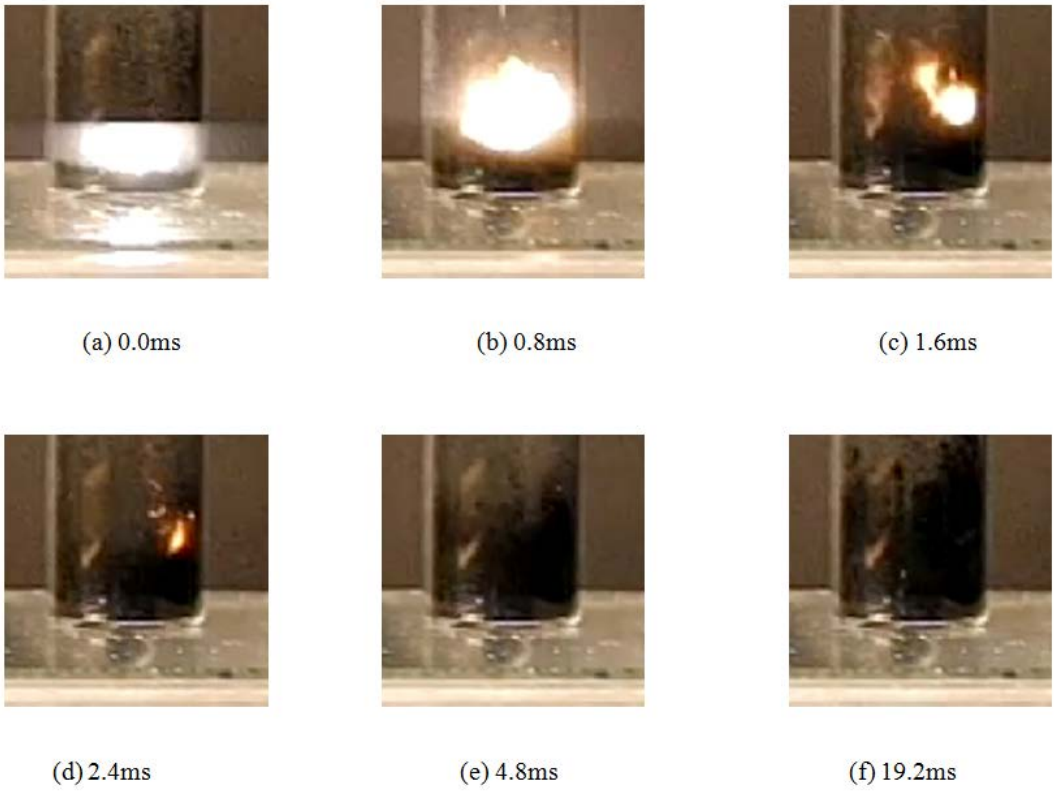

Figure 6.4: High speed camera photos of the laser initiation of APSWCNT/PETN (1:1, 20mg total). Times shown is the time since the first frame where a reaction can be seen (a), i.e. the first frame captured upon laser impact.

A comparison of previous results for the initiation of APSWCNT is shown in Figure 6.5. With no PETN the flame produced is much smaller and diminishes more rapidly within two frames. This result proves that PETN was at least partially ignited by the nanotubes.

Figure 6.5: High speed camera photos of the laser initiation of APSWCNT (10mg) displaying the comparatively smaller reaction with no PETN present. (Reused from Chapter 4.2)

In order to enhance the contact between the APSWCNT and the PETN, acetone (~2mL) was added which dissolved the PETN. The sample was then mixed in the flask shaker and left at room temperature for one hour for the acetone to evaporate and for the PETN to recrystallise in direct contact with the nanotube bundles. Some formed on the glass sample container instead, so a ratio of APSWCNT/PETN (1:3, 40mg total) was used to compensate for those losses. Large crystals of PETN were not visible in this sample since they recrystallised evenly across the APSWCNT and the sample container so the size and shape of PETN crystals would be changed. As a control for this experiment, a sample of APSWCNT was shaken with acetone and allowed to dry. This process increased the density of the previously 'fluffy' sample by forcing the nanotube bundles to settle in a more closely packed fashion as the acetone evaporated.

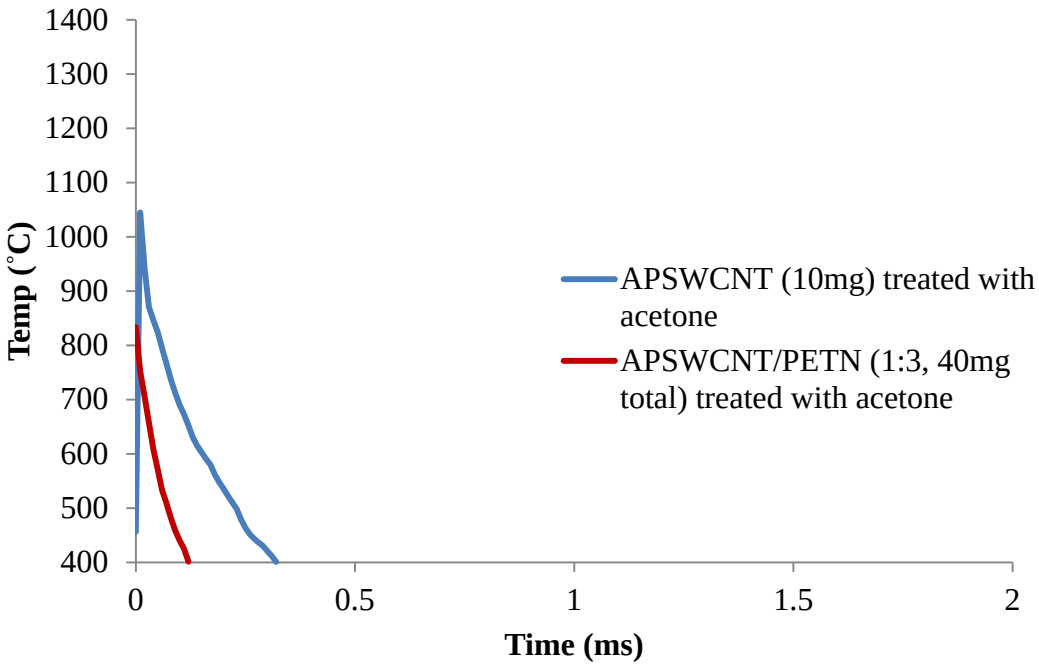

Figure 6.6: Ignition response of APSWCNT and PETN mixed by dissolving in acetone and evaporating.

Figure 6.6 shows that when the sample is mixed by dissolving in acetone, the reaction is significantly worse when there is PETN present with the APSWCNT due to the lower peak temperature and shorter overall reaction time. This result suggests that a chemical interaction between the PETN and nanotubes has been formed when they are mixed together in acetone as opposed to simply shaking the powders together. The interaction has reduced the sensitivity to the laser beam significantly though, which is an undesired result. The random orientation of bundles of nanotubes in the sample allows energy to dissipate throughout the sample easier when the density is higher[21] due to a lower thermal diffusivity. More PETN would be attached to CNT walls rather than tips which means the heat flow is mostly radial rather than axial. Additionally, crystals of PETN evaporated onto the surfaces of nanotube bundles may also inhibit the flow of oxygen into the nanotubes and thus decrease the reaction. The increased density of PETN would reduce its thermal diffusivity in this reaction and the significantly altered crystal shape of PETN may play a role in the output reaction.

The energy of the laser beam was increased to 800mJ and a new sample was initiated to investigate whether energy absorption was inhibited by the PETN. Despite creating a larger reaction as a result of the significantly increased input laser beam energy, the same trend was still visible in Figure 6.7. The reaction with PETN added to the nanotubes was weaker than without PETN, so even with a very high energy input the sample is not sufficiently initiated to ignite the PETN and the PETN acts instead to inhibit the reaction.

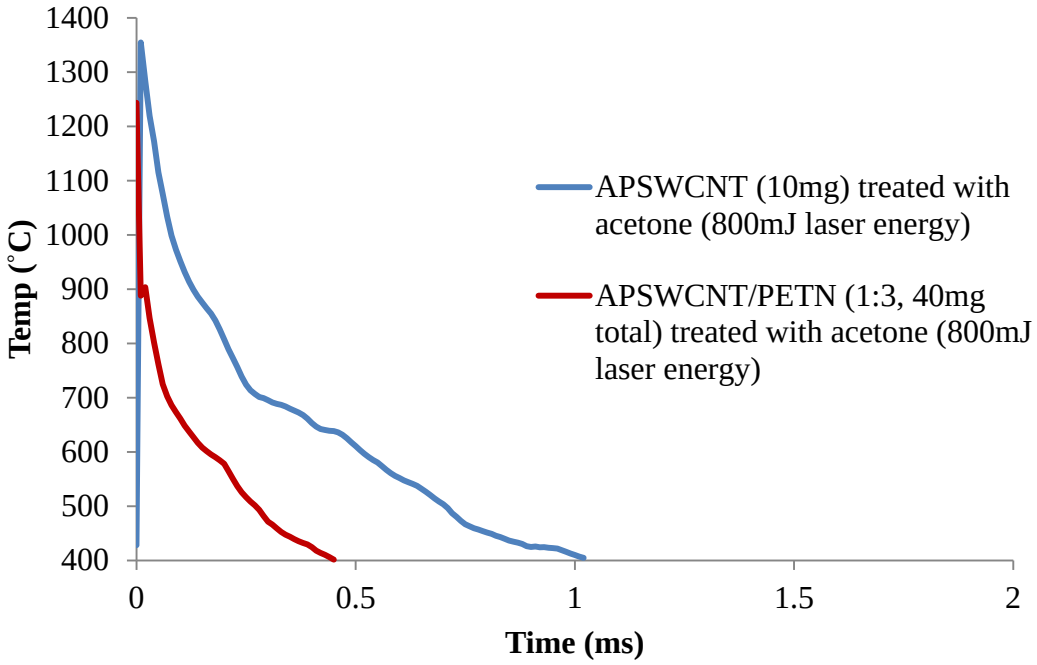

Figure 6.7: Ignition response at 800mJ of laser energy of APSWCNT and PETN mixed by dissolving in acetone and evaporating.

On the advice of Orica, a mixture of APSWCNT (1mg) with PETN (33mg) was prepared for ignition. This is only 3% by weight nanotubes and supports the research of Kim *et al*. where 1-3% nanotubes was found to best ignite a metal nanoparticle/oxidizer mix.[22] This experiment was performed with the laser at 800mJ to input a large amount of energy on the sample. Figure 6.8 shows the initiation of the sample compared to a 1mg sample of APSWCNT. Very little difference was observed visually in the reaction, and the results support

that the PETN only provided a small increase in total ignition time suggesting that the APSWCNT reaction again has not transferred enough energy to the PETN to initiate it completely. The particle scattering at 800mJ may also work to inhibit the transfer of energy to the PETN and cool it down.

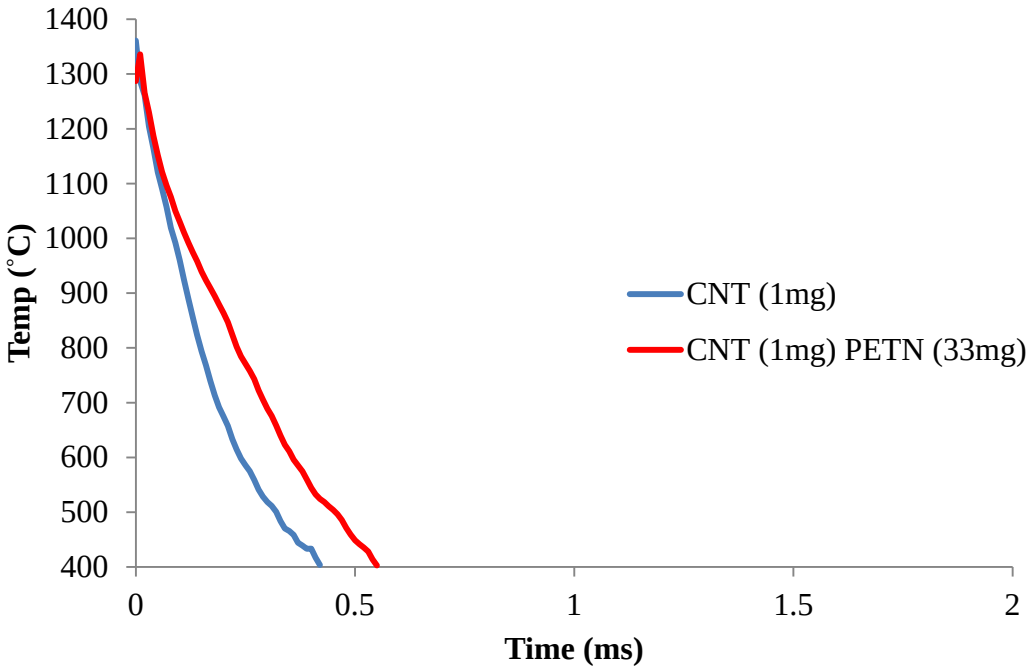

Figure 6.8: Laser initiation of APSWCNT/PETN (1:33, 34mg total) at 800mJ laser energy highlighting only a minor increase in reaction with PETN compared to APSWCNT only.

6.3: Addition of Ferrocene to APSWCNTs with PETN

Previous chapters have shown that the laser ignition of carbon nanotubes is enhanced by the addition of ferrocene. Ferrocene may act as a fuel to allow a sample to burn for a time much greater than 1ms. It was previously found that a ratio of APSWCNT/ferrocene (1:2) worked most successfully for ignition of samples, and that ferrocene created a higher initial temperature and made samples burn for up to 200ms from laser ignition.

A sample of APSWCNT/ferrocene/PETN (1:2:5, 16mg total) was prepared and initiated by the laser at 150mJ, Figure 6.9. As a comparison, a sample without PETN was also initiated. The results show that PETN addition has caused the samples to burn initially at 300˚C higher than with no PETN present. A separate sample was also dissolved in acetone first and dried as described with APSWCNT/PETN to create a closer bond between the three materials, and Figure 6.9 shows again that the reactivity is significantly reduced by dissolution in acetone. In addition to the PETN crystals having a better ability to shield and reflect the laser light as observed in Figure 6.6, the size and shape of PETN crystals is significantly changed and the structure may be insufficient for a reaction to occur.

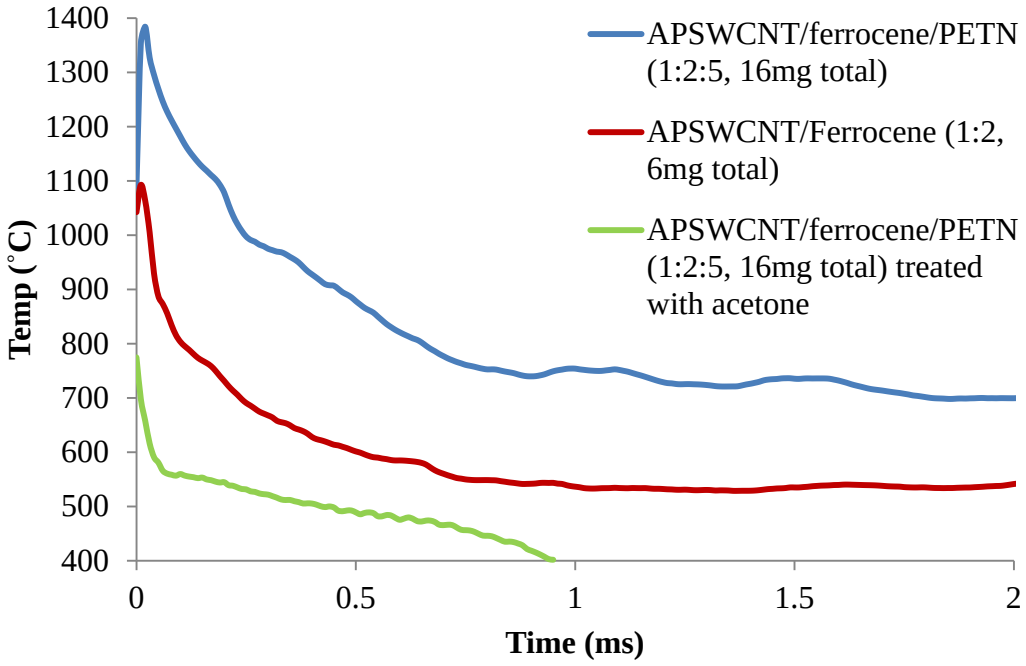

Figure 6.9: Laser initiation of APSWCNT/ferrocene/PETN (1:2:5, 16mg total) compared to without PETN. Bottom trace (green) shows a sample of APSWCNT/ferrocene/PETN after being dissolved in acetone and air dried.

Another characteristic of the ignition of nanotubes with ferrocene in previous chapters has shown that after the initial peak, the temperature drops before rising again to a secondary peak as the ferrocene was ignited by the

reaction of the nanotubes. Only the first 2ms of the reaction is displayed in Figure 6.9. The full reaction of the sample with PETN present and compared to without PETN is displayed in Figure 6.10. The sample with the PETN ignited for 46ms while the sample without PETN ignited for 127ms. The PETN sample has no secondary peak from the ferrocene igniting, and the total reaction time is approximately half that of the sample with no PETN. A stronger and faster reaction in the first 5ms may leave less material to burn causing a shorter overall reaction. Stronger reactivity initially within the first 2ms is more desirable for the outcome of using samples to initiate less sensitive explosives in a more controllable way. The PETN appears to ignite when initiated by the APSWCNT much faster than ferrocene (0-2ms compared to 5-10ms) and subsequently provide enough additional heat to burn the ferrocene much more rapidly.

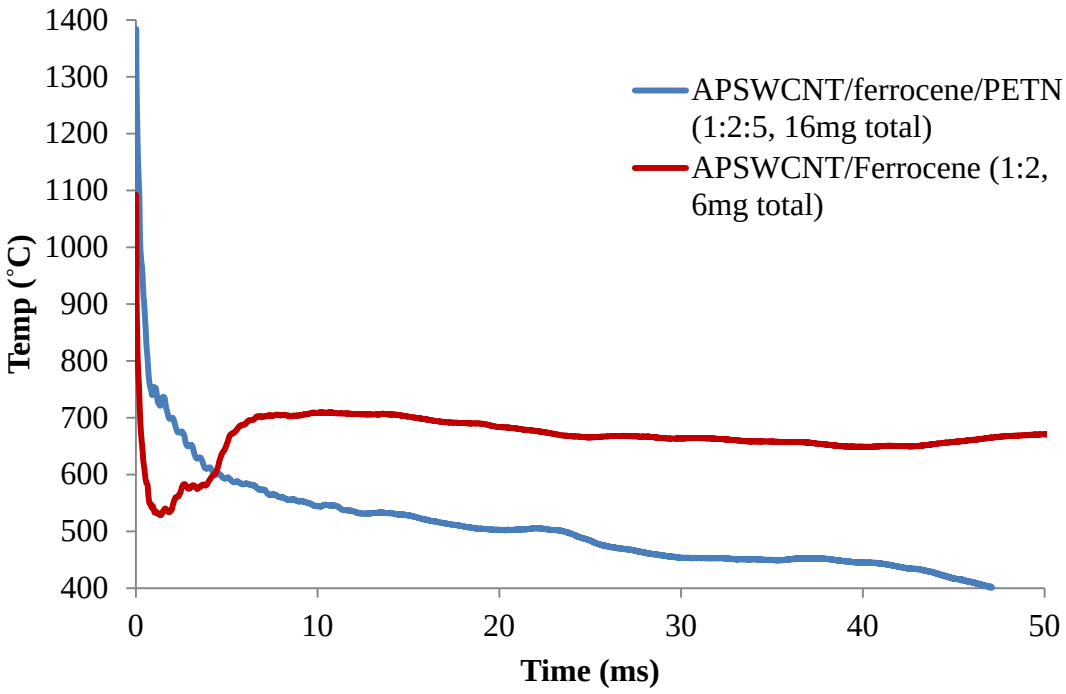

Figure 6.10: Laser initiation of APSWCNT/ferrocene/PETN (1:2:5) compared to without PETN, x-axis changed to show full reaction time of the PETN containing sample.

High speed video of the ignitions were recorded and frames for APSWCNT/ferrocene/PETN (1:2:5, 16mg total) are displayed in Figure 6.11. In

frames (a-c) the initial rapid ignition from the PETN triggered by the APSWCNTs is displayed. This overlaps with the subsequent ignition and burning of the ferrocene (d) and presumably consumes some of the ferrocene in the first 5ms. The fireball from a combination of all the materials burning rapidly rises and particles scatter (e) before the whole reaction is complete at 53.6ms (f) with burnt material stuck to the sides of the sample container.

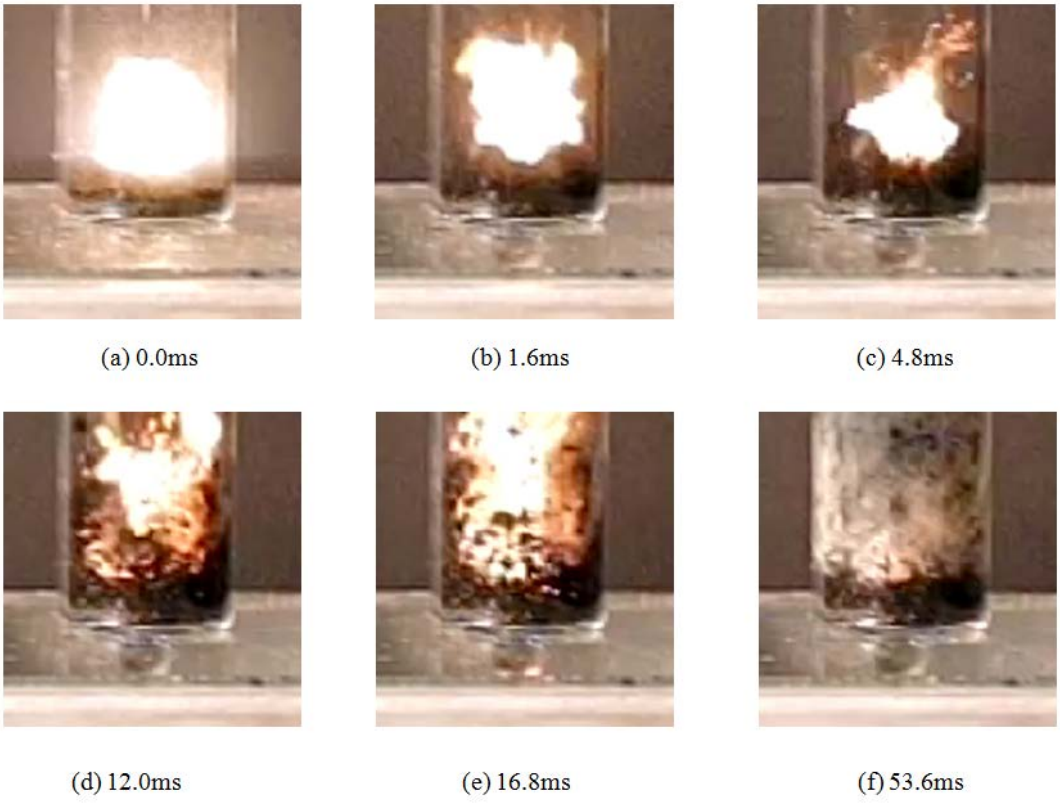

Figure 6.11: High speed camera photos of the laser initiation of APSWCNT/ferrocene/PETN (1:2:5, 16mg total) showing a rapid and intense ignition (a-c) as a result of the PETN which causes ferrocene to ignite quickly (d-e).

By contrast, APSWCNT/ferrocene (1:2, 6mg total) is displayed in Figure 6.12. The bright flash from APSWCNT initiating is seen in (a), it then almost completely diminishes in the first 12ms (d) before a secondary flame rises (e-f) after 20ms as a result of the ferrocene reacting and igniting. The secondary ignition from ferrocene includes particles scattering from the laser and burnt matter sticking to the sides of the sample container.

Overall, the inclusion of PETN increases the rate of the ignition by allowing the ferrocene to burn earlier and faster. In turn, compared to Figure 6.4 where APSWCNT and PETN complete the reaction within 1.6ms and initially peak at 1050˚C, when ferrocene is added the initial ignition in Figure 6.11 from the PETN lasts for 4.8ms and the initial peak temperature is nearly 1400˚C. PETN and ferrocene appear to complement each other to produce faster and hotter reactions.

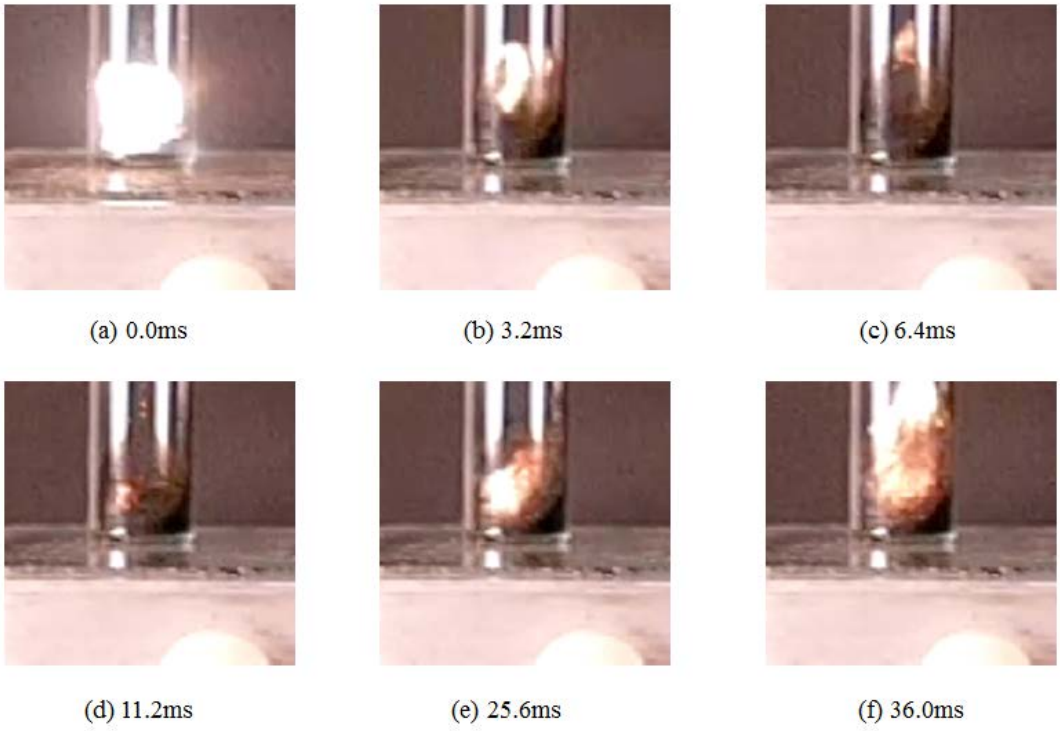

Figure 6.12: High speed camera photos of the laser initiation of APSWCNT/ferrocene (1:2, 6mg total) displaying the initial ignition (a-d) followed by a secondary ignition (e-f) when the ferrocene is initiated.

6.4: Reaction of PETN with Iron Nanoparticles

Iron nanoparticles (26nm) were found to ignite and oxidize when exposed to the laser. A sample of iron nanoparticles (5mg) was mixed with a sample of

PETN (5mg) to observe whether the oxidation reaction of the nanoparticles can trigger the ignition of PETN. Results were shown at high laser power (850mJ) since 150mJ displayed no reaction on the pyrometer. No difference was observed between reactions at 800mJ and 850mJ. Figure 6.13 shows the reaction compared to iron nanoparticles without PETN. Very little difference is observed in the initial temperature and the overall reaction time. Additionally, the reaction pathway looks similar. After the reaction PETN crystals were still visible in the sample suggesting that PETN did not react in the presence of iron nanoparticles suggesting that there was insufficient heat transfer from the metal nanoparticles to the PETN. This may also be because there is no fuel in the reaction to burn and allow a deflagration to detonation transition to occur.

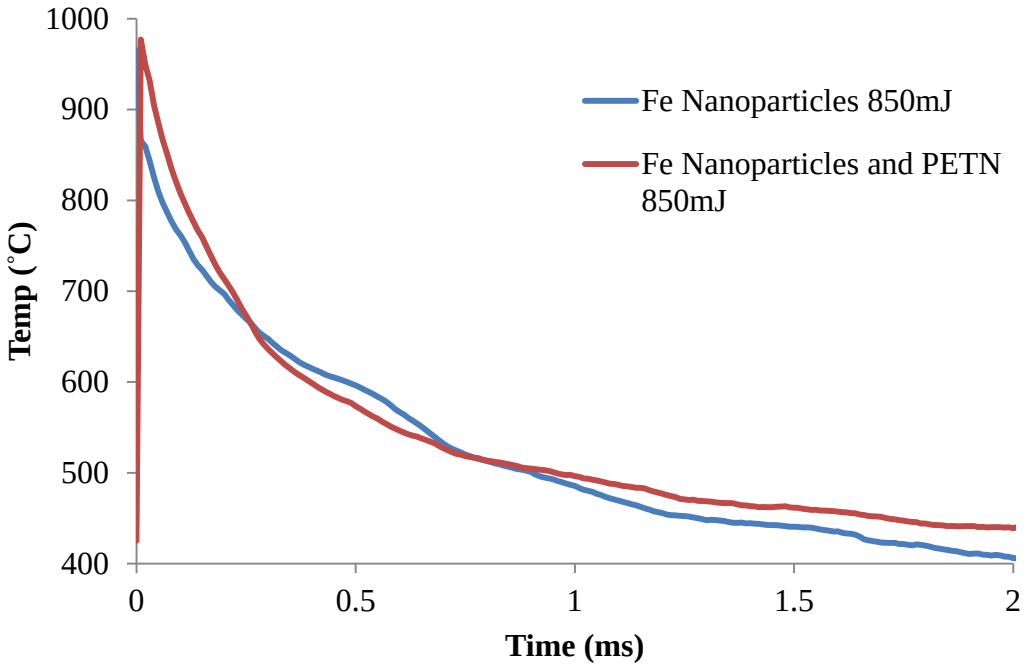

Figure 6.13: Initiation of iron nanoparticles with and without PETN (1:1) at 850mJ.

Nanoparticles were considered as initiators for PETN since their exothermic oxidation in carbon nanotubes was considered a critical part of light ignition. In this thesis it has been determined that nanotubes play a very important role and are important in absorbing light energy and converting it to thermal

energy. Nanoparticles alone do not appear to absorb enough transferable energy to initiate a reaction.

6.5: CVD Grown Vertically Aligned Carbon Nanotubes with PETN

Vertically aligned MWCNTs grown on silicon were charged with PETN for ignition. To do this, ~5-10mg of PETN was placed on top of the MWCNT surface. Then a 15µL aliquot of acetone was added in one drop to the PETN. This caused the PETN crystals to dissolve and spread across the surface with the expanding acetone droplet. Rapid evaporation of the acetone droplet on the sample (<5 seconds) caused recrystallisation of the PETN onto the surface of the nanotubes in a thin layer of PETN. In total, 3 drops of acetone were added allowing evaporation between each drop to create the PETN layers.

As the PETN travelled rapidly in the acetone drop radially outwards from the centre of the drop, and then radially inwards as a result of evaporation from the edge, the crystal surfaces of the PETN were found to be aligned in the direction of movement. This was examined by optical microscopy through the WITec confocal Raman microscope, shown in Figure 6.14. At the microscale, the PETN has recrystallised in an ordered and aligned layer on the surface. Using the z-axis of the microscope and comparing the difference between the height of the focal plane of the PETN layer and the MWCNT surface layer across several points, the thickness of the PETN layer was determined to be in the range of ~5-40µm, measured from multiple points in multiple samples.

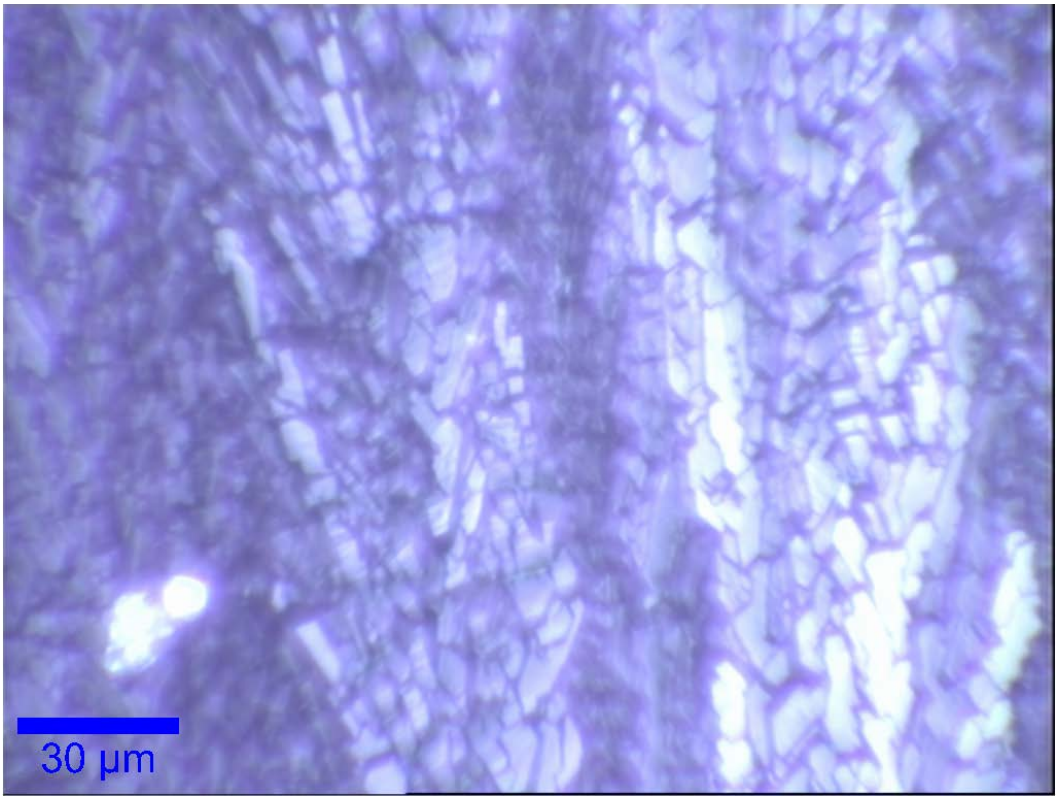

Figure 6.14: Optical microscopy image of a PETN layer on vertically aligned MWCNTs. PETN crystals have formed in an aligned fashion due to the movement of the expanding then evaporating acetone droplet.

The PETN layer of a different sample prepared and analysed in the same way is shown in Figure 6.15. In this surface, the PETN crystal fractures are much larger than those observed in Figure 6.14. This difference can be attributed to the particle size variation of the PETN sample - smaller particles will dissolve much more readily than larger particles. The acetone treatment does not completely dissolve the PETN all at once so under the same treatment conditions, different sized crystals will be formed from different sized particles. Therefore the technique used in this thesis is somewhat limited in reproducibility since the PETN surface thickness and the critical surface area properties of the samples cannot easily be controlled which will lead to variations in the light initiation properties of samples. Variations in the reaction from sample to sample are expected.

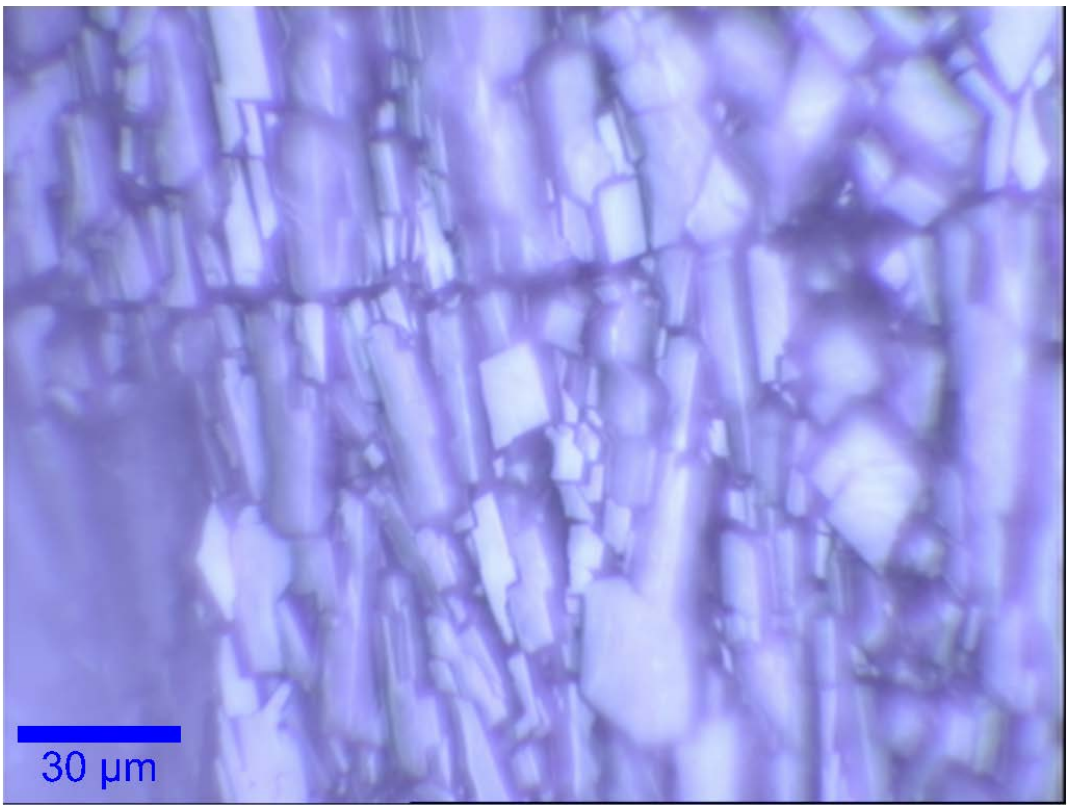

Figure 6.15: Optical microscopy image of a PETN layer on vertically aligned MWCNTs illustrating a different sample with different PETN crystal morphology.

It was postulated that in addition to forming a thin layer of PETN on the surface of the nanotube array, some PETN can travel between the nanotubes on the surface through the acetone wetting the sample. Functionalisation of the walls of vertically aligned nanotubes has been previously reported which demonstrates that there is space for molecules to exist between nanotubes.[23,24] In this system, the mechanism for light initiation may be via a thermopower wave along the length of the nanotubes as described in Chapter 1.8[25-27] in addition to the surface layer of PETN igniting.

Proving the existence of PETN within the nanotube array as well as on the surface is not trivial. This was attempted by Raman spectroscopy of a MWCNT surface with PETN loaded on it. The sample analysed contained nanotubes of length ~2mm. Longer nanotubes were examined to make microscopy of the side easier to perform. The sample was examined from the side rather than the top to

directly observe the side walls of the nanotubes. An optical microscope image of the sample is shown in Figure 6.16. The bright white area in the top left is the silicon surface that the nanotubes are gown on. Nanotubes are excellent absorbers of light so typically appear very dark, and make up the bulk of the sample image. Reflective areas on the nanotubes are believed to be PETN, which is a bright white reflective material.

Raman spectra obtained were then compared to the spectra for MWCNTs and for PETN respectively. These spectra are displayed in Figure 6.17, highlighting the agreement of peak locations to the relevant reference spectra. The green spectrum is collected from the circled area shown in Figure 6.16. The spectra recorded for PETN agrees with that found in the literature.[28-30] Important peaks for PETN include the large peak at 100cm^{-1} which is due to crystal lattice vibrations,[28] the nitro group stretching at 1300cm^{-1} (not seen in the combined sample due to the carbon nanotube D-band) and CH_3 stretching at 3000cm^{-1} while other peaks for PETN are attributed to CH bends.[30] PETN is much less Raman-active than MWCNTs so the peaks for PETN are comparatively smaller in the combined sample. The PETN CH_3 stretch at 3000cm^{-1} is broadened and unresolved in the combined sample most likely due to chemical interactions with the nanotubes. Raman spectra recorded on the top of samples (from the perspective of images shown in Figure 6.14 and Figure 6.15) display only PETN, no nanotube peaks. This data collected from the side suggests that during acetone evaporation onto samples, PETN does travel between nanotubes as well as crystallising in a layer on top.

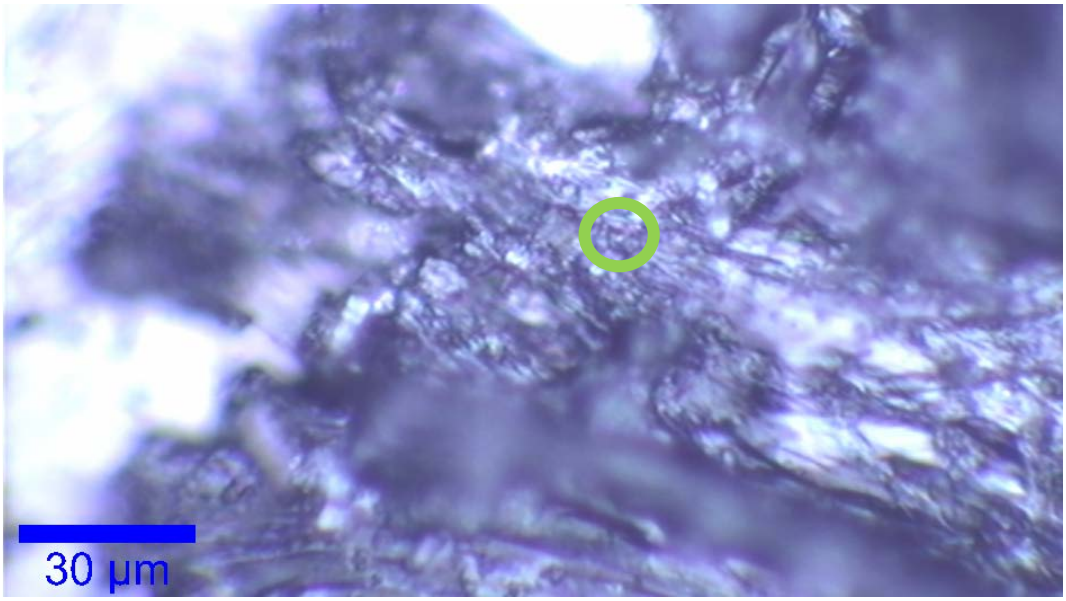

Figure 6.16: Optical microscopy image of a MWCNT surface loaded with PETN. The right white area out of focus is the silicon surface, the dark material is MWCNTs, and the reflective parts on it is PETN. The green circle shows where Raman spectra was collected from.

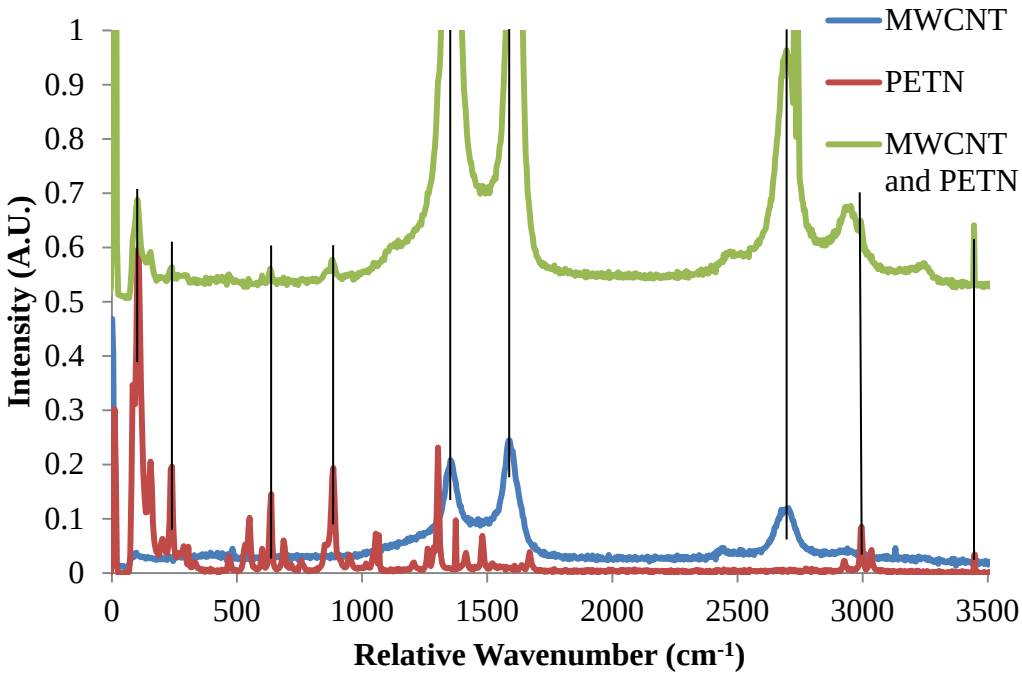

Figure 6.17: Raman spectra of the side of a MWCNT surface with PETN loading (green) in comparison to reference spectra of MWCNT and PETN (blue and red respectively).

Samples of MWCNTs were grown on silicon wafers ~1cm^2 so in all cases, the 2mm radius laser spot was used to initiate a quarter region of the sample before PETN loading, then PETN was added to the opposite region. This meant comparison could be made with and without PETN on exactly the same surface of MWCNTs for every sample initiated to remove variations between MWCNTs as a variable. One sample is displayed in Figure 6.18. Acetone treatment was previously shown to weaken the ignition in APSWCNTs (Figure 6.6 and Figure 6.7) and this trend is displayed again in the MWCNT surface. A much lower initial temperature is observed. However, ignitions with PETN present were much more violent than with no PETN. Louder pops were heard and samples were seen to jump around the sample stage. Transferring energy into kinetic energy may reduce the thermal energy produced, and as soon as the sample moves away from the focal point of the pyrometer head it is no longer able to directly collect thermal data from the sample. Two extra peaks were observed in the PETN loaded sample. This could possibly be due to firstly PETN within the nanotube array in contact with the sides of the nanotubes igniting (thermopower wave) and secondly the PETN layer on the surface igniting. The frame rate of the high speed camera is not high enough to examine this in depth.

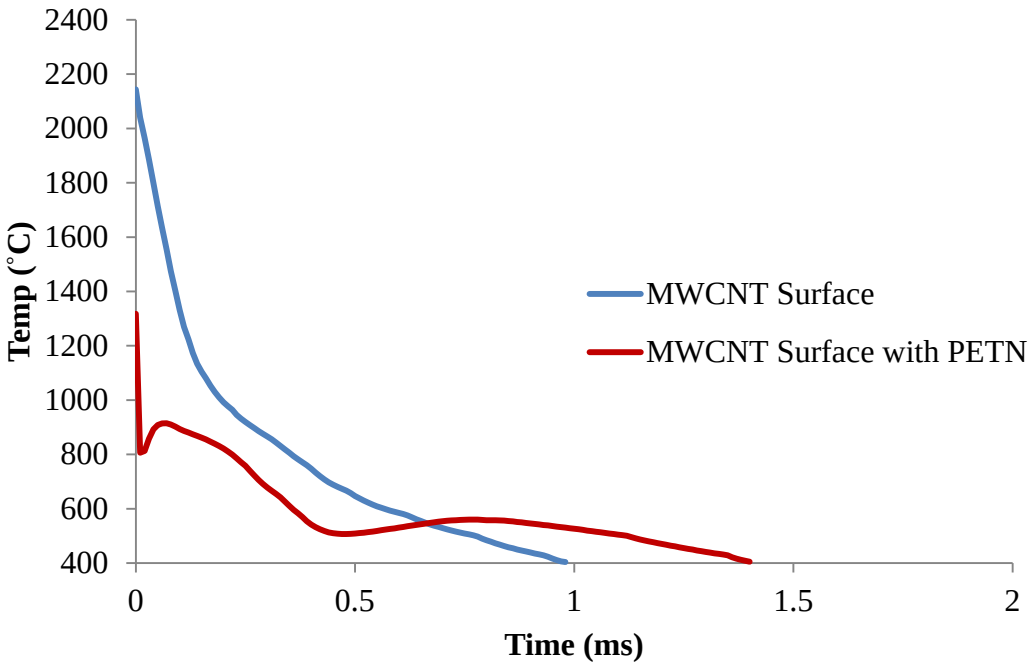

Figure 6.18: Laser initiation of a vertically aligned MWCNT surface with and without a PETN layer on the surface.

A high speed camera was used in conjunction with the pyrometer for the data shown in Figure 6.18. The first three frames of ignition for the MWCNT surface is displayed in Figure 6.19(a-c) while the first three frames of the sample when loaded with a PETN layer is displayed in (d-f). The ignition with PETN visually appears much larger and stronger than without PETN. The temperature of ignition may be lower due to the low absorbance of the PETN on the surface.

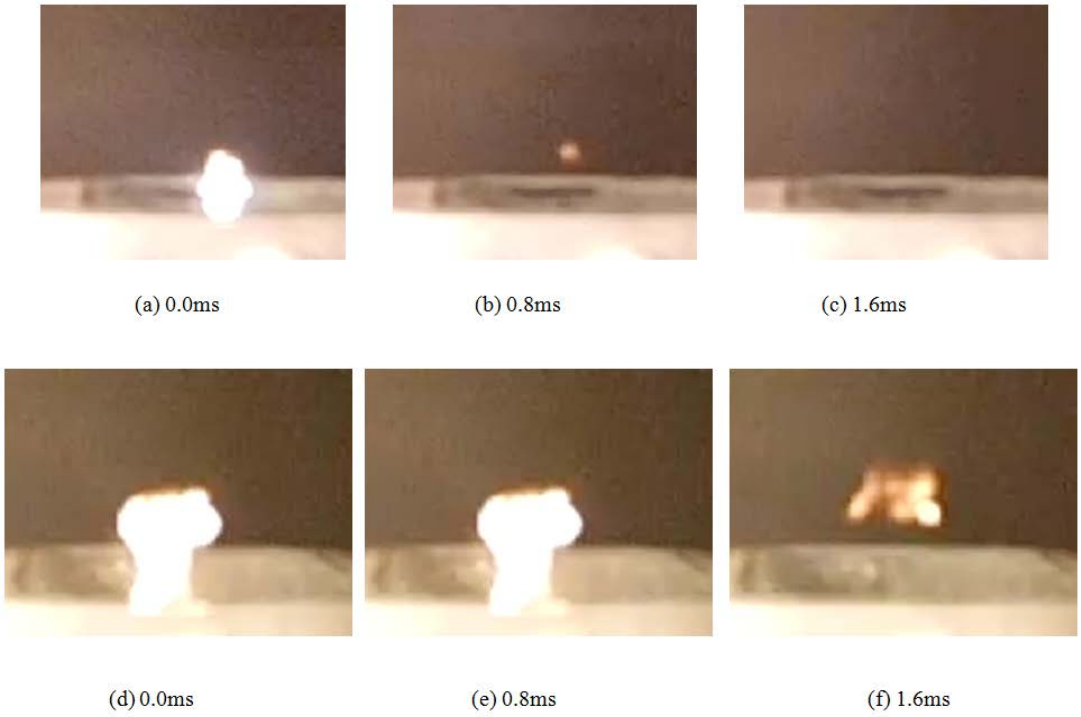

Figure 6.19: High speed camera frames of the laser initiation of a MWCNT surface (a-c) and the same sample with a layer of PETN (d-f).

As well as a larger explosion on the surface of the sample, the entire silicon wafer was seen to jump up off of the sample stage and flip through the air in total 540º (1.5 revolutions). The photos of this are shown in Figure 6.20. This suggests that a successful detonation of the PETN has occurred and produced enough downward force on the sample to force it to become airborne. An explosion travelling down the length of the vertical nanotubes would account for this reaction. Alignment of nanotubes in arrays as compared to random orientation of APSWCNT samples allows the energy to be more focused as it is unidirectional.

Figure 6.20: High speed camera photos of the MWCNT surface with PETN layer displaying the silicon wafer flipping through the air.

Laser initiation of a supported metal surface has been shown to produce an ablation plasma and possible shockwave which can ignite small amounts of PETN.[2] As a control experiment, in order to show that the MWCNT growth on the silicon surface plays an important role in the ignition of PETN here, a silicon wafer with the sputtered aluminium and iron layers (support and catalyst respectively for MWCNT growth) but no nanotubes was charged with PETN using the acetone evaporation technique. Optical microscopy of the surface (Figure 6.21) revealed a region of PETN ~10-12μm thick and another region just 4μm thick. Both were initiated with the laser and compared to the laser initiation of the sputtered silicon wafer.

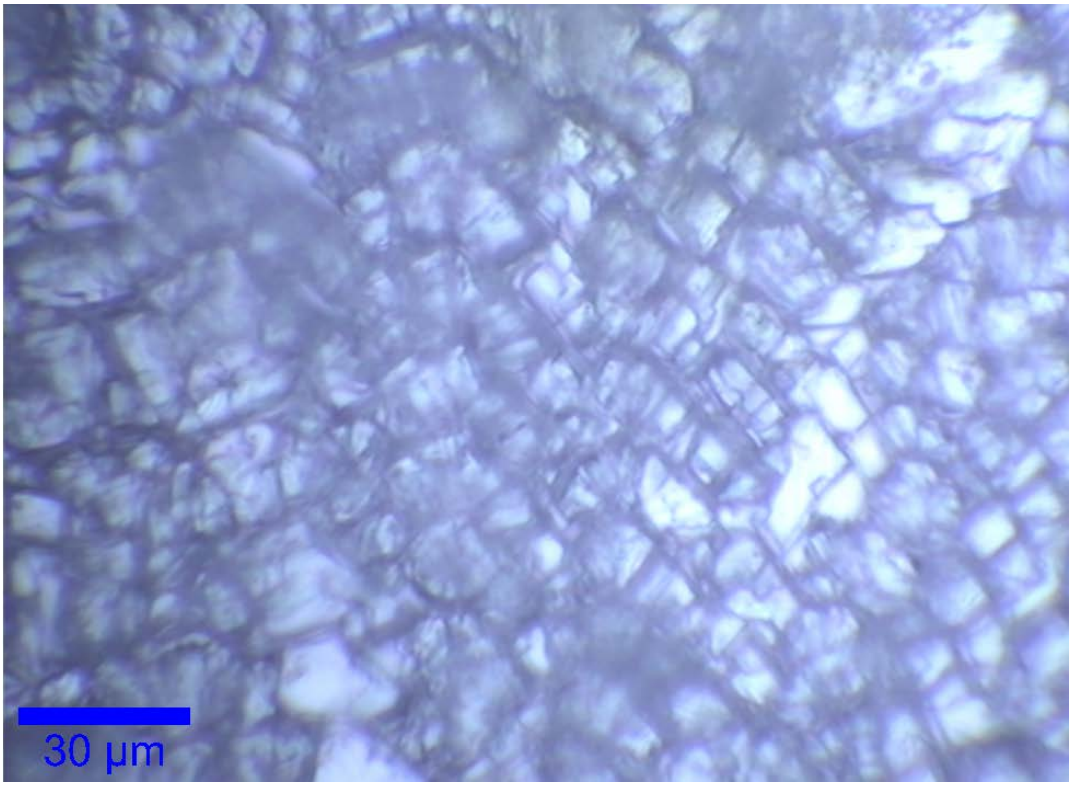

Figure 6.21: Optical microscope image of the PETN layer (10-12µm) on a silicon wafer.

Figure 6.22 displays the results of the control experiment. The metal on the surface of the silicon wafer appeared to heat up to ~1650˚C as a result of laser ablated plasma. In the 10-12µm region of PETN, a peak at ~2400˚C was first observed which rapidly cools within 0.25ms. No movement of the silicon wafer was observed and no pop was heard, the PETN was ablated off of the surface. The 4µm region displayed very little reaction either on the pyrometer or visually. No sign of ignition of the PETN was observed in either case. A high speed camera was not available at the time of these experiments. The amount of PETN used in these experiments is far below the 1-2mm thickness used by Nagayama[2] and the detonation of samples observed here on the MWCNT surfaces suggests that the nanotubes play a key role in increasing the sensitivity of the PETN and causing detonation of PETN.

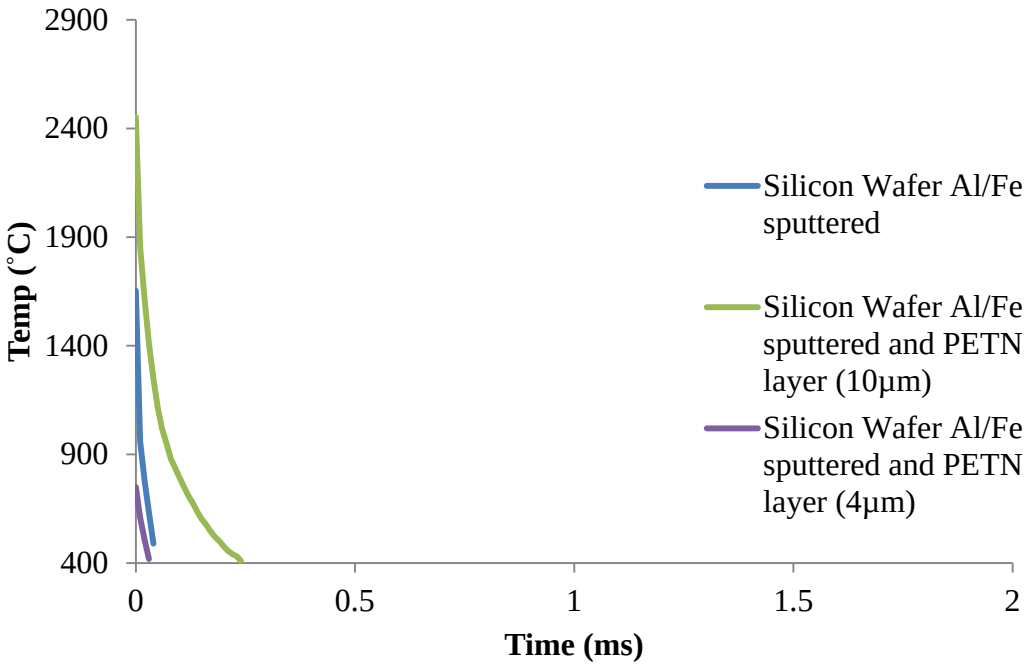

Figure 6.22: Laser initiation of a silicon wafer sputtered with aluminium and iron. The wafer was then charged with a PETN layer and initiated.

A different MWCNT sample prepared with the same techniques was initiated with and without PETN loaded to compare the result to Figure 6.18 and examine the reproducibility of ignitions between samples. The result of the new sample is presented in Figure 6.23. The samples differ by much lower initial temperatures (1500˚C compared to 2200˚C for MWCNTs and 950˚C compared to 1350˚C with PETN loaded) and the total ignition time is shorter. However, the overall trend of PETN producing a lower initial temperature and a similar ignition time is repeated. Differences may be due more to differences in the MWCNTs than the PETN layers since results without PETN differed. Density and height of MWCNTs has not been measured for every sample.

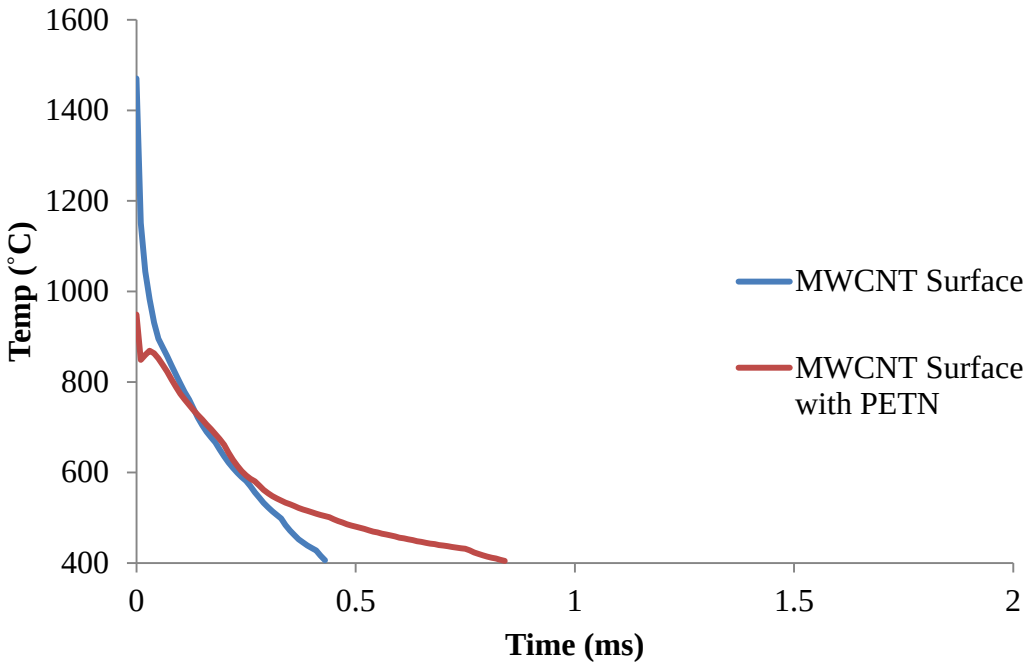

Figure 6.23: Laser initiation of a vertically aligned MWCNT surface with and without a PETN layer on the surface.

A sample of MWCNTs with nanotubes of length ~2mm was produced. A much greater length than the ~200µm of most of the samples may allow more PETN to get between nanotubes compared to on top. The same amount of catalyst was used to make this sample, so the ratio of nanotube: catalyst is also much lower than for the shorter nanotubes. While loading with acetone, some of the structure collapsed due to the length of the nanotubes, resulting in channels on the surface which could affect ignition properties. For this reason alone, more reliable systems may use shorter nanotubes.

The sample was first ignited without PETN loading, Figure 6.24. An initial temperature of 2200˚C was achieved, and the sample burned for a total of 1.25ms. A shoulder on the initial peak at 0.05ms suggests a second reaction starting, possibly the catalyst particles oxidizing or the nanotubes exothermically reconstructing. After PETN is loaded onto the sample, it was initiated at 150mJ in a different surface region. Figure 6.24 shows a lower initial temperature of

1400˚C and a shorter reaction time again with a pronounced shoulder peak from a secondary ignition. Finally, the sample was initiated with the laser power at 850mJ. In this reaction, a full secondary peak appears and the secondary peak rises back up to the initial temperature of 1000˚C. As the nanotubes are the particles absorbing light, the higher secondary peak present due to increased laser energy can be attributed to nanotubes. A much greater amount of energy absorbed allows more of the strong covalent bonds to break and exothermic oxidation and reconstruction of the nanotubes can occur. The enhanced explosion as a result of PETN is not seen on the pyrometer results. High speed video of the three ignitions was recorded to view the ignitions.

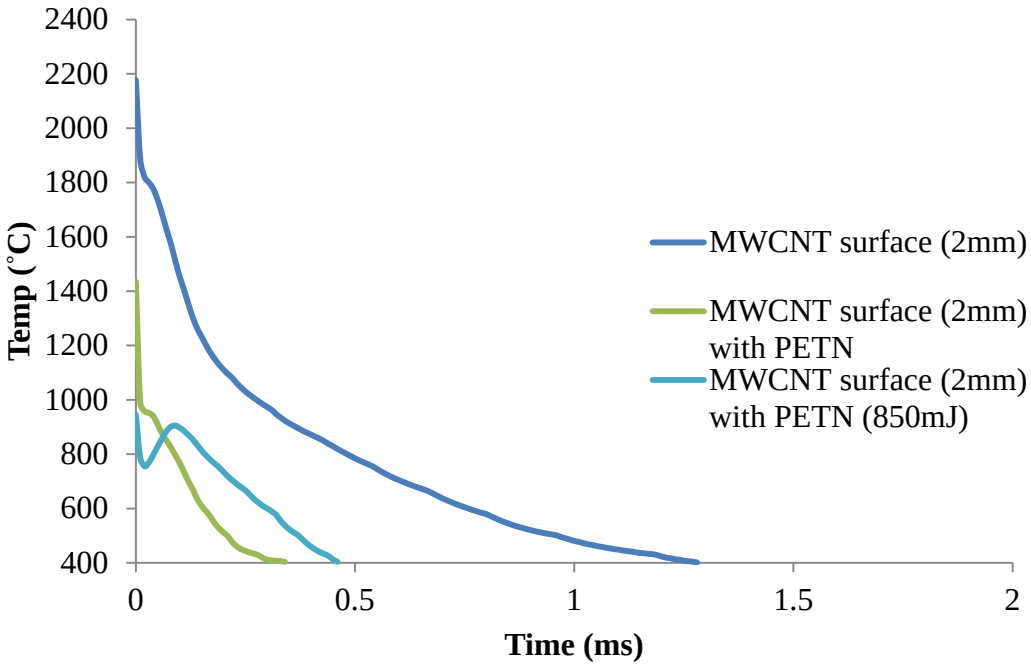

Figure 6.24: Laser initiation of a vertical MWCNT array of length ~2mm displaying first the ignition of the nanotubes, then the sample loaded with PETN. Finally the laser energy was increased to 850mJ to initiate another region of the sample.

Figure 6.25 shows the ignition of the aligned 2mm MWCNTs without PETN. The bright flash was only observed in a single frame, which suggests it exists for <0.8ms. As the pyrometer showed a reaction time of 1.25ms, the remaining time after the flash was most likely the time taken for the sample to

cool down. No particle matter was scattered from the surface as a result of the reaction. The ignition appears to not be on the surface of the sample, it may have originated on the surface but moved too rapidly for the camera to capture.

Figure 6.25: High speed camera frames of MWCNT (~2mm) array initiated by laser. Only one frame of flame is observed and very little ablation of particles can be seen.

Figure 6.26 displays the reaction of the MWCNT surface loaded with PETN at laser energy of 150mJ. In (a), the roughness on the right side of the sample is visible compared to in Figure 6.25. This is due to the acetone treatment collapsing some of the structure of the nanotubes. The ignition is brighter than with no PETN, and this time significant particle scattering can be seen in (c) and (d). Scattering sideways from the sample may be due to the new alignment of the nanotubes in the region that the laser impacted.

In Figure 6.27, the ignition of the sample with the laser at 850mJ energy is shown. The first frame of ignition (a) displays a very large flame above the sample compared to at 150mJ despite the lower initial temperature recorded in Figure 6.24. The reaction is faster than the reaction at 150mJ since the particles are already scattering rapidly by 0.8ms (b) and the energy of the ignition is high enough to flip the whole sample over (c-f).

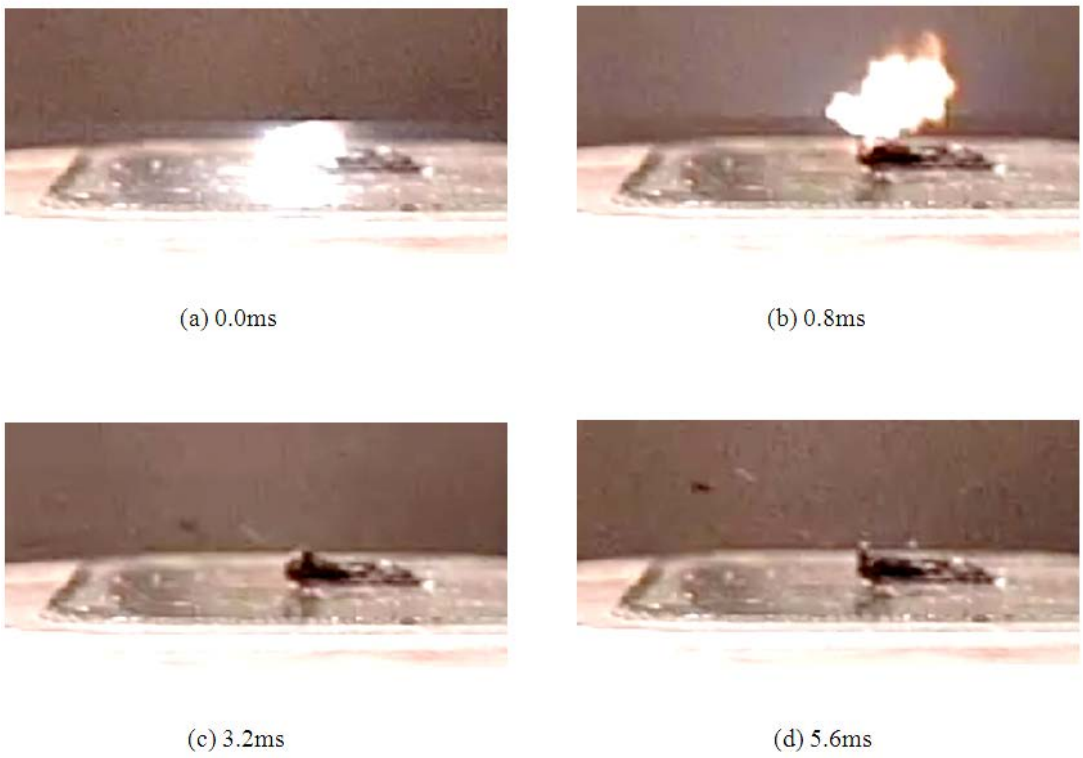

Figure 6.26: High speed camera frames of MWCNT (~2mm) array with PETN loaded initiated by laser (150mJ). Particle matter is seen firing to the left of the sample (c-d) after the initial ignition.

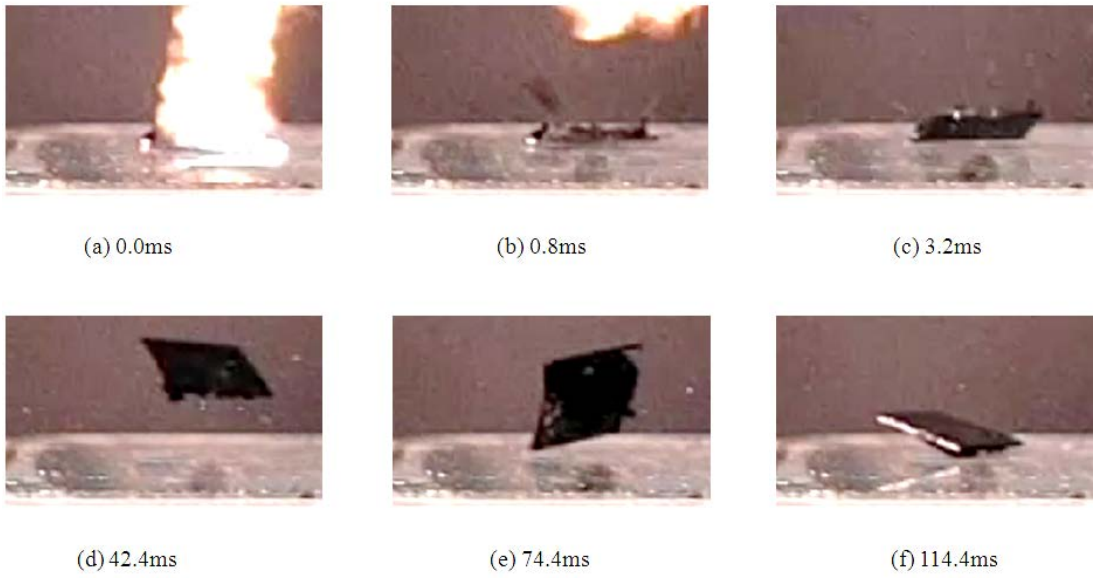

Figure 6.27: High speed camera frames of MWCNT (~2mm) array with PETN loaded initiated by laser (850mJ). A large ignition is first seen (a) and lots of particles scatter (b) before the whole silicon wafer flips over (c-f).

Another MWCNT sample was prepared and loaded with PETN for ignition in conjunction with the high speed camera. This sample reacted very explosively and destroyed the silicon wafer that the MWCNTs were supported on, shown in Figure 6.28. In (a), the first frame from laser initiation is observed, and the wafer has already appeared to crack with a large bright flash appearing above the sample. Reaction is rapid, with the flames almost completely gone after one frame (b). The shattered parts of the sample scatter away from the point of laser initiation (c-d). Similar reaction was observed in the fragments of the sample multiple times.

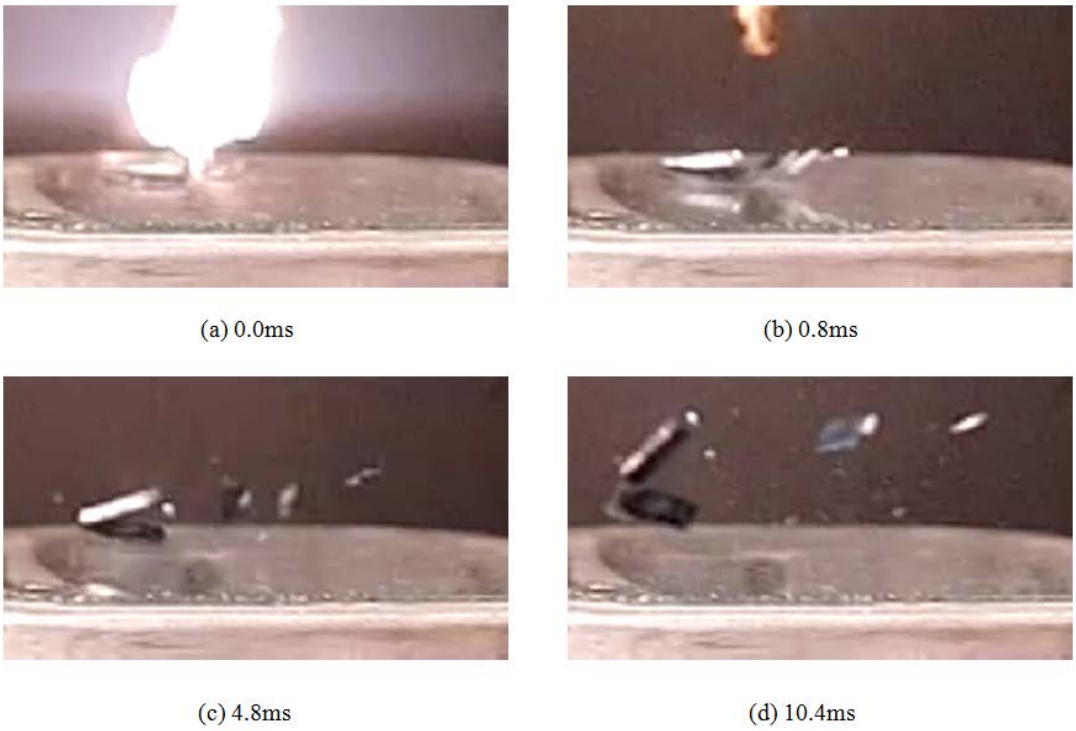

Figure 6.28: High speed camera frames of the laser initiation of a MWCNT surface loaded with PETN displaying a rapid explosion and shattering of the silicon wafer.

The pyrometer result for this explosion is shown in Figure 6.29. As observed previously, a lower initial temperature is seen with the PETN present, and a faster overall reaction is seen. The secondary peak in the PETN sample is 150˚C higher than the initial peak, which was not seen in other samples. This means a more energetic reaction is produced as a result of the initial MWCNT absorption, possibly triggering an explosion in the PETN on the surface.

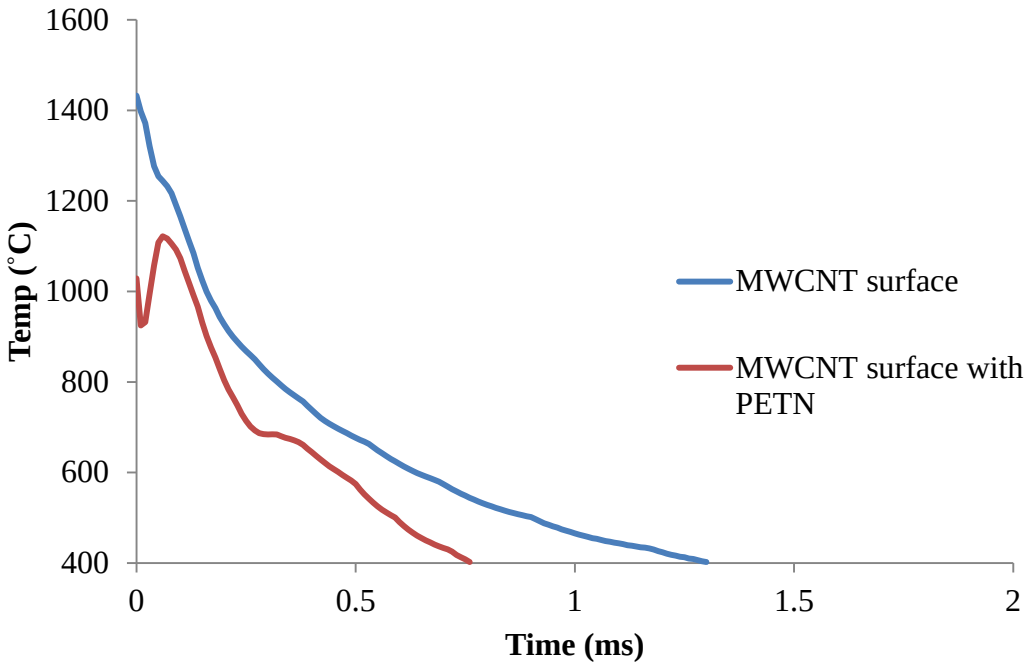

Figure 6.29: Laser initiation of a vertically aligned MWCNT surface with and without a PETN layer on the surface.

It is not known why this sample reacted much more violently than other samples. The variables have not been fully investigated. Examination of the sample suggests that the nanotube length is relatively short (~150µm) which means there is more percentage mass of iron catalyst. The PETN layer appeared thin so a higher portion could be within the nanotube array rather than on top. Figure 6.28 (a) shows that a small point of the flame has extended down through the sample to the sample stage suggesting that the more energetic part of the explosion was closer to the silicon wafer than the surface. This high explosion occurred on three different samples only, but could not be controllably reproduced. A more thorough investigation into all the variables that affect the reaction is required, but surface bound vertically aligned MWCNTs have shown great potential for explosive applications here.

6.6: Chapter Conclusions

PETN was found to be optically inactive to the IR (1064nm) laser when initiated alone which supported the low absorption found in the literature. In laser initiated reactions with APSWCNTs, partial ignition of PETN was evident through a higher temperature on the pyrometer and a brighter flash observed in high frame rate photos. A poor contact between APSWCNTs and PETN resulting in low thermal transfer coupled with particle scattering was attributed to the incomplete reaction.

Dissolving and recrystallising PETN directly onto APSWCNT samples was unsuccessful due in part to the insulating effect of the PETN, the altered crystal shape and the increased density of the randomly oriented nanotube bundles allowing greater heat dissipation.

Initiating samples with the optimal ratio of ferrocene present (1:2) produced an enhanced reaction as a result of the PETN igniting. The higher initial temperature from ferrocene produced enough energy transfer to the PETN to ignite it which in turn increased the overall reaction rate and displayed much more energy early in the reaction with no delayed secondary peak arising. This powder mixture has strong potential for future investigations into energetic material initiation.

Thin (5-40µm) layers of PETN were successfully evaporated onto vertically aligned surface bound MWCNTs by acetone recrystallization. Some aspects of these layers were investigated by optical and Raman microscopy to show the structure of the crystalline layers and indicate that PETN was able to reach between nanotubes as well as creating a surface layer.

The resulting laser initiated reactions displayed reduced temperatures on the pyrometer due to a partial blocking of input laser radiation. However, high speed camera photos showed very fast reaction rates and energies high enough to force the silicon wafer substrates to become airborne and in some cases shatter. Vertically aligned arrays of nanotubes appear to have excellent potential as light initiated explosive devices and exhibit many advantages over powder samples including removing the influence of density and greater control of surface structure. However, more work is required to investigate and control the variables which influence ignition properties and develop controllable methods to attach energetic materials to them.

6.7: References

1 Bourne, N.K., On the Laser Ignition and Initiation of Explosives. *Proceedings of the Royal Society of London. Series A: Mathematical, Physical and Engineering Sciences* **457** (2010), 1401-1426 (2001).

2 Nagayama, Kunihito, Inou, Kazunari, and Nakahara, Motonao, Initiation of PETN Powder by Pulse Laser Ablation. *Shock Compression of Condensed Matter: 12th APS Topical Conference* **620** (1), 995-998 (2002).

3 Watson, S., Gifford, M. J., and Field, J. E., The Initiation of Fine Grain Pentaerythritol Tetranitrate by Laser-Driven Flyer Plates. *Journal of Applied Physics* **88** (1), 65-69 (2000).

4 Aluker, E. D. *et al.*, Efficiency of Laser Initiation and Absorption Spectra of PETN. *Russ. J. Phys. Chem. B* **4** (1), 63-65 (2010).

5 Aluker, E. D. *et al.*, Laser Initiation of PETN in the Mode of Resonance Photoinitiation. *Russ. J. Phys. Chem. B* **5** (1), 67-74 (2011).

6 Aluker, E. D. *et al.*, Effect of Temperature on the Laser Initiation of Pentaerythritol Tetranitrate (PETN). *Russ. J. Phys. Chem. B* **2** (3), 375-377 (2008).

7 Borg, Rodney A, Diffuse Reflectance Spectra of Energetic Material, DTIC Document, (1994).

8 Nagayama, Kunihito, Kotsuka, Yuriko, Nakahara, Motonao, and Kubota, Shiro, Pulse Laser Ablation of Ground Glass Surface and Initiation of PETN Powder. *Sci. Technol. Energ. Mater* **66** (6), 416-420 (2005).

9 Meyer, Rudolf, Köhler, Josef, and Homburg, Axel, *Explosives*, 6th edition. pp 250-269 (Wiley-VCH Verlag GmbH & Co. KGaA, 2007).

10 Zhuang, Li, Gui, Lai, and Gillham, Robert W., Degradation of Pentaerythritol Tetranitrate (PETN) by Granular Iron. *Environmental Science & Technology* **42** (12), 4534-4539 (2008).

11 Luebcke, P. E., Dickson, P. M., and Field, J. E., Deflagration-to-Detonation Transition in Granular Pentaerythritol Tetranitrate. *Journal of Applied Physics* **79** (7), 3499-3503 (1996).

12 Petel, O. E. *et al.*, Minimum Propagation Diameter and Thickness of High Explosives. *Journal of Loss Prevention in the Process Industries* **20** (4–6), 578-583 (2007).
13 Khasainov, B. A., Ermolaev, B. S., Presles, H. N., and Vidal, P., On the Effect of Grain Size on Shock Sensitivity of Heterogeneous High Explosives. *Shock Waves* **7** (2), 89-105 (1997).
14 Davis, Tenney L., *The Chemistry of Powder and Explosives*. pp 500 (New York: Wiley, 1966).
15 Cooper, P.W., *Explosives Engineering*. pp 460 (New York, NY: Wiley-VCH, Inc., 1996).
16 Tarzhanov, V. I. *et al.*, Laser Initiation of PETN. *Combust Explos Shock Waves* **32** (4), 454-459 (1996).
17 Jaffe, Irving, Determination of the Critical Diameter of Explosive Materials. *ARS Journal* **32** (7), 1060-1065 (1962).
18 Tappan, Alexander S. *et al.*, Critical Detonation Thickness in Vapor-Deposited Pentaerythritol Tetranitrate (PETN) Films. *AIP Conference Proceedings* **1426** (1), 677-680 (2012).
19 Petel, Oren E., Higgins, Andrew J., Yoshinaka, Akio C., and Zhang, Fan, Effect of Shock Precompression on the Critical Diameter of Liquid Explosives. *AIP Conference Proceedings* **845** (1), 998-1001 (2006).
20 Paisley, Dennis L., Prompt Detonation of Secondary Explosives by Laser, presented at the Ninth Symposium (International) on Detonation, Portland, Oregon, pp. 1110-1117, 1989.
21 Ajayan, P. M. *et al.*, Nanotubes in a Flash--Ignition and Reconstruction. *Science* **296** (5568), 705- (2002).
22 Kim, Ji Hoon, Ahn, Ji Young, Park, Hyun Seol, and Kim, Soo Hyung, Optical Ignition of Nanoenergetic Materials: The Role of Single-Walled Carbon Nanotubes as Potential Optical Igniters. *Combustion and Flame* **160** (4), 830-834 (2013).
23 Lau, Kenneth K. S. *et al.*, Superhydrophobic Carbon Nanotube Forests. *Nano Letters* **3** (12), 1701-1705 (2003).
24 Nguyen, Cattien V. *et al.*, Preparation of Nucleic Acid Functionalized Carbon Nanotube Arrays. *Nano Letters* **2** (10), 1079-1081 (2002).
25 Abrahamson, Joel T. *et al.*, Excess Thermopower and the Theory of Thermopower Waves. *ACS Nano* **7** (8), 6533-6544 (2013).
26 Choi, Wonjoon, Abrahamson, Joel T., Strano, Jennifer M., and Strano, Michael S., Carbon Nanotube-Guided Thermopower Waves. *Materials Today* **13** (10), 22-33 (2010).
27 Choi, Wonjoon *et al.*, Chemically Driven Carbon-Nanotube-Guided Thermopower Waves. *Nat Mater* **9** (5), 423-429 (2010).
28 Fell, Nicholas F *et al.*, Fourier Transform Raman (FTR) Spectroscopy of Some Energetic Materials and Propellant Formulations II, (1995).
29 Lewis, Ian R., Daniel, Nelson W., and Griffiths, Peter R., Interpretation of Raman Spectra of Nitro-Containing Explosive Materials. Part I: Group Frequency and Structural Class Membership. *Applied Spectroscopy* **51** (12), 1854-1867 (1997).
30 Nagli, L., Gaft, M., Fleger, Y., and Rosenbluh, M., Absolute Raman Cross-Sections of Some Explosives: Trend to UV. *Optical Materials* **30** (11), 1747-1754 (2008).

Chapter 7: Conclusions and Future Direction

7.1: Introduction

This thesis sought to investigate the light initiation of carbon nanotubes to ignite energetic materials for use as detonators in blasting systems. To achieve this, firstly the research set out to reliably measure the output speed and energy of light initiated carbon nanotube ignition reactions and thus to investigate variables which alter the reaction properties.

Secondly, the study aimed to optimise the reaction in terms of thermal energy output and reaction rate. This was to be performed by investigating the influence of various novel techniques and material additives to the light initiated nanotubes.

Thirdly, the aim was to trigger the ignition of an energetic material by using light initiated carbon nanotubes. This final research aim was to be performed by drawing on the other goals and outcomes to use optimised conditions and techniques in preparing samples for the light initiated ignition of energetic materials and investigate the reactions achieved.

A comprehensive study into the literature to date was presented in Chapter 1.7-1.9. In summary, research has mostly included analysis of sample chemistry and molecules before and after the light initiation reaction to examine the chemical and physical changes. There remains speculation surrounding the mechanism that causes the light initiation of carbon nanotubes. Additionally, conflicting reports relating to the sensitivity and reactivity of different types of nanotubes and the influence of the catalyst exist. There have been very few

studies that attempt to measure or record properties of the ignition reaction as it occurs and those were limited to microphones to measure the photoacoustic signal and high speed cameras to observe the reaction rate. As such, investigations into the enhancement of the light initiated reaction of nanotubes have not been previously performed.

The combination of carbon nanotubes with energetic materials has previously been reported, most notably with the enhanced sensitivity of explosive nanoparticle/oxide mixtures due to the addition of nanotubes and the investigation of thermopower waves. This research has so far examined the electrical impulse generated rather than the explosion.

7.2: Research Findings

Chapter 3 explored the most commonly reported light initiation source – a camera flash unit. Experimental results found a flash unit was successful in igniting SWCNTs and that the reaction was enhanced by addition of ferrocene, which supported the literature. It was found that direct measuring of the triggered reaction was difficult due to optical interference from the flash unit. This obstacle directed research to the use of a laser with a much shorter (5ns) pulsewidth in order to measure carbon nanotube ignitions without interference on equipment.

A comparison into the differences between light initiation from the flash unit and from the laser using high speed camera frames and the pyrometer revealed that the reaction rate is much faster from laser initiation than it is from flash unit initiation. It appeared that the flash unit produced a surface propagated deflagration of samples while the reaction from the laser produced a reaction far closer to an explosion due to the high reaction rate and the fireball observed.

Consequently, as well as the improved ability to measure the reaction in the laboratory, it can be concluded that this difference is also a key reason to use a laser for initiation in the application of energetic material ignition at a commercial scale rather than a flash unit. Rate of reaction and delay between triggering and ignition are very important properties. This conclusion is supported by the findings of Manaa *et al*. where the flash initiation of carbon nanotubes was reported to cause detonation of a steel tube of K-6 explosives only after a delay of 1.5 minutes of deflagration before detonation occurred.[1] A laser would potentially provide a much faster detonation reaction.

A high speed pyrometer was used throughout this thesis to measure the temperature of light initiated reactions with respect to time. In itself, this is a novel approach to examining the light initiated reactions of carbon nanotubes in applications where a comparison between sample reactivity is required. A reproducible measurement of the reaction is acquired that can be easily compared to other samples. These results provided good synergy with the high speed camera to allow comprehensive examination and comparison of results between samples.

As such, in Chapter 4 and Chapter 5 many variables were investigated that had been previously reported in the literature with conflicting light sensitivity results such as as-prepared SWCNTs, purified SWCNTs, MWCNTs and various contents of metal catalyst. Under IR (1064nm) laser radiation at 150mJ, optimal parameters with respect to output energy were reported as Carbon Solutions APSWCNTs/ferrocene (1:2) partially confined in a glass sample vial to reduce scattered particles. However, all other samples did initiate from the laser. It is concluded from these results that any sample of carbon nanotube is capable of light initiated ignition if the radiation is of a high enough energy. Many reports in the literature use a much lower energy flash unit which does not seem to be directly comparable to laser initiation.

Chapter 4 attempted investigate the influence of the type and concentration of the residual metal catalyst. It was found that a higher metal content did enhance the light initiated reaction. However, purification of samples in Chapter 5.2 conflicted with this conclusion. Our experiments were limited to investigating only the metal content and it does appear that other properties of nanotube samples play an important role in the initiation reaction which has not yet been investigated.

Iron and nickel nanoparticles were found to ignite via the flash unit and the laser on their own. However, they were unable to transfer energy to other materials. Successful initiation of samples with almost no metal content indicates the importance of carbon nanotubes in the reaction.

Discovering or proposing the mechanism of light initiation of carbon nanotubes was not directly in the scope of this thesis. However, we suggest that proposals stating that the residual metal catalyst particles are entirely responsible for the ignition are incorrect since reactions have been observed in samples with little to no metal catalyst. Kang *et al*. also used an IR laser and reported no difference in reactivity between samples of varying catalyst content.[2]

The light initiation of surface bound vertically aligned arrays of MWCNTs was investigated in Chapter 5 and the ignition reactions were found to be superior to ‘fluffy’ APSWCNTs. The key advantages of these samples over powder samples were reported. In summary, the alignment means light travels down the length of the nanotubes rather than hitting a randomly oriented bundle which provides enhanced light absorption and particle scattering is greatly reduced so less energy is lost to kinetic energy. A further advantage is that reaction properties are not affected by confinement or density as with powder samples. As such, surface-bound samples appear to be a good choice for initiating systems.

Chapter 6 was solely dedicated to the aim of igniting a secondary energetic material (PETN) with light initiated carbon nanotubes. This was successfully achieved with APSWCNT/ferrocene (1:2) and with vertically aligned MWCNTs. Mixing of samples is easily achieved with powder samples, however, contact between particles may not be high enough to initiate a complete reaction unless pressure is used, and the effect of density and pressure on samples is still not fully understood.

On the other hand, vertically aligned surface bound nanotubes reduce the influence of sample packing and density, but adding energetic materials to them in a controllable method presents its own challenges. The technique used in this thesis was to dissolve the PETN into the nanotube surface with acetone. This technique was limited by the lack of control and reproducibility. While very strong potential for the system was shown, there is still a need to investigate the variables which influence the reaction and introduce reproducibility into systems. Additionally, reactions observed via high speed camera did appear to somewhat contradict the results recorded by the pyrometer in that the pyrometer suggested weaker reactions occurred with PETN addition while the high speed showed the opposite. It may be that the temperature reached was indeed lower with PETN on the surface, or the rapid movement of samples out of the focal point of the pyrometer optics may have reduced the signal received. Clearly further investigation is required to develop the analysis methods.

7.3: Future Directions

There are many potential applications of light initiated carbon nanotubes and the phenomenon is still relatively new. To begin, the full mechanism and thus the variables that influence the light initiated reactions still needs to be investigated further. This may be difficult since synthesis of nanotubes with controllable properties is not trivial and modifying variables such as metal content

without affecting other variables like sample density is problematic. A significant difference in reactions with flash units and with a laser has been demonstrated. Analysis of any differences in chemical changes of nanotubes as a result of the reactions would be interesting.

Applications relating to the ignition of fuels were reported in the literature (Chapter 1.9) and the results appear to be quite promising.[3-5] In those experiments a camera flash was used and flash initiation should not be discounted for all applications as a result of this thesis. The ability to initiate a large area at one time provides advantage over many current systems for fuels and explosives that contain a single point source initiation. Chapter 3.4 showed that laser beam divergence could be used with similar effect but potentially greater overall power if required.

The simple light initiation of nanotubes was shown to be capable of creating instant localised temperatures in the region of 1000˚C. There may be potential for this to be used as a reaction cell to initiate reactions of other materials which require high temperatures without the need for a furnace. Reconstruction of nanotube structure has also been demonstrated.[6,7] An investigation into the lower threshold energy requirements for different types of samples could provide a method of purification. If, for example, at a low energy some nanotubes are combusted and reconstructed but others are not, light initiated reactions could selectively destroy some types or lengths of nanotubes only. Oxidation purification techniques have shown smaller diameter SWCNTs oxidise at lower temperatures than larger diameter nanotubes.[8] Similar differences may exist for light initiated nanotubes. Chemical reconstruction and degradation of nanotubes has been shown even without combustion[9] so light energy could be reduced significantly. Much more research is needed to investigate the minimum energy levels required and what properties of any given nanotube sample influences the minimum energy of light initiation.

There are many established and preliminary techniques to chemically attach different functional groups to carbon nanotubes. Light initiation of covalently functionalised nanotubes has not been investigated yet. Direct chemical attachment will decrease the need to transfer heat efficiently to other materials and may potentially enhance reactions. For example, covalent attachment of NO_2 functional groups to carbon nanotubes has been demonstrated by electrochemistry and by substitution of a carboxylic acid functional group respectively.[10,11] This may improve the energetic output of light initiation. Covalent attachment of ferrocene to carbon nanotubes has previously been demonstrated[12] and the light initiation compared to simple powder mixing of ferrocene would be interesting.

There are many more potential future investigations directly related to the goals and outcomes of this thesis. It was found that the use of powder samples was limited by the need to carefully monitor density and by the transfer of heat when particle scattering occurs or additives are not in close enough contact. Vertically aligned surface bound samples solved many of those problems, however, they presented difficulties in reproducibly mixing controlled volumes and surface morphologies of energetic materials. For as-prepared nanotubes, a particle structure clearly needs to be developed to prevent heat dissipation and improve heat flow to energetic materials. For vertically aligned arrays, control and reproducibility is needed in the thin films of energetic materials. Suggested future directions for both are presented in the following.

Recently, carbon nanotubes have been grown radially outwards from the surface of metal nanoparticles (~200nm diameter) in the gas phase.[13-15] This technique was capable of producing ‘sea urchin-like’ structures with the carbon nanotubes on metal particles. The TEM image is displayed in Figure 7.1. This structure is very novel and significantly reduces the heat dissipation pathways to other nanotubes when compared to ‘fluffy’ APSWCNTs by reduced cross-linking and less bundles so it may form an excellent starting point for light initiation.

Further, the energy can be all directed to the nanoparticle and produce a lot of heat in the particle as opposed to randomly aligned bundles where heat can dissipate in any direction through neighbouring nanotubes.

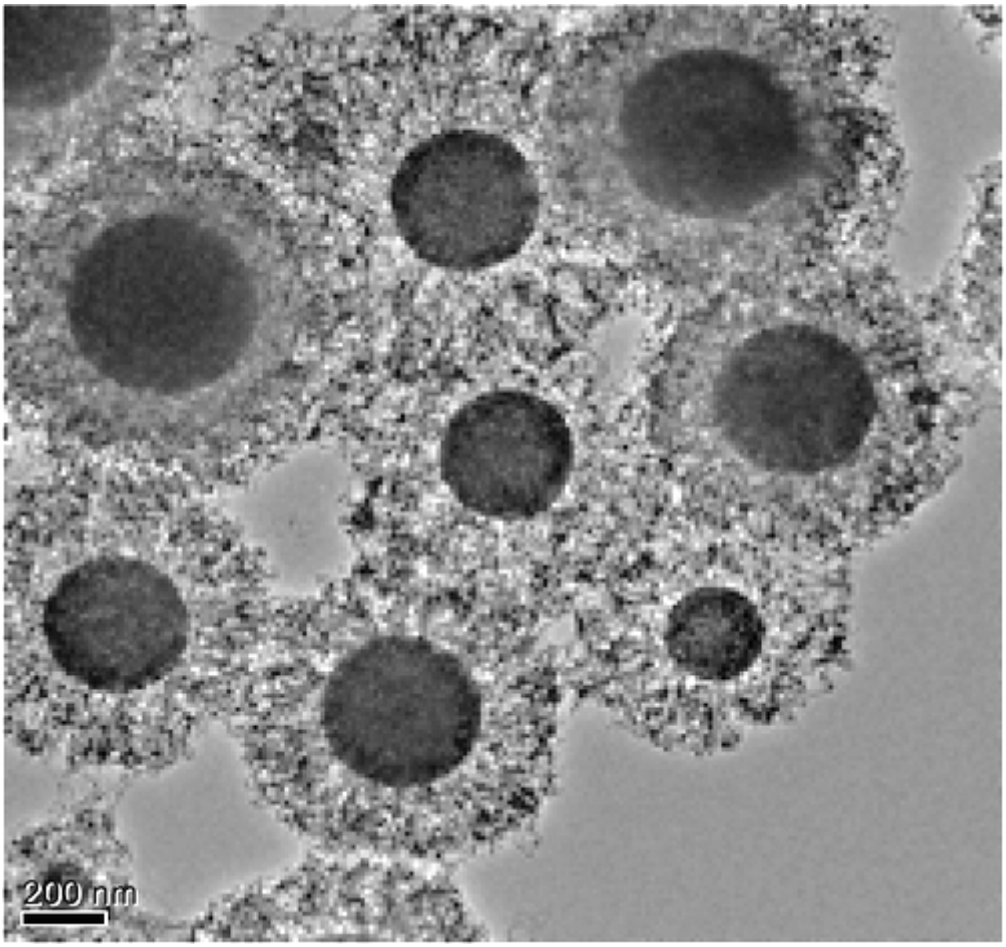

Figure 7.1: TEM image of the metal nanoparticles with 'sea urchin-like' structure of carbon nanotubes grown out of the surface. (*Moon, 2009*)

Kim *et al*. has very recently (article in press) used the 'sea urchin-like' particles as part of a light initiated system for underwater explosives.[16] The particles were combined with aluminium (fuel) and copper oxide (oxidiser) nanoparticles and pressed into a pellet. A hydrophobic film of nitrocellulose was then applied to allow the pellets to ignite underwater via a flash unit initiation of the nanotubes. This outcome proves contrary to current belief that, under the right conditions, pressurised nanotubes can be successfully light initiated because heat

dissipation pathways are not increased in these particles with pressure. This opens up many more potential uses if pellets of nanotubes and energetic materials can be light initiated since controlled volumes and consistent surface areas would be much easier to handle and much more predictable than with loose powder.

In 2013, Jeong *et al*. reported on the use of nanotubes in aluminium nanoparticles to enhance their thermal oxidation properties.[17] A ball-milling process was used with MWCNTs and aluminium nanoparticles (200nm) to combine them. Longer milling time changed the structure in three different morphologies. Firstly, nanotubes coated the outside of the particles. Secondly, nanotubes became embedded in the particles with a portion still remaining at the surface. Thirdly, nanotubes were embedded completely inside the particles. The second stage of this presents an alternate method to produce 'sea urchin-like' particles with nanotubes that potentially can be scaled up far easier through the simple ball milling process. In addition, the nanotubes are embedded into the metal nanoparticles which may provide greater heat transfer to the energetic aluminium than surface growth. TGA found that oxidation rates were increased and onset oxidation temperature was decreased at the second stage when nanotubes were embedded and still at the surface due to the surface portion of the nanotubes transferring heat into the core of the aluminium nanoparticles. Light initiation of these particles should be performed and their combination with secondary energetic materials would be an interesting study.

Improving the methods of growing vertically aligned carbon nanotubes for greater reproducibility would be advantageous. Subsequently, improving the attachment of PETN is required to build control and reproducibility of reactions. The PETN layers should be investigated more thoroughly to attempt to determine how the differences in the microstructure effect the ignition. Greater control may be achieved by dissolving PETN in a solution at a known concentration first and then applying measured volumes to the vertically aligned nanotube surfaces. Other techniques may also be explored such as physical vapour deposition of

PETN as demonstrated by Tappan *et al*.[18] which may provide better control and reproducibility of the PETN layer.

PETN is only one energetic component of many current initiating systems and an extensive study could be performed examining the carbon nanotube light initiation of other secondary energetic materials. RDX has been evaporated into carbon nanotubes to investigate the production of an electrical impulse.[19] This could be investigated in direct comparison to PETN.

Experiments in this thesis have been performed with a large Nd-YAG laser in the laboratory which is impractical for use in commercial devices. Portable lasers or light sources will eventually be required. To this end, further studies should be performed using small diode lasers to investigate the reactions. The experimental method developed in this thesis involved directing the laser beam from above a silicon substrate which contained vertically aligned MWCNTs and a top layer of PETN. The laser beam therefore had to travel through the PETN before reaching the MWCNTs. It has been previously shown that vertically aligned arrays of nanotubes can be grown on quartz.[20,21] Using an optically transparent substrate like quartz will potentially allow the laser beam to be directed from directly beneath the sample substrate and thus the MWCNTs will initiate from their base (at the substrate surface) and the energy will travel towards the top layer of PETN instead. This method would also allow the top layer of PETN to be in contact with and initiate a larger bulk charge of secondary energetic material.

Finally, the ignition of milligram quantities of PETN has been successfully demonstrated via the light initiation of carbon nanotubes. Scaling up these experiments and attempting to ignite larger charges of energetic materials with the nanotube/PETN systems is required. Manaa *et al*. have already demonstrated the detonation of a copper cylinder of K-6 explosive by flash unit

initiation of carbon nanotubes at one end.[1] However, a deflagration to detonation delay of 1.5 minutes was found. A similar experiment could be performed with laser initiation to reduce or remove the delay. Implementation of a vertically aligned CNT system to such experiments could also be performed. A thorough investigation into explosion delays and shockwave speeds could be performed.

7.4: References

1 Manaa, M. Riad *et al.*, Flash Ignition and Initiation of Explosives−Nanotubes Mixture. *Journal of the American Chemical Society* **127** (40), 13786-13787 (2005).

2 Kang, Bin, Dai, Yaodong, Chang, Shuquan, and Chen, Da, Explosion of Single-Walled Carbon Nanotubes in Suspension Induced by a Large Photoacoustic Effect. *Carbon* **46** (6), 978-981 (2008).

3 Berkowitz, Andrew M. and Oehlschlaeger, Matthew A., The Photo-Induced Ignition of Quiescent Ethylene/Air Mixtures Containing Suspended Carbon Nanotubes. *Proceedings of the Combustion Institute* **33** (2), 3359-3366 (2011).

4 Danczyk, SA *et al.*, in *53rd JANNAF Joint Propulsion Meeting, 2nd Liquid Propulsion Subcommittee and Spacecraft Propulsion Subcommittee* (Monterey, CA, 2005).

5 Finigan, Daniel J, Dohm, Brian D, Mockelman, Jeffrey A, and Oehlschlaeger, Matthew A, Deflagration-to-Detonation Transition Via the Distributed Photo Ignition of Carbon Nanotubes Suspended in Fuel/Oxidizer Mixtures. *Combustion and Flame* **159** (3), 1314-1320 (2012).

6 Ajayan, P. M. *et al.*, Nanotubes in a Flash--Ignition and Reconstruction. *Science* **296** (5568), 705- (2002).

7 Smits, Jan *et al.*, Response of Fe Powder, Purified and as-Produced HiPCO Single-Walled Carbon Nanotubes to Flash Exposure. *Materials Science and Engineering A* **358** (1-2), 384-389 (2003).

8 Chiang, I. W. *et al.*, Purification and Characterization of Single-Wall Carbon Nanotubes (SWNTs) Obtained from the Gas-Phase Decomposition of CO (HiPCO Process). *The Journal of Physical Chemistry B* **105** (35), 8297-8301 (2001).

9 Tseng, Shih H. *et al.*, Ignition of Carbon Nanotubes Using a Photoflash. *Carbon* **45** (5), 958-964 (2007).

10 Forohar, Farhad, Whitaker, Craig M., Uber, Ian C., and Bellitto, Victor, Synthesis and Characterization of Nitro-Functionalized Single-Walled Carbon Nanotubes. *Journal of Energetic Materials* **30** (1), 55-71 (2011).

11 Wang, Yubing, Malhotra, Sanjay V., Owens, Frank J., and Iqbal, Zafar, Electrochemical Nitration of Single-Wall Carbon Nanotubes. *Chemical Physics Letters* **407** (1–3), 68-72 (2005).

12 Yu, Jingxian *et al.*, Electron-Transfer Characteristics of Ferrocene Attached to Single-Walled Carbon Nanotubes (SWCNT) Arrays Directly Anchored to Silicon(1 0 0). *Electrochimica Acta* **52** (21), 6206-6211 (2007).

13 Kim, S. H., Wang, C., and Zachariah, M. R., Aerosol Formation of Sea-Urchin-Like Nanostructures of Carbon Nanotubes on Bimetallic Nanocomposite Particles. *J Nanopart Res* **13** (1), 139-146 (2011).

14 Kim, Whi Dong *et al.*, Tailoring the Carbon Nanostructures Grown on the Surface of Ni–Al Bimetallic Nanoparticles in the Gas Phase. *Journal of Colloid and Interface Science* **362** (2), 261-266 (2011).

15 Moon, Young Kyun *et al.*, Synthesis of Length-Controlled Aerosol Carbon Nanotubes and Their Dispersion Stability in Aqueous Solution. *Langmuir* **25** (3), 1739-1743 (2009).

16 Kim, Ji Hoon *et al.*, Flash-Ignitable Nanoenergetic Materials with Tunable Underwater Explosion Reactivity: The Role of Sea Urchin-Like Carbon Nanotubes. *Combustion and Flame* (in Press), http://dx.doi.org/10.1016/j.combustflame.2014.1011.1011 (2014).

17 Jeong, Hye Yun *et al.*, Tailoring Oxidation of Al Particles Morphologically Controlled by Carbon Nanotubes. *Energy* **55**, 1143-1151 (2013).

18 Tappan, Alexander S. *et al.*, Critical Detonation Thickness in Vapor-Deposited Pentaerythritol Tetranitrate (PETN) Films. *AIP Conference Proceedings* **1426** (1), 677-680 (2012).

19 Choi, Wonjoon *et al.*, Chemically Driven Carbon-Nanotube-Guided Thermopower Waves. *Nat Mater* **9** (5), 423-429 (2010).

20 Hata, Kenji *et al.*, Water-Assisted Highly Efficient Synthesis of Impurity-Free Single-Walled Carbon Nanotubes. *Science* **306** (5700), 1362-1364 (2004).

21 Murakami, Yoichi *et al.*, Growth of Vertically Aligned Single-Walled Carbon Nanotube Films on Quartz Substrates and Their Optical Anisotropy. *Chemical Physics Letters* **385** (3–4), 298-303 (2004).

Appendix

A.1: Labview Program Front Panel

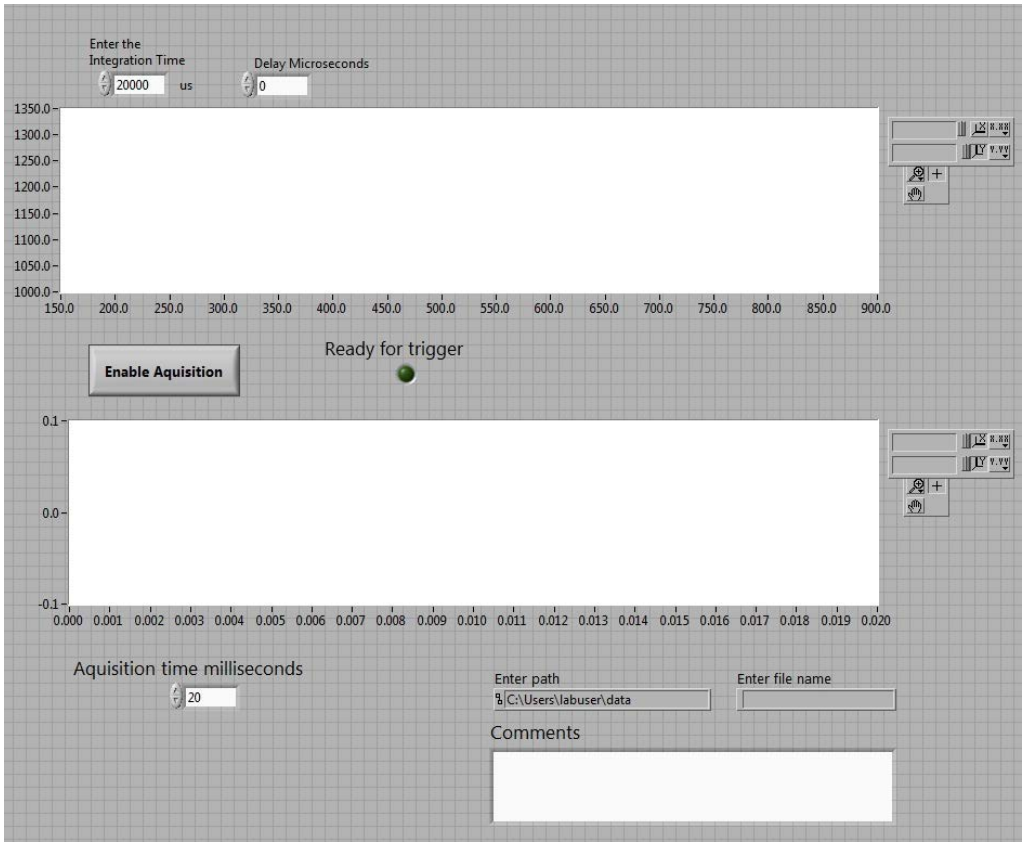

A.2: Labview VI Block Diagram

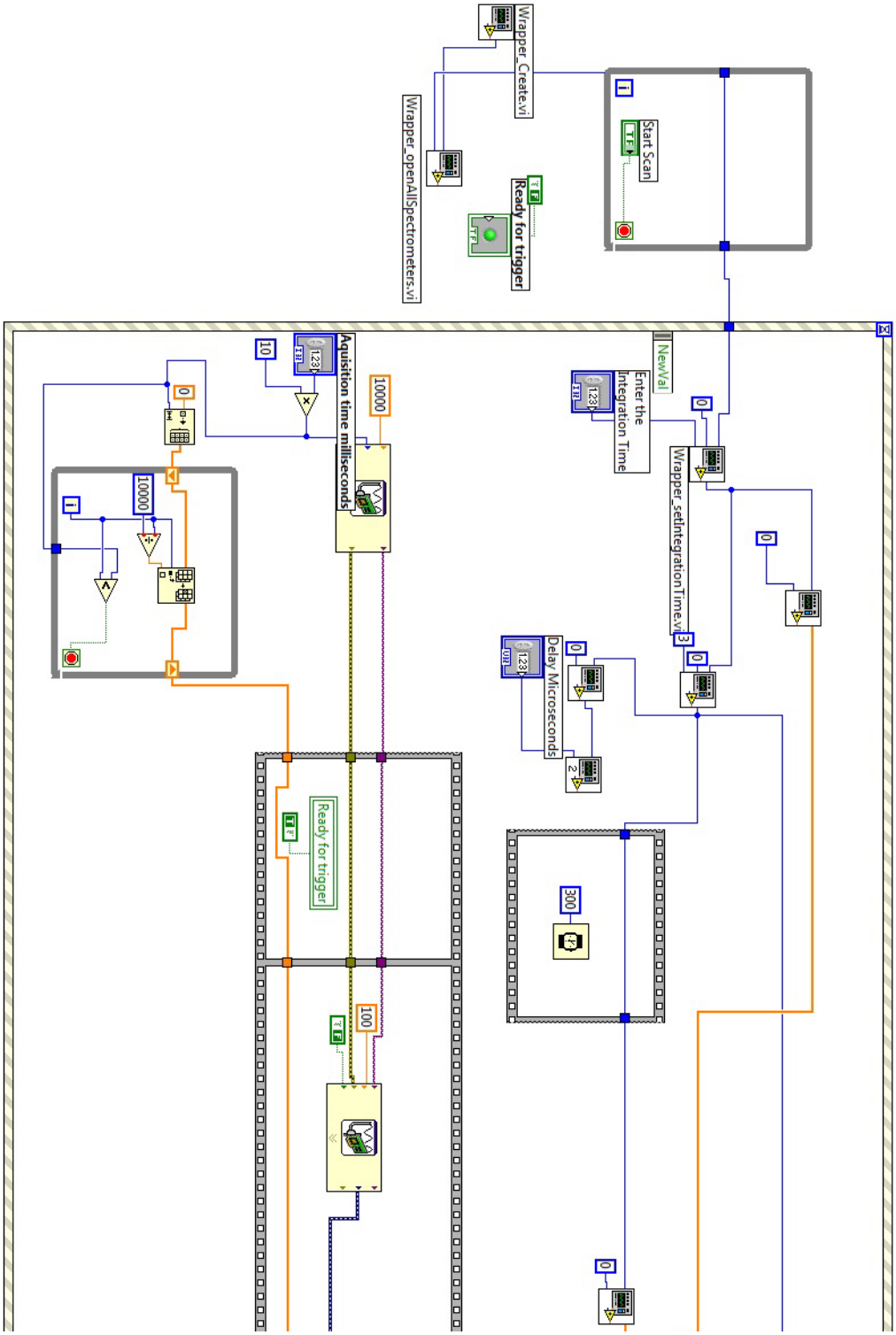

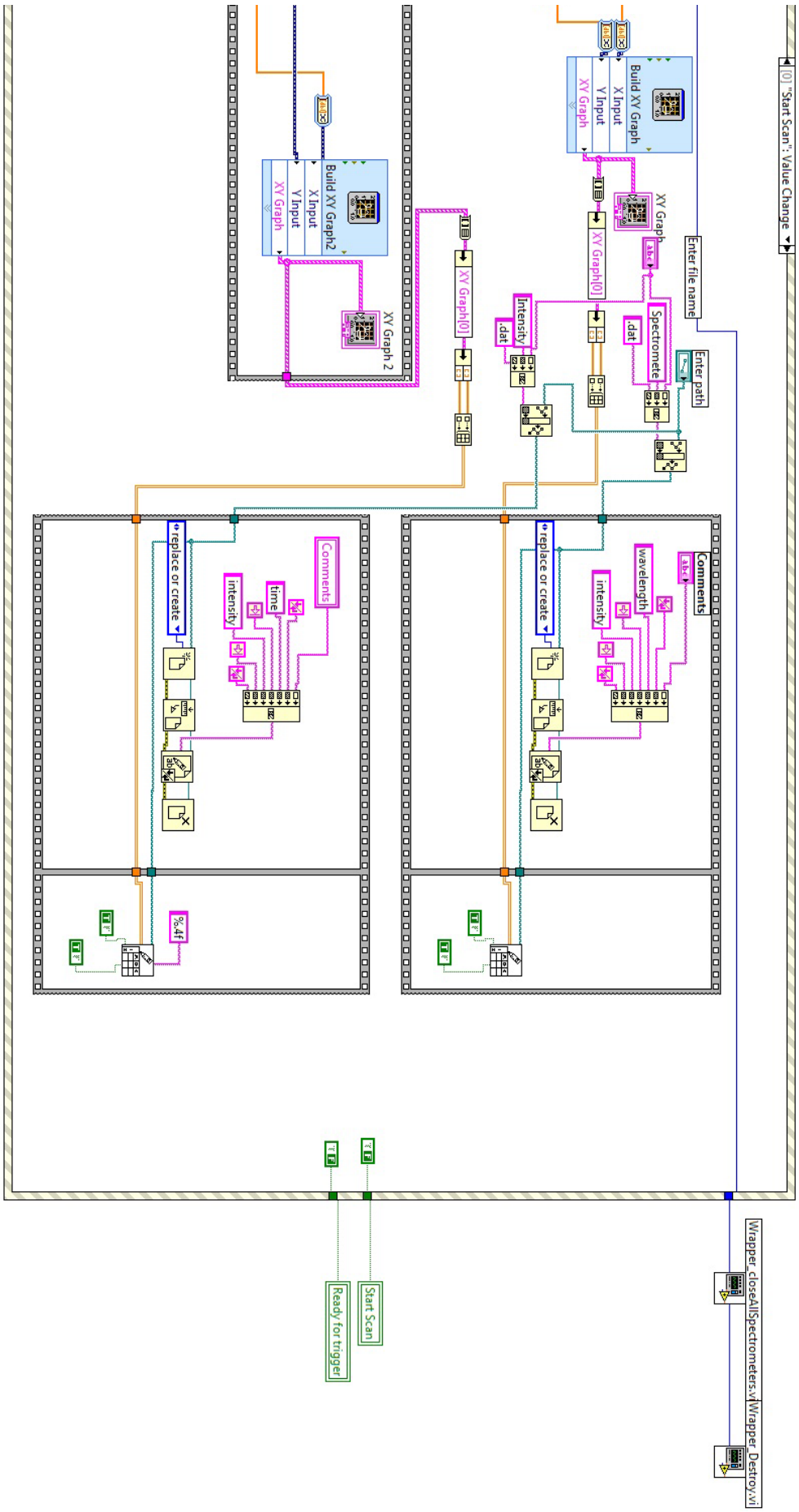
Build XY Graph
X Input
Y Input
XY Graph
Build XY Graph2
XY Graph 2
XY Graph[0]
Enter file name
Enter path
Intensity .dat
Spectromete
.dat
replace or create
intensity
time
Comments
wavelength
%.4f
Ready for trigger
Start Scan
Wrapper_closeAllSpectrometers.vi
Wrapper_Destroy.vi